VOLUME 106 PART C NUMBER 10 SEPTEMBER 1959

The Proceedings

OF

THE INSTITUTION OF ELECTRICAL ENGINEERS

FOUNDED 1871: INCORPORATED BY ROYAL CHARTER 1921

PART C

MONOGRAPHS Nos. 327–339

SAVOY PLACE · LONDON W.C.2

Price Fifteen Shillings

The Institution of Electrical Engineers

FOUNDED 1871
INCORPORATED BY ROYAL CHARTER 1921

PATRON: HER MAJESTY THE QUEEN

COUNCIL 1958–1959

President

S. E. GOODALL, M.Sc.(Eng.)., F.Q.M.C.

Past-Presidents

W. H. ECCLES, D.Sc., F.R.S.
The RT. HON. THE EARL OF MOUNT EDGCUMBE, T.D.
J. M. DONALDSON, M.C.
PROFESSOR E. W. MARCHANT, D.Sc.
H. T. YOUNG.
SIR GEORGE LEE, O.B.E., M.C.
SIR ARTHUR P. M. FLEMING, C.B.E., D.Eng., LL.D.
J. R. BEARD, C.B.E., M.Sc.
SIR NOEL ASHBRIDGE, B.Sc.(Eng.).
SIR HARRY RAILING, D.Eng.
P. DUNSHEATH, C.B.E., M.A., D.Sc.(Eng.).
SIR VINCENT Z. DE FERRANTI, M.C.
T. G. N. HALDANE, M.A.
PROFESSOR E. B. MOULLIN, M.A., Sc.D., LL.D.
SIR ARCHIBALD J. GILL, B.Sc.(Eng.).
SIR JOHN HACKING.
COLONEL B. H. LEESON, C.B.E., T.D.
SIR HAROLD BISHOP, C.B.E., B.Sc.(Eng.).
SIR JOSIAH ECCLES, C.B.E., D.Sc.
SIR GEORGE H. NELSON, Bart.
SIR GORDON RADLEY, K.C.B., C.B.E., Ph.D.(Eng.).
T. E. GOLDUP, C.B.E.

Vice-Presidents

SIR WILLIS JACKSON, D.Sc., D.Phil., Dr.Sc.Tech., F.R.S.
G. S. C. LUCAS, O.B.E.
SIR HAMISH D. MACLAREN, K.B.E., C.B., D.F.C., LL.D., B.Sc.
C. T. MELLING, C.B.E., M.Sc.Tech.
A. H. MUMFORD, O.B.E., B.Sc.(Eng.).

Honorary Treasurer

E. LEETE.

Ordinary Members of Council

J. A. BROUGHALL, B.Sc.(Eng.).
PROFESSOR M. W. HUMPHREY DAVIES, M.Sc.
SIR JOHN DEAN, B.Sc.
B. DONKIN, B.A.
J. M. FERGUSON, B.Sc.(Eng.).
D. C. FLACK, B.Sc.(Eng.), Ph.D.
J. S. FORREST, D.Sc., M.A.
R. J. HALSEY, C.M.G., B.Sc.(Eng.).
E. M. HICKIN.
J. B. HIGHAM, Ph.D., B.Sc.
F. C. MCLEAN, C.B.E., B.Sc.
B. L. METCALF, B.Sc.(Eng.).
J. R. MORTLOCK, Ph.D., B.Sc.(Eng.).
R. H. PHILLIPS, T.D.
H. V. PUGH.
J. R. RYLANDS, M.Sc., J.P.
D. P. SAYERS, B.Sc.
C. E. STRONG, O.B.E., B.A., B.A.I.
D. H. TOMPSETT, B.Sc.(Eng.).
H. WATSON-JONES, M.Eng.
H. WEST, M.Sc.

Chairmen and Past-Chairmen of Sections

Electronics and Communications
G. MILLINGTON, M.A., B.Sc.
*J. S. MCPETRIE, Ph.D., D.Sc.

Measurement and Control:
J. K. WEBB, M.Sc.(Eng.), B.Sc.Tech.
*H. S. PETCH, B.Sc.(Eng.).

Supply:
D. P. SAYERS, B.Sc.
*PROFESSOR M. G. SAY, Ph.D., M.Sc., F.R.S.E.

Utilization:
R. A. MARRYAT, B.Sc.(Eng.).
*J. VAUGHAN HARRIES.

Chairmen and Past-Chairmen of Local Centres

East Midland Centre:
D. E. LAMBERT, B.Sc.(Eng.).
*J. D. PIERCE.

Mersey and North Wales Centre:
J. COLLINS.
*T. MAKIN.

North Midland Centre:
J. D. NICHOLSON, B.Sc.
*A. J. COVENEY.

North-Eastern Centre:
A. T. CRAWFORD, B.Sc.
*T. W. WILCOX.

North-Western Centre:
PROFESSOR F. C. WILLIAMS, O.B.E., D.Sc., D.Phil., F.R.S.
*F. R. PERRY, M.Sc.Tech.

Northern Ireland Centre:
D. S. MCILLHAGGER, Ph.D., M.Sc.
*C. M. STOUPE, B.Sc.

Western Centre:
R. W. STEEL.
*J. F. WRIGHT.

Scottish Centre:
R. J. RENNIE, B.Sc.
*E. O. TAYLOR, B.Sc., F.R.S.E.

South Midland Centre:
J. ASHMORE.
*L. L. TOLLEY, B.Sc.(Eng.).

Southern Centre:
G. BISHOP, B.Sc.
*L. G. A. SIMS, M.Sc., Ph.D., D.Sc.

* Past Chairman.

Secretary

W. K. BRASHER, C.B.E., M.A., M.I.E.E.

Deputy Secretary

F. JERVIS SMITH, M.I.E.E.

Principal Assistant Secretary

F. C. HARRIS.

Editor-in-Chief

G. E. WILLIAMS, B.Sc.(Eng.), M.I.E.E.

THE PROCEEDINGS OF
THE INSTITUTION OF ELECTRICAL ENGINEERS

EDITED UNDER THE SUPERINTENDENCE OF W. K. BRASHER, C.B.E., M.A., M.I.E.E., SECRETARY

VOL. 106. PART C. NO. 10. SEPTEMBER 1959

621.318.13 : 621.316.5

The Institution of Electrical Engineers
Monograph No. 327 M
Feb. 1959

THE SQUARE-LOOP FERRITE CORE AS A CIRCUIT-ELEMENT

By C. H. LINDSEY, M.A., Ph.D.

(*The paper was first received 5th August, and in revised form 5th November*, 1958. *It was published as an* INSTITUTION MONOGRAPH *in February*, 1959.)

SUMMARY

A quantitative theory is presented to explain the shape of the output waveforms when square-loop ferrite cores are switched. This is based on the qualitative theory of Menyuk and Goodenough.[3] Various useful equations arising from the theory are deduced, and it is shown that the agreement with experiment is reasonable. The theory indicates which parameters of the material need to be known in order to predict its behaviour.

LIST OF SYMBOLS

μ_r = Residual permeability.
$F = F(r) = F(B)$ = Distribution function.
v = Radial velocity of domain wall.
t = Time.
p = Probability of an element $(d\theta)$ reaching radius r.
α, a = Arbitrary areas.
ρ = Density of domain centres.
H_m = Magnetizing force.
H_c = Coercive force.
$H = H_m - H_c$.
B = Flux density.
B_m = Saturation flux density.
X_0 = Loss parameter of the material: $dB/dt = X_0 F H$, ohms/m.
k_1, k_2 = Constants.
T = Switching time.
i_0 = Applied current.
i_c = Coercive current.
$i = i_0 - i_c$.
V_{max} = Peak output voltage per turn.
R_0 = Loss resistance of a core: $V_{max} = R_0 i$.
R = Instantaneous loss resistance = $R_0 F$.
Φ = Magnetic flux.
Φ_m = Saturation flux.

Correspondence on Monographs is invited for consideration with a view to publication.
Dr. Lindsey is now with Ferranti Ltd., and was formerly at the University Mathematical Laboratory, Cambridge.

(1) INTRODUCTION

It is found impossible to describe the behaviour of a square-loop ferrite core in terms of an equivalent circuit composed of linear elements, owing to the essential non-linearity of the material. The major property of the core to be taken into account when it is switched at high speeds is its residual loss, which makes the core itself appear resistive rather than inductive. The effect of this residual loss will be considered in some detail, and a method of calculating the behaviour of any particular core circuit will be described. This method does, in fact, predict the behaviour of a core with more than sufficient accuracy for the design of switching circuits, although it does not take into account the higher-order effects which are relevant when considering the suitability of the material for storage.

(2) D.C. PROPERTIES

The properties of the material at zero and low frequencies are described completely by its well-known hysteresis loop. An idealized hysteresis loop is shown in Fig. 1. The origin has

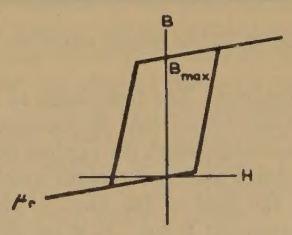

Fig. 1.—Idealized hysteresis loop.

been chosen so that in one of the remanent states B is zero. This is convenient because B_{max} then represents the change in B when the core is fully switched, and because in practice the core is never likely to be completely demagnetized. Two values of the permeability of the material are of interest, namely the residual permeability (μ_r), which is small, and the permeability on the steep part of the loop, which is so large that it may, as is

shown later, be considered infinite. The values of the field at the knee of the curve and at the saturation point are not vastly different, owing to the high permeability in this region, and so both these values will be loosely referred to as the 'coercive force'. A more precise and convenient definition of this quantity will be given later.

So long as the fields applied do not exceed the coercive force, the material behaves as an ordinary linear magnetic material of permeability μ_r. This causes any winding on a core to have an inductance (with a mutual inductance to any other winding), and this effect of the residual permeability is often of importance when the core is not actually being switched. While the core is being switched, the effect becomes of secondary importance, and in the following discussion it will be neglected.

(3) A.C. PROPERTIES

(3.1) Losses

An ordinary metallic ferromagnetic material has an eddy-current loss due to currents in the material itself. It also has a 'residual loss', which is a fundamental property of the material, but this is usually negligible because of the much larger eddy-current effect. In the case of a ferrite, the resistivity is so high that eddy currents can be entirely neglected, so that the residual loss becomes the dominant factor.

If a core is switched by a step function of current applied to a winding, then, in principle, the output voltage should be a spike of infinite amplitude lasting for an infinitesimal time. In practice, it is observed to be of finite amplitude and to last for a finite length of time, i.e. longer than the rise time of the current (see Fig. 2). Thus the core is giving a voltage output while its input current is constant, which implies a resistance

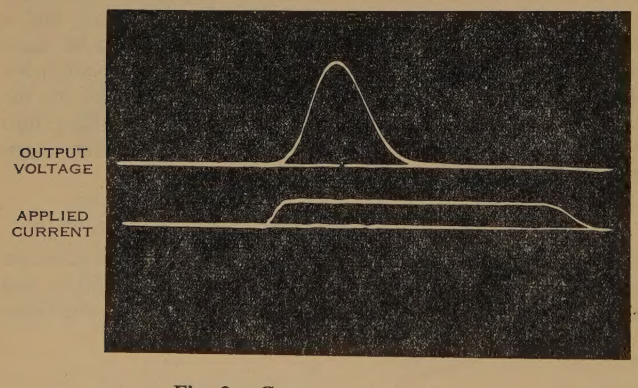

Fig. 2.—Core output waveform.

rather than an inductance. The time taken to switch the core is found to decrease as the current is increased. In order to switch it in about a microsecond, the applied field must be about twice the coercive force and is therefore much larger than the difference between the field at the knee of the hysteresis loop and that at the saturation point. It is for this reason that the slope on the steep part of the loop can be considered infinite, since it plays a very small part in determining the output voltage when the core is switched at these high speeds; in the rest of the paper it will be assumed to be infinite.

It is found experimentally that, if the peak output voltage is plotted against the switching current, a straight line is obtained as in Fig. 3, provided that the rise time of the current is short compared with the switching time. The coercive force will be defined, for the purpose of this paper, to be the intercept of this line on the current (or magnetizing force) axis (H_c in Fig. 3).

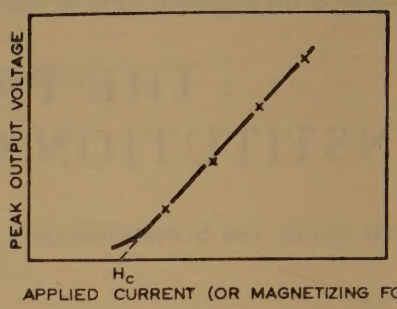

Fig. 3.—Variation of peak output voltage with applied field.

This definition has also been used by Karnaugh,[1] who called it the 'pseudo-coercive force'. It is a quantity which is precisely determined and of considerable use, being somewhat larger than the coercive force as usually defined, namely the field necessary to reduce the magnetization from remanence to zero.

(3.2) Approximate Equivalent Circuit

It is found that the graph of Fig. 3 is accurately a straight line, limited only at large currents by stray capacitances of the windings. The slope of this line, when current is plotted against voltage, has the dimensions of resistance, and is of the order of half an ohm for typical cores. The properties of the core when it is being switched can be approximately represented by a fictitious resistor of this value, connected to a fictitious single-turn winding, the core being regarded as a perfect transformer provided that the magnetizing force exceeds the coercive value and that the coercive force is subtracted from the magnetizing force before the output voltage is calculated. This equivalent circuit for a core was first suggested, in connection with metal cores, by Sands.[2]

Although this simple representation of a core is adequate for rough calculations, it does not give a true picture of its behaviour. The equivalent circuit implies that when a current step of amplitude i_0 is applied, the output should be a square voltage pulse of amplitude $R(i_0 - i_c)$. This is roughly what is observed with metal cores, which is to be expected, since their losses are due to the resistance of the material, which the fictitious resistor R should be able to represent fairly well. With ferrites, however, the output pulses are observed to be far from square, and are in fact more nearly triangular, as is shown in Fig. 2. An explanation of this phenomenon will now be given.

(4) THEORY OF SWITCHING

(4.1) Shape of Output Waveform: Qualitative Theory

(4.1.1) Domain Wall Movement.

A qualitative explanation of the phenomenon has been given by Menyuk and Goodenough.[3] Their theory applies to both metal and ferrite cores, the only differences being that, for the metal core, there is an extra term due to the eddy-current loss and the saturation magnetization is greater, which leads to a different switching time. They suppose that, when the material is magnetized in one direction, small domains of reverse magnetization exist at the grain boundaries, and also at voids in the material in the case of ferrites, or that such reverse domains are formed by the application of a small reverse field, the latter mechanism tending to give a squarer hysteresis loop. The boundaries between such domains and the adjacent ones are 180° Bloch walls—the directions of magnetization on opposite sides of such a wall being 180° apart. It is proposed that the reversal of magnetization takes place by the movement of these

Bloch walls in a direction at right angles to that of magnetization. A picture is presented of cylindrical or ellipsoidal domains of reverse magnetization growing by increasing their diameter, until they either reach the grain boundaries or meet with other such growing domains.

Menyuk and Goodenough then go on to suggest that a Bloch wall will not move until a certain minimum field has been applied, and that when it does the only significant retarding force is a viscous one, which is due in part to the eddy-current loss, if any, and in part to the spin-relaxation effect. (The latter occurs because any attempt to rotate an electron spin by applying a magnetic field will, by classical theory, cause the electron to precess, so that if it is required to turn it over quickly, a large field must be applied.) The viscous force implies that the velocity of the Bloch wall is proportional to the amount by which the applied field exceeds the minimum field necessary for motion to start.

(4.1.2) **Voltage Output.**

The voltage output from the core is proportional to the rate of change of flux within it, and therefore to the rate of change of cross-sectional area of the growing reverse domains. Since the radius of these domains increases at a constant rate for a constant applied field, and since the cross-sectional area is proportional to the square of this radius, the output voltage initially increases with time. Later, when the growing domains begin to coalesce, the rate of increase of the area diminishes again, and thus accounts for the roughly triangular shape of the observed output waveform. The following equation [eqn. (6) of Reference 3] is proposed:

$$\frac{d\Phi}{dt} = \frac{16 I_s (\cos\theta)^3}{\beta} \mathrm{F}(r)(H_m - H_0) \quad . \quad . \quad (1)$$

where I_s is the saturation magnetization of the material, β is the viscous damping parameter, H_m is the applied field, H_0 is the critical field mentioned, and θ is the angle between the easy direction of magnetization and the field. $\mathrm{F}(r)$ is a distribution function which takes account of the variations in the rate of change of the area as the radius of the domains increases. The form of $\mathrm{F}(r)$ is not given, but it will be calculated in the following Section.

The above is an outline of Menyuk and Goodenough's theory, and the experimental evidence quoted in their paper, and in another paper,[4] indicates that this outline probably represents the true mechanism of the process. They also give some further quantitative detail of the probable magnitudes of some of the quantities involved, in an effort to predict in what direction improvement of the material is likely to lie. The correctness or otherwise of these details does not affect the validity of the basic outline, neither does it affect what follows.

(4.1.3) **Effect of θ.**

In a polycrystalline material, the directions of easy magnetization of the grains are not necessarily parallel to the applied field, which accounts for the term in θ in eqn. (1). The effect of this cannot be large, however, since the ferrite materials in question have cubic structures, so that any given direction cannot be far from one of the three possible directions of easy magnetization. An attempt to take account of this effect in a theory will lead to much complication; it will probably be invalid because of the fields due to poles set up in the material wherever grains with different orientations meet, and because of the stresses which exist in ferrite toroids and which, by symmetry, must be either tangential or radial, and therefore either parallel or perpendicular to the applied field. Either way will tend to align the easy directions of magnetization, either parallel to the applied field or perpendicular to it, depending upon the sign of the magnetostriction coefficient, and this will probably invalidate any attempt to bring θ into the theory. In any case, the only effect of having the direction of easy magnetization not parallel to the field would be to reduce the velocity of the Bloch walls, and this would not affect the shape of the output waveform basically. In the following treatment, therefore, the effect of θ will be neglected.

(4.2) Quantitative Theory

(4.2.1) **Calculation of F(r).**

It is assumed that reversal of magnetization takes place by the growth of cylindrical domains which are parallel to the applied field. The centres from which these domains start are scattered at random throughout the material. At time $t = 0$, all the domains are assumed to be of zero radius, at which time a field H_m is applied. The domains then expand with radial velocity proportional to $(H_m - H_c)$, where H_c is the coercive force.

It is necessary to consider only a typical cross-section of the material perpendicular to the field, so that the domains become circles. Let the radius of a domain be r, and let the domain walls move outward with velocity v [proportional to $(H_m - H_c)$]. The area inside a domain, A, is πr^2;

$$\text{therefore} \qquad \frac{dA}{dt} = 2\pi r \frac{dr}{dt} = 2\pi r v \quad . \quad . \quad . \quad . \quad . \quad (2)$$

It is now necessary to consider the annihilation of domain walls by the coalescence of the expanding domains (see Fig. 4).

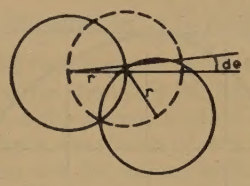

Fig. 4.—Intersection of two domain walls.
The applied field is perpendicular to the paper.

Consider an element of domain wall subtending an angle $d\theta$ at the centre of the domain. If, when the domain reaches a radius r, this element meets another domain wall, also of radius r, the centre of this second domain must lie on a circle of radius r (dotted in Fig. 4), centred at the point of intersection. If the centre of a second domain had lain within this circle, the element $d\theta$ of the first domain would never have got this far. Therefore the probability that this element reaches a radius r is the same as the probability of finding no other domain centre within this circle of radius r (or within any other circle of radius r, since domain centres are scattered at random). Let this probability be p. Then p also represents the proportion of such elements which survive until they reach a radius r. Thus the rate of change of the area enclosed by the circles, divided by the number of circles, is given by

$$\frac{dA}{dt} = 2\pi r v p \quad . \quad . \quad . \quad . \quad . \quad . \quad (3)$$

It is now necessary to calculate the probability p. Consider an area α, and within it an area a. If a particle is put in α, the probability of finding it in a is a/α, and the probability of not finding it in a is $(1 - a/\alpha)$, so that, if n particles are put in α, the probability of finding no particle in a is $(1 - a/\alpha)^n$.

If ρ is the density of the particles, $\rho = n/\alpha$, and $\alpha = n/\rho$.

Therefore the probability of finding no particles is

$$p = (1 - a\rho/n)^n$$

Now $\lim_{n\to\infty} p = \varepsilon^{-a\rho}$. Thus, if a is the area of a circle of radius r,

$$p = \varepsilon^{-\pi r^2\rho} \quad . \quad . \quad . \quad . \quad . \quad . \quad . \quad (4)$$

Combining eqns. (3) and (4),

$$\frac{dA}{dt} = 2\pi r v \varepsilon^{-\pi r^2\rho} \quad . \quad . \quad . \quad . \quad . \quad (5)$$

But v is proportional to $(H_m - H_c)$, and the rate of change of flux density ($= dB/dt$) is proportional to dA/dt,

Therefore $$\frac{dB}{dt} \propto (H_m - H_c) r \varepsilon^{-\pi r^2\rho} \quad . \quad . \quad . \quad (6)$$

so that the required distribution function is given by

$$\mathrm{F}(r) = K r \varepsilon^{-\pi r^2\rho} \quad . \quad . \quad . \quad . \quad . \quad (7)$$

where K is an arbitrary constant.

Since, however, the value of B at time t, being proportional to A, is a function of r, it is more convenient for practical purposes to express the distribution function $\mathrm{F}(r)$ as a function of B. (Note that $B = 0$ when the material is fully saturated in one direction.) This function is shown, in Appendix 8.1, to be

$$\mathrm{F} = \mathrm{F}(B) = \sqrt{(2\varepsilon)}\sqrt{\left[\log_\varepsilon\left(\frac{B_m}{B_m - B}\right)\right]}\left(\frac{B_m - B}{B_m}\right) \quad . \quad (8)$$

The variation of F with B/B_m is shown in Fig. 5.

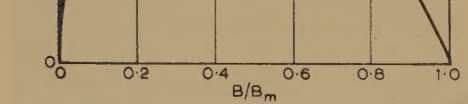

Fig. 5.—Variation of F with B/B_m.

From eqns. (6) and (7),

$$\frac{dB}{dt} \propto \mathrm{F}(H_m - H_c)$$

Let $(H_m - H_c) = H$, and let

$$dB/dt = X_0 \mathrm{F} H \quad . \quad . \quad . \quad . \quad . \quad . \quad (9)$$

Then X_0 is a fundamental parameter of the material, depending on the velocity of the domain walls for a given field H, on the density of the reverse domain centres ρ, and on the saturation flux density B_m.

(4.2.2) **Constant Field Case.**

A case of particular interest arises when the applied field H_m does not vary with time, so that v is constant. This corresponds to a step function of current applied to the core.

Now $r = vt$, so that eqn. (5) becomes

$$\frac{dA}{dt} = 2\pi v^2 t \varepsilon^{-\pi v^2 t^2 \rho}$$

and therefore

$$\frac{dB}{dt} = k_1 (H_m - H_c)^2 t \varepsilon^{-k_2 (H_m - H_c)^2 t^2}$$

$$= k_1 H^2 t \varepsilon^{-k_2 H^2 t^2} \quad . \quad . \quad . \quad . \quad . \quad . \quad . \quad (10)$$

where k_1 is a constant depending on the saturation flux density and on the ratio of v to $(H_m - H_c)$, and k_2 is a constant depending on the same ratio and on ρ.

This, therefore, is the form of the output pulse with a step-current input, and it will be seen to be at least similar to the observed waveform (Fig. 2). A detailed comparison of the predicted and observed waveforms will be given later.

The maximum value of dB/dt, which is, of course, proportional to the peak output voltage, occurs when F has its maximum value of unity.

Therefore, from eqn. (9),

$$\left(\frac{dB}{dt}\right)_{max} = X_0 H \quad . \quad . \quad . \quad . \quad . \quad . \quad (11)$$

Thus the value of X_0 may be determined easily be measuring the peak output voltage of a core for various currents, and plotting a graph such as that of Fig. 3.

(4.2.3) **Switching Time.**

Eqn. (10) shows that it takes an infinite time for the material to saturate completely. Any definition of switching time must therefore be arbitrary. In the past, many workers have defined switching to be complete when, with a step function of current applied, the output voltage has decreased to one-tenth of its peak value. This definition is obviously unsatisfactory, since it cannot be applied when the current is not constant during switching. A more logical way is to define switching to be complete when B/B_m reaches some suitable value, which will be chosen, for convenience, to correspond to the instant when the output voltage has decreased to one-tenth of its peak value in the constant-current case. It is shown in Appendix 8.2 that, at this time,

$$B/B_m = 0{\cdot}978 \quad . \quad . \quad . \quad . \quad . \quad . \quad (12)$$

and, in Appendix 8.3, that in the constant-current case the actual switching time is given by

$$T = 1{\cdot}67 \frac{B_m}{X_0 H} \quad . \quad . \quad . \quad . \quad . \quad (13)$$

It should be noted that the switching time thus defined is a function of the applied current, and is not the same as the 'switching time of the material'—a term used when describing the properties of a material to be used for storage purposes, when the current is fixed by other considerations.

(4.2.4) **Behaviour of a Core.**

So far, we have considered the properties of the material in bulk. Consider now a core of mean radius r and cross-sectional area A. Let a current of i_0 ampere-turns flow through a single-turn winding. Let the coercive current be i_c, and let $i = i_0 - i_c$. In Appendix 8.4 it is shown that the peak output voltage per turn, when i is a step function, is given by

$$V_{max} = \frac{2X_0 A i}{r} = R_0 i \quad . \quad . \quad . \quad . \quad . \quad (14)$$

where $R_0 = 2X_0 A/r$. R_0, which has the dimensions of resistance, is obviously the slope of the line in Fig. 3. It also follows that X_0 should be measured in ohms per metre (unrationalized).

Hence, for a single core, eqns. (8), (9) and (13) become

$$F(\Phi) = \sqrt{(2\varepsilon)}\sqrt{\left[\log\left(\frac{\Phi_m}{\Phi_m - \Phi}\right)\right]\left(\frac{\Phi_m - \Phi}{\Phi_m}\right)} \quad . \quad (15)$$

$$\frac{d\Phi}{dt} = R_0 F i \quad . \quad . \quad . \quad . \quad . \quad . \quad . \quad (16)$$

$$T = 1{\cdot}67\frac{\Phi_m}{R_0 i} \quad . \quad . \quad . \quad . \quad . \quad . \quad . \quad (17)$$

The output voltage is therefore, in general, given by

$$V = R_0 F i = Ri \quad . \quad . \quad . \quad . \quad . \quad . \quad (18)$$

where

$$R = R_0 F \quad . \quad . \quad . \quad . \quad . \quad . \quad . \quad (19)$$

This implies that the current equivalent circuit for a core is as described in Section 3.2, except that the fictitious resistor R is now variable, of magnitude $R = R_0 F$. It is suggested that the quantity R_0 should be termed the 'loss resistance' of the core.

(4.2.5) **Energy Required to Switch a Core.**

If a core is switched by a constant field H_m, the energy required per unit volume is

$$\frac{1}{4\pi}B_m H_m = \frac{1}{4\pi}B_m(H_c + H)$$

$$= \frac{1}{4\pi}B_m\left(H_c + 1{\cdot}67\frac{B_m}{X_0 T}\right) \text{ from eqn. (13)}$$

$$= \frac{1}{4\pi}H_c B_m + \frac{1{\cdot}67}{4\pi}\frac{B_m^2}{X_0 T} \quad . \quad . \quad . \quad . \quad . \quad (20)$$

The first term represents the hysteresis loss, and the second term the residual loss.

(4.3) Experimental Evidence

(4.3.1) **General Experimental Evidence.**

The fact that a linear relationship exists between the peak voltage from a core and the input current (Fig. 3) supports the above theory, but it is necessary to show also that, with a step-function input, the output voltage is of the predicted form [eqn. (10)], and that, in other cases, the application of eqn. (8) yields the correct result.

(4.3.2) **Experimental Details.**

The experiment was carried out with 3 mm cores in grade D2 material. Two input windings and a 'read' winding (all of 10 turns) were put upon the core. A 'reset' pulse of 2·5 ampere-turns was applied to one input, and a pulse of variable amplitude, with a rise time of 0·2 microsec, to the other. The output was applied to a double-beam oscillograph, and the trace was photographed. The voltage across a 100-ohm resistor carrying the current pulse was applied to the other beam. Fig. 2 is one of these photographs. In this Figure the current appears to rise before the voltage: this is due to the delay in the amplifier, and also to the finite rise-time of the current and the coercive force of the core. The finite rise-time of the current also causes the voltage waveform to be concave upwards at the start, whereas the theory predicts that the voltage should rise almost linearly at first, and then become concave downwards. That this is the correct explanation is clear, since the effect is only marked when the switching time of the core is comparable with the rise time of the current.

The bandwidth of the amplifier, which is a limiting factor in this experiment, was greater on the ranges with less gain, so that it was necessary to use rather a small trace on the screen and, in doubtful cases, to photograph the same waveform with different gain settings. The photographs finally selected were considered to be a fair representation of the true waveform, but owing to the small traces, the accuracy of the experiment could not be very high.

The photographs were traced on to graph paper in an enlarger, and were measured. Fig. 6 shows the resulting traces taken

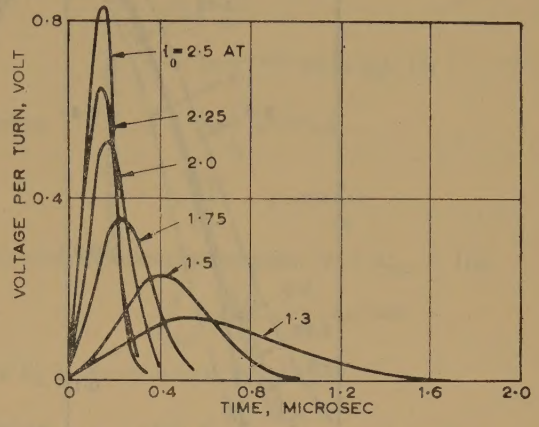

Fig. 6.—Observed output waveforms (3 mm core).

with input currents varying between 2·5 and 1·3 ampere-turns. (At the higher current, the switching time is comparable with the rise time of the current, and the lower current is only slightly higher than the coercive value.) A plot of peak voltage versus current produced values of R_0 and i_c for the core [see Section (4.2.4)]; the area under the curves gave Φ_m.

The curves were then normalized by multiplying the voltages by $\frac{0{\cdot}428}{R_0(i_0 - i_c)}$, and the times by $\sqrt{\left(\frac{\varepsilon}{2}\right)}\frac{R_0(i_0 - i_c)}{\Phi_m}$ (0·428 being the peak value of the function $x\varepsilon^{-x^2}$). If the theory is correct, all the normalized curves should fit the function $x\varepsilon^{-x^2}$. Owing to the finite rise-time of the current, with the resulting error at the beginning of the output waveforms, it was necessary to take as the origin of the time axis the instant when the voltage reached its maximum value. The results are plotted in Fig. 7, together with the function $x\varepsilon^{-x^2}$. It will be seen that the discrepancy is greater for the initial voltages, and especially at the larger input currents, which is almost certainly due to the current rise-time. The scatter of the curves amongst themselves is within the limits of the experimental error.

It will be seen from Fig. 7 that the observed voltage waveforms fit the theory reasonably well, allowing for the limitations mentioned above. There appears to be a tendency for the observed values to be less than those predicted in the region $x = 1$. This may be due to overshoot on the part of the amplifier, but it may be a genuine effect. When the input current approaches the coercive value, the agreement is not so good. This is probably due to higher-order effects not taken account of in the theory, which one would expect to be more noticeable when the current is only slightly greater than the coercive value.

(4.3.3) **Currents other than Step Functions.**

That the theory still holds when the current applied to the core is not a step function can best be shown by loading the core with some impedance, the actual current applied then being the difference between the step function and the current drawn by this impedance. Fig. 8 shows the form of the output voltage, measured as in the previous case, with a 46-ohm resistor across one of the 10-turn windings. The current step was 164 mA in 10 turns. The theoretical waveform for this case, which was

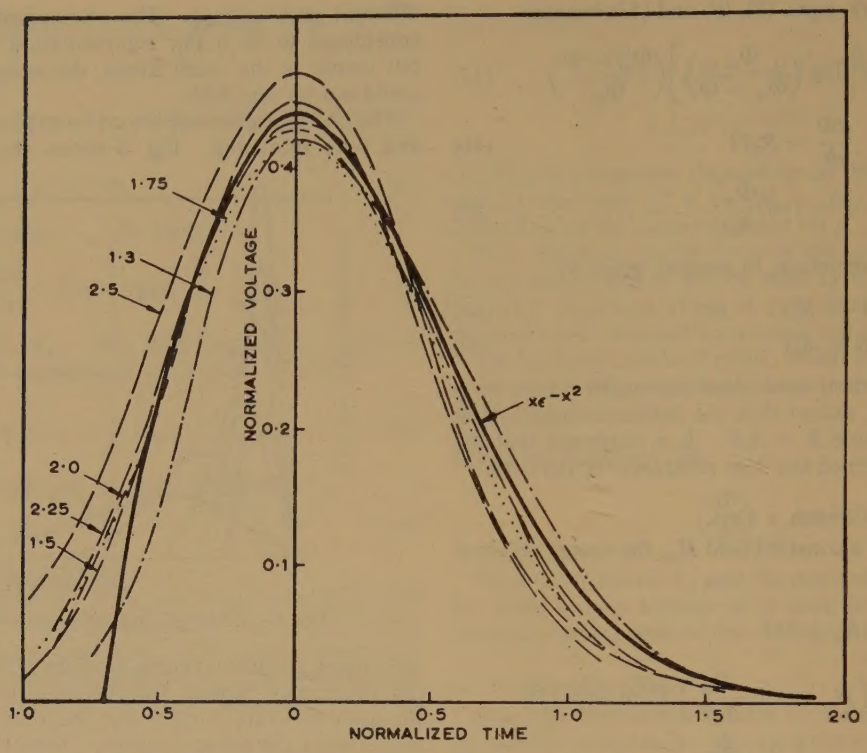

Fig. 7.—Comparison of observed and theoretical waveforms.

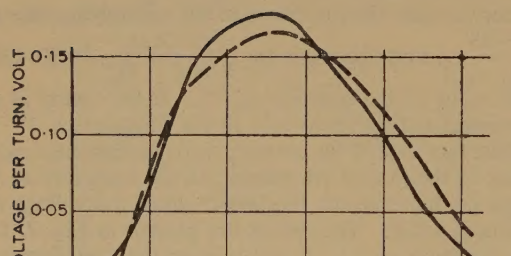

Fig. 8.—Output waveform with resistive load.

——— Observed waveform.
- - - - Calculated waveform.

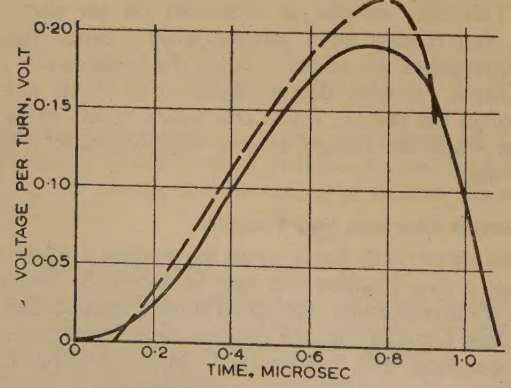

Fig. 9.—Output waveform with capacitive load.

——— Observed waveform.
- - - - Calculated waveform.

obtained by solving eqn. (15) numerically, using the Edsac, is also shown in Fig. 8. It will be seen that the agreement is reasonable.

Fig. 9 shows the results of a similar experiment using a $0{\cdot}009\,\mu$F condenser across 10 turns.

(4.3.4) **The Effect of not Switching a Core fully.**

The above theory has assumed that, before switching, the core has previously been saturated in the reverse direction. If it has only been partially switched in that direction, it is found that R_0 is reduced when the core is subsequently switched forwards. The extent of this reduction cannot be predicted from the theory, but it has been examined experimentally.

A 3 mm core was partially set by a current pulse of variable amplitude, and the flux change which occurred was measured

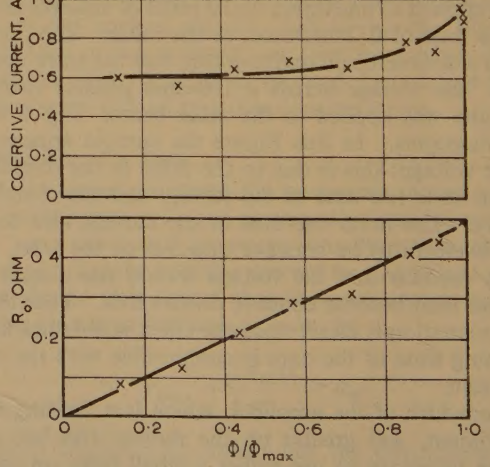

Fig. 10.—Variation of coercive current and loss resistance with flux change (3 mm core).

with a Miller integrator. It was reset with current steps of various known amplitudes, and the peak output voltage was measured at this time with a diode and condenser circuit followed by a slide-back voltmeter. (This method of measurement removes the uncertainty due to the poor frequency response of the amplifier when an oscillograph is used to measure peak voltages.) For each value of the flux change, the output voltage was plotted against the switching current to obtain values for R_0 and the coercive current, i_c. The values obtained are shown plotted against Φ/Φ_{max} in Fig. 10, from which it will be seen that R_0 is directly proportional to the flux change. However, i_c does not follow any such simple law, but it does exhibit a marked increase as saturation is approached. The scatter of the points in the i_c plot is rather great, since i_c is measured as the intercept on the current axis when the output voltage is plotted against current, a method which does not lead to great accuracy.

(5) CONCLUSIONS

A quantitative theory has been presented which explains the observed output waveforms from cores switched at high speeds. In view of the simplifying assumptions made, it is not exact, but it is quite adequate to assist in the design of switching circuits, and the qualitative concepts contained in it will be of use to the engineer in understanding the waveforms that he sees.

It is now apparent that the behaviour of these materials can be adequately described for most purposes by four parameters, namely:

μ_r = Residual permeability.
B_m = Maximum flux density. (If μ_r is significantly different from unity, B_m should be the remanent rather than the saturation value.)
H_c = Pseudo-coercive force as defined in Section 3.1.
X_0 = Loss parameter.

The engineer designing circuits needs to know the values of these four quantities for the material that he is using, and the extent to which they are likely to vary between different samples. This information, other than the mean values of the remanence and the ordinary coercive force, is not at present obtainable from manufacturers' literature. This situation is to be regretted, and it is hoped that it will be remedied in the future.

(6) ACKNOWLEDGMENTS

I am grateful to the Director of the University Mathematical Laboratory, Cambridge, for providing the facilities for this research, and to Ferranti Ltd. for a maintenance grant.

(7) REFERENCES

(1) KARNAUGH, M.: 'Pulse-Switching Circuits using Magnetic Cores', *Proceedings of the Institute of Radio Engineers*, 1955, **43**, p. 570.
(2) SANDS, E. A.: 'The Behaviour of Rectangular Hysteresis-Loop Magnetic Materials under Current Pulse Conditions', *ibid.*, 1952, **40**, p. 1246.
(3) MENYUK, N., and GOODENOUGH, J. B.: 'Magnetic Materials for Digital Computer Components—I. A Theory of Flux Reversal in Polycrystal Ferromagnetics', *Journal of Applied Physics*, 1955, **26**, p. 8.
(4) MENYUK, N.: 'Magnetic Materials for Digital Computer Components—II. Magnetic Characteristics of Ultra Thin Molybdenum-Permalloy Cores', *ibid.*, 1955, **26**, p. 692.

(8) APPENDICES

(8.1) *To express* F(r) *as a function of B.*

Now
$$\frac{dA}{dr} = \frac{dt}{dr}\frac{dA}{dt}$$
$$= \frac{1}{v}\frac{dA}{dt}$$
$$= 2\pi r\varepsilon^{-\pi r^2\rho} \text{ from eqn. (5)}$$

Therefore
$$A = 2\pi\int_0^r r\varepsilon^{-\pi r^2\rho}dr$$
$$= \frac{1}{\rho}\left[1 - \varepsilon^{-\pi r^2\rho}\right]_0^r$$

Since, when switching is complete, $A = A_{max} = 1/\rho$,

$$\frac{A}{A_{max}} = \frac{B}{B_m} = 1 - \varepsilon^{-\pi r^2\rho}$$

where B_m is the saturation flux density.

Therefore
$$\varepsilon^{-\pi r^2\rho} = \frac{B_m - B}{B_m}$$

whence
$$\pi r^2\rho = \log_\varepsilon\left(\frac{B_m}{B_m - B}\right)$$

so that
$$r = \frac{1}{\sqrt{(\pi\rho)}}\sqrt{\left[\log_\varepsilon\left(\frac{B_m}{B_m - B}\right)\right]}$$

and the required function is

$$\mathrm{F}(B) = \mathrm{F}(r)$$
$$= Kr\varepsilon^{-\pi r^2\rho} \text{ from eqn. (7)}$$
$$= \frac{K}{\sqrt{(\pi\rho)}}\sqrt{\left[\log_\varepsilon\left(\frac{B_m}{B_m - B}\right)\right]}\left(\frac{B_m - B}{B_m}\right)$$

K is an arbitrary constant. It is convenient to choose K so that the maximum value of F is unity.

Let
$$\frac{B_m}{B_m - B} = y$$

Then
$$F = \frac{K}{\sqrt{(\pi\rho)}}\sqrt{\log_\varepsilon y}\left(\frac{1}{y}\right)$$

and
$$\frac{d\mathrm{F}}{dy} = \frac{K}{\sqrt{(\pi\rho)}}\frac{1 - 2\log_\varepsilon y}{2y^2\sqrt{(\log_\varepsilon y)}}$$

For maximum F, $\log_\varepsilon y = \frac{1}{2}$, i.e. $y = \sqrt{\varepsilon}$.

Therefore
$$\mathrm{F}_{max} = \frac{K}{\sqrt{(\pi\rho)}}\frac{1}{\sqrt{(2\varepsilon)}}$$
$$= 1 \text{ by hypothesis}$$

so that
$$\frac{K}{\sqrt{(\pi\rho)}} = \sqrt{(2\varepsilon)}$$

and
$$\mathrm{F}(B) = \sqrt{(2\varepsilon)}\sqrt{\left[\log_\varepsilon\left(\frac{B_m}{B_m - B}\right)\right]}\left(\frac{B_m - B}{B_m}\right) \quad . \quad (8)$$

(8.2) *To find* B/B_m *when the output voltage has dropped to one-tenth of its peak value, the input current being constant.*

At this time, $\mathrm{F} = \frac{1}{10}$

From eqn. (8), putting $\frac{B_m}{B_m - B} = y$

$$\frac{1}{10} = \frac{\sqrt{(2\varepsilon \log_\varepsilon y)}}{y}$$

whence $$\frac{1}{200\varepsilon} = \frac{\log_\varepsilon y}{y^2}$$

which gives $$y = 45{\cdot}5$$

and $$B/B_m = 0{\cdot}978 \quad . \quad . \quad . \quad . \quad . \quad . \quad (12)$$

(8.3) *To find the switching time in the constant-current case.*

Eqn. (10) states that $\frac{dB}{dt} = k_1 H^2 t \varepsilon^{-k_2 H^2 t^2}$

Therefore $$\frac{d^2B}{dt^2} = (k_1 H^2 - 2k_1 k_2 H^4 t^2)\varepsilon^{-k_2 H^2 t^2}$$

For maximum $\frac{dB}{dt}$, $1 = 2k_2 H^2 t^2$

which gives $$t = \frac{1}{H\sqrt{(2k_2)}}$$

Therefore $$\left(\frac{dB}{dt}\right)_{max} = \frac{k_1}{\sqrt{(2k_2)}} \frac{H}{\sqrt{\varepsilon}} \quad . \quad . \quad . \quad . \quad (21)$$

But, from eqn. (11), $\left(\frac{dB}{dt}\right)_{max} = X_0 H$

Therefore $$\frac{k_1}{\sqrt{(2k_2)}} \frac{1}{\sqrt{\varepsilon}} = X_0 \quad . \quad . \quad . \quad . \quad . \quad (22)$$

Integrating eqn. (10), we obtain

$$B_m = k_1 H^2 \int_0^\infty t\varepsilon^{-k_2 H^2 t^2} dt$$

$$= \frac{k_1}{2k_2} \quad . \quad . \quad . \quad . \quad . \quad . \quad . \quad . \quad (23)$$

From eqns. (22) and (23),

$$\frac{B_m}{X_0} = \sqrt{\frac{\varepsilon}{2k_2}} \quad . \quad . \quad . \quad . \quad . \quad (24)$$

Switching is defined to be complete when the output voltage has dropped to one-tenth of its peak value, at which time, from eqns. (10) and (21),

$$\frac{1}{10} \frac{k_1}{\sqrt{(2k_2)}} \frac{H}{\sqrt{\varepsilon}} = k_1 H^2 t \varepsilon^{-k_2 H^2 t^2}$$

Therefore $$\frac{1}{10\sqrt{(2\varepsilon)}} = \sqrt{(k_2)} H t \varepsilon^{-k_2 H^2 t^2}$$

$$= x\varepsilon^{-x^2}$$

where $x = \sqrt{(k_2)}Ht$, so that $x = 1{\cdot}95$, and the switching time is given by

$$t = \mathrm{T} = \frac{1{\cdot}95}{\sqrt{(k_2)}H}$$

$$= 1{\cdot}95\sqrt{\left(\frac{2}{\varepsilon}\right)} \frac{B_m}{X_0 H} \text{ from eqn. (24)}$$

$$= 1{\cdot}67 \frac{B_m}{X_0 H} \quad . \quad . \quad . \quad . \quad . \quad . \quad . \quad . \quad (13)$$

(8.4) *To calculate the output voltage of a core.*

It follows from Ampère's theorem that $2\pi r H_m = 4\pi i_0$.

Therefore $H_m = 2i_0/r$, and likewise $H_c = 2i_c/r$ and $H = 2i/r$.

Let the flux in the core be Φ ($\Phi = 0$ for one state of saturation).

Then $$\Phi = AB$$

Eqn. (11) then becomes $\frac{1}{A}\left(\frac{d\Phi}{dt}\right)_{max} = X_0 \frac{2i}{r}$

so that the peak output voltage per turn is

$$V_{max} = \left(\frac{d\Phi}{dt}\right)_{max}$$

$$= \frac{2X_0 Ai}{r}$$

$$= R_0 i \quad . \quad . \quad . \quad . \quad . \quad . \quad (14)$$

where $R_0 = 2X_0 A/r$.

Note that if X_0 is expressed in rationalized units, $V_{max} = R_0 i$ where $R_0 = X_0 A/2\pi r$.

Note*

Since writing the monograph, I have come across a paper by Haynes,† in which he performs a similar calculation assuming ellipsoidal domains rather than cylindrical ones. He thus arrives at an output waveform for the constant-current case which is of the form $x^2\varepsilon^{-x^3}$, as opposed to $x\varepsilon^{-x^2}$. The cylindrical approximation is more likely to be correct if the ellipsoids are so eccentric that their major axes are large compared with the dimensions of the grains of the material whilst their minor axes are still small. The ellipsoids are then truncated by the grain boundaries and therefore approximate to cylinders.

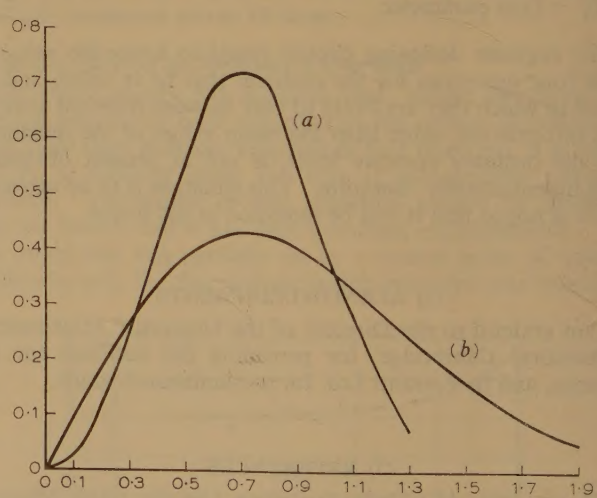

Fig. 11

(*a*) $2{\cdot}83x^2\varepsilon^{-1{\cdot}89x^3}$
(*b*) $x\varepsilon^{-x^2}$

Fig. 11 shows the two curves, normalized to have the same area and the same peaking time, and I think it will be agreed that the curve for $x\varepsilon^{-x^2}$ appears more like the shape of the observed output waveforms, as shown in Fig. 7. One therefore deduces that the ellipsoidal domains must be highly eccentric indeed.

* The note was received 24th July, 1959.

† HAYNES, M. K.: 'Model for Nonlinear Flux Reversals of Square-Loop Polycrystalline Magnetic Cores', *Journal of Applied Physics*, 1958, 29, p. 472.

21.372.6 : 621–52

The Institution of Electrical Engineers
Monograph No. 328 M
Feb. 1959

THE STABILITY CRITERIA FOR LINEAR SYSTEMS

By O. P. D. CUTTERIDGE, M.Sc.(Eng.), Ph.D., Associate Member.

(*The paper was first received* 18*th September, and in revised form* 22*nd November*, 1958. *It was published as an* INSTITUTION MONOGRAPH *in February*, 1959.)

SUMMARY

It is shown that the various stability criteria for linear systems can be conveniently obtained, and interrelated, by means of continued fractions. A new canonical form for a Hurwitz polynomial as a product of continued fractions is also given, together with an alternative set of determinantal criteria with determinants of about half the order of the Hurwitz determinants.

(1) INTRODUCTION

As is well known, the question of the stability or instability of a lumped linear system reduces to a consideration of the position of the zeros of a polynomial in p, the complex frequency, on the complex p-plane. If all the zeros lie in the left half p-plane, the system is stable, otherwise it is unstable. The various stability criteria express the restrictions on the coefficients of the various powers of p in the polynomial, corresponding to the restriction of its zeros to the left half-plane. Routh[1, 2] was the first to derive such a set of stability criteria. Later Hurwitz[3] independently obtained the result in another form.* Alternative derivations of the Hurwitz determinantal criteria have been given, for example, by Orlando[4] and Schur.[5]

(2) THE FUNDAMENTAL PROPERTY OF HURWITZ POLYNOMIALS

The fundamental property of Hurwitz polynomials, namely that the zeros of the odd and even parts are simple, purely imaginary and separate one another, was first shown by Routh,[1, 2] by using a theorem of Cauchy. It can, however, be demonstrated more simply as follows:

Let $$f(p) = a_0 + a_1p + a_2p^2 + \ldots + a_np^n \quad . \quad . \quad . \quad (1)$$

where $a_0, a_1, \ldots a_n$ are real, and consider the phase of $f(p)$ when $p = j\omega$ and ω is real. If all the zeros of $f(p)$ are in the left half-plane, the increase in phase of $f(p)$, as ω increases from $-\infty$ to $+\infty$, is $n\pi$. If i zeros of $f(p)$ lie in the right half-plane, the corresponding phase-increase in $f(p)$ is $(n - 2i)\pi$, since, as ω increases from $-\infty$ to $+\infty$, a phase increase of π is contributed by each left-half-plane zero and a phase decrease of π by each right-half-plane zero. Thus a polynomial whose zeros are confined to the left half-plane might be styled a 'maximum-phase polynomial', since such phase increases would then be a maximum for polynomials of given degree.

Now $$\tan [\text{phase } f(j\omega)] = \frac{a_1\omega - a_3\omega^3 + a_5\omega^5 - \ldots}{a_0 - a_2\omega^2 + a_4\omega^4 - \ldots} \quad . \quad (2)$$

and, bearing in mind the properties of the tangent function, it is evident that a phase increase in $f(j\omega)$, of either $n\pi$ or $-n\pi$ for an increase in ω of from $-\infty$ to $+\infty$, implies that the zeros of both numerator and denominator in eqn. (2) are real, simple and separate one another, and conversely. The phase increase in $f(j\omega)$ will be $n\pi$ or $-n\pi$ according as a_1 and a_0 (or a_{n-1} and a_n) have the same or opposite signs.

Thus the necessary and sufficient conditions for a polynomial with real coefficients to have its zeros confined to either the left or right half-planes are:

(*a*) The odd part of the polynomial should have a simple zero at the origin, and simple zeros distributed in conjugate-complex pairs on the imaginary axis.

(*b*) The even part of the polynomial should have simple zeros distributed in conjugate-complex pairs on the imaginary axis, interlacing with the zeros of the odd part.

If, in addition, a_1 and a_0 (or a_{n-1} and a_n) have the same sign, the polynomial is Hurwitz, otherwise anti-Hurwitz.*

(3) THE CONTINUED-FRACTION TEST FOR STABILITY AND SOME APPLICATIONS

(3.1) The Continued-Fraction Test

It has been shown by Guillemin[6] (and from a rather more general point of view by Wall[7]) that continued fractions can provide a neat test for the Hurwitz character of a polynomial.

Thus if

$$\phi(p) = \frac{a_np^n + a_{n-2}p^{n-2} + \ldots}{a_{n-1}p^{n-1} + a_{n-3}p^{n-3} + \ldots} \quad . \quad . \quad . \quad (3)$$

$$= \alpha_1 p + \cfrac{1}{\beta_1 p + \cfrac{1}{\alpha_2 p + \cfrac{1}{\beta_2 p + \ldots}}} \quad . \quad (4)$$

the original polynomial, $f(p)$, will have its zeros confined to the left half-plane if all the α's and β's are positive; if any are negative then one or more zeros lie in the right half-plane. When n is even, $\phi(p)$ is the ratio of even to odd parts of $f(p)$ and inversely when n is odd. In general, when n is even, there are $n/2$ α's and $n/2$ β's, and when n is odd, $(n + 1)/2$ α's and $(n - 1)/2$ β's. Premature termination of the continued fraction in eqn. (4) is, by Euclid's algorithm, indicative of a common factor between the even and odd parts of $f(p)$ and is inconsistent with $f(p)$ being Hurwitz.

(3.2) Connection with the Hurwitz Criteria

The following expressions, giving the α's and β's of eqn. (4) in terms of the a's of eqn. (3), can easily be obtained and have been given in References 8, 9, and 10:

$$\left.\begin{aligned}
\alpha_1 &= \frac{a_n}{a_{n-1}} \\
\beta_1 &= \frac{a_{n-1}}{\Delta_2/a_{n-1}} = \frac{\Delta_1^2}{\Delta_2} \\
\alpha_2 &= \frac{\Delta_2/a_{n-1}}{\Delta_3/\Delta_2} = \frac{\Delta_2^2}{\Delta_1\Delta_3} \\
\beta_2 &= \frac{\Delta_3/\Delta_2}{\Delta_4/\Delta_3} = \frac{\Delta_3^2}{\Delta_2\Delta_4} \\
&\ldots\ldots \\
\alpha_i &= \frac{\Delta_{2i-2}/\Delta_{2i-3}}{\Delta_{2i-1}/\Delta_{2i-2}} = \frac{\Delta_{2i-2}^2}{\Delta_{2i-3}\Delta_{2i-1}} \\
\beta_i &= \frac{\Delta_{2i-1}/\Delta_{2i-2}}{\Delta_{2i}/\Delta_{2i-1}} = \frac{\Delta_{2i-1}^2}{\Delta_{2i-2}\Delta_{2i}}
\end{aligned}\right\} \quad . \quad . \quad . \quad (5)$$

* For this reason, a polynomial where zeros are confined to the left half-plane is often referred to as a Hurwitz polynomial.

* An anti-Hurwitz polynomial is one whose zeros are confined to the right half-plane.

Correspondence on Monographs is invited for consideration with a view to publication.

Dr. Cutteridge is at the Manchester College of Science and Technology.

where $\Delta_1 = a_{n-1}$, $\Delta_2 = \begin{vmatrix} a_{n-1} & a_{n-3} \\ a_n & a_{n-2} \end{vmatrix}$

$$\Delta_3 = \begin{vmatrix} a_{n-1} & a_{n-3} & a_{n-5} \\ a_n & a_{n-2} & a_{n-4} \\ 0 & a_{n-1} & a_{n-3} \end{vmatrix}$$

$$\Delta_i = \begin{vmatrix} a_{n-1} & a_{n-3} & a_{n-5} & a_{n-7} & \cdots \\ a_n & a_{n-2} & a_{n-4} & a_{n-6} & \cdots \\ 0 & a_{n-1} & a_{n-3} & a_{n-5} & \cdots \\ 0 & a_n & a_{n-2} & a_{n-4} & \cdots \\ 0 & 0 & a_{n-1} & a_{n-3} & \cdots \\ 0 & 0 & a_n & a_{n-2} & \cdots \\ 0 & 0 & 0 & a_{n-1} & \cdots \\ & \cdots & \cdots & \cdots & \end{vmatrix} \quad \left.\begin{array}{l} \\ \\ \\ \\ \\ \\ \\ \end{array}\right\} \quad \ldots \quad (6)$$

Δ_i is an ith-order determinant. The determinants Δ will be recognized as the Hurwitz determinants.*

From eqns. (5), it is evident that, for the α's and β's to be positive,

$$\left.\begin{array}{l} a_n, \Delta_1, \Delta_3, \Delta_5, \ldots \text{ must all have the same sign} \\ \text{and} \quad \Delta_2, \Delta_4, \Delta_6, \ldots \text{ must all be positive} \end{array}\right\} \quad \ldots \quad (7)$$

If $f(p)$ is normalized so that $a_n > 0$, this reduces to the usual form for the Hurwitz criteria,

$$\Delta_i > 0, \; i = 1, 2, 3, \ldots n \quad \ldots \quad (8)$$

(3.3) Connection with the Routh Criteria

It can be seen from eqns. (5) that the condition for positive α's and β's is equivalent to the $(n+1)$ terms in the following sequence:

$$a_n, a_{n-1}, \Delta_2/a_{n-1}, \Delta_3/\Delta_2, \Delta_4/\Delta_3, \ldots \Delta_n/\Delta_{n-1} \quad \ldots \quad (9)$$

all having the same sign.

Since $$\Delta_n/\Delta_{n-1} = a_0 \quad \ldots \quad (10)$$

sequence (9) can be rewritten

$$a_n, a_{n-1}, \Delta_2/a_{n-1}, \Delta_3/\Delta_2, \ldots \Delta_{n-1}/\Delta_{n-2}, a_0 \quad \ldots \quad (11)$$

This is the second form of the rule given by Routh (see Reference 2, Article 301), in which he gave a simple method of calculating any quotient, in the above sequence, from the preceding. The first form of Routh's rule (see Reference 2, Article 297) is, in effect, a method of drawing up the triangular array of coefficients of the various powers of p in the successive divisors used to obtain the continued fraction in eqn. (4).

(3.4) A Canonical Form for a Hurwitz Polynomial

For concreteness, take the case of a polynomial of the 4th degree, and consider the expression

$$F(p) = \left(1 + c_1 p + \cfrac{1}{c_2 p + \cfrac{1}{c_3 p + \cfrac{1}{c_4 p}}}\right) \left(c_2 p + \cfrac{1}{c_3 p + \cfrac{1}{c_4 p}}\right)\left(c_3 p + \frac{1}{c_4 p}\right)(c_4 p) \quad \ldots \quad (12)$$

$F(p)$ is a quartic polynomial with constant term equal to unity.

Writing $$F(p) = F_1(p) + F_2(p) \quad \ldots \quad (13)$$

* Except that Hurwitz wrote his original polynomial $a_0 x^n + a_1 x^{n-1} + \ldots + a_n$.

where $F_1(p)$ is the even part of $F(p)$ and $F_2(p)$ its odd part, we have

$$F_1(p) = \left(c_1 p + \cfrac{1}{c_2 p + \cfrac{1}{c_3 p + \cfrac{1}{c_4 p}}}\right) \left(c_2 p + \cfrac{1}{c_3 p + \cfrac{1}{c_4 p}}\right)\left(c_3 p + \frac{1}{c_4 p}\right)(c_4 p) \quad \ldots \quad (14)$$

and $$F_2(p) = \left(c_2 p + \cfrac{1}{c_3 p + \cfrac{1}{c_4 p}}\right)\left(c_3 p + \frac{1}{c_4 p}\right)(c_4 p) \quad \ldots \quad (15)$$

Thus the ratio of even to odd parts of $F(p)$ is

$$c_1 p + \cfrac{1}{c_2 p + \cfrac{1}{c_3 p + \cfrac{1}{c_4 p}}} \quad \ldots \quad (16)$$

Hence, by the continued-fraction test, $F(p)$ will be a Hurwitz polynomial provided that $c_1, c_2, c_3, c_4 > 0$.

Similarly, the expression

$$c_0 \left[1 + c_1 p + \cfrac{1}{c_2 p + \cfrac{1}{c_3 p + \cfrac{\vdots}{\cdots + \cfrac{1}{c_n p}}}}\right] \left[c_2 p + \cfrac{1}{c_3 p + \cfrac{\vdots}{\cdots + \cfrac{1}{c_n p}}}\right] \left[c_3 p + \cfrac{1}{c_4 p + \cfrac{\vdots}{\cdots + \cfrac{1}{c_n p}}}\right] \cdots \left(c_{n-1} p + \frac{1}{c_n p}\right)(c_n p) \quad \ldots \quad (17)$$

is a Hurwitz polynomial of the nth degree, provided that

$$c_i > 0, \; i = 1, 2, 3, \ldots n \quad \ldots \quad (18)$$

c_0, a normalizing constant equal to the constant term, can have any value.

The canonical form of a Hurwitz polynomial, given by Bückner,[11, 12] can be easily obtained from the form given here. For example, for a quartic polynomial with constant term equal to unity, we have, from eqn. (12),

$$F(p) = \begin{vmatrix} 1 + c_1 p + \cfrac{1}{c_2 p + \cfrac{1}{c_3 p + \cfrac{1}{c_4 p}}} & -1 & 0 & 0 \\ 0 & c_2 p + \cfrac{1}{c_3 p + \cfrac{1}{c_4 p}} & -1 & 0 \\ 0 & 0 & c_3 p + \frac{1}{c_4 p} & -1 \\ 0 & 0 & 0 & c_4 p \end{vmatrix} \quad \ldots \quad (19)$$

with $c_1, c_2, c_3, c_4 > 0$

Taking 1st column + $\left(\dfrac{1}{c_2p + \dfrac{1}{c_3p + \dfrac{1}{c_4p}}}\right)$ × 2nd column,

2nd column + $\left(\dfrac{1}{c_3p + \dfrac{1}{c_4p}}\right)$ × 3rd column and finally

3rd column + $\left(\dfrac{1}{c_4p}\right)$ × 4th column, the determinant in eqn. (19)

is transformed into

$$\begin{vmatrix} 1+c_1p & -1 & 0 & 0 \\ 1 & c_2p & -1 & 0 \\ 0 & 1 & c_3p & -1 \\ 0 & 0 & 1 & c_4p \end{vmatrix} \quad \ldots \quad (20)$$

which is Bückner's form.

Alternatively, Bückner's form can be obtained directly from the continued-fraction test in two stages. First, write the continued fraction as the ratio of two continuants,* one of which will be the odd part and the other the even part of a polynomial. Secondly, write the sum of these two continuants as a single determinant, which is Bückner's form. Thus, for the fourth order case,

$$c_1p + \cfrac{1}{c_2p + \cfrac{1}{c_3p + \cfrac{1}{c_4p}}} = \frac{\begin{vmatrix} c_1p & -1 & 0 & 0 \\ 1 & c_2p & -1 & 0 \\ 0 & 1 & c_3p & -1 \\ 0 & 0 & 1 & c_4p \end{vmatrix}}{\begin{vmatrix} c_2p & -1 & 0 \\ 1 & c_3p & -1 \\ 0 & 1 & c_4p \end{vmatrix}} \quad \ldots \quad (21)$$

and

$$\begin{vmatrix} c_1p & -1 & 0 & 0 \\ 1 & c_2p & -1 & 0 \\ 0 & 1 & c_3p & -1 \\ 0 & 0 & 1 & c_4p \end{vmatrix} + \begin{vmatrix} c_2p & -1 & 0 \\ 1 & c_3p & -1 \\ 0 & 1 & c_4p \end{vmatrix} = \begin{vmatrix} 1+c_1p & -1 & 0 & 0 \\ 1 & c_2p & -1 & 0 \\ 0 & 1 & c_3p & -1 \\ 0 & 0 & 1 & c_4p \end{vmatrix} \quad (22)$$

(3.5) An Alternative Set of Determinantal Criteria obtained from the Continued-Fraction Expansion

The following expressions for the α's and β's of eqn. (4) can be obtained from first principles or by condensing the Hurwitz determinants, as shown in Appendix 7.1.

$$\left.\begin{aligned} \alpha_1 &= \frac{a_n}{a_{n-1}} & \beta_1 &= \frac{D_1^2}{D_2} \\ \alpha_2 &= \frac{D_2^2}{D_1D_3} & \beta_2 &= \frac{D_3^2}{D_2D_4} \\ &\ldots\ldots & & \\ \alpha_i &= \frac{D_{2i-2}^2}{D_{2i-3}D_{2i-1}} & \beta_i &= \frac{D_{2i-1}^2}{D_{2i-2}D_{2i}} \end{aligned}\right\} \quad \ldots \quad (23)$$

where $D_1 = a_{n-1}$ $\quad D_2 = \begin{vmatrix} a_{n-1} & a_{n-3} \\ a_n & a_{n-2} \end{vmatrix}$

$$\left.\begin{aligned} D_3 &= \begin{vmatrix} a_{n-1} & a_{n-3} \\ a_na_{n-3} & a_na_{n-5} + \begin{vmatrix} a_{n-2} & a_{n-4} \\ a_{n-1} & a_{n-3} \end{vmatrix} \end{vmatrix} \\ D_4 &= \begin{vmatrix} \begin{vmatrix} a_{n-1} & a_{n-3} \\ a_n & a_{n-2} \end{vmatrix} & \begin{vmatrix} a_{n-1} & a_{n-5} \\ a_n & a_{n-4} \end{vmatrix} \\ \begin{vmatrix} a_{n-1} & a_{n-5} \\ a_n & a_{n-4} \end{vmatrix} & \begin{vmatrix} a_{n-1} & a_{n-7} \\ a_n & a_{n-6} \end{vmatrix} + \begin{vmatrix} a_{n-3} & a_{n-5} \\ a_{n-2} & a_{n-4} \end{vmatrix} \end{vmatrix} \\ D_5 &= \begin{vmatrix} a_{n-1} & a_{n-3} & a_{n-5} \\ a_na_{n-3} & a_na_{n-5} + \begin{vmatrix} a_{n-2} & a_{n-4} \\ a_{n-1} & a_{n-3} \end{vmatrix} & a_na_{n-7} + \begin{vmatrix} a_{n-2} & a_{n-6} \\ a_{n-1} & a_{n-5} \end{vmatrix} \\ a_na_{n-5} & a_na_{n-7} + \begin{vmatrix} a_{n-2} & a_{n-6} \\ a_{n-1} & a_{n-5} \end{vmatrix} & a_na_{n-9} + \begin{vmatrix} a_{n-2} & a_{n-8} \\ a_{n-1} & a_{n-7} \end{vmatrix} + \begin{vmatrix} a_{n-4} & a_{n-6} \\ a_{n-3} & a_{n-5} \end{vmatrix} \end{vmatrix} \\ D_6 &= \begin{vmatrix} \begin{vmatrix} a_{n-1} & a_{n-3} \\ a_n & a_{n-2} \end{vmatrix} & \begin{vmatrix} a_{n-1} & a_{n-5} \\ a_n & a_{n-4} \end{vmatrix} & \begin{vmatrix} a_{n-1} & a_{n-7} \\ a_n & a_{n-6} \end{vmatrix} \\ \begin{vmatrix} a_{n-1} & a_{n-5} \\ a_n & a_{n-4} \end{vmatrix} & \begin{vmatrix} a_{n-1} & a_{n-7} \\ a_n & a_{n-6} \end{vmatrix} + \begin{vmatrix} a_{n-3} & a_{n-5} \\ a_{n-2} & a_{n-4} \end{vmatrix} & \begin{vmatrix} a_{n-1} & a_{n-9} \\ a_n & a_{n-8} \end{vmatrix} + \begin{vmatrix} a_{n-3} & a_{n-7} \\ a_{n-2} & a_{n-6} \end{vmatrix} \\ \begin{vmatrix} a_{n-1} & a_{n-7} \\ a_n & a_{n-6} \end{vmatrix} & \begin{vmatrix} a_{n-1} & a_{n-9} \\ a_n & a_{n-8} \end{vmatrix} + \begin{vmatrix} a_{n-3} & a_{n-7} \\ a_{n-2} & a_{n-6} \end{vmatrix} & \begin{vmatrix} a_{n-1} & a_{n-11} \\ a_n & a_{n-10} \end{vmatrix} + \begin{vmatrix} a_{n-3} & a_{n-9} \\ a_{n-2} & a_{n-8} \end{vmatrix} + \begin{vmatrix} a_{n-5} & a_{n-7} \\ a_{n-4} & a_{n-6} \end{vmatrix} \end{vmatrix} \end{aligned}\right\} \quad \ldots \quad (24)$$

etc.

* See, for example, Reference 13.

As with the Hurwitz determinants, the criterion for stability, with $a_n > 0$, is

$$D_i > 0, i = 1, 2, 3, \ldots n \quad . \quad . \quad . \quad . \quad (25)$$

For example, for $n = 5$, with $a_5 > 0$, the above stability criteria reduce to

$$\left.\begin{array}{l} a_4 > 0, \quad \begin{vmatrix} a_4 & a_2 \\ a_5 & a_3 \end{vmatrix} > 0 \quad \begin{vmatrix} a_4 & a_2 \\ a_5 a_2 & a_5 a_0 + \begin{vmatrix} a_3 & a_1 \\ a_4 & a_2 \end{vmatrix} \end{vmatrix} > 0 \\ \qquad \begin{vmatrix} \begin{vmatrix} a_4 & a_2 \\ a_5 & a_3 \end{vmatrix} & \begin{vmatrix} a_4 & a_0 \\ a_5 & a_1 \end{vmatrix} \\ \begin{vmatrix} a_4 & a_0 \\ a_5 & a_1 \end{vmatrix} & \begin{vmatrix} a_2 & a_0 \\ a_3 & a_1 \end{vmatrix} \end{vmatrix} > 0 \\ \begin{vmatrix} a_4 & a_2 & a_0 \\ a_5 a_2 & a_5 a_0 + \begin{vmatrix} a_3 & a_1 \\ a_4 & a_2 \end{vmatrix} & a_3 a_0 \\ a_5 a_0 & a_3 a_0 & a_1 a_0 \end{vmatrix} > 0 \end{array}\right\} \quad . \quad . \quad . \quad (26)$$

As before, the last determinant may be replaced by

$$a_0 > 0 \quad . \quad . \quad . \quad . \quad . \quad . \quad . \quad . \quad (27)$$

(4) SIMPLIFICATION OF THE SETS OF STABILITY CRITERIA

Fuller[14] has recently shown that about half the Hurwitz criteria can be replaced by much simpler conditions involving the sign of every other coefficient in the given polynomial. This result is obtained here using a theorem in continued fractions and is also applicable to the alternative set of determinantal criteria derived in Section 3.5.

Consider first the case of n even. Let P be a polynomial in x of degree $m - 1$, and Q a polynomial in x of degree m, and suppose that the coefficients of the highest powers of x in P and Q have the same sign. Then

$$\frac{P}{Q} = \cfrac{1}{\gamma_1 x + \cfrac{1}{\delta_1 + \cfrac{1}{\gamma_2 x + \cfrac{1}{\delta_2 + \cfrac{\quad\vdots\quad}{\cfrac{1}{\gamma_m x + \cfrac{1}{\delta_m}}}}}}} \quad . \quad . \quad . \quad . \quad . \quad (28)$$

and it is shown in Appendix 7.2, Theorem 1, that the necessary and sufficient conditions for P and Q to have only simple real zeros, with the zeros of P interlacing those of Q, are that

$$\gamma_i > 0, i = 1, 2, 3, \ldots m \quad . \quad . \quad . \quad . \quad (29)$$

If all the zeros of Q are negative then $\delta_i > 0$; every negative δ indicates a positive zero of Q. (This is proved in Appendix 7.2, Theorem 3.) Evidently, if $\gamma_i > 0$, the condition $\delta_i > 0$ can be replaced by the simpler condition that all the coefficients in the polynomial Q must have the same sign.

Writing p^2 for x in eqn. (28), we have

$$\frac{P(p^2)}{Q(p^2)} = \cfrac{1}{\gamma_1 p^2 + \cfrac{1}{\delta_1 + \cfrac{1}{\gamma_2 p^2 + \cfrac{1}{\delta_2 + \cfrac{\quad\vdots\quad}{\cfrac{1}{\gamma_m p^2 + \cfrac{1}{\delta_m}}}}}}} \quad . \quad . \quad . \quad . \quad (30$$

or

$$\frac{Q(p^2)}{pP(p^2)} = \gamma_1 p + \cfrac{1}{\delta_1 p + \cfrac{1}{\gamma_2 p + \cfrac{1}{\delta_2 p + \cfrac{\quad\vdots\quad}{\cfrac{1}{\gamma_m p + \cfrac{1}{\delta_m p}}}}}} \quad . \quad . \quad . \quad (31$$

Now, the condition that P(x) and Q(x) should have interlacin negative real zeros is equivalent to the zeros in p of P(p^2) an Q(p^2) interlacing on the positive imaginary and negativ imaginary p-axes, and therefore to Q(p^2) and pP(p^2) being th even and odd parts respectively of a Hurwitz polynomial o degree $2m$. Comparing eqn. (31) with eqn. (4) it is seen tha for an even polynomial of degree n, the Hurwitz criteria can b reduced to

$$\left.\begin{array}{l} a_{n-1}, \Delta_3, \Delta_5, \ldots \Delta_{n-3}, \Delta_{n-1} \\ a_n, a_{n-2}, a_{n-4}, \ldots a_2, a_0 \end{array}\right\} \text{ must have the same sign} \quad (32$$

In expression (32), the alternative set of determinants, D_i, ca replace the Hurwitz determinants Δ_i.

Consider now the case of n odd. Let X and Y be polynomial in x of degree m, and suppose that the coefficients of the highes powers of x in X and Y have the same sign.

Then

$$\frac{X}{Y} = \cfrac{1}{\eta_1 + \cfrac{1}{\theta_1 x + \cfrac{1}{\eta_2 + \cfrac{1}{\theta_2 x + \cfrac{\quad\vdots\quad}{\cfrac{1}{\theta_m x + \cfrac{1}{\eta_{m+1}}}}}}}} \quad . \quad . \quad . \quad . \quad (33$$

It is shown in Appendix 7.2, Theorem 2, that the necessar and sufficient conditions for X and Y to have only simple rea zeros, with the zeros of X interlacing the zeros of Y, and with zero of X the most positive, are that

$$\theta_i > 0, i = 1, 2, 3, \ldots m \quad . \quad . \quad . \quad . \quad (34$$

If all the zeros of X are negative then $\eta_i > 0$; every negative indicates a positive zero of X. (Appendix 7.2, Theorem 4 Similarly to the previous case, if $\theta_i > 0$, the condition $\eta_i >$

can be replaced by the condition that all the coefficients in the polynomial X must have the same sign.

Writing p^2 for x in eqn. (33) we have finally

$$\frac{pY(p^2)}{X(p^2)} = \eta_1 p + \cfrac{1}{\theta_1 p + \cfrac{1}{\eta_2 p + \cfrac{1}{\theta_2 p + \cfrac{1}{\ddots + \cfrac{1}{\theta_m p + \cfrac{1}{\eta_{m+1} p}}}}}} \quad \ldots \quad (35)$$

and the condition that $X(x)$ and $Y(x)$ should have interlacing negative real zeros [with the most positive zero belonging to $X(x)$] is equivalent to $pY(p^2)$ and $X(p^2)$ being the odd and even parts respectively of a Hurwitz polynomial of degree $2m + 1$. Comparing eqn. (35) with eqn. (4), it is seen that, for an odd polynomial of degree n, the Hurwitz criteria can be reduced to

$$\left.\begin{array}{l} \Delta_2, \Delta_4, \Delta_6, \ldots \Delta_{n-1} > 0 \\ \text{and} \quad a_n, a_{n-1}, a_{n-3}, a_{n-5}, \ldots a_2, a_0 \quad \text{must have same sign} \end{array}\right\} \quad \ldots \quad (36)$$

Once again the alternative determinants D_i can replace the Hurwitz determinants Δ_i in the above. For example, for $n = 5$, the set of criteria can be written

$$\left.\begin{array}{l} \begin{vmatrix} \begin{vmatrix} a_4 & a_2 \\ a_5 & a_3 \end{vmatrix} & \begin{vmatrix} a_4 & a_0 \\ a_5 & a_1 \end{vmatrix} \\ \begin{vmatrix} a_4 & a_0 \\ a_5 & a_1 \end{vmatrix} & \begin{vmatrix} a_2 & a_0 \\ a_3 & a_1 \end{vmatrix} \end{vmatrix} > 0 \qquad \begin{vmatrix} a_4 & a_2 \\ a_5 & a_3 \end{vmatrix} > 0 \\ a_5, a_4, a_2, a_0 \text{ must have the same sign} \end{array}\right\} \quad \ldots \quad (37)$$

(5) CONCLUSIONS

It has been shown that the various sets of stability criteria for linear systems, including the set recently given by Fuller,[14] can easily be derived using some simple theorems in continued fractions. A method of condensing the Hurwitz determinants to about half their original order yields alternative sets of determinantal criteria.

As pointed out by Fuller, this material on stability is intimately related to criteria for the realizability of two element-kind networks and to the so-called aperiodicity criteria, and corresponding results exist in these latter fields. For example, the aperiodicity criteria could be written in continued-fraction form and criteria for the realizability of an *RC* impedance could be written using the condensed Hurwitz determinants.

Finally, it has been shown that a canonical form for a Hurwitz polynomial exists as a product of continued fractions.

(6) REFERENCES

(1) ROUTH, E. J.: 'A Treatise on the Stability of a Given State of Motion' (Macmillan, 1877).

(2) ROUTH, E. J.: 'Dynamics of a System of Rigid Bodies', 6th edition (Macmillan, 1905), Part II, Chapter VI.

(3) HURWITZ, A.: 'Ueber die Bedingungen, unter welchen eine Gleichung nur Wurzeln mit negativen reelen Theilen besitzt', *Mathematische Annalen*, 1895, **46**, p. 273.

(4) ORLANDO, L.: 'Sul problema di Hurwitz relativo alle parti reali delle radici di un'equazione algebrica', *ibid.*, 1912, **71**, p. 233.

(5) SCHUR, J.: 'Über algebraische Gleichungen, die nur Wurzeln mit negativen Realteilen besitzen', *Zeitschrift für angewandte Mathematik und Mechanik*, 1921, **1**, p. 307.

(6) GUILLEMIN, E. A.: 'The Mathematics of Circuit Analysis' (John Wiley, 1949), p. 401.

(7) WALL, H. S.: 'Analytic Theory of Continued Fractions' (D. Van Nostrand, 1948), Chapter X, p. 173.

(8) BADER, W.: 'Beitrag zur Verwirklichung von Wechselstromwiderständen vorgeschriebener Frequenzabhängigkeit', *Archiv für Elektrotechnik*, 1940, **34**, p. 293.

(9) BADER, W.: 'Polynomvierpole vorgeschriebener Frequenzabhängigkeit', *ibid.*, 1940, **34**, p. 181.

(10) VAN DER POL, B., and BREMMER, H.: 'Operational Calculus' (Cambridge University Press, 1950), p. 187.

(11) BÜCKNER, H.: 'A Formula for an Integral occurring in the Theory of Linear Servomechanisms and Control-Systems', *Quarterly of Applied Mathematics*, 1952–53, **10**, p. 205.

(12) BASHKOW, T. R., and DESOER, C. A.: 'A Network Proof of a Theorem on Hurwitz Polynomials and its Generalization', *ibid.*, 1956–57, **14**, p. 423.

(13) AITKEN, A. C.: 'Determinants and Matrices', 6th edition (Oliver and Boyd, 1949), Section 53, p. 126.

(14) FULLER, A. T.: 'Stability Criteria for Linear Systems and Realizability Criteria for *RC* Networks', *Proceedings of the Cambridge Philosophical Society*, 1957, **53**, p. 878.

(7) APPENDICES

(7.1) Condensation of the Hurwitz Determinants Δ_i

Consider first the case of i even, and consider the result of premultiplying Δ_i by the following determinant, of value $(a_{n-1})^{i/2}$, in the usual matrix fashion:

$$\left.\begin{array}{|cccccccccccc|} 1 & 0 & . & . & . & . & . & . & . & . & . & . \\ 0 & 0 & 1 & 0 & . & . & . & . & . & . & . & . \\ 0 & 0 & 0 & 0 & 1 & 0 & . & . & . & . & . & . \\ . & . & . & . & . & . & . & . & . & . & . & . \\ . & . & . & . & . & . & . & . & . & . & . & . \\ 0 & . & . & . & . & . & . & . & . & . & 1 & 0 \\ 0 & . & . & . & . & . & . & . & . & . & -a_n & a_{n-1} \\ . & . & . & . & . & . & . & . & . & . & . & . \\ . & . & . & . & . & . & . & . & . & . & . & . \\ 0 & 0 & -a_n & a_{n-1} & . & . & . & . & . & . & . & a_{n-i+3} \\ -a_n & a_{n-1} & -a_{n-2} & a_{n-3} & . & . & . & . & . & . & . & a_{n-i+1} \end{array}\right\} \begin{array}{l} \} \, i/2 \text{ rows} \\ \\ \} \, i/2 \text{ rows} \end{array}$$

The resulting product is

$$
\left|\begin{array}{cccccccccc}
a_{n-1} & a_{n-3} & a_{n-5} & \cdots & & & & & & \\
0 & a_{n-1} & a_{n-3} & \cdots & & & & & & \\
\cdot & \cdot & \cdot & \cdots & & & & & & \\
\cdot & \cdot & \cdot & \cdots & & & & & & \\
0 & \cdot & \cdot & 0 & a_{n-1} & a_{n-3} & \cdots & & & \\
0 & \cdot & \cdot & \cdot & 0 & \begin{vmatrix} a_{n-1} & a_{n-3} \\ a_n & a_{n-2} \end{vmatrix} & \begin{vmatrix} a_{n-1} & a_{n-5} \\ a_n & a_{n-4} \end{vmatrix} & \begin{vmatrix} a_{n-1} & a_{n-7} \\ a_n & a_{n-6} \end{vmatrix} & \cdots \\
0 & \cdot & \cdot & \cdot & 0 & \begin{vmatrix} a_{n-1} & a_{n-5} \\ a_n & a_{n-4} \end{vmatrix} & \begin{vmatrix} a_{n-1} & a_{n-7} \\ a_n & a_{n-6} \end{vmatrix} + \begin{vmatrix} a_{n-3} & a_{n-5} \\ a_{n-2} & a_{n-4} \end{vmatrix} & \begin{vmatrix} a_{n-1} & a_{n-9} \\ a_n & a_{n-8} \end{vmatrix} + \begin{vmatrix} a_{n-3} & a_{n-7} \\ a_{n-2} & a_{n-6} \end{vmatrix} & \cdots \\
0 & \cdot & \cdot & \cdot & 0 & \begin{vmatrix} a_{n-1} & a_{n-7} \\ a_n & a_{n-6} \end{vmatrix} & \begin{vmatrix} a_{n-1} & a_{n-9} \\ a_n & a_{n-8} \end{vmatrix} + \begin{vmatrix} a_{n-3} & a_{n-7} \\ a_{n-2} & a_{n-6} \end{vmatrix} & \begin{vmatrix} a_{n-1} & a_{n-11} \\ a_n & a_{n-10} \end{vmatrix} + \begin{vmatrix} a_{n-3} & a_{n-9} \\ a_{n-2} & a_{n-8} \end{vmatrix} + \begin{vmatrix} a_{n-5} & a_{n-7} \\ a_{n-4} & a_{n-6} \end{vmatrix} & \cdots \\
\cdot & \cdot & \cdot & \cdots & & & & & & \\
\cdot & \cdot & \cdot & \cdots & & & & & &
\end{array}\right|
$$

(first group of rows: $i/2$ rows; second group of rows: $i/2$ rows; left block: $i/2$ columns; right block: $i/2$ columns)

and hence, for i even, Δ_i is equal to D_i, where

$$
\underset{(i \text{ even})}{D_i =} \left|\begin{array}{cccc}
\begin{vmatrix} a_{n-1} & a_{n-3} \\ a_n & a_{n-2} \end{vmatrix} & \begin{vmatrix} a_{n-1} & a_{n-5} \\ a_n & a_{n-4} \end{vmatrix} & \begin{vmatrix} a_{n-1} & a_{n-7} \\ a_n & a_{n-6} \end{vmatrix} & \cdots \\
\begin{vmatrix} a_{n-1} & a_{n-5} \\ a_n & a_{n-4} \end{vmatrix} & \begin{vmatrix} a_{n-1} & a_{n-7} \\ a_n & a_{n-6} \end{vmatrix} + \begin{vmatrix} a_{n-3} & a_{n-5} \\ a_{n-2} & a_{n-4} \end{vmatrix} & \begin{vmatrix} a_{n-1} & a_{n-9} \\ a_n & a_{n-8} \end{vmatrix} + \begin{vmatrix} a_{n-3} & a_{n-7} \\ a_{n-2} & a_{n-6} \end{vmatrix} & \cdots \\
\begin{vmatrix} a_{n-1} & a_{n-7} \\ a_n & a_{n-6} \end{vmatrix} & \begin{vmatrix} a_{n-1} & a_{n-9} \\ a_n & a_{n-8} \end{vmatrix} + \begin{vmatrix} a_{n-3} & a_{n-7} \\ a_{n-2} & a_{n-6} \end{vmatrix} & \begin{vmatrix} a_{n-1} & a_{n-11} \\ a_n & a_{n-10} \end{vmatrix} + \begin{vmatrix} a_{n-3} & a_{n-9} \\ a_{n-2} & a_{n-8} \end{vmatrix} + \begin{vmatrix} a_{n-5} & a_{n-7} \\ a_{n-4} & a_{n-6} \end{vmatrix} & \cdots \\
\cdots & \cdots & \cdots & \cdots \\
\cdots & \cdots & \cdots & \cdots
\end{array}\right| \quad \cdots \quad (38)
$$

For i even, D_i is symmetrical, and of order $i/2$.

When i is odd, condensation of Δ_i can be achieved by premultiplying by the following determinant of value $(a_{n-1})^{(i-1)/2}$:

$$
\left|\begin{array}{cccccccccc}
1 & 0 & \cdot & \cdot & \cdot & \cdot & \cdot & \cdot & \cdot & \cdot \\
0 & 0 & 1 & 0 & \cdot & \cdot & \cdot & \cdot & \cdot & \cdot \\
0 & 0 & 0 & 0 & 1 & 0 & \cdot & \cdot & \cdot & \cdot \\
\cdot & \cdot & \cdot & \cdot & \cdot & \cdot & \cdot & \cdot & \cdot & \cdot \\
\cdot & \cdot & \cdot & \cdot & \cdot & \cdot & \cdot & \cdot & \cdot & \cdot \\
0 & \cdot & \cdot & \cdot & \cdot & \cdot & \cdot & \cdot & \cdot & 1 \\
0 & \cdot & \cdot & \cdot & \cdot & \cdot & \cdot & a_n & -a_{n-1} & a_{n-2} \\
\cdot & \cdot & \cdot & \cdot & \cdot & \cdot & \cdot & \cdot & \cdot & \cdot \\
0 & 0 & a_n & -a_{n-1} & \cdot & \cdot & \cdot & \cdot & \cdot & a_{n-i+3} \\
a_n & -a_{n-1} & a_{n-2} & -a_{n-3} & \cdot & \cdot & \cdot & \cdot & \cdot & a_{n-i+1}
\end{array}\right|
$$

(first group of rows: $(i+1)/2$ rows; second group of rows: $(i-1)/2$ rows)

The resulting product is

$$
\left|\begin{array}{cccccccccc}
a_{n-1} & a_{n-3} & \cdots & & & & & & & \\
0 & a_{,-1} & a_{n-3} & \cdots & & & & & & \\
\cdot & \cdot & \cdot & \cdots & & & & & & \\
\cdot & \cdot & \cdot & \cdots & & & & & & \\
0 & \cdot & \cdot & \cdot & a_{n-1} & a_{n-3} & \cdots & & & \\
0 & \cdot & \cdot & \cdot & 0 & a_{n-1} & a_{n-3} & a_{n-5} & \cdots & \\
0 & \cdot & \cdot & \cdot & 0 & a_n a_{n-3} & a_n a_{n-5} + \begin{vmatrix} a_{n-2} & a_{n-4} \\ a_{n-1} & a_{n-3} \end{vmatrix} & a_n a_{n-7} + \begin{vmatrix} a_{n-2} & a_{n-6} \\ a_{n-1} & a_{n-5} \end{vmatrix} & \cdots & \\
0 & \cdot & \cdot & \cdot & 0 & a_n a_{n-5} & a_n a_{n-7} + \begin{vmatrix} a_{n-2} & a_{n-6} \\ a_{n-1} & a_{n-5} \end{vmatrix} & a_n a_{n-9} + \begin{vmatrix} a_{n-2} & a_{n-8} \\ a_{n-1} & a_{n-7} \end{vmatrix} + \begin{vmatrix} a_{n-4} & a_{n-6} \\ a_{n-3} & a_{n-5} \end{vmatrix} & \cdots & \\
\cdot & \cdot & \cdot & \cdots & & & & & & \\
\cdot & \cdot & \cdot & \cdots & & & & & &
\end{array}\right|
$$

(first group of rows: $(i-1)/2$ rows; second group of rows: $(i+1)/2$ rows; left block: $(i-1)/2$ columns; right block: $(i+1)/2$ columns)

and thus, for i odd, Δ_i is equal to D_i, where

$$D\hat{\imath} = \begin{vmatrix} a_{n-1} & a_{n-3} & a_{n-5} & \cdots \\ a_n a_{n-3} & a_n a_{n-5} + \begin{vmatrix} a_{n-2} & a_{n-4} \\ a_{n-1} & a_{n-3} \end{vmatrix} & a_n a_{n-7} + \begin{vmatrix} a_{n-2} & a_{n-6} \\ a_{n-1} & a_{n-5} \end{vmatrix} & \cdots \\ a_n a_{n-5} & a_n a_{n-7} + \begin{vmatrix} a_{n-2} & a_{n-6} \\ a_{n-1} & a_{n-5} \end{vmatrix} & a_n a_{n-9} + \begin{vmatrix} a_{n-2} & a_{n-8} \\ a_{n-1} & a_{n-7} \end{vmatrix} + \begin{vmatrix} a_{n-4} & a_{n-6} \\ a_{n-3} & a_{n-5} \end{vmatrix} & \cdots \\ \cdots & \cdots & \cdots & \cdots \end{vmatrix} \quad (i \text{ odd}) \quad \ldots (39)$$

For i odd, D_i is of order $(i+1)/2$, and would be symmetrical if the elements in the first row were multiplied by a_n.

(7.2) Some Theorems on Continued Fractions

Theorem 1

If P is a polynomial in x of degree $m-1$, and Q is a polynomial in x of degree m, and the coefficients of the highest powers of x in P and Q have the same sign, the necessary and sufficient conditions for P and Q to have only simple real zeros, with the zeros of P interlacing the zeros of Q, are that the coefficients γ_i in the following continued fraction should all be positive:

$$\frac{P}{Q} = \cfrac{1}{\gamma_1 x + \cfrac{1}{\delta_1 + \cfrac{1}{\gamma_2 x + \cfrac{1}{\delta_2 + \cfrac{\ddots}{\cfrac{1}{\gamma_m x + \cfrac{1}{\delta_m}}}}}}} \quad \ldots (40)$$

The necessity of these conditions will first be shown.

The first two steps in the process of forming this continued fraction are

$$\frac{P}{Q} = \frac{1}{\gamma_1 x + \dfrac{Q_1}{P}} \quad \ldots (41)$$

$$\frac{Q_1}{P} = \frac{1}{\delta_1 + \dfrac{P_1}{Q_1}} \quad \ldots (42)$$

Thus $$Q_1 = Q - P\gamma_1 x \quad \ldots (43)$$

and $$P_1 = P - Q_1\delta_1 \quad \ldots (44)$$

Q_1 being of degree $m-1$, P_1 of degree $m-2$ and $\gamma_1 > 0$, since the coefficients of the highest powers of x in P and Q have the same sign.

As only one zero of Q occurs between two adjacent zeros of P, Q must have opposite signs at adjacent zeros of P. But, from eqn. (43), Q_1 is equal to Q at zeros of P. Therefore Q_1 has opposite signs at adjacent zeros of P, and therefore Q_1 has one zero, or an odd number of zeros, between adjacent zeros of P. As the total numbers of zeros of P and Q_1 are equal, since they are of the same degree, only one zero of Q_1 lies between two adjacent zeros of P; the remaining zero of Q_1 lies either to the left of the most negative zero of P or to the right of the most positive zero of P. If the former, P and Q_1 have opposite signs at infinity; if the latter, P and Q_1 have the same sign at infinity. In either case the zeros of Q_1 are all real and simple and interlace the zeros of P.

Now, from eqn. (44), P_1 is equal to P at zeros of Q_1, and therefore exactly one zero of P_1 must lie between adjacent zeros of Q_1, since the degree of P_1 is one less than that of Q_1. Thus the zeros of P_1 and Q_1 are real, simple and interlaced. Further, as P and Q_1 have the same sign at infinity when a zero of Q_1 is the most positive, and opposite signs at infinity when a zero of P is the most positive, it follows, since P_1 is equal to P at zeros of Q_1, that P_1 and Q_1 have the same sign at infinity. Therefore the ratio P_1/Q_1 has the same properties as the original ratio P/Q, but the degrees of both numerator and denominator have been reduced by one. As the above argument can now be repeated with P_2/Q_2 and P_1/Q_1 instead of P_1/Q_1 and P/Q respectively, γ_2 must be positive, and hence by continual repetition of the same argument, $\gamma_3, \gamma_4, \ldots \gamma_m$ must all be positive.

By the same type of argument, which therefore will not be given in full, the sufficiency of the conditions in Theorem 1 can easily be demonstrated. Using eqns. (43) and (44), it can be shown that, if P_1/Q_1 is a function of the type considered in the theorem, P/Q will also be a function of that type, provided γ_1 is positive and regardless of the sign of δ_1. But as P_{m-1}/Q_{m-1}, equal to $1/(\gamma_m x + 1/\delta_m)$, is a function of that type, so therefore are P_{m-2}/Q_{m-2}, P_{m-3}/Q_{m-3}, $\ldots$ P_1/Q_1, P/Q, which proves the sufficiency of the conditions.

In the course of the proof of Theorem 1, the following theorem has also been proved.

Theorem 2

If X and Y are polynomials in x of degree m, and the coefficients of the highest powers of x in X and Y have the same sign, the necessary and sufficient conditions for X and Y to have only simple real zeros, with the zeros of X interlacing the zeros of Y and a zero of X the most positive, are that the coefficients θ_i in the following continued fraction should all be positive:

$$\frac{X}{Y} = \cfrac{1}{\eta_1 + \cfrac{1}{\theta_1 x + \cfrac{1}{\eta_2 + \cfrac{1}{\theta_2 x + \cfrac{\ddots}{\cfrac{1}{\theta_m x + \cfrac{1}{\eta_{m+1}}}}}}}} \quad \ldots (45)$$

The following two theorems give methods of counting the number of positive zeros in the denominator polynomials Q and Y respectively.

Theorem 3

If in the continued fraction of eqn. (40) all the coefficients γ_i are positive, then the total number of the coefficients δ_i that are negative is equal to the number of positive zeros of Q.

The proof follows by an extension of the argument used for Theorem 1. From eqn. (43), it is evident that, since γ_1 is positive, Q_1 has the same sign as P at negative zeros of Q, and the opposite sign to P at positive zeros of Q. Thus a zero of

Q_1 lying between adjacent zeros of P will always lie to the *left* of the corresponding zero of Q if this is a *negative* zero, but to the *right* of the corresponding zero of Q if this is a *positive* zero. There are now three cases to consider: either all the zeros of Q are negative, or they are all positive, or some are negative and some positive.

If all the zeros of Q are negative, the remaining zero of Q_1 (see the proof of Theorem 1) must lie to the right of the most positive zero of P, and hence δ_1 in eqn. (44) will be positive; also the zeros of Q_1 will all be negative. If all the zeros of Q are positive, the remaining zero of Q_1 must lie to the left of the most negative zero of P, and hence δ_1 in eqn. (44) will be negative; also the zeros of Q_1 will all be positive. If some of the zeros of Q are negative and some positive, it is impossible to state definitely where the remaining zero of Q_1 lies and what the sign of Q_1 is at infinity. However, if Q_1 does have the same sign as P at infinity, then δ_1 in eqn. (44) will be positive, and the numbers of positive zeros of Q_1 and Q will be equal. Whereas, if Q_1 has the opposite sign at infinity to P, then δ_1 in eqn. (44) will be negative, and the number of positive zeros of Q_1 will be one less than the number of positive zeros of Q. As the argument can now be repeated with $Q_2, Q_3, \ldots Q_{m-1}$, it is evident that the number of positive zeros of Q is equal to the number of the coefficients $\delta_1, \delta_2, \ldots \delta_m$ that are negative.

In the course of the proofs of Theorems 1 and 3 the following theorem has also been proved.

Theorem 4

If in the continued fraction of eqn. (45) all the coefficients θ_i are positive, then the total number of the coefficients η_i that are negative is equal to the number of positive zeros of Y.

(7.3) Complete Expressions for the Stability Criteria using the Condensed Hurwitz Determinants

Given below are complete sets of stability criteria for values of n from 1 to 8. They are developed from eqns. (32) for n even and from eqns. (36) for n odd, using the condensed Hurwitz determinants. The criteria represent the conditions under which a polynomial with real coefficients

$$f(p) = a_0 + a_1 p + a_2 p^2 + \ldots + a_{n-1}p^{n-1} + a_n p^n$$

has its zeros confined to the left half p-plane.

(a) $n = 1$: a_1, a_0 must have the same sign

(b) $n = 2$: a_2, a_1, a_0 must have the same sign

(c) $n = 3$: $\begin{vmatrix} a_2 & a_0 \\ a_3 & a_1 \end{vmatrix} > 0$; a_3, a_2, a_0 must have the same sign

(d) $n = 4$: $\begin{vmatrix} a_3 & a_1 \\ a_4 a_1 & \begin{vmatrix} a_2 & a_0 \\ a_3 & a_1 \end{vmatrix} \end{vmatrix}$, a_4, a_3, a_2, a_0 must have the same sign

(e) $n = 5$: $\left.\begin{array}{l} \begin{vmatrix} \begin{vmatrix} a_4 & a_2 \\ a_5 & a_3 \end{vmatrix} & \begin{vmatrix} a_4 & a_0 \\ a_5 & a_1 \end{vmatrix} \\ \begin{vmatrix} a_4 & a_0 \\ a_5 & a_1 \end{vmatrix} & \begin{vmatrix} a_2 & a_0 \\ a_3 & a_1 \end{vmatrix} \end{vmatrix} > 0 \quad \begin{vmatrix} a_4 & a_2 \\ a_5 & a_3 \end{vmatrix} > 0; \\ a_5, a_4, a_2, a_0 \text{ must have the same sign} \end{array}\right\}$

(f) $n = 6$: $\left.\begin{array}{l} \begin{vmatrix} a_5 & a_3 & a_1 \\ a_6 a_3 & a_6 a_1 + \begin{vmatrix} a_4 & a_2 \\ a_5 & a_3 \end{vmatrix} & \begin{vmatrix} a_4 & a_0 \\ a_5 & a_1 \end{vmatrix} \\ a_6 a_1 & \begin{vmatrix} a_4 & a_0 \\ a_5 & a_1 \end{vmatrix} & \begin{vmatrix} a_2 & a_0 \\ a_3 & a_1 \end{vmatrix} \end{vmatrix}, \quad \begin{vmatrix} a_5 & a_3 \\ a_6 a_3 & a_6 a_1 + \begin{vmatrix} a_4 & a_2 \\ a_5 & a_3 \end{vmatrix} \end{vmatrix}, \\ a_6, a_5, a_4, a_2, a_0 \text{ must have the same sign} \end{array}\right\}$

(g) $n = 7$: $\left.\begin{array}{l} \begin{vmatrix} \begin{vmatrix} a_6 & a_4 \\ a_7 & a_5 \end{vmatrix} & \begin{vmatrix} a_6 & a_2 \\ a_7 & a_3 \end{vmatrix} & \begin{vmatrix} a_6 & a_0 \\ a_7 & a_1 \end{vmatrix} \\ \begin{vmatrix} a_6 & a_2 \\ a_7 & a_3 \end{vmatrix} & \begin{vmatrix} a_6 & a_0 \\ a_7 & a_1 \end{vmatrix} + \begin{vmatrix} a_4 & a_2 \\ a_5 & a_3 \end{vmatrix} & \begin{vmatrix} a_4 & a_0 \\ a_5 & a_1 \end{vmatrix} \\ \begin{vmatrix} a_6 & a_0 \\ a_7 & a_1 \end{vmatrix} & \begin{vmatrix} a_4 & a_0 \\ a_5 & a_1 \end{vmatrix} & \begin{vmatrix} a_2 & a_0 \\ a_3 & a_1 \end{vmatrix} \end{vmatrix} > 0 \\ \begin{vmatrix} \begin{vmatrix} a_6 & a_4 \\ a_7 & a_5 \end{vmatrix} & \begin{vmatrix} a_6 & a_2 \\ a_7 & a_3 \end{vmatrix} \\ \begin{vmatrix} a_6 & a_2 \\ a_7 & a_3 \end{vmatrix} & \begin{vmatrix} a_6 & a_0 \\ a_7 & a_1 \end{vmatrix} + \begin{vmatrix} a_4 & a_2 \\ a_5 & a_3 \end{vmatrix} \end{vmatrix} > 0 \quad \begin{vmatrix} a_6 & a_4 \\ a_7 & a_5 \end{vmatrix} > 0; \\ a_7, a_6, a_4, a_2, a_0 \text{ must have the same sign} \end{array}\right\}$

(h) $n = 8$: $\left.\begin{array}{l} \begin{vmatrix} a_7 & a_5 & a_3 & a_1 \\ a_8 a_5 & a_8 a_3 + \begin{vmatrix} a_6 & a_4 \\ a_7 & a_5 \end{vmatrix} & a_8 a_1 + \begin{vmatrix} a_6 & a_2 \\ a_7 & a_3 \end{vmatrix} & \begin{vmatrix} a_6 & a_0 \\ a_7 & a_1 \end{vmatrix} \\ a_8 a_3 & a_8 a_1 + \begin{vmatrix} a_6 & a_2 \\ a_7 & a_3 \end{vmatrix} & \begin{vmatrix} a_6 & a_0 \\ a_7 & a_1 \end{vmatrix} + \begin{vmatrix} a_4 & a_2 \\ a_5 & a_3 \end{vmatrix} & \begin{vmatrix} a_4 & a_0 \\ a_5 & a_1 \end{vmatrix} \\ a_8 a_1 & \begin{vmatrix} a_6 & a_0 \\ a_7 & a_1 \end{vmatrix} & \begin{vmatrix} a_4 & a_0 \\ a_5 & a_1 \end{vmatrix} & \begin{vmatrix} a_2 & a_0 \\ a_3 & a_1 \end{vmatrix} \end{vmatrix}, \\ \begin{vmatrix} a_7 & a_5 & a_3 \\ a_8 a_5 & a_8 a_3 + \begin{vmatrix} a_6 & a_4 \\ a_7 & a_5 \end{vmatrix} & a_8 a_1 + \begin{vmatrix} a_6 & a_2 \\ a_7 & a_3 \end{vmatrix} \\ a_8 a_3 & a_8 a_1 + \begin{vmatrix} a_6 & a_2 \\ a_7 & a_3 \end{vmatrix} & \begin{vmatrix} a_6 & a_0 \\ a_7 & a_1 \end{vmatrix} + \begin{vmatrix} a_4 & a_2 \\ a_5 & a_3 \end{vmatrix} \end{vmatrix}, \\ \begin{vmatrix} a_7 & a_5 \\ a_8 a_5 & a_8 a_3 + \begin{vmatrix} a_6 & a_4 \\ a_7 & a_5 \end{vmatrix} \end{vmatrix}, \quad a_8, a_7, a_6, a_4, a_2, a_0 \text{ must have the same sign} \end{array}\right\}$

It will be noted that, where a number of determinants occur in one set of criteria, e.g. when $n = 7$, the various determinants are successive minors with respect to the elements in the last row and last column. Thus if D is the highest order determinant in (g), the other two can be written as D_{33} and D_{3322}. By repeated use of Jacobi's theorem (see, for example, Reference 13) it can be shown that the three determinants in the set can be taken, more generally, as D, D_{ii} and D_{iijj} where i, j are selected from 1, 2, 3. In this case, therefore, the set of determinantal criteria can be expressed in a total of six different ways. Similar results apply to each of the other cases.

The non-determinantal members of each set of criteria can also be varied somewhat from those given above. Two possibilities have been given by Fuller,[14] and various others can be obtained by using either of these in conjunction with the determinantal members of the set. For example, when $n = 5$, the condition

a_5, a_4, a_2, a_0 must have the same sign

can be replaced either by

a_5, a_3, a_2, a_0 must have the same sign

or a_5, a_3, a_1, a_0 must have the same sign

621.317.333.82

The Institution of Electrical Engineers
Monograph No. 329 M
Feb. 1959

THE EFFECT OF IRRADIATION ON THE BREAKDOWN VOLTAGE OF SPHERE-GAPS IN AIR UNDER DIRECT AND ALTERNATING VOLTAGES

By E. KUFFEL, M.Sc., A.Inst.P.

(*The paper was first received 2nd October, and in revised form 4th December, 1958. It was published as an* INSTITUTION MONOGRAPH *in February, 1959.*)

SUMMARY

Breakdown voltages have been measured with and without the irradiation from 0·5 mg of radium. Spheres of diameters 2 to 25 cm were used and some experiments were made with parallel-plate electrodes. The irradiation lowered the breakdown voltage by as much as 4% in some circumstances. A maximum effect was obtained with a particular gap length, and this length depended on the size of the sphere electrodes.

(1) INTRODUCTION

The influence of irradiation on the impulse breakdown voltage of sphere-gaps in air has been studied by various workers.[1–4] The methods employed for irradiation have included[4–6] radioactive materials, mercury arcs and subsidiary sparks or corona discharges. An extensive summary of the results can be found in a paper by Meek.[1]

However, little information is available concerning the effect of irradiation on gap breakdowns with direct or alternating voltages. Whitehead and Castellain[7] studied qualitatively the effect of irradiation from a carbon arc with alternating voltages and they reported a small reduction of the breakdown voltages.

Edwards and Smee,[8] using 50 c/s alternating voltages and 1·3 cm-diameter spheres, showed that the breakdown voltage for an unirradiated gap of 0·5 mm was variable from day to day. Values were obtained as high as 80% in excess of the corresponding breakdown voltages with irradiation. The difference was reduced as the gap length was increased. Similar results on d.c. were reported earlier by Klemm.[9]

Recently Hardy and Broadbent[10] studied the effect of irradiation on the gap between 2 cm-diameter spheres. With gaps up to 0·5 cm they reported that the presence of radium did not appreciably change the direct breakdown voltage. However, a decrease of over 2% was recorded for a gap of 0·8 cm, but no attempt was made to explain this effect.

The purpose of the present work was to establish whether it is necessary to use additional irradiation in accurate direct or alternating voltage sphere-gap calibrations. Other factors influencing the breakdown voltage, such as humidity, temperature and pressure, were carefully measured and the clearance of nearby objects was adjusted in accordance with B.S. 358.[11]

The results indicate that the irradiation effect varies with the sphere spacing, and consequently with the breakdown mechanism involved.

The mechanism of breakdown in air between sphere electrodes depends on the air-gap length. Two mechanisms are suggested by Loeb and Meek.[12, 13] In short gaps at the minimum breakdown voltage an electron avalanche travels across the gap from cathode to anode. In longer gaps the field is non-uniform and an avalanche does not cross the full gap since the voltage gradient in the middle of the gap is too weak to cause ionization by collision. High gradients will be present near the surfaces of electrodes, and when one electrode is earthed the higher gradient will occur at the high-voltage electrode. Thus the breakdown will be initiated near that electrode. At the breakdown voltage, Meek[13] proposes a gradient sufficiently high to give a transition from an avalanche to a streamer, which in turn propagates across the gap to form a conducting filament between the electrodes. A transition point or critical sphere-spacing is then expected, below which one mechanism applies and above which a second mechanism operates. Toepler[14, 15] has shown that the experimental breakdown curves for sphere-gaps can be matched by two empirical curves, and that there is a discontinuity in the slopes of the two curves at the point of their meeting. The sphere spacing at which the discontinuity occurs depends on the diameter of the sphere. Claussnitzer[16] has studied this phenomenon in detail for spheres of various diameters. He found that at gap lengths up to $0{\cdot}5d_k$, where d_k is the gap length corresponding to Toepler's discontinuity, the breakdown voltage of sphere-gaps corresponded closely to the uniform field breakdown. Between $0{\cdot}5d_k$ and d_k the breakdown voltage was higher than that of a uniform field, while above d_k the breakdown values were lower than those for a uniform field. An interpretation of Claussnitzer's observations has been made in terms of a transition from one mechanism to another by Meek[13] and also by Jørgensen.[17]

(2) APPARATUS AND MEASUREMENT PROCEDURE

(2.1) Gap Arrangement

The 2·0, 6·25 and 12·5 cm-diameter spheres were mounted with a vertical axis and the lower sphere was earthed. The gap assembly was enclosed in a chamber 8 × 8 × 10 ft tall, with clearances to neighbouring objects in accordance with B.S. 358.[11] The adjustment of the gap was effected by an electric motor controlled from outside the chamber. The setting arrangement was calibrated with block gauges and was found to be accurate to ±0·1% for spacings above 0·5 cm.

The measurements with 25 cm-diameter spheres and with parallel-plane electrodes were made in the normal laboratory atmosphere. The electrodes were mounted with the axis horizontal. The spheres were made of copper, with the exception of those of 6·25 cm diameter, for which both copper and aluminium were used. They were normally polished with metal polish and washed with ether.

(2.2) Voltage Supply and Measurement

The direct voltages were derived from a Cockcroft–Walton type of rectifier circuit. The input was supplied from a motor-generator set whose speed was stabilized to within ±0·1%. The field of the generator was supplied from a constant-current source. The voltages at the input and output points of the rectifying circuit were found to be stable to within ±0·1% of their mean values. The ripple superimposed on the direct-voltage output was less than 0·1% and was neglected.

The direct voltage across the test gap was measured with a

Correspondence on Monographs is invited for consideration with a view to publication.
Mr. Kuffel is in the Research Department, Metropolitan-Vickers Electrical Co., Ltd.

resistance voltage divider and a potentiometer by comparing a known fraction of the total voltage with that of a standard cell. The resistance divider consisted of an oil-immersed wire-wound resistor and a standard decade resistance box. The h.v. resistance was 300·0 megohms ±0·1%.

In practice, and after the first trial breakdown of the test gap, the voltage was set to a value approximately 1% less than the expected breakdown voltage. It was then increased slowly by a fine control, so that the changing voltage could be followed by manipulating the potentiometer dials. A series of 20 breakdowns was made and the mean value was taken as the breakdown voltage. The interval between successive breakdowns was about 20 sec. Preliminary investigations showed that when the gap was inside the test chamber no change in breakdown voltage was observed during the first 100 tests or so, but after a large number of tests the results became more erratic. Consequently it was a standard practice to clean the spheres after about 100 tests and provision was made for this, using a chamois leather from outside the chamber without disturbing the test conditions.

When tests were carried out in the open laboratory it was found necessary to clean the spheres after about 50 breakdowns.

The measurement of the direct voltage applied to the test gap was accurate to ±0·2% of the true value. The measurements were consistent with each other for the whole investigation within ±0·1% but in most cases of comparison the results were obtained over short periods of time and the measurement consistency was well within 0·1%.

An alternating voltage was obtained from the transformer used to supply the rectifying circuit. The output voltage was measured by a Chubb and Fortescue type of peak voltmeter which consisted of a standard compressed-gas capacitor and a high-speed relay which was used as a mechanical rectifier. The mean current through the capacitor was measured by a moving-coil microammeter. For comparative purposes the measurements are considered to be accurate to within ±0·2%.

(2.3) Irradiation Technique

All sphere electrodes were hollow, and the gap was irradiated by positioning 0·5 mg of radium inside the top electrode. The capsule was so arranged that it could be moved to the top of the shank (about 30 in long) supporting the top electrode. The movement was effected from outside the chamber without disturbing the gap setting. Preliminary experiments showed that when the radium was moved back more than 15 in from the electrode it had little effect on the breakdown voltage. Series of readings were taken alternately with and without the radium and usually the sequence was repeated several times.

When experiments were made in the open laboratory, the radium was pushed through the hollow shank on the end of a rod so that it touched the inside surface of the electrode. It was removed after a set of readings was taken, without disturbing the gap setting.

Preliminary work showed that the effect of irradiation was the same whether the radium was placed in the h.v. electrode or in the earthed one. The thickness of the electrode was about 1·0 mm. The ionization current in the gap was measured with an electrometer. For 12·5 cm-diameter spheres 2·0 cm apart and with 240 volts between them, the current was approximately $3{\cdot}3 \times 10^{-11}$ amp; for 6·25 cm-diameter spheres 2·0 cm apart and with 240 volts between them, it was $3{\cdot}1 \times 10^{-11}$ amp.

(2.4) Other Measurements

The measured breakdown voltages were reduced to a standard barometric pressure of 760 mm Hg and a temperature of 20° C. When tests were made inside the chamber the temperature was measured with a thermocouple and was accurate to 0·1° C. The pressure was obtained from a barometer situated in the laboratory. The difference between atmospheric pressure and the pressure inside the test chamber was measured with an oil-filled manometer and was added to the barometer reading. The humidity was controlled with chemical salts and remained at about 4·0 mm Hg vapour pressure. It was measured with a dew-point hygrometer which was originally checked by measuring the humidities maintained by saturated solutions of various chemical salts. The measured relative humidities were correct within 2%.

(3) RESULTS

The actual breakdown voltages with unirradiated gaps generally agreed within 1% of those quoted in B.S. 358 for negative unidirectional voltages. However, the results for small spheres (2 cm diameter) differed from the corresponding values of B.S. 358 by as much as 3% in some cases, but agreed with those of Hardy and Broadbent[10] within 1%. Further work on sphere-gap calibrations is in progress and it is hoped to publish the results later. For the present purposes the paper is concerned with the influence of irradiation, and only the differences between the voltages for irradiated and unirradiated gaps have been considered here. The experimental results for direct voltages are plotted in Fig. 1, which shows the reduction

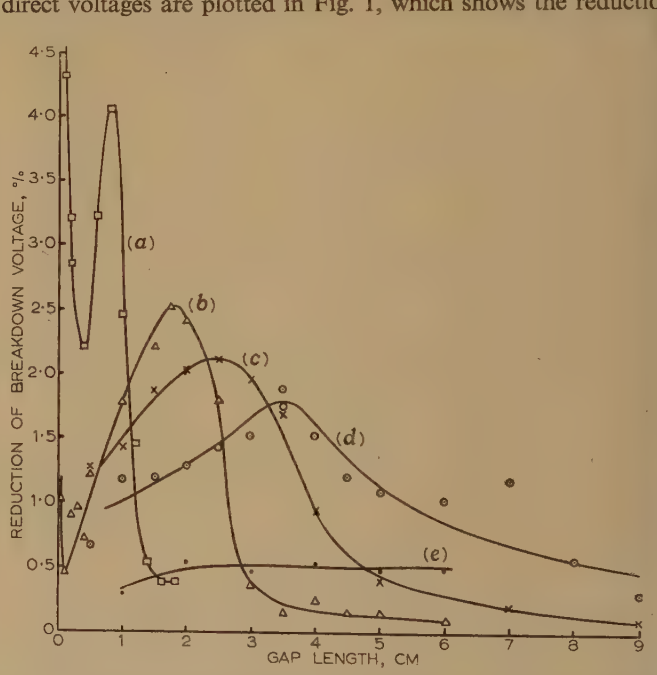

Fig. 1.—Effect of gap irradiation on the direct voltage breakdown of sphere-gaps.

(*a*) 2 cm-diameter spheres.
(*b*) 6·25 cm-diameter spheres.
(*c*) 12·5 cm-diameter spheres.
(*d*) 25·0 cm-diameter spheres.
(*e*) Parallel-plane electrodes.

of the breakdown voltages when 0·5 mg of radium was inserted inside one electrode. Except on very small gaps the irradiation effect increased with gap length, until a maximum effect was obtained at a fairly well-defined setting. Thereafter, in the case of sphere electrodes, the ionization effect decreased as the gap length was increased. The observed change due to radium was greater for spheres of smaller diameter. Furthermore, maximum ionization effect occurred at gap lengths which appeared to be a function of the sphere diameters or of the field distribution, as will be discussed later.

The effect of irradiation with 2·0 and 6·25 cm-diameter spheres was investigated for gaps down to 0·5 mm. With 2·0 cm spheres the effect increased considerably with very small gaps (0·5 mm), which is in agreement with the early results of Klemm[9] and the results of Edwards and Smee.[8] The results for 2·0 and 12·5 cm spheres are reproduced in Fig. 2, together with the maximum

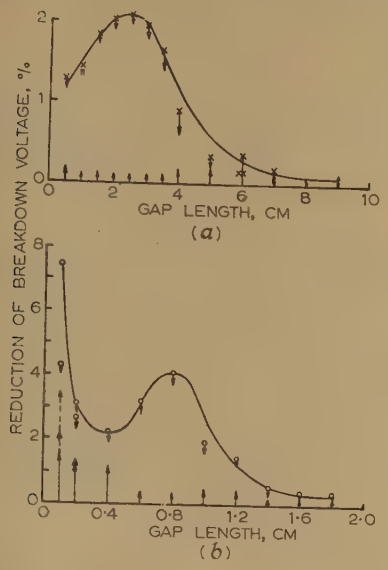

Fig. 2.—Dispersion of breakdown voltages.
(*a*) 12·5 cm-diameter spheres.
(*b*) 2 cm-diameter spheres.
Curves (*a*) and (*b*) are the same as (*c*) and (*a*) in Fig. 1.
↓ Arrow length gives maximum dispersion of breakdown voltages above the mean value for an irradiated gap.
↑ Arrow length gives maximum dispersion below the mean breakdown voltage for an unirradiated gap.

scatter observed in the measurements. As will be seen later, the irradiation effect for very small gaps can be related to the scatter. In the case of 6·25 cm spheres the same effect occurred with very small gaps, but it was much less pronounced and the scatter was correspondingly less.

The results shown in Fig. 1 were obtained for copper spheres. Measurements were also made with 6·25 cm-diameter aluminium spheres, and the results are plotted in Fig. 3 with the corresponding results for copper spheres. The irradiation effect was the

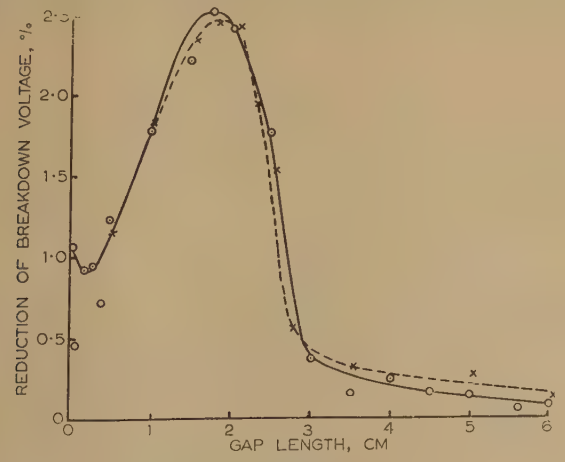

Fig. 3.—Effect of electrode material.
○—○— Copper spheres, 6·25 cm diameter.
×---×--- Aluminium spheres, 6·25 cm diameter.

same in both cases within the experimental error, indicating that the effect was independent of the material of the electrodes. The corresponding mean breakdown voltages for copper and aluminium electrodes agreed within 0·5%, the results with aluminium being slightly lower than with copper.

The effect of irradiation with 6·25 cm-diameter copper spheres was also studied for alternating voltages, and the results are included in Fig. 4. They show similar characteristics to the

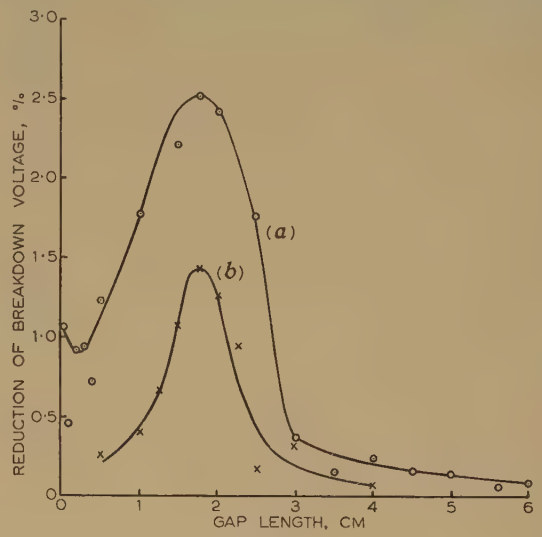

Fig. 4.—Irradiation effect for direct and alternating voltages.
Sphere diameter, 6·25 cm; material, copper.
(*a*) Direct voltage.
(*b*) Alternating voltage.

corresponding direct voltage results, but the effect was smaller. The peak value of the mean alternating voltage was within 0·5% of the mean direct voltage which caused breakdown.

The effects of irradiation were investigated with direct voltages of positive and negative polarity. Tests were made with 6·25 and 12·5 cm-diameter spheres. The effect was found to be slightly higher for negative polarity, but the difference was small and was within the limits of normal scatter of the results. Negative polarity was used for the main experiments.

The effect of irradiation was also investigated with direct voltage for gaps with small clearance. The radial clearance was reduced to 1·2 times the sphere diameter by enclosing the 6·25 cm-diameter sphere-gap in an earthed metal cylinder of 6 in diameter. The results are included in Fig. 6. The breakdown voltage for gaps larger than 1 cm was considerably lower than that for the corresponding gaps with normal clearance. It will be noticed that the reduction of clearance shifted the maximum ionization effects towards the smaller gap length.

Tests were also carried out in a mixture of approximately 1 part of argon in 10 parts of air by volume. In this case the ionization effect was the same as in normal air, but the corresponding breakdown voltages were reduced by approximately 13%.

(4) ANALYSIS OF RESULTS AND DISCUSSION

(4.1) Scatter of Results with Very Small Gaps

The rather large effect of irradiation under conditions of small sphere-spacing may be explained by considering the scatter of the results. The measured breakdown voltages of unirradiated gaps of less than 1·0 mm were widely scattered (e.g. in the case of 2·0 cm-diameter spheres and 0·5 mm gap, the maximum scatter in a set of 50 readings was about ±11% of the mean

breakdown voltage). It was found that with very small gaps the observed breakdown voltage depended greatly on the rate of voltage application. This effect may be attributed to the scarcity of electrons in the small gap.

For a breakdown to occur, there is an effective volume of air in which the voltage gradient must equal or exceed the minimum gradient required to produce an electron avalanche by electron collision, and some free electrons must be present or appear in that volume while the voltage is maintained. As an example, consider that the effective volume is a cylinder of air along the axis of the gap. If the gap breakdown is to be within 4% of the minimum value for an 0·5 mm gap between 2·0 cm-diameter spheres, the effective volume will be bounded by the axial cylinder whose side is approximately 4% longer than the shortest distance between the spheres. The radius of this cylinder is approximately $4{\cdot}4 \times 10^{-2}$ cm and the length is substantially the gap spacing, so that the effective volume is about 3×10^{-4} cm^3. Breakdown would occur if at any time at least one free electron was found in this volume, i.e. if the average concentration of free electrons was greater than say 3000/cm^3. In the absence of additional ionization, Geiger-counter experiments in the laboratory gave approximately 20 counts/sec/cm^3. Considering that the mean free life of an electron in air is very short ($\simeq 10^{-7}$ sec) the voltage may have to be maintained for as long as 2–3 minutes before breakdown occurs in the example quoted.

The experimental scatter was reduced to a very small value when the gap was irradiated with radium. Thus, the initial large difference between the irradiated and the unirradiated gap was dependent only on the level of the ionization existing in the very small gaps.

(4.2) Irradiation Effect with Moderate Gap Lengths

When the gap was increased beyond the very small gaps discussed in Section 4.1, the irradiation effect also increased (see Fig. 1). The effect cannot be explained by reference to scatter of the measured breakdown voltages, and an analysis of the corresponding results for an irradiated and a non-irradiated gap shows that the extreme measured results of the two cases did not overlap. This is illustrated in Fig. 2, where the arrows indicate maximum and minimum scatters obtained in the investigations with 2·0 and 12·5 cm-diameter sphere-gaps. Furthermore, the voltage could be set below the minimum breakdown value for the non-irradiated gap and then the gap could be made to break down by slowly lowering the radium inside the upper sphere.

The gradual increase of the ionization effect with gap length is difficult to explain. Assuming that Townsend's mechanism applies in this region, there will be a continuous development of an electron avalanche maintained from behind by a secondary process. The latter is effective when it moves towards the cathode, and is most effective when it acts at the cathode itself. One or more of the secondary processes will depend on the nature and the geometry of the cathode.[18] In the present case the possibility of a significant increase of ionization due to secondary effects with the material of the cathode surface may be excluded on the evidence of Fig. 3, which shows the same results for both copper and aluminium electrodes.

(4.3) Gas and Space Charge Effects

A more likely explanation of the increase in the ionization effect with gap length is the field distortion due to space charge. It is usually considered that space-charge distortion is likely with currents over 10^{-8} A/cm^2. Approximate evaluations of the exponent in the equation for the gas amplified current $i = i_0 \varepsilon^{\int_0^x \alpha dx}$ are given in Table 1. In the equation, i and i_0 are the total

Table 1

Approximate Current Density for 2·0 and 6·25 cm Diameter Spheres Irradiated with 0·5 mg of Radium

2·0 cm spheres			6·25 cm spheres		
Gap length	$\int_0^d \alpha dx$	i	Gap length	$\int_0^d \alpha dx$	i
cm	ε	A/cm^2	cm	ε	A/cm^2
0·4	$8{\cdot}0 \times 10^5$	4×10^{-6}	0·5	$4{\cdot}8 \times 10^5$	$7{\cdot}7 \times 10^{-8}$
0·6	$5{\cdot}2 \times 10^6$	$2{\cdot}6 \times 10^{-5}$	1·0	$2{\cdot}9 \times 10^7$	$4{\cdot}7 \times 10^{-6}$
0·8	$1{\cdot}8 \times 10^8$	9×10^{-4}	1·5	$5{\cdot}7 \times 10^8$	$9{\cdot}1 \times 10^{-5}$
			1·75	$3{\cdot}9 \times 10^9$	$6{\cdot}3 \times 10^{-4}$

and initial currents respectively, x is the distance from the cathode (or across the gap in this example) and α is the Townsend first ionization coefficient. The integral $\int_0^x \alpha dx$ was evaluated using Simpson's rule from plots of α against gap length (e.g. Fig 5).

The initial current in the gap was approximately 3×10^{-11} amp. Assuming the current to be uniformly distributed over one-half of the sphere, in the case of 6·25 cm-diameter spheres the initial current density was approximately $1{\cdot}6 \times 10^{-13}$ A/cm^2 and for 2·0 cm-diameter spheres it was about 5×10^{-12} A/cm^2.

The amplified current per unit area calculated for the measured breakdown voltages is given in Table 1. The current increases considerably with increasing gap length and exceeds the value of 10^{-8} A/cm^2 suggested above by a factor of several orders of magnitude.

This explanation would account qualitatively for the experimental results with gaps up to the point where the irradiation effect was a maximum. It would not be simple to demonstrate the effects quantitatively and precisely because, with the curved electrodes, the ion current density would vary with radial distance from the gap axis.

(4.4) Gap Length for Maximum Irradiation Effect

Some other breakdown mechanism may come into play when the ionization effect reaches its maximum value (see Fig. 1) and decreases with further increases of gap length.

An analysis was made of the distribution of the ionization coefficient, α, across the critical gap for each size of sphere electrodes. This showed that the maximum influence of radium

Table 2

Distribution of the Ionization Coefficients along the Axis of the Gaps at Spacings Corresponding to Maximum Ionization Effect

Sphere diameter	Gap length	E_{max}	E_{min}	α_{max}	α_{min}	$\int_0^d \alpha dx$	α_A
cm	cm	kV/cm	kV/cm				
2·0	0·80	41·0	27·2	60·0	7·5	19·0	23·8
6·25	1·75	34·4	26·2	26·8	6·2	22·1	12·6
12·5	2·50	31·8	26·1	18·3	6·1	23·0	9·2
25·0	3·50	30·0	26·1	13·2	6·1	29·6	8·5

on the gap breakdown voltages occurred when the minimum value of α was approximately the same in all cases.

The results are given in Table 2, where E is the voltage gradient

and α_A is an average value for α. The field distribution along the axis of the gap was calculated from the expression[19]

$$E = \frac{2d[d^2(f+1) + 4y^2(f-1)]V}{[d^2(f+1) - 4y^2(f-1)]^2}$$

where

$$f = \frac{\frac{d}{r} + 1 + \sqrt{\left[\left(\frac{d}{r}+1\right)^2 + 8\right]}}{4}$$

d = Gap length.
y = Distance of the point under consideration from the mid-point on the line joining the centres of the spheres.
r = Radius of the spheres.
V = Potential difference between the spheres.

The above expression assumes that both spheres are isolated from earth, but Reference 19 (p. 27) indicates that the effect of earthing one sphere would be small when $d/r \leqslant 0{\cdot}5$ (e.g. the error in E would be about 0·5% or less, except for the 2 cm spheres where it might be about 2%). In the case of the 2 cm spheres the calculated values of E in the centre of the gap may be high, which would make α change to a higher value.

The field distribution and the distribution of α along the axis of the gap in the case of 6·25 cm spheres at maximum ionization effect are illustrated in Fig. 5. The values of α used in plotting Fig. 5 and also for Table 1 are those of Harrison and Geballe.[20]

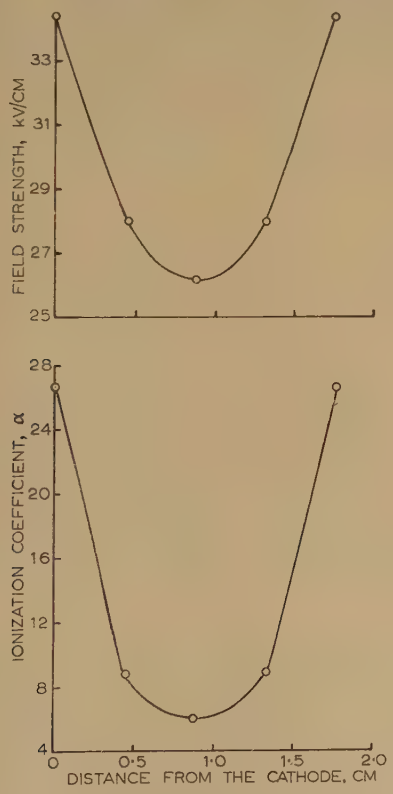

Fig. 5.—Distribution of field strength and ionization coefficient along the axis of the gap.

Sphere diameter, 6·25 cm.
Gap length, 1·75 cm, giving maximum irradiation effect.

Thus, at the gap lengths which gave the maximum ionization effect the field strength distribution and the distribution of α along the axis of the gap vary widely for different sizes of sphere. Nevertheless the minimum field strength in the middle of the gap was approximately the same in each case, and in air it was about 26 kV/cm. This gives an ionization coefficient of 6–7·5 (see Table 2). If the attachment coefficient η is taken into account, the extent of ionization by collision processes will be dependent on the difference $(\alpha - \eta)$. This difference will be less than α by a factor of about 2 near the centre of the gap. In such a case a single avalanche is unlikely to traverse the full gap.

An attempt was made to demonstrate that the gap which gave the maximum ionization effect depended on the distribution of α along the axis of the gap. The gap field was distorted by reducing the radial clearance with an earthed metal cylinder. This cylinder, of radius equal to 1·2 times the sphere diameter, was positioned concentrically with the gap axis to surround the gap. Fig. 6 compares the results of this arrangement with those

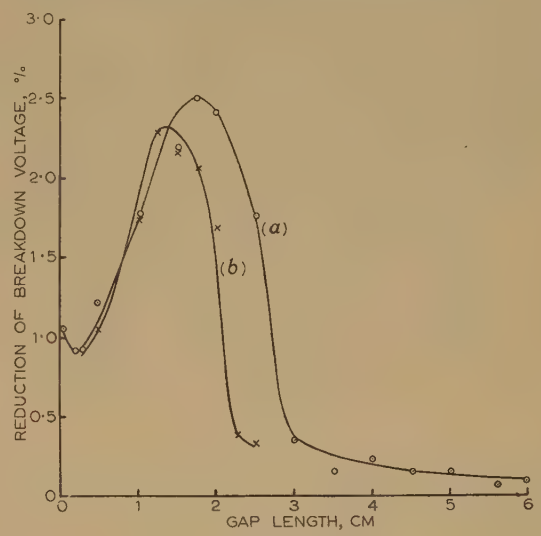

Fig. 6.—Influence of clearance from the gap to surrounding objects on the irradiation effect.

(*a*) Normal clearance, as in Fig. 1, Curve (*b*).
(*b*) Radial clearance from gap axis reduced to 7·5 cm by an earthed cylinder.
Sphere diameter, 6·25 cm.
Sphere material, copper.

for a normal clearance for 6·25 cm-diameter spheres. (It should be noted that in order to make an appreciable change in the field distribution of a small gap the clearance had to be changed to a small value.)

Fig. 6 demonstrates that the irradiation effect with the distorted field followed a similar trend to that for a normal field distribution, but the maximum effect occurred at a notably different gap setting. The breakdown voltage for the distorted field was 2·5% less than the normal value for this gap, from which it is inferred that the voltage gradient along the axis of the gap was less uniform than normal, as might be expected.

When the field was less uniform, the ratio between the maximum and minimum voltage gradient in the gap would be increased and the whole arrangement would tend to give the effect of smaller sphere sizes (see Table 2). In consequence, the gap which gave the maximum ionization effect would be less than for a normal field. It is assumed that the breakdown with a distorted field occurred when the minimum voltage gradient was about 26 kV/cm.

A further experiment was made to demonstrate the dependence of the gap length for maximum ionization effect on the distribution of α. The effect was studied for a mixture of air and argon in the proportion 10 : 1 by volume. The gap length at which the maximum ionization effect occurred coincided with that in normal air, but the breakdown voltage was reduced by about 13%. The presence of argon augmented the value of α con-

siderably, and consequently the minimum field strength in the middle of the gap required to give the minimum value of α was reduced below 26 kV/cm.

The gap lengths corresponding to the peaks of Fig. 1 may be considered as the critical lengths above which a second breakdown mechanism begins to apply. In the region of the decreasing ionization effect either mechanism might be possible.

The gap lengths with maximum irradiation effect (Fig. 1) were in the region between $\frac{1}{2}d_k$ and d_k, where d_k is the gap length corresponding to Toepler's discontinuity.

The values for d_k as reported by Claussnitzer are given in Table 3. The values of d_k for 6·25 and 12·5 cm diameter sphere

Table 3

CLAUSSNITZER'S GAP LENGTHS FOR TOEPLER'S DISCONTINUITIES AND THE GAP LENGTHS AT WHICH MAXIMUM IONIZATION EFFECT OCCURRED

Sphere diameter	Toepler's values for d_k	Observed gap length for maximum irradiation effect
cm	cm	cm
2·0	0·90	0·80
5·0	2·05	—
6·25	(2·50)	1·75
10	3·65	—
12·5	(4·65)	2·50
15	5·0	—
25	7·15	3·50

electrodes have been interpolated approximately and inserted in brackets; the gap lengths for maximum irradiation effect are also given. The Table shows that these gaps become progressively closer to d_k as the sphere size is reduced.

Claussnitzer,[15] Hueter[21] and Dattan[22, 23] reported an increase in the scatter of the breakdown voltages in the region between $\frac{1}{2}d_k$ and d_k. The present investigation also showed a slight increase in scatter in the region where the ionization effect was decreasing. This greater scatter was least pronounced in the case of the smallest spheres, but was considerable with the larger spheres. This is shown in Fig. 2, where the largest scatter for 2·0 and 12·5 cm-diameter spheres is included. No explanation of the apparent difference in scatter for different sizes of spheres can be offered at this stage.

Finally, there was a difference in the irradiation effects with direct and alternating voltages. Fig. 4 shows that the shape of the curves is the same in each case, and that the same gap lengths gave the maximum effect. However, the magnitudes of the effect were different. This suggests that the magnitude of the effect may be dependent partly on the time of voltage application.

(5) CONCLUSIONS

The present investigations extend the available information on the influence of irradiation on the direct-voltage breakdown of sphere-gaps. Brief checks were also made with 50 c/s alternating voltages. A study was made over a wide range of sphere-gaps with spheres of different diameters. This showed that 0·5 mg of radium, suitably placed inside one sphere, lowered the breakdown voltage appreciably. A small reduction was also observed with parallel-plane electrodes (Fig. 1). The extent of the reduction varied with the electrode spacing for a particular size of sphere electrode. It varied also with the size of the spheres, and the greatest reduction was obtained with the smallest spheres.

In all the cases (except when the parallel-plane electrodes were used) the irradiation had a maximum effect with a particular spacing which was found to depend on the distribution of the ionization coefficient α across the gap.

It is suggested that this spacing defines a maximum gap length below which one breakdown mechanism operates. When the gap length is increased beyond this spacing, some other breakdown mechanism begins to have an influence.

The spacing which gave the maximum effect of irradiation was within the range of gap lengths between $\frac{1}{2}d_k$ and d_k. Meek[13] considers that there is a change from one mechanism to another in this region.

The irradiation effect was comparatively large with very small gaps of 1 mm or less, and this was due to scarcity of electrons to initiate the breakdown. The phenomenon occurred with direct voltages, even when the time of voltage application was effectively several seconds, and it has also been noticed with alternating voltages.[8] With both small and large gaps it constitutes the cause of the statistical delay for an impulse-voltage breakdown.

When the gap length was increased to 1–5 mm the radium had an effect which was smaller than that noted for very short gaps. Further increases in gap length resulted in an increasing radium effect, which continued to increase with gap length until the maximum effect was obtained at a particular spacing as noted above. The effect of irradiation in this range of gap lengths may be explicable by considering the field distortion caused by small space charges. Thus, the longer the gap the larger was the gas-amplified current and the greater was the distortion. Consequently, when radium was present there was a larger initial ion current in the gap and the correspondingly large degree of field distortion resulted in a reduced breakdown voltage.

In the region of gap lengths greater than that which gave the maximum influence of irradiation, the ionization coefficient α at the centre of the gap fell to a value less than 7·5. Then a different mechanism is thought to come into play. The integral $\int_0^d \alpha dx$ increases with gap length, and with it the distortion is likely to increase, but the effect becomes progressively masked, possibly by some secondary effect which may become prominent with longer gaps.

Finally, the investigations indicate that in specifying the minimum breakdown for direct and alternating voltages it is necessary to define carefully the level of initial ionization.

It is suggested in B.S. 358 that for voltages below 50 kV additional ionization should be used. This statement is clearly insufficient. As is seen from the present work, the presence of 0·5 mg of radium will change the breakdown voltage of 6·25 cm-diameter spheres at about 50 kV by more than 2·5% and that of 12·5 cm-diameter spheres at 70 kV by more than 2%.

(6) ACKNOWLEDGEMENTS

The author wishes to thank Mr. A. S. Husbands for his suggestions and encouragement, Mr. K. J. Cornick for the development and construction of the measuring and control equipment and for his participation in the measurements, and Mr. F. S. Edwards for his support and encouragement of the programme.

The author is grateful to Sir Willis Jackson, F.R.S., Director of the Research and Education Departments, Metropolitan-Vickers Electrical Co. Ltd. and Dr. J. M. Dodds, Manager of the Research Department for permission to publish the paper.

(7) REFERENCES

(1) MEEK, J. M.: 'The Influence of Irradiation on the Measurement of Impulse Voltages with Sphere Gaps', *Journal I.E.E.*, 1946, **93**, Part II, p. 97.

(2) HAGENGUTH, J. H.: 'Short-time Spark-Over of Gaps', *Transactions of the American I.E.E.*, 1937, **56**, p. 67.
(3) GARFITT, D. E. M.: 'The Measurement of Impulse Voltages by Means of Small Sphere Gaps', *Proceedings of the Physical Society*, 1942, **54**, p. 109.
(4) NORD, G. L.: 'Effect of Ultraviolet on Breakdown Voltage', *Transactions of the American I.E.E.*, 1935, **54**, p. 955.
(5) BERKEY, W. E.: 'Radium Improves Operation of Spark Gaps', *Electric Journal*, 1934, **31**, p. 101.
(6) ROGOWSKI, W., and JAM, R.: 'Quecksilberlampe und Radium als Vorionisatoren. Ihr Einflus auf den elektrischen Funken', *Archiv für Elektrotechnik*, 1928, **20**, p. 107.
(7) WHITEHEAD, S., and CASTELLAIN, A. P.: 'Sphere-Gap Calibration', *Journal I.E.E.*, 1931, **69**, p. 898.
(8) EDWARDS, F. S., and SMEE, J. F.: 'The Calibration of the Sphere Spark-Gap for Voltage Measurement up to One Million Volts at 50 cycles', *ibid.*, 1938, **82**, p. 655.
(9) KLEMM, A.: 'Anfangsspannungen und Durchbruchsfeldstärke von Kugelektroden bei Gleichspannung', *Archiv für Elektrotechnik*, 1923, **12**, p. 553.
(10) HARDY, D. R., and BROADBENT, T. E.: 'The Effect of Irradiation on the Calibration of 2·0-cm-diameter Sphere-Gaps', *Proceedings I.E.E.*, Paper No. 1682 M, August, 1954 (**101**, Part II, p. 438).
(11) 'Measurement of Voltage with Sphere Gaps', B.S. 358 : 1939.
(12) LOEB, L. B., and MEEK, J. M.: 'The Mechanism of the Electric Spark' (Oxford University Press, 1941).
(13) MEEK, J. M.: 'The Electric Spark in Air', *Journal I.E.E.*, 1942, **89**, Part I, p. 335.
(14) TOEPLER, M.: 'Knickstelle in Verlaufe der Anfangspannung', *Elektrotechnische Zeitschrift*, 1932, **53**, p. 1219.
(15) TOEPLER, M.: 'Zur Spannungsmessung mittels Grenzspannungen und Funkenspannungen', *Archiv für Elektrotechnik*, 1936, **30**, p. 663.
(16) CLAUSSNITZER, J.: 'Zur Messung mit Kugelfunkenstrecken', *Elektrotechnische Zeitschrift*, 1936, **57**, p. 177.
(17) JØRGENSEN, M. O.: 'Elektrische Funkenspannungen' (Copenhagen, 1943).
(18) LLEWELLYN JONES, F.: 'Electrical Discharges', *Reports on Progress in Physics*, 1953, **16**, p. 216.
(19) DEAN, G. E., quoted by PEEK, F. W.: 'Dielectric Phenomena in High Voltage Engineering' (McGraw-Hill, 1929), pp. 27 and 69.
(20) HARRISON, M. A., and GEBALLE, R.: 'Simultaneous Measurement of Ionization and Attachment Coefficients', *Physical Review*, 1953, **91**, p. 1.
(21) HUETER, E.: 'Über die Messung des Schneitelwertes Wechselspannungen Mitels der Kugelfunkenstrecke', *Elektrotechnische Zeitschrift*, 1936, **57**, p. 621.
(22) DATTAN, W.: 'Beitrag zur Frage des Anordnungsspannung bei Einpoliggeerdeten Kugelfunkenstrecken', *Archiv für Elektrotechnik*, 1937, **31**, p. 342.
(23) DATTAN, W.: 'Zur Eichung von Kugelfunkenstrecken bei Stosspannungen und Normal Frequenz', *Elektrotechnische Zeitschrift*, 1936, **57**, pp. 377 and 412.

621.3.011.1 : 621.319.7

The Institution of Electrical Engineers
Monograph No. 330
Mar. 1959

A METHOD OF SERIES SUMMATION AND ITS APPLICATION TO THE ELECTRIC FORCE IN SPHERE-GAPS

By C. V. JONES, M.Eng., B.Sc., Associate Member.

(*The paper was first received 9th October*, 1958, *and in revised form 16th January*, 1959. *It was published as an* INSTITUTION MONOGRAPH *in March*, 1959.)

SUMMARY

The paper sets out a simple procedure of general application whereby any function represented by a power series may be replaced by a sequence of rational functions, the advantage of such representation being that in many cases the rational functions converge much more rapidly than does the series. It often happens that the rational-function form continues to represent the given function accurately for values of the argument which make the series form diverge.

The procedure is illustrated with a worked example, and the method is then applied to determine a simple expression for the maximum electric intensity between two equal charged spheres, when the sphere-gap is small compared with the diameters.

(1) INTRODUCTION

Infinite power series occur in the solution of many engineering problems, notably in electromagnetism, and it frequently happens that over the range of values of most practical interest the series either converge very slowly or else diverge.

The paper sets out a simple procedure of general application, whereby any power series may be replaced by a sequence of rational functions, the advantage of such representation being that in many cases the rational functions converge much more rapidly than does the series. When both forms of a given function are considered together, it frequently happens that the rational-function form continues to represent the given function accurately for values of the argument which make the series form diverge.

The procedure to be described was developed by the author from first principles to sum a particular ill-conditioned series, but it would seem to be basically similar to a method first invented by Euler[1,2] and later extended by Gauss,[3] Stieljes[4] and other mathematicians.[5,6] The differences of the present treatment are considered in the conclusion.

The result of the process may be illustrated by means of the following rational function (to be derived later):

$$f(x) = \frac{60x + 60x^2 + 11x^3}{60 + 90x + 36x^2 + 3x^3} \quad . \quad . \quad . \quad . \quad (1)$$

For small values of x, the function may be converted into a power series by simple long division, giving:

$$f(x) = x - \tfrac{1}{2}x^2 + \tfrac{1}{3}x^3 - \tfrac{1}{4}x^4 + \tfrac{1}{5}x^5 - \tfrac{1}{6}x^6 \quad . \quad . \quad (2)$$

the first six terms shown being those of the series expansion of $\log(1 + x)$. For small values of x both expressions give the same result. For $x = 0{\cdot}1$, for example, both give the correct value of 0·095 310 for log 1·1.

The situation is quite different for larger values of x. In the first place there is a limit to the range of convergence of the power series which occurs for $x = 1$, and here the value of 0·6167 given by the sum of the six terms shown in eqn. (2) is but a poor approximation to log 2. The rational function, however, gives 0·693 12, which compares favourably with the correct value of 0·693 15. For $x = 2$ the power series diverges, whereas the rational function gives 1·0980, a fair approximation to the correct value of 1·0986 (log 3).

Eqn. (1) is the rational function obtained from the first six terms of the power series given by eqn. (2). By taking different numbers of terms in turn, a sequence of rational functions is obtained, and the advantage of the process is that the ranges of convergence of the series and the sequence are quite different and frequently to the marked advantage of the latter, as in the example.

(2) DERIVATION OF THE RATIONAL FUNCTIONS

The rational functions are most conveniently derived from the power series in two stages. First, the power series

$$f(x) = a_1x + a_2x^2 + a_3x^3 + a_4x^4 + \ldots \quad . \quad (3)$$

is replaced by the continued fraction

$$f(x) = \cfrac{b_1x}{1 + \cfrac{b_2x}{1 + \cfrac{b_3x}{1 + \ldots}}} \quad . \quad . \quad (4)$$

It is a simple matter to derive general expressions for the b-coefficients in terms of the a-coefficients, but it is more satisfactory to derive their numerical values individually for each particular series according to the method shown in Table 1.

Table 1

DERIVATION OF CONTINUED FRACTION FROM POWER SERIES

b	x	x^2	x^3	x^4	x^5	x^6
	1					
	1	−1/2	1/3	−1/4	1/5	−1/6
1	1	−1/2	1/3	−1/4	1/5	−1/6
	1/2	−1/3	1/4	−1/5	1/6	
1/2	1	−2/3	1/2	−2/5	1/3	
	1/6	−1/6	3/20	−2/15		
1/6	1	−1	9/10	−4/5		
	1/3	−2/5	2/5			
1/3	1	−6/5	6/5			
	1/5	−3/10				
1/5	1	−3/2				
	3/10					
3/10	1					

In the body of the Table, the first row consists of unity in the left-hand column, and the second row the coefficients of the power series under consideration—here the logarithmic series is again chosen as illustration. The third row is obtained by dividing the second row by the coefficient of the first term in that row. The fourth row is obtained by subtracting the third

Correspondence on Monographs is invited for consideration with a view to publication.

Mr. Jones is in the Department of Electrical Engineering, University of Liverpool.

row from the first and moving the new coefficients one place to the left. These two basic processes are then repeated alternately on successive rows. The b-coefficients of the continued fraction are the divisors shown to the left of the main Table.

The continued fraction for the logarithmic series is thus

$$f(x) = \cfrac{x}{1 + \cfrac{\frac{1}{2}x}{1 + \cfrac{\frac{1}{6}x}{1 + \cfrac{\frac{1}{3}x}{1 + \cfrac{\frac{1}{5}x}{1 + \cfrac{\frac{3}{10}x}{1 + \ldots}}}}}} \quad \ldots \quad (5)$$

In the second stage, the continued fraction is replaced by its successive convergents $c_1, c_2, \ldots c_n, \ldots$, where the nth convergent c_n is obtained by rationalizing the first n terms of the fraction. The following recurrence formulae are readily derived by induction:

$$c_n = A_n/B_n \quad \ldots \quad (6)$$

$$\left.\begin{aligned} A_n &= A_{n-1} + b_n x A_{n-2} \\ B_n &= B_{n-1} + b_n x B_{n-2} \end{aligned}\right\} \quad \ldots \quad (7)$$

with $A_0 = 0$, $A_1 = b_1 x$, $B_0 = B_1 = 1$.

Eqn. (1) is the 6th convergent found from eqn. (5) in this manner. In general, however, it is more satisfactory to introduce numerical values before determining the convergents rather than to evaluate the rational functions.

Table 2

RATIONAL FUNCTION APPROXIMATIONS TO LOG $(1 + x)$

$x = 1$	$x = 2$	$x = -1$	$x = -2$
$\log 2 = 0{\cdot}693\,15$	$\log 3 = 1{\cdot}098\,61$	$\log 0 = -\infty$	$\log(-1) = j\pi$
1	2	-1	-2
0·67	1	-2	∞
0·70	1·14	$-2\frac{1}{2}$	4
0·692	1·091	-3	0
0·693 3	1·101	$-3\frac{1}{3}$	$-2{\cdot}7$
0·693 12	1·098 0	$-3\frac{2}{3}$	∞
0·693 15	1·098 8	$-3\frac{1}{11}\frac{1}{2}$	3·6
	1·098 6	$-4\frac{1}{6}$	0

Table 2 shows successive convergents for log 2 and log 3 derived from eqns. (5), (6) and (7). It is seen that convergence is rapid.

(3) TESTS FOR CONVERGENCE

Convergence of the rational functions depends upon the convergence of the continued fraction, since the derivation of this form from the original series is always legitimate. The general problem of the convergence of continued fractions is exceedingly complex.[5] A simple test of limited application is the following. The continued fraction will converge[2] if $b_n x > 0$ and if the series $\sum_{n=1}^{\infty} 1/b_n x$ is divergent. It so happens that for the logarithmic series considered above a general expression for b_n can be derived [$b_n = (n-1)/4n$ if n is odd; $b_n = n/4(n-1)$ if n is even], and it is easily confirmed that eqn. (5) converges for all positive values of x.

For most practical series, however, it is not possible to deduce a general form of expression for b_n, nor is the quantity $b_n x$ invariably positive, so that the simple test for convergence is not applicable.

Engineering problems are concerned with the values of specific continued fractions for one or more specific values of x rather than with the general analytical problem of convergence, and under these conditions the following very simple test may be used. It follows at once from eqns. (6) and (7) that, if two successive convergents c_{n-2} and c_{n-1} have the same value c, then c_n and all following convergents have the same value c, which is the value of the function. In practical problems exact equality between two successive convergents cannot be expected, but it is sufficient to continue the calculation until the difference is less than the tolerable error.

Reference to Table 2 shows that convergence is obvious for $x = 1$ and $x = 2$. For $x = -1$ it is clear that the differences between the successive convergents shown are

$$-1, -1, -\tfrac{1}{2}, -\tfrac{1}{2}, -\tfrac{1}{3}, -\tfrac{1}{3}, -\tfrac{1}{4}, \ldots$$

so that the sequence is divergent to $-\infty$. This is the value of the corresponding function log 0. As a final example the values for $x = -2$ are shown in Table 2. The logarithmic function now has an imaginary value, and this is indicated by the fact that successive convergents now oscillate. In short, it is believed that both convergence, which is normal, and non-convergence, which is very rare, will at once be apparent from the general behaviour of the sequence.

It has been convenient to use the logarithmic series by way of illustration, but the process is of general application and a practical problem is now considered.

(4) ELECTRIC FORCE BETWEEN TWO EQUAL SPHERES

The sphere-gap is the standard apparatus for the measurement of high voltages, and a knowledge of the intensity of the electric field between the electrodes is of value.

From an expression given by Dean[7] for the voltage distribution between two equal charged conducting spheres of radii a and spacing $2d$, the following expressions for the per-unit gradients on the line of centres may be found. A is a point on the electrode and B is the centre of the system.

$$E'_A = \frac{c}{a}\left(\sqrt{\frac{d+a}{2a}}\right)(S+T) \quad \ldots \quad (8)$$

$$E'_B = 2\frac{(d-a)}{c}(S-T) \quad \ldots \quad (9)$$

where

$$S = \sum_{m=0}^{\infty} (-1)^m \frac{(2m+1)}{y^{2m+1}-1} \quad \ldots \quad (10)$$

$$T = \sum_{m=0}^{\infty} (-1)^m \frac{(2m+1)}{y^{2m+1}+1} \quad \ldots \quad (11)$$

and

$$y = \sqrt{\left(\frac{c+d}{a}\right)} \qquad c^2 = d^2 - a^2 \quad \ldots \quad (12)$$

The S and T series converge rapidly for large values of the ratio d/a, but the gradient is of most interest in practice for small air-gaps, that is for d/a, and hence y, close to unity. That both series are ill-conditioned for such values is best seen by considering a numerical example.

Let $d/a = 1{\cdot}01$. Then $c/a = 0{\cdot}141\,77$ and $y = 1{\cdot}073\,2$. The first terms in the S series are

$$S = 13{\cdot}660 - 12{\cdot}707 + 11{\cdot}800 - 10{\cdot}942 + 10{\cdot}128 \quad (13)$$

It is clear that the series converges slowly, and summation by conventional methods would be difficult. Routine application

of the rational-function approximation gives the following continued fraction:

$$S = \cfrac{13{\cdot}660}{1 + \cfrac{0{\cdot}93024}{1 - \cfrac{0{\cdot}00154}{1 + \cfrac{0{\cdot}925}{1 - \cfrac{0{\cdot}004}{1 + \ldots}}}}} \quad . \; . \; (14)$$

the corresponding convergents being

$$13{\cdot}7,\ 7{\cdot}076,\ 7{\cdot}072,\ 7{\cdot}0740,\ 7{\cdot}0740 \quad . \; . \; (15)$$

Convergence is beyond doubt, the sum of the series to five figures being

$$S = 7{\cdot}0740 \quad . \; . \; . \; . \; . \; . \; . \; (16)$$

The first terms in the T series are

$$T = 0{\cdot}48235 - 1{\cdot}3417 + 2{\cdot}0630 - 2{\cdot}6518 + 3{\cdot}1154 \ldots \quad . \; . \; . \; (17)$$

This series would appear to diverge. The continued fraction is

$$T = \cfrac{0{\cdot}48235}{1 + \cfrac{2{\cdot}7815}{1 - \cfrac{1{\cdot}2439}{1 + \cfrac{0{\cdot}3118}{1 - \cfrac{0{\cdot}0011}{1 + \ldots}}}}} \quad . \; . \; (18)$$

and the convergents are

$$0{\cdot}48,\ 0{\cdot}13,\ -0{\cdot}046,\ 0{\cdot}0088,\ 0{\cdot}0088 \quad . \; . \; (19)$$

In spite of an initial oscillation, final convergence is again beyond doubt, since two successive convergents are equal. The sum of this series to the same scale as before is

$$T = 0{\cdot}0088 \; . \; . \; . \; . \; . \; . \; . \; (20)$$

From eqns. (8), (9), (16) and (20), the values of the per-unit gradients are

$$E'_A = 1{\cdot}0067 \qquad E'_B = 0{\cdot}9967 \quad . \; . \; . \; (21)$$

The effectiveness of the rational function method in summing these difficult series, coupled with the fact that the final gradients are both close to unity, suggests that in this particular case the method might be used to derive power series for the gradients. Let $y = 1 + \varepsilon$, where ε is small: then from eqns. (10) and (11) it is possible to express the a-terms of the S and T series as power series in ε. The results are shown in the top sections of Table 3. The expressions for S and T given in eqns. (10) and (11) may be converted into power series by the artifice of multiplying each term inside the summation sign by x^m. It is the coefficients of powers of x which are given in the top sections of the Table. The b-coefficients of the continued fractions may then be derived as in Table 1. The results are given in the middle sections of Table 3. Finally with $x = 1$ the convergents of the continued fractions, shown in the bottom sections, are evaluated. The sums of the series expressed as power series in ε are therefore

$$S = \frac{1}{2\varepsilon}(1 + \tfrac{1}{2}\varepsilon - \tfrac{1}{6}\varepsilon^2 + \tfrac{1}{12}\varepsilon^3 - \tfrac{11}{180}\varepsilon^4 + \tfrac{1}{20}\varepsilon^5 \ldots) \quad . \; (22)$$

$$T = \frac{1}{2\varepsilon}(\qquad \tfrac{1}{4}\varepsilon^2 - \tfrac{1}{8}\varepsilon^3 + \tfrac{3}{16}\varepsilon^4 - \tfrac{7}{32}\varepsilon^5 \ldots) \quad . \; (23)$$

Table 3

EXAMPLE OF THE APPLICATION OF THE RATIONAL-FUNCTION APPROXIMATION

S Series

$$\begin{aligned}
a_1 &= \quad 1/\varepsilon \\
a_2 &= -1/\varepsilon(1 - \varepsilon + 2\varepsilon^2/3 - \varepsilon^3/3 + \varepsilon^4/9 + 0\varepsilon^5) \\
a_3 &= \quad 1/\varepsilon(1 - 2\varepsilon + 2\varepsilon^2 - \varepsilon^3 - \varepsilon^4/5 + 4\varepsilon^5/5) \\
a_4 &= -1/\varepsilon(1 - 3\varepsilon + 4\varepsilon^2 - 2\varepsilon^3 - 2\varepsilon^4 + 4\varepsilon^5) \\
a_5 &= \quad 1/\varepsilon(1 - 4\varepsilon + 20\varepsilon^2/3 - 10\varepsilon^3/3 - 62\varepsilon^4/9 + 12\varepsilon^5) \\
a_6 &= -1/\varepsilon(1 - 5\varepsilon + 10\varepsilon^2 - 5\varepsilon^3 - 17\varepsilon^4 + 28\varepsilon^5)
\end{aligned}$$

$$\begin{aligned}
b_1 &= 1/\varepsilon \\
b_2 &= 1 - \varepsilon + 2\varepsilon^2/3 - \varepsilon^3/3 + \varepsilon^4/9 + 0\varepsilon^5 \\
b_3 &= \quad - \varepsilon^2/3 + 2\varepsilon^3/3 - 29\varepsilon^4/45 + 4\varepsilon^5/15 \\
b_4 &= 1 - \varepsilon - 4\varepsilon^2/5 + 13\varepsilon^3/5 \\
b_5 &= \quad - 16\varepsilon^2/15 + 32\varepsilon^3/15 \\
b_6 &= 1 - \varepsilon
\end{aligned}$$

$$\begin{aligned}
c_1 &= 1/\varepsilon \\
c_2 &= 1/2\varepsilon(1 + \varepsilon/2 - \varepsilon^2/12 \ldots) \\
c_3 &= 1/2\varepsilon(1 + \varepsilon/2 - \varepsilon^2/4 \ldots) \\
c_4 &= 1/2\varepsilon(1 + \varepsilon/2 - \varepsilon^2/6 + \varepsilon^3/12 - \varepsilon^4/120 \ldots) \\
c_5 &= 1/2\varepsilon(1 + \varepsilon/2 - \varepsilon^2/6 + \varepsilon^3/12 - 7\varepsilon^4/180 \ldots) \\
c_6 &= 1/2\varepsilon(1 + \varepsilon/2 - \varepsilon^2/6 + \varepsilon^3/12 - 11\varepsilon^4/180 + \varepsilon^5/20)
\end{aligned}$$

T Series

$$\begin{aligned}
a_1 &= \quad 1/2(1 - \varepsilon/2 + \varepsilon^2/4 - \varepsilon^3/8 + \varepsilon^4/16) \\
a_2 &= -3/2(1 - 3\varepsilon/2 + 3\varepsilon^2/4 + 5\varepsilon^3/8 - 21\varepsilon^4/16) \\
a_3 &= \quad 5/2(1 - 5\varepsilon/2 + 5\varepsilon^2/4 + 35\varepsilon^3/8 - 115\varepsilon^4/16) \\
a_4 &= -7/2(1 - 7\varepsilon/2 + 7\varepsilon^2/4 + 105\varepsilon^3/8 - 329\varepsilon^4/16) \\
a_5 &= \quad 9/2(1 - 9\varepsilon/2 + 9\varepsilon^2/4 + 231\varepsilon^3/8 - 711\varepsilon^4/16)
\end{aligned}$$

$$\begin{aligned}
b_1 &= \quad 1/2(1 - \varepsilon/2 + \varepsilon^2/4 - \varepsilon^3/8 + \varepsilon^4/16) \\
b_2 &= \quad 3(1 - \varepsilon + 0\varepsilon^2 + \varepsilon^3 - \varepsilon^4) \\
b_3 &= -4/3(1 - \varepsilon + 5\varepsilon^2/4 - 3\varepsilon^3/2 - 9\varepsilon^4/4) \\
b_4 &= \quad 1/3(1 - \varepsilon + 2\varepsilon^2 - 3\varepsilon^3 - 36\varepsilon^4) \\
b_5 &= -60(\quad . \quad . \quad . \qquad + \varepsilon^4)
\end{aligned}$$

$$\begin{aligned}
c_1 &= 1/2 - \varepsilon/4 \ldots \\
c_2 &= 1/8 + \varepsilon/32 \ldots \\
c_3 &= -1/16 + 31\varepsilon/128 \ldots \\
c_4 &= \quad \varepsilon/8 - \varepsilon^2/16 + 3\varepsilon^3/32 - 71\varepsilon^4/64 \ldots \\
c_5 &= \quad \varepsilon/8 - \varepsilon^2/16 + 3\varepsilon^3/32 + 89\varepsilon^4/64 \ldots
\end{aligned}$$

It is more convenient to express the results in terms of δ rathe than ε, where $d/a = 1 + \delta$. From eqn. (12),

$$\varepsilon = \sqrt{\tfrac{1}{2}\delta^{1/2}} + \tfrac{1}{4}\delta - \tfrac{1}{32}\delta^2 + \tfrac{1}{128}\delta^3 \ldots \quad . \; (2$$

Substitution of eqn. (24) into eqns. (22) and (23) gives the sum of the S and T series as power series in δ:

$$S = \frac{1}{\sqrt{(2\delta)}}(1 + \tfrac{1}{24}\delta - \tfrac{29}{2880}\delta^2 \ldots) \quad . \; . \; . \; . \; . \; (2$$

$$T = \frac{1}{\sqrt{(2\delta)}}(\qquad \tfrac{1}{8}\delta + \tfrac{1}{64}\delta^2 \ldots) \quad . \; . \; . \; . \; . \; (2$$

Half powers of δ disappear inside the brackets in each serie The multiplying powers expressed in terms of δ become, fro eqns. (8) and (9),

$$\frac{c}{a}\sqrt{\left(\frac{d+a}{2a}\right)} = \sqrt{(2\delta)}(1 + \tfrac{1}{2}\delta) \quad . \; . \; . \; . \; . \; (2$$

$$\frac{2(d-a)}{c} = \sqrt{(2\delta)}(1 - \tfrac{1}{4}\delta + \tfrac{3}{32}\delta^2 \ldots) \quad . \; . \; (2$$

so that the final power series for the gradients become

$$E'_A = 1 + \tfrac{2}{3}\delta + \tfrac{4}{45}\delta^2 \ldots \quad (29)$$

$$E'_B = 1 - \tfrac{1}{3}\delta + \tfrac{4}{45}\delta^2 \ldots \quad (30)$$

It follows that the rational-function method has been used to convert series which converge rapidly for large values of d/a into series which converge rapidly for small ones, and that in the course of the conversion the nature of the series has been changed completely.[8,9]

(5) CONCLUSION AND ACKNOWLEDGMENTS

It would be easy to extend the number of illustrations of the application of the rational-function approximation method, but the examples given are sufficient to show its power and versatility.

The author is grateful to Professor J. M. Meek for continued encouragement. He also wishes to express his thanks to Dr. C. W. Jones, who made a valuable criticism of the first draft of the paper and referred him to the work of Euler, Gauss and Chrystal.

He is indebted to a referee for pointing out that the problem considered is an aspect of the 'problem of moments' and for bringing to his notice the treatises of Wall and of Shohat and Tamarkin. He is indebted to Dr. L. R. Shenton for reading the manuscript and for suggesting further references.[10,11]

From a study of the references above, it seems clear that the method described in the paper is not basically new. Unfortunately the standard textbooks[5,6] can only be understood by those who are thoroughly familiar with advanced concepts of mathematical analysis, so that it seems unlikely that the important results contained in them can be known to more than a few electrical engineers. The treatment given in the paper differs from that in the references in its simplicity and its immediate practical application, questions of generality and rigour having been given the bare minimum of attention.

(6) REFERENCES

(1) EULER, L.: 'De Transformatione Serierum in Fractiones Continuas', Opuscula Analytica (Petropoli, 1785), Vol. 2, p. 138.

(2) CHRYSTAL, G.: 'Algebra', Part II (Adam and Charles Black, Edinburgh, 1889).

(3) GAUSS, K. F.: 'Disquisitiones generales circa seriem infinitam', Werke (Göttingen, 1866), Vol. 3, p. 125.

(4) STIELTJES, T. J.: 'Recherches sur les fractions continues', Oeuvres Complètes (Noordhoff, Groningen, 1918), Vol. 2, p. 398.

(5) WALL, H. S.: 'Continued Fractions' (Van Nostrand, 1948).

(6) SHOHAT, J. A., and TAMARKIN, J. D.: 'The Problem of Moments' (American Mathematical Society, New York, 1943).

(7) DEAN, G. R.: 'The Potential and Electrostatic Force in the Field of two Metal, Spherical Electrodes', *Physical Review*, 1912, **35**, p. 459.

(8) RUSSELL, A.: 'The Dielectric Strength of Air', *Philosophical Magazine*, 1906, **1**, p. 237.

(9) KIRCHHOFF, G. R.: 'Über die Vertheilung der Elektricität auf zwei leitenden Kugeln', *Gesammelte Abhandlungen* (Leipzig, 1882), p. 78.

(10) SHENTON, L. R.: 'A Determinantal Expansion for a Class of Definite Integral', *Edinburgh Mathematical Proceedings*, 1957, **10**, p. 152.

(11) HILDEBRAND, F. B.: 'Introduction to Numerical Analysis' (McGraw-Hill, 1956).

621.372.543.2

The Institution of Electrical Engineers
Monograph No. 331 E
Mar. 1959

TRANSIENT RESPONSE OF BAND-PASS FILTERS TO MODULATED SIGNALS

By D. Q. MAYNE, M.Sc.(Eng.), Graduate.

(*The paper was first received 25th August, and in revised form 12th December*, 1958. *It was published as an* INSTITUTION MONOGRAPH *in March*, 1959.)

SUMMARY

The process of obtaining the transient response of band-pass filters to a suddenly applied carrier of frequency equal to or differing from the mid-band frequency of the filter is shown to be simplified by the use of Laurent's low-pass band-pass transformation together with suitable approximations. The method is illustrated by an analysis of the *m*-derived band-pass filter. The effect of elements possessing a finite Q-factor is considered and an estimation of the errors due to the approximations used is made.

LIST OF PRINCIPAL SYMBOLS

p = Heaviside's operator.
P = Low-pass band-pass transformation.
$\omega_0/2\pi$ = Mid-band frequency of band-pass filter.
$\omega_f/2\pi$ = Frequency of applied carrier.
$\Delta\omega = \omega_f - \omega_0$.
R_0 = Characteristic resistance of filter.
$\omega_c/2\pi$ = Cut-off frequency of low-pass filter.
$n\omega_0/2\pi$ = Bandwidth of band-pass filter.
$P_1 = 2mP/n\omega_0$.
$p_1 = 2mp/n\omega_0$.
$\Delta\omega_1 = 2m\Delta\omega/n\omega_0$.
$\tau = n\omega_0 t/2m$.
$\alpha = m^2/2$.
$\omega = m\sqrt{(1 - m^2/4)}$.
Q = Q-factor of LC circuit.
$\beta = \omega_0/2Q$.
$\beta_1 = 2m\beta/n\omega_0$.
$a(t)$ = In-phase component of response.
$b(t)$ = Quadrature component of response.

(1) INTRODUCTION

The low-pass band-pass transformation has often been used in the frequency domain to aid the analysis of band-pass filters in terms of the known properties of low-pass filters.[1,2,3] Laurent[4] first applied this transformation, suitably generalized, to the analysis of the transient response of band-pass filters subjected to the unit step function, and summarized his method in a complex formula analogous to Heaviside's expansion theorem. By means of this formula the response of a complex filter (e.g. a band-pass filter) could be expressed in terms of the known response of a simple filter (e.g. a low-pass filter) from which the complex filter was derived by substituting for p a function $P(p)$. Laurent's method has not been employed subsequently for transient analysis apart from an attempt by Tucker,[5] who reports that incorrect amplitude terms were obtained. In order to obtain the response of an *m*-derived band-pass filter to a suddenly applied carrier of mid-band frequency (subsequently called the symmetric case) Tucker resorted to semi-empirical methods. However, he employed in his analysis a factor $M = (m/n)(p/\omega_0 + \omega_0/p)$ which is very similar to the low-pass band-pass transformation employed by Laurent. Eaglesfield[6] showed that, for a narrow pass-band, the factor M could be considerably simplified in the transient analysis for the symmetric case. Eaglesfield's result revealed, for the particular case considered, that the envelope of the response is equal to the response to a step function of a *m*-derived low-pass filter of cut-off frequency equal to half the bandwidth of the band-pass filter.

The solution for the symmetric case is relatively simple. However, in the circuits used in selective sideband apparatus, in stagger-tuned intermediate-frequency amplifiers and in other cases when the frequency of the applied carrier does not correspond to the mid-band frequency of the network, the solution becomes more complex. In these asymmetric cases, not only the envelope of the response but also the phase undergoes change. The response may therefore be regarded as having in-phase and quadrature components, $a(t)$ and $b(t)$ respectively, relative to the applied carrier, the envelope of the response being $\sqrt{(a^2 + b^2)}$. Because of the quadrature component, the waveform of the response depends on the depth to which a carrier is modulated by a step function and the simple transient low-pass band-pass analogy does not hold, except for two limiting cases of low-modulation or symmetrically-placed carrier, where the quadrature component becomes negligible.[7,8]

It is the purpose of the paper to present a general method of analysis for the response of band-pass filters when subjected to a carrier modulated by a step function, the analysis being valid for large modulation factors in the asymmetric case. As most filters are of T or π configuration, a general transfer function for each of these networks is given. Laurent's transformation is presented and it is shown how it is radically simplified for the case of a narrow pass-band. For the symmetric case, the solution reduces to that obtained by Eaglesfield.[6] A detailed derivation of the approximation for narrow pass-band is given, thus permitting an estimation of the error due to approximation to be made. It is shown how the effect of elements possessing finite, instead of infinite, Q-factors can be taken into account. The entire analysis is illustrated by its application to the *m*-derived band-pass filter, an example first considered by Tucker.[5]

In the analysis which follows, operational as opposed to symbolic calculus is employed. Thus, the operator p must be understood as $1/Q$ where $Q = \int_0^t dt$. The use of the operator Q has been amply justified by Jeffreys[10] and Dalton.[11] It is interesting to note that, because the operational method employs integration over a finite time, it is equipped to handle functions of time such as $\exp(\alpha t^2)$ which cause divergence when the Laplace transform is employed. However, this is not fundamental to the present paper. The expansion formula, e.g. eqn. (6), can be derived using the classical method, operational calculus or symbolic calculus.

(2) TRANSFER FUNCTION OF T AND π NETWORKS

The T and π networks form the basic elements of most filter circuits and their symmetry facilitates the analysis of transient

Correspondence on Monographs is invited for consideration with a view to publication.
Mr. Mayne is in the Department of Electrical Engineering, University of Witwatersrand, Johannesburg.

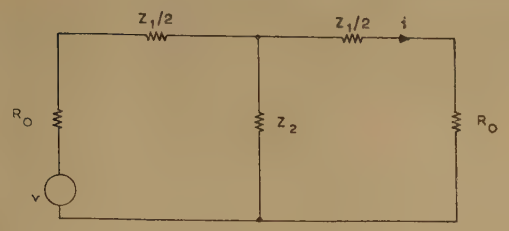

Fig. 1.—Single T element.

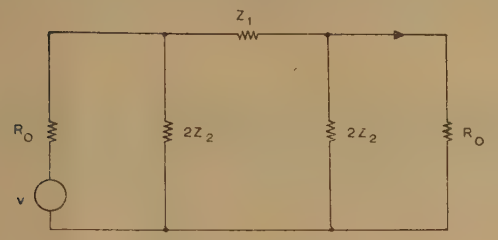

Fig. 2.—Single π element.

response. The equation relating response, i, to input, v, for the single T element (Fig. 1) is

$$i = \frac{1}{(1 + Z_1/2R_0)(1 + Z_1/4Z_2 + R_0/2Z_2)} \frac{v}{2R_0} \quad . \quad (1)$$

so that the transfer function is $1/2R_0[(1 + Z_1/2R_0)(1 + Z_1/4Z_2 + R_0/2Z_2)]$.

The corresponding equation for the single π element (Fig. 2) is

$$i = \frac{1}{(1 + R_0/2Z_2)(1 + Z_1/2R_0 + Z_1/4Z_2)} \frac{v}{2R_0} \quad . \quad (2)$$

so that the transfer function is

$$1/2R_0[(1 + R_0/2Z_2)(1 + Z_1/2R_0 + Z_1/4Z_2)]$$

As the denominator of the transfer functions possess two factors, the transient analysis (which always involves factorization) is simplified.

(3) LOW-PASS BAND-PASS TRANSFORMATION

It is found inconvenient to use Laurent's method in the form he suggested. The low-pass band-pass transformation $P = p(1 + \omega_0^2/p^2)$, where $\omega_0^2 = 1/LC$, which he employs is, however, very useful. For convenience, this transformation will be modified slightly to give

$$P = \tfrac{1}{2}(p + \omega_0^2/p) \quad . \quad . \quad . \quad . \quad . \quad . \quad (3)$$

where $\omega_0^2 = 1/LC$

This transformation changes a simple inductor of value L into an inductor of value $L/2$ in series with a capacitor, the resonant frequency of the combination being $\omega_0/2\pi$. Thus, pL becomes $PL = pL/2 + \omega_0^2 L/2p = pL/2 + 1/p2C$. A capacitor of value C is transformed into a parallel circuit consisting of a capacitor of value $C/2$ and an inductor, the resonant frequency of the combination being $\omega_0/2\pi$. Thus $1/pC$ becomes

$$\frac{1}{PC} = \frac{1}{(pC/2 + \omega_0^2 C/2p)} = \frac{p2L(2/pC)}{p2L + 2/pC}$$

Terman,[12] in the design of low-pass sections, expresses all inductances in terms of inductance $L_k' = 2R_0/\omega_c$, where $\omega_c/2\pi$ is the cut-off frequency. Applying the transformation of eqn. (3) would yield inductance $L_k = L_k'/2 = R_0/\omega_c$. However, the corresponding inductance employed by Terman for the design of a band-pass section is $L_k = 2R_0/n\omega_0$, where $n\omega_0/2\pi$ is the bandwidth, so that $\omega_c = n\omega_0/2$. Therefore application of the transformation to a conventional low-pass network yields a band-pass network, of central frequency $\omega_0/2\pi$, having a bandwidth $n\omega_0/2\pi$ equal to twice the cut-off frequency $\omega_c/2\pi$ of the original low-pass network.

(4) APPROXIMATION FOR NARROW PASS-BAND

An important simplification can be made if the pass-band is small compared with the centre frequency of the filter. If $A(p)/B(p)$ is the transfer function of the filter, the response to a suddenly applied carrier of frequency $\omega_f/2\pi$ is $[A(p)/B(p)] \exp(j\omega_f t)H(t)$, where $H(t)$ is the unit step function. This can be expressed as

$$\exp(j\omega_f t)[A(p + j\omega_f)/B(p + j\omega_f t)]H(t)$$

by the application of Heaviside's shifting theorem. $[A(p + j\omega_f)/B(p + j\omega_f)]H(t)$ will be called the modulation function and is denoted $g(t)$.

More generally, the response to a sudden application $\exp(j\omega_f t)H(t - t_0)$, at an arbitrary phase, $(\omega_f t_0)$, of the carrier is $\exp(j\omega_f t)g(t - t_0)$, so that the modulation function, referred to the instant $t = t_0$ of application, is independent of the carrier phase at this instant. In particular, the in-phase and quadrature components of the modulation function are also independent of carrier phase.

A band-pass circuit has the characteristic that its natural modes are clustered about the frequency $\omega_0/2\pi$ which is the centre of the pass-band. This is illustrated in Fig. 3, where the

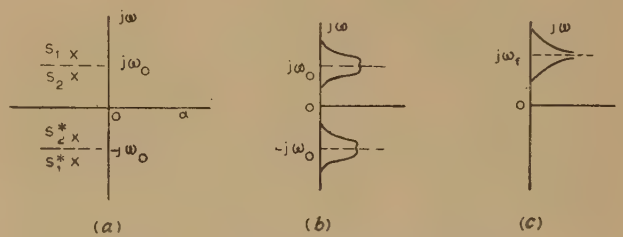

Fig. 3.—Typical properties of $A(p)/B(p)$.
(a) Distribution of poles.
(b) Frequency characteristic, $|A(j\omega)/B(j\omega)|$.
(c) Spectrum, $|1/j(\omega - \omega_f)|$ of applied voltage.

poles S_1, S_1^*, S_2, S_2^*, etc., of $A(p)/B(p)$ are shown. The modulus of $A(p)/B(p)$ would then vary along the imaginary axis as shown by the plot of $|A(j\omega)/B(j\omega)|$, which is the conventional frequency characteristic of the filter. The spectrum $|V(j\omega)| = |1/j(\omega - \omega_f)|$ of the applied voltage $\exp(j\omega_f t)H(t)$ for the general case $\omega_f \neq \omega_0$ is also shown. The fact that p is replaced by $p + j\omega_f$ to obtain the modulation function means that the entire plot on the complex-frequency plane will be displaced by an amount $-j\omega_f$, as shown in Fig. 4. There are two sets of poles: one set, $S_a = (S_1 - j\omega_f)$, $S_b = (S_2 - j\omega_f)$, etc., is clustered about the point $-j(\omega_f - \omega_0)$; the other set, $S_\alpha = (S_1^* - j\omega_f)$, $S_\beta = (S_2^* - j\omega_f)$, etc., is clustered about the point $-j(\omega_f + \omega_0)$. The spectrum of the applied voltage is now symmetrically disposed about the axis $j\omega = 0$ and is, in fact, the spectrum $|1/j\omega|$ of $H(t)$. If $\omega_f + \omega_0$ is very large compared with the pass-band $n\omega_0$, the spectrum, $1/\omega$, of the applied voltage will fall to a negligible value near the point $-j(\omega_f + \omega_0)$. This means that the natural modes S_α, S_β, etc.,

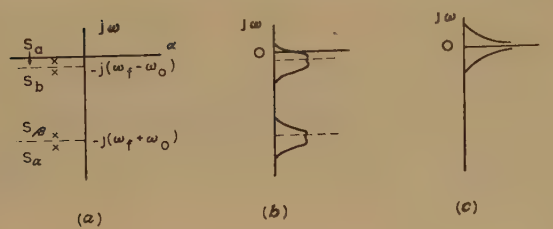

Fig. 4.—Typical properties of $A(p+j\omega_f)/B(p+j\omega_f)$.
(*a*) Distribution of poles.
(*b*) Frequency characteristic, $|A[j(\omega+\omega_f)]/B[j(\omega+\omega_f)]$.
(*c*) Spectrum $|1/j\omega|$ of $H(t)$.

will not be excited and the response (i.e. the modulation function) will be due only to those poles S_a, S_b, etc., which are clustered about the point $-j(\omega_f-\omega_0)$. In operational form, this approximation can be derived as follows. The modulation function is

$$g(t)=\frac{A(p+j\omega_f)}{B(p+j\omega_f)}H(t)$$

$$=\frac{C(p)}{D(p)}H(t) \quad . \quad . \quad . \quad . \quad . \quad . \quad (4)$$

where $C(p)=A(p+j\omega_f)$, $D(p)=B(p+j\omega_f)$

or $$g(t)=I_a\exp(S_at)+I_b\exp(S_bt)+\ldots$$
$$+I_\alpha\exp(S_\alpha t)+I_\beta\exp(S_\beta t)+\ldots \quad . \quad (5)$$

assuming the zeros S_a, S_b, . . . S_α, S_β . . . of $D(p)$ are all simple and distinct, where, by the expansion formula,†

$$I_r=\left[\frac{(p-S_r)C(p)}{pD(p)}\right]_{p=S_r},\ r=a,b\ldots\alpha,\beta \quad . \quad (6)$$

since $D(p)=K(p-S_a)(p-S_b)\ldots(p-S_\alpha)(p-S_\beta)\ldots$

If the filter possesses a narrow pass band (i.e. n small) and if $\omega_f-\omega_0$ is small, then $|S_a|$, $|S_b|$, etc., will be small (of the order $n\omega_0/2$) and $|S_\alpha|$, $|S_\beta|$, etc., will be large (of the order $2\omega_0$). The limiting case of an infinitely narrow relative band-pass filter is obtained by allowing $n\to 0$, preserving the band-pass characteristic (and therefore maintaining the values of S_a, S_b, etc.) by keeping $n\omega_0$ constant. For finite bandwidth, $n\omega_0$, as $n\to 0$, $\omega_0\to\infty$. Under these conditions $|S_\alpha|$, $|S_\beta|$, etc., tend to infinity while $|S_a|$, $|S_b|$, etc., remain unaltered. Also $K\to 0$ in such a way that $KS_\alpha S_\beta\ldots$ remains constant and therefore finite. Therefore, for infinitely narrow relative pass band,

$$I_a=\lim_{\omega_0,\omega_f\to\infty}\left[\frac{(p-S_a)C(p)}{pD(p)}\right]_{p=S_a}$$

$$=\lim_{\omega_0,\omega_f\to\infty}\frac{C(S_a)}{S_aK(S_a-S_b)(S_a-S_c)\ldots(S_a-S_\alpha)(S_a-S_\beta)\ldots}$$

or $$I_a=\frac{C(S_a)}{S_aK(S_a-S_b)(S_a-S_c)\ldots(-S_\alpha)(-S_\beta)\ldots} \quad . \quad (7)$$

Similar expressions exist for I_b, I_c, etc.

The same result is obtained if $\lim_{\omega_0,\omega_f\to\infty}\frac{C(p)}{D(p)}$ is obtained prior to application of the expansion theorem. As $\omega_0\to\infty$, so do the roots S_α, S_β, etc., resulting in the replacement of the factors $(p-S_\alpha)$, $(p-S_\beta)$, etc., of $D(p)$ by $(-S_\alpha)$, $(-S_\beta)$, etc. This reduces the degree of $D(p)$, facilitating both the process of finding the roots S_a, S_b, etc., and the calculation of I_a, I_b, etc.

For the infinitely narrow relative pass-band,

$$I_\alpha=\lim_{\omega_0,\omega_f\to\infty}\left[\frac{(p-S_\alpha)C(p)}{pD(p)}\right]_{p=S_\alpha} \quad . \quad . \quad . \quad (8)$$

While $\frac{(p-S_\alpha)}{D(p)}$ will have a finite value at $p=S_\alpha$, even if ω_0 and therefore S_α, approach infinity, $1/p$ becomes $1/s_\alpha$, which will be zero in the limit. Therefore $I_\alpha=I_\beta=I_\gamma\ldots\to 0$ as $\omega_0\to\infty$.

(5) MODIFICATION OF LOW-PASS BAND-PASS TRANSFORMATION FOR MODULATED SIGNALS

If $Y(p)$ is the transfer function of a low-pass filter, the response of a band-pass filter to a suddenly applied carrier $\exp(j\omega_f t)H(t)$ is

$$i=Y(P)\,.\,\exp(j\omega_f t)H(t),\ \text{where } P=P(p)$$

or $$i=\exp(j\omega_f t)Y[P(p+j\omega_f)]H(t) \quad . \quad . \quad . \quad . \quad (9)$$

The modulation function is

$$g(t)=Y[P(p+j\omega_f)]H(t) \quad . \quad . \quad . \quad . \quad (10)$$

For a narrow band-pass filter the approximation outlined in Section 4 can be employed.

Thus $$g(t)\simeq\lim_{\omega_0,\omega_f\to\infty}[P(p+j\omega_f)]H(t)$$

$$=Y[\lim_{\omega_0,\omega_f\to\infty}P(p+j\omega_f)]H(t) \quad . \quad . \quad . \quad (11)$$

Using eqn. (3) and allowing ω_0 and ω_f to tend to infinity, keeping $(\omega_f-\omega_0)$ constant, yields

$$\lim_{\omega_0,\omega_f\to\infty}P(p+j\omega_f)=\lim_{\omega_0,\omega_f\to\infty}\frac{(p+j\omega_f)^2+\omega_0^2}{2(p+j\omega_f)}$$

$$=p+j(\omega_f-\omega_0)$$

i.e. $$\lim_{\omega_0,\omega_f\to\infty}P(p+j\omega_f)=p+j\Delta\omega \quad . \quad . \quad . \quad (12)$$

where $$\Delta\omega=\omega_f-\omega_0$$

Thus, in order to obtain the transient response of a narrow band-pass filter to a suddenly applied carrier of frequency $\omega_f/2\pi$, the function $P=p+j\Delta\omega$ is substituted for p in the transfer function of the equivalent low-pass filter from which the band-pass filter was derived by the transformation P. The expression for the modulation function becomes

$$g(t)=Y(p+j\Delta\omega)H(t) \quad . \quad . \quad . \quad . \quad (13)$$

For the symmetric case, $\Delta\omega=0$. Therefore, from eqn. (13) the expression for the modulation function becomes

$$g(t)=Y(p)H(t) \quad . \quad . \quad . \quad . \quad . \quad (14)$$

Eqn. (14) is the response to a step function of the equivalent low-pass filter. Thus, the modulation function of the response of a narrow band-pass filter to a suddenly applied carrier of mid-band frequency is identical to the response to a step function of the equivalent low-pass filter from which the band-pass filter is derived by the transformation P. In many cases the equivalent low-pass filter has a cut-off frequency equal to half the band width of the band-pass filter.

† Strictly, this should be written

$$I_r=\left[\frac{(S-S_r)C(S)}{SD(S)}\right]_{S=S_r},\quad r=a,b\ldots\alpha,\beta\ldots$$

where S is a complex number in contrast to the operator p. However, it is thought unlikely that confusion will arise.

(6) EFFECT OF FINITE Q-FACTOR

The analysis so far developed is based on the assumption that all elements employed have an infinite Q-factor. The actual Q-factor of the LC circuits used in the filter considered by Tucker was 100; it will be shown that a value even as high as 100 modifies the response appreciably.

The substitution of $p + \beta$ for p transforms a loss-free circuit into a circuit with loss. Thus, pL becomes $pL + \beta L$, i.e. an inductor is transformed into the same inductor in series with a resistor βL. Also, pC becomes $pC + \beta C$, i.e. a capacitor is transformed into the same capacitor in parallel with a resistor of conductance βC. Applying this transformation to the loss-less parallel tuned circuit of Fig. 5(*a*) yields the circuit of

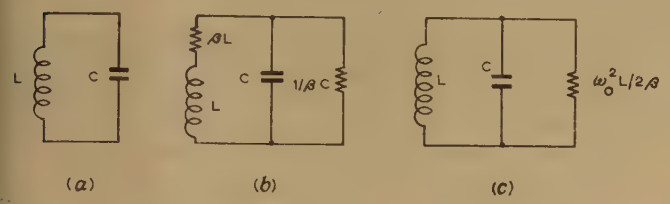

Fig. 5.—Application of transformation $(p + \beta)$ to parallel LC circuit.
(*a*) Lossless parallel circuit.
(*b*) Transformed parallel circuit.
(*c*) Equivalent circuit at $\omega = \omega_0$.

Fig. 5(*b*). At the resonant frequency $\omega_0/2\pi = 1/2\pi\sqrt{(LC)}$, the resistor βL in series with L can be replaced by a parallel resistor $\omega_0^2L^2/\beta L$ provided $\omega_0 \gg \beta$. Since $\omega_0^2L^2/\beta L = \omega_0^2L/\beta$ and the resistance associated with the capacitor is $1/\beta C = \omega_0^2L/\beta$, the circuit finally reduces to that of Fig. 5(*c*) at the resonant frequency $\omega_0/2\pi_0$. The effective Q-factor at ω_0 is thus given by

$$Q\omega_0 L = \omega_0^2 L/2\beta$$

i.e. $$Q = \omega_0/2\beta, \text{ or } \beta = \omega_0/2Q \quad . \quad . \quad . \quad . \quad (15)$$

The transformation $(p + \beta)$ results in equal dissipation factors being associated with inductance and capacitance, whereas in a practical circuit most of the loss occurs in the inductor. The practical circuit can therefore be represented by a resistor of value $\omega^2L/2\beta$ in parallel with a lossless LC circuit, whereas the circuit obtained by the transformation $(p + \beta)$ results in two resistors ω^2L/β and ω_0^2L/β in parallel with the LC circuit. Provided ω does not differ much from ω_0, i.e. provided none of the frequencies in the response differ appreciably from $\omega_0/2\pi$, the transformation gives a reasonable approximation to the practical circuit.

The series LC circuit of Fig. 6(*a*) is transformed into the circuit of Fig. 6(*b*) by means of the transformation $(p + \beta)$. At the resonant frequency $\omega_0/2\pi = 1/2\pi\sqrt{(LC)}$, if $\omega_0 \gg \beta$ the

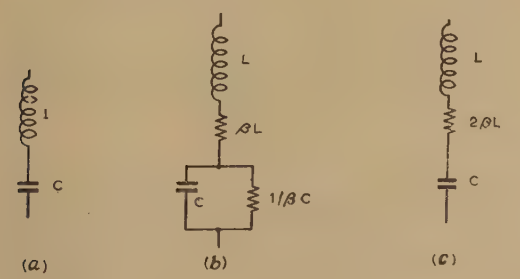

Fig. 6.—Application of transformation $(p + \beta)$ to series LC circuit.
(*a*) Lossless series circuit.
(*b*) Transformed series circuit.
(*c*) Equivalent circuit at $\omega = \omega_0$.

parallel impedance of the capacitor and resistor becomes $\beta/\omega_0^2C - j/\omega_0C = \beta L - j/\omega_0C$ so that the circuit reduces to that of Fig. 7(*c*), where $Q = \omega_0L/2\beta L = \omega_0/2\beta$ as before. The transformation is subject to the same error as outlined for the parallel LC circuit since the effective series resistance of the capacitor is a function of frequency and is equal to βL only at ω_0. Provided that all the frequencies in the response are sufficiently close to $\omega_0/2\pi$ this results in small error.

The transformation $P = p + j\Delta\omega$ of eqn. (12), which gives the modulation function of the response to a suddenly applied carrier of an infinite Q-factor band-pass filter, therefore becomes

$$P = p + \beta + j\Delta\omega \quad . \quad . \quad . \quad . \quad . \quad (16)$$

for the finite Q-factor filter.

(7) ESTIMATION OF ERROR DUE TO APPROXIMATION

From eqn. (5) the expression for the modulation function is

$$g(t) = I_a \exp(S_at) + I_b \exp(S_bt) + \ldots + I_\alpha \exp(S_\alpha t) + I_\beta \exp(S_\beta t) + \ldots$$

The approximation consists in obtaining $\lim_{\omega_0,\, \omega_f \to \infty} \frac{C(p)}{D(p)}$ prior to the application of the expansion theorem. This results in two errors: (i) an incorrect estimation of I_a, I_b, etc., and (ii) an error in assigning the value zero to I_α, I_β, etc.

Considering error (i), the exact expression for I_a is

$$I_a = \frac{C(S_a)}{KS_a(S_a - S_b)(S_a - S_c)\ldots(S_a - S_\alpha)(S_a - S_\beta)\ldots}$$

or $$I_a = \frac{C(S_a)}{KS_a(S_a - S_b)(S_a - S_c)\ldots(-S_\alpha)(1 - S_a/S_\alpha)(-S_\beta)(1 - S_a/S_\beta)} \quad . \quad . \quad . \quad . \quad (17)$$

The approximation expression for I_a is

$$I_a' = \frac{C(S_a)}{KS_a(S_a - S_b)(S_a - S_c)\ldots(-S_\alpha)(-S_\beta)\ldots} \quad . \quad (18)$$

so that $$\frac{I_a'}{I_a} = \left(1 - \frac{S_a}{S_\alpha}\right)\left(1 - \frac{S_a}{S_\beta}\right)\left(1 - \frac{S_a}{S_\gamma}\right)\ldots \quad . \quad . \quad . \quad (19)$$

To estimate the error, it will be sufficient to put

$$S_\alpha = S_\beta = S_\gamma = -j2\omega_0$$

Then $$\frac{I_a'}{I_a} = \left(1 + j\frac{S_a}{2\omega_0}\right)^u$$

$$= 1 + j\frac{uS_a}{2\omega_0}\ldots \quad . \quad . \quad . \quad . \quad . \quad . \quad . \quad (20)$$

where u = number of poles S_a, S_b, S_c, etc., of the modulation function which are clustered around the point $S = -j(\omega_f - \omega_0)$, i.e. half the total number of roots of $D(p)$.

To estimate the magnitudes of I_α, I_β, etc., an alternative form of the expansion formula will be employed. The modulation function of the response is given by eqn. (4):

$$g(t) = \frac{A(p + j\omega f)}{B(p + j\omega f)}H(t)$$

which has poles S_a, S_b, $S_c \ldots S_\alpha$, S_β, $S_\gamma \ldots$

where $$S_a = S_1 - j\omega_f,\ S_b = S_2 - j\omega_f \ldots$$
$$S_\alpha = S_1^* - j\omega_f,\ S_\beta = S_2^* - j\omega_f \ldots$$

and where S_1, S_1^*, S_2, S_2^* . . . are the poles of the original function $A(p)/B(p)$.

Then
$$I_a = \left[\frac{A(p+j\omega_f)}{pB'(p+j\omega_f)}\right]_{p=S_a} = \frac{1}{S_a}\left[\frac{A(S_1)}{B'(S_1)}\right]$$

and
$$I_\alpha = \frac{1}{S_\alpha}\left[\frac{A(S_1^*)}{B'(S_1^*)}\right]$$

$\frac{A(S_1^*)}{B'(S_1^*)}$ is the conjugate of $\frac{A(S_1)}{B(S_1)}$ and therefore has the same magnitude, so that

$$\frac{|I_\alpha|}{|I_a|} = \frac{|S_a|}{|S_\alpha|} = \frac{|S_a|}{2\omega_0} \quad . \quad . \quad . \quad . \quad . \quad (20a)$$

Similarly, the magnitude of I_β, I_γ, etc., can be estimated.

(8) THE M-DERIVED BAND-PASS FILTER

The m-derived band-pass filter, together with the low-pass filter from which it is derived by the transformation P, is shown in Fig. 7. By virtue of the transformation P, $L_1 = L_1'/2$, whence $\omega_c = n\omega_0/2$.

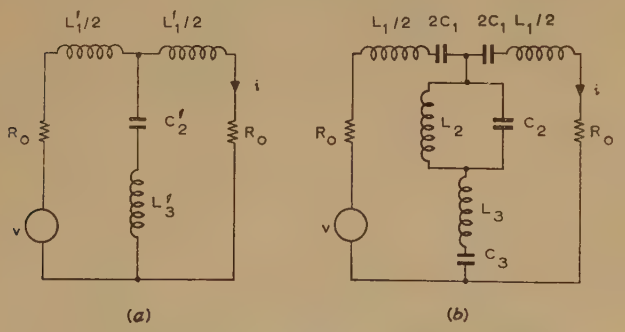

Fig. 7.—m-derived low-pass and band-pass filters.

(a) Low-pass filter.
$L_1'/2 = mR_0/\omega_c$, $C_2' = 2m/\omega_c R_0$, $L_3' = (1-m^2)R_0/2m\omega_c$
(b) Band-pass filter.
$L_1/2 = mR_0/n\omega_0$, $C_2 = 2m/n\omega_0 R_0$, $L_3 = (1-m^2)R_0/2mn\omega_0$
$2C_1 = n/mR_0\omega_0$, $L_2 = nR_0/2m\omega_0$, $C_3 = 2mn/(1-m^2)R_0\omega_0$

The response, i, of a T network to a voltage, v, is given by eqn. (1). Using the values L_1', C_2' and L_3' for the low-pass filter, Fig. 7(a) gives

$$Z_1' = pL_1' = 2p_1R_0 \text{ where } p_1 = mp/\omega_c = 2mp/n\omega_0$$

$$Z_2' = pL_3' + 1/pC_2' = \frac{(1-m^2)p_1^2 + m^2}{m^2 p_1}\,\frac{R_0}{2}$$

Substituting these values of Z_1' and Z_2' into eqn. (1) gives the following expression for the response of the low-pass filter to a step function:

$$i = \frac{E}{2R_0}\,\frac{(1/m^2)(1-m^2)p_1^2 + 1}{(p_1+1)(p_1^2/m^2 + p_1 + 1)}H(t) \quad . \quad . \quad (21)$$

From eqns. (12), (13), (14) and (16), the modulation function of the response of the band-pass filter to a suddenly applied carrier $E\exp(j\omega_f t)H(t)$ is given by the substitution of:

$P = p + \beta + j\Delta\omega$ for p for the finite Q-factor filter, asymmetric case ($\omega_f \neq \omega_0$).

$P = p + j\Delta\omega$ for p for the infinite Q-factor filter, asymmetric case.

$P = p + \beta$ for p for the finite Q-factor filter, symmetrical case ($\omega_f = \omega_0$).

$P = p$ for p for the infinite Q-factor filter, symmetrical case.

On division by $n\omega_0/2m$, these transformations become

$$\left.\begin{aligned} P_1 &= p_1 + \beta_1 + j\Delta\omega_1 \\ P_1 &= p_1 + j\Delta\omega_1 \\ P_1 &= p_1 + \beta_1 \\ P_1 &= p_1 \end{aligned}\right\} \quad . \quad . \quad . \quad . \quad (22)$$

where $P_1 = 2mP/n\omega_0$, $p_1 = 2mp/n\omega_0$,† $\beta_1 = 2m\beta/n\omega_0$, $\Delta\omega_1 = 2m\Delta\omega/n\omega_0$.

To obtain the modulation function of the response to a suddenly applied carrier $E\exp(j\omega_f t)H(t)$, $P = (p + \beta + j\Delta\omega)$ must replace p in eqn. (21), or $P_1 = 2mP/n\omega_0$ must replace $p_1 = 2mp/n\omega_0$.

Therefore the expression for the modulation function is

$$g(t) = \frac{E}{2R_0}\,\frac{(1-m^2)(1/m^2)P_1^2 + 1)}{(P_1+1)(P_1^2/m^2 + P_1 + 1)}H(t) \quad . \quad (23)$$

where P_1 is given by eqn. (22).

Eqn. (23) can be expanded into partial fractions:

$$g(t) = \frac{E}{2R_0}\left(\frac{1}{P_1+1} - \frac{m^2P_1}{P_1^2 + m^2P_1 + m^2}\right)H(t) \quad . \quad (24)$$

(8.1) Transient Response of Finite Q-Factor Filter, Asymmetric Case

The modulation function is given by eqn. (24) where $P_1 = p_1 + \beta_1 + j\Delta\omega_1$:

$$g(t) = \frac{E}{2R_0}\left[\frac{1}{p_1 + \beta_1 + j\Delta\omega_1 + 1} - \frac{m^2(p_1 + \beta_1 + j\Delta\omega_1)}{(p_1 + \beta_1 + j\Delta\omega_1)^2 + m^2(p_1 + \beta_1 + j\Delta\omega_1) + m^2}\right]H(t)$$
$$. \quad . \quad . \quad . \quad . \quad (25)$$

This reduces to

$$g(t) = \frac{E}{2R_0}[a(t) + jb(t)] \quad . \quad . \quad . \quad . \quad (26)$$

where
$$a(t) = a_1(t) - a_2(t)$$

and
$$b(t) = b_1(t) - b_2(t)$$

and $a_1(t)$, $a_2(t)$, $b_1(t)$ and $b_2(t)$ are shown in the appendix to be

$$a_1(t) = \frac{\cos^2\phi_1}{1+\beta_1} - \exp[-(1+\beta_1)\tau]\frac{\cos\phi_1}{1+\beta_1}\cos(\Delta\omega_1\tau + \phi_1)$$

$$b_1(t) = \frac{-\sin\phi_1\cos\phi_1}{1+\beta_1} + \exp[-(1+\beta_1)\tau]\frac{\cos\phi_1}{1+\beta_1}\sin(\Delta\omega_1\tau + \phi_1)$$

$$a_2(t) = \mathscr{R}C + \exp[-(\alpha+\beta_1)\tau]\left[\cos\Delta\omega_1\tau\left(\mathscr{R}A\cos\omega\tau + \frac{\mathscr{R}B - \alpha\mathscr{R}A}{\omega}\sin\omega\tau\right) + \sin\Delta\omega_1\tau\left(\mathscr{I}A\cos\omega\tau + \frac{\mathscr{I}B - \alpha\mathscr{I}A}{\omega}\sin\omega\tau\right)\right]$$

† The time scale corresponding to the operator p_1 is $\tau = n\omega_0 t/2m$, since, by well-known theorem, if $F(p)H(t) = f(t)$, $F(p/a)H(t) = f(at)$.

$$b_2(t) = \mathscr{I}C + \exp[-(\alpha+\beta_1)\tau]$$
$$\left[-\sin\Delta\omega_1\tau\left(\mathscr{R}A\cos\omega\tau + \frac{\mathscr{R}B - \mathscr{R}A}{\omega}\sin\omega\tau\right)\right.$$
$$\left. + \cos\Delta\omega_1\tau\left(\mathscr{I}A\cos\omega\tau + \frac{\mathscr{I}B - \alpha\mathscr{I}A}{\omega}\sin\omega\tau\right)\right]$$

where

$\tau = n\omega_0 t/2m$, $\Delta\omega_1 = 2m\Delta\omega/n\omega_0$, $\Delta\omega = \omega_f - \omega_0$

$\beta_1 = 2m\beta/n\omega_0$, $\beta = \omega_0/2Q$, $\tan\phi_1 = \Delta\omega_1/(1+\beta_1)$, $\alpha = m^2/2$

$\omega = m\sqrt{(1-m^2/4)}$

$$A = -\frac{\beta_1 + j\Delta\omega_1}{(1 - \Delta\omega_1^2/m^2 + \beta_1 + \beta_1^2/m^2) + j\Delta\omega_1(1+2\beta_1/m^2)}$$

$$B = \frac{m^2}{(1 - \Delta\omega_1^2/m^2 + \beta_1 + \beta_1^2/m^2) + j\Delta\omega_1(1+2\beta_1/m^2)}$$

$$C = \frac{\beta_1 + j\Delta\omega_1}{(1 - \Delta\omega_1^2/m^2 + \beta_1 + \beta_1^2/m^2) + j\Delta\omega_1(1+2\beta_1/m^2)} \quad . \quad . \quad . \quad . \quad (27)$$

and $\mathscr{R}$ and $\mathscr{I}$ are used to denote the real and imaginary parts of A, B and C.

The output current is therefore

$$i = g(t)\exp(j\omega_f t)H(t)$$
$$= \frac{E}{2R_0}[a(t) + jb(t)]\exp(j\omega_f t)H(t)$$

or
$$i = \frac{E}{2R_0}(a^2 + b^2)\exp(j\omega_f t + \phi) \quad . \quad . \quad . \quad (28)$$

where $\phi = \arctan(b/a)$.

$a(t)$ and $b(t)$ are known as the in-phase and quadrature components of the response. Both the amplitude, $\sqrt{(a^2+b^2)}$, and the phase angle, arc tan (b/a), of the response vary with time.

As an illustration, the particular circuit values employed by Tucker[5] in one of his experiments may be considered. These are

$$\omega_0 = 2\pi \times 2650,\ \omega_f = 2\pi \times 2550,\ \Delta\omega = -2\pi \times 100$$
$$m = 0{\cdot}884,\ n = 0{\cdot}037,\ Q = 100 \quad . \quad . \quad . \quad (29)$$

Thus, $\Delta\omega_1 = -1{\cdot}8$, $\beta_1 = 0{\cdot}238$ and $\tau = 349t$ and the in-phase and quadrature components become

$$a(t) = -0{\cdot}009 - 0{\cdot}458\varepsilon^{-1{\cdot}238\tau}\cos(1{\cdot}8\tau + 0{\cdot}969)$$
$$+ \varepsilon^{-0{\cdot}628\tau}[0{\cdot}271\cos(1{\cdot}8\tau)\sin(0{\cdot}792\tau + 1{\cdot}43)$$
$$+ 0{\cdot}499\sin(1{\cdot}8\tau) \times \sin(0{\cdot}792\tau - 0{\cdot}8)]$$

$$b(t) = 0{\cdot}020 - 0{\cdot}458\varepsilon^{-1{\cdot}238\tau}\sin(1{\cdot}8\tau + 0{\cdot}969)$$
$$+ \varepsilon^{-0{\cdot}628\tau}[0{\cdot}271\sin(1{\cdot}8\tau)\sin(0{\cdot}792\tau + 1{\cdot}43)$$
$$- 0{\cdot}499\cos(1{\cdot}8\tau) \times \sin(0{\cdot}792\tau - 0{\cdot}8)]$$
$$. \quad . \quad . \quad . \quad (30)$$

The envelope, $\sqrt{(a^2+b^2)}$, of the response is plotted in Fig. 8, where it can be compared with the response assuming an infinite Q-factor (Section 8.2).

The envelope of the decay when the carrier is removed may be derived as follows.

The in-phase and quadrature components of the response to a suddenly applied carrier, which are independent of the carrier phase at the instant of switching, have constant and transient terms,

$$\left.\begin{aligned} a(t) &= c + d(t) \\ b(t) &= e + f(t) \end{aligned}\right\} \quad . \quad . \quad . \quad . \quad . \quad (31)$$

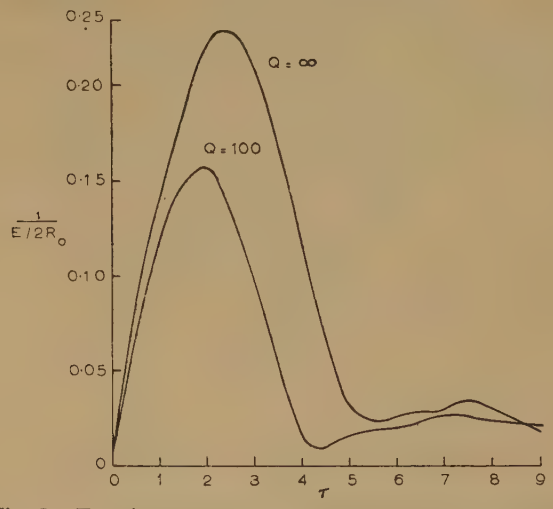

Fig. 8.—Transient response of band-pass filter, asymmetric case.

The effect of removing the carrier is equivalent to the application of a cancelling carrier when the transient terms have died away. The values of the in-phase and quadrature components for the decay become

$$\left.\begin{aligned} a'(t) &= c - a(t) = -d(t) \\ b'(t) &= e - b(t) = -f(t) \end{aligned}\right\} \quad . \quad . \quad . \quad . \quad (32)$$

The envelope $\sqrt{[(a')^2 + (b')^2]}$ of the decay is thus obtained by taking the root of the sum of the squares of the transient parts of the in-phase and quadrature components of the rise.

(8.2) Transient Response of Infinite Q-Factor Filter, Asymmetric Case

For $Q = \infty$, $\beta = \beta_1 = 0$ and the response is again given by eqn. (26), with A, B, and C of eqn. (27), however, simplified:

$$\left.\begin{aligned} A &= -\frac{j\Delta\omega_1}{1 - \Delta\omega_1^2/m^2 + j\Delta\omega_1} \\ B &= \frac{m^2}{1 - \Delta\omega_1^2/m^2 + j\Delta\omega_1} \\ C &= \frac{j\Delta\omega_1}{1 - \Delta\omega_1^2/m^2 + j\Delta\omega_1} \end{aligned}\right\} \quad . \quad . \quad . \quad (33)$$

Using again the values of eqn. (29),

$$a(t) = -0{\cdot}010 - 0{\cdot}486\varepsilon^{-\tau}\cos(1{\cdot}8\tau + 1{\cdot}063)$$
$$+ \varepsilon^{-0{\cdot}39\tau}[0{\cdot}272\cos(1{\cdot}8\tau)\sin(0{\cdot}792\tau + 1{\cdot}135)$$
$$+ 0{\cdot}553\sin(1{\cdot}8\tau)\sin(0{\cdot}792\tau - 0{\cdot}89)]$$

$$b(t) = -0{\cdot}006 - 0{\cdot}486\varepsilon^{-\tau}\sin(1{\cdot}8\tau + 1{\cdot}063)$$
$$+ \varepsilon^{-0{\cdot}39\tau}[0{\cdot}272\sin(1{\cdot}8\tau)\sin(0{\cdot}792\tau + 1{\cdot}135)$$
$$- 0{\cdot}553\cos(1{\cdot}8\tau)\sin(0{\cdot}792\tau - 0{\cdot}89)]$$
$$. \quad . \quad . \quad . \quad (34)$$

where $\tau = 349t$.

The envelope of the response, $\sqrt{(a^2+b^2)}$, is plotted in Fig. 8.

(8.3) Transient Response of Finite Q-Factor Filter, Symmetric Case

For the symmetric case, $\Delta\omega_1 = 0$, $\tan\phi_1 = \phi_1 = 0$ so that substitution in eqn. (27) yields

$$\mathscr{R}A = -\frac{\beta_1}{1+\beta_1+\beta_1^2/m^2}, \quad \mathscr{R}B = \frac{m^2}{1+\beta_1+\beta_1^2/m^2},$$
$$\mathscr{R}C = \frac{\beta_1}{1+\beta_1+\beta_1^2/m^2}$$

$\mathscr{I}A = \mathscr{I}B = \mathscr{I}C = 0$ and eqn. (26) reduces to

$$g(t) = \frac{E}{2R_0}\left\{\frac{1+(1-m^2)\beta_1^2/m^2}{(1+\beta_1)(1+\beta_1+\beta_1^2/m^2)}\right.$$
$$-\frac{1}{1+\beta_1}\exp[-(1+\beta_1)\tau] + \exp[-(\alpha+\beta_1)\tau]$$
$$\left.\left[-\frac{m^2(1+\beta_1/2)}{\omega(1+\beta_1+\beta_1^2/m^2)}\sin\omega\tau + \frac{\beta_1}{1+\beta_1+\beta_1^2/m^2}\cos\omega\tau\right]\right\} \quad . \quad . \quad . \quad (35)$$

Substituting the values of eqn. (29) yields

$$g(t) = \frac{E}{2R_0}[0{\cdot}626 - 0{\cdot}808\varepsilon^{-1{\cdot}238\tau}$$
$$- 0{\cdot}861\varepsilon^{-0{\cdot}628\tau}\sin(0{\cdot}792\tau - 0{\cdot}213)] \quad . \quad (36)$$

This result is plotted in Fig. 9. For comparison with Tucker's results, eqn. (36) is divided by 0·626 to give a final response of

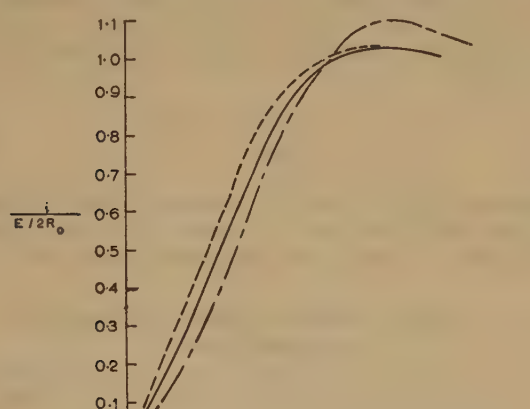

Fig. 9.—Transient response of band-pass filter, symmetric case.
---- Experimental (from Tucker).
—— Theoretical, $Q = 100$.
---- Theoretical, $Q = \infty$

unity. The curve for an infinite value of Q (Section 8.4) is also plotted. It is seen that the error in assuming Q infinite is appreciable. The curve for a finite Q-factor gives good agreement when t is large (in particular, the overshoot corresponds very closely to that obtained experimentally). For t small, the slope of the theoretical curve is less than it should be, owing, no doubt, to the neglected higher frequencies.

(8.4) Transient Response of Infinite Q-Factor Filter, Symmetric Case

The solution for this case can be obtained from eqn. (35) by putting $\beta_1 = 0$:

$$g(t) = \frac{E}{2R_0}\left(1 - \varepsilon^{-\tau} - \frac{m^2}{\omega}\varepsilon^{-\alpha\tau}\sin\omega\tau\right) \quad . \quad . \quad (37)$$

where $\tau = n\omega_0 t/2m$.

It can also be obtained using the general rule stated i Section 5 for narrow pass-band filters. The response of th low-pass filter from which the band-pass filter is derived known to be[9]

$$i = \frac{E}{2R_0}\left[1 - \varepsilon^{-\omega_c t/m} - \frac{m}{\sqrt{(1-m^2/4)}}\varepsilon^{-m\omega_c t/2}\sin\sqrt{(1-m^2/4)}\omega_c t\right.$$
. . . . (38

The modulation function of the response of the band-pass filte to a suddenly applied carrier of mid-band frequency is obtaine by replacing ω_0 by $n\omega_0/2$:

$$g(t) = \frac{E}{2R_0}\left[1 - \varepsilon^{-n\omega_0 t/2m}\right.$$
$$\left. - \frac{m}{\sqrt{(1-m^2/4)}}\varepsilon^{-mn\omega_0 t/4}\sin\sqrt{(1-m^2/4)}n\omega_0 t/2\right] \quad . \quad (39$$

which, since $\tau = n\omega_0 t/2m$, $\omega = m\sqrt{1-m^2/4}$ and $\alpha = m^2/2$, i identical with eqn. (37). Eqn. (37) for the values of eqn. (29 becomes

$$g(t) = \frac{E}{2R_0}[1 - \varepsilon^{-\tau} - 0{\cdot}985\varepsilon^{-0{\cdot}39\tau}\sin 0{\cdot}792\tau] \quad . \quad (40$$

and is plotted in Fig. 9.

(8.5) Estimation of Error

As an illustration the infinite Q-factor filter, the asymmetri case will be considered (Section 8.2). From eqns. (22) and (24 the modulation function is

$$g(t) = \frac{E}{2R_0}\left[\frac{1}{p_1+1+j\Delta\omega_1}\right.$$
$$\left. - \frac{m^2(p_1+j\Delta\omega_1)}{(p_1+j\Delta\omega_1)^2 + m^2(p_1+j\Delta\omega_1)+m^2}\right]H(t) \quad . \quad (41$$

Thus, one of the three poles of the modulation function clustere near the point $-j(\omega_f - \omega_0)$ is $S_a = -\frac{n\omega_0}{2m}(1+j\Delta\omega_1)$ o $S_a = -\left(\frac{n\omega_0}{2m} + j\Delta\omega\right)$. This gives rise to a term of the form $I_a'\varepsilon^{-\tau} \times \varepsilon^{-j\Delta\omega_1\tau}$ in the response. I_a' is, however, not the tru magnitude, and the error can be calculated from eqn. (20), s that

$$\frac{I_a'}{I_a} = 1 - j\frac{3}{2\omega_0}\left(\frac{n\omega_0}{2m} + j\Delta\omega\right)$$
$$= 1 + \frac{3\Delta\omega}{2\omega_0} - j\frac{3n}{4m} \quad . \quad . \quad . \quad . \quad . \quad . \quad (42$$

If $3\Delta/2\omega_0$ and $3n/4m$ are both $\ll 1$, then $3\Delta\omega/2\omega_0$ is th approximate per-unit error in magnitude and $3n/4m$ is th approximate error in phase angle. For the particular values o eqn. (29), eqn. (42) becomes

$$\frac{I_a'}{I_a} = 1 - 0{\cdot}057 - j0{\cdot}031$$
$$I_a = 1{\cdot}06\angle 1{\cdot}9° \times I_a' \quad . \quad . \quad . \quad . \quad . \quad (43$$

Similarly, the errors in obtaining I_b and I_c can be obtained noting that

$$I_a\varepsilon^{s_a t} = a_1(t) + jb_1(t)$$

and $I_b\varepsilon^{s_b t} + I_c\varepsilon^{s_c} = -[(a_2(t) + jb_2(t)]$

The amplitudes of the neglected modes can be estimated from eqn. (20*a*). Thus

$$\frac{|I_\alpha|}{|I_a|} = \frac{|S_a|}{2\omega_0} = \sqrt{\left[\frac{n^2}{4m} + \left(\frac{\Delta\omega}{2\omega_0}\right)^2\right]} \quad . \quad . \quad . \quad (44)$$

For the particular values of eqn. (29), eqn. (44) becomes

$$\frac{|I_\alpha|}{|I_a|} = 0{\cdot}022 \quad . \quad . \quad . \quad . \quad . \quad . \quad (45)$$

Similarly, the magnitudes of I_β, I_γ . . . can be estimated.

(9) CONCLUSIONS

(*a*) The substitution $P = \frac{1}{2}[p + \omega_0^2/p]$ transforms a low-pass filter into a band-pass filter of central frequency $\omega_0/2\pi$. To obtain the transient response of a band-pass filter to a step function, $P = \frac{1}{2}[p + \omega_0^2/p]$ is substituted for p in the operational expression for the transient response to a step-function of the original low-pass filter.

(*b*) To obtain the modulation function of the transient response of a band-pass filter to a suddenly applied carrier of frequency $\omega_f/2\pi$, $P = \dfrac{(p + j\omega_f)^2 + \omega_0^2}{2(p + j\omega_f)}$ is substituted for p in the operational expression for the transient response to a step-function of the original low-pass filter.

(*c*) For a narrow band-pass filter and for $\Delta\omega = \omega_f - \omega_0 \ll \omega_0$, the transformation for the modulation function of the transient response of a band-pass filter to a suddenly applied carrier reduces to $P = p + j\Delta\omega$.

(*d*) If the elements of the band-pass filter possess a finite value of Q, the transformation of (*c*) becomes

$$P = p + \beta + j\Delta\omega$$

where $\beta = \omega_0/2Q$.

(*e*) The error in calculating the magnitude of mode S_a in the modulation function due to the approximation outlined in (*c*) is given by

$$\frac{I_a'}{I_a} = 1 + j\frac{uS_a}{2\omega_0}$$

where I_a' is the magnitude as calculated by the approximate method, I_a is the correct magnitude and u is the number of poles S_a, S_b, S_c . . . of the modulation function which are clustered about the point $-j(\omega_f - \omega_0)$. Similarly, the errors in obtaining I_b, I_c . . . , etc., can be estimated.

(*f*) The approximate magnitudes of the neglected modes S_α, S_β, S_γ . . . can be obtained from the relations

$$\frac{|I_\alpha|}{|I_a|} = \frac{|S_a|}{2\omega_0}, \quad \frac{|I_\beta|}{|I_b|} = \frac{|S_b|}{2\omega_0}, \text{ etc.}$$

The transformations of (*c*) and (*d*) were applied to a *m*-derived band-pass filter considered by Tucker. For the symmetrical case $\Delta\omega = 0$ transformation (*d*) gives good agreement with his experimental results. For the asymmetrical case, the transformation gives results having the same general shape of oscillograms as those obtained by Tucker.

(11) REFERENCES

(1) LANDON, V. D.: 'The Band-Pass Low-Analogy', *Proceedings of the Institute of Radio Engineers*, 1936, **24**, p. 1582.

(2) LAURENT, T.: 'Transformation frequentielle des lignes artificielles correctrices d'affaiblissment', *Ericsson Technics*, 1935, p. 15.

(3) LAURENT, T.: 'New Principles for Practical Computation of Filter Attenuations by means of Frequency Transformations', *ibid.*, 1939, p. 57.

(4) LAURENT, T.: 'Frequency Transformations applied on the Heaviside Expansion Theorem', *Ericsson Review*, 1937, p. 40.

(5) TUCKER, D. G.: 'Transient Response of Filters', *Wireless Engineer*, 1946, **23**, pp. 36 and 84.

(6) EAGLEFIELD, C. C.: 'Transient Response of Filters', *ibid.*, 1946, **23**, p. 306.

(7) EAGLEFIELD, C. C.: 'Carrier Frequency Amplifiers—Transient Response with Detuned Carriers', *ibid.*, 1946, **23**, p. 67.

(8) AGRAIN, P. R., TEARE, B. R., and WILLIAMS, E. M.: 'Generalized Theory of the Band-pass Low-pass Analogy', *Proceedings of the Institute of Radio Engineers*, 1949, **37**, p. 1152.

(9) KALLMAN, H. E., SPENCER, R. E., and SINGER, C. P.: 'Transient Response', *ibid.*, 1945, **33**, p. 169.

(10) JEFFREYS, H. and B. S.: 'Mathematical Physics' (University Press, Cambridge, 1946).

(11) DALTON, J. P.: 'Symbolic Operators' (Witwatersrand University Press, 1954).

(12) TERMAN, F. E.: 'Radio Engineers Handbook' (McGraw-Hill, 1943).

(12) APPENDIX

Eqn. (25) is

$$g(t) = \frac{E}{2R_0}\left[\frac{1}{p_1 + 1 + \beta_1 + j\Delta\omega_1} - \frac{m^2(p_1 + \beta_1 + j\Delta\omega_1)}{(p_1 + \beta_1 + j\Delta\omega_1)^2 + m^2(p_1 + \beta_1 + j\Delta\omega_1) + m^2}\right]H(t)$$

The first term of this equation is

$$\frac{1}{p_1 + 1 + \beta_1 + j\Delta\omega_1}H(t) = \left[\frac{1}{1 + \beta_1 + j\Delta\omega_1}\right][1 - \varepsilon^{-(1+\beta_1)\tau}\varepsilon^{-j\Delta\omega_1\tau}] \quad . \quad (46)$$

Letting $$\tan\phi_1 = \Delta\omega_1/(1 + \beta_1) \quad . \quad . \quad . \quad . \quad (47)$$

then $$\frac{1}{1 + \beta_1 + j\Delta\omega_1} = \frac{\cos\phi_1}{1 + \beta_1}\varepsilon^{-j\phi_1} \quad . \quad . \quad . \quad (48)$$

and eqn. (46) becomes

$$\frac{\cos\phi_1}{1 + \beta_1}[\varepsilon^{-j\phi_1} - \varepsilon^{-(1+\beta_1)\tau}\varepsilon^{-j(\Delta\omega_1\tau + \phi_1)}]$$
$$= \left[\frac{\cos^2\phi_1}{1 + \beta_1} - \frac{\cos\phi_1}{1 + \beta_1}\varepsilon^{-(1+\beta_1)\tau}\cos(\Delta\omega_1\tau + \phi_1)\right]$$
$$+ j\left[\frac{-\sin\phi_1\cos\phi_1}{1 + \beta_1} + \frac{\cos\phi_1}{1 + \beta_1}\varepsilon^{-(1+\beta_1)\tau}\sin(\Delta\omega_1\tau + \phi_1)\right]$$
$$= a_1(t) + jb_1(t) \quad . \quad . \quad . \quad . \quad . \quad . \quad . \quad . \quad . \quad . \quad (49)$$

The second term of eqn. (25) is

$$\frac{m^2(p_1 + \beta_1 + j\Delta\omega_1)}{(p_1 + \beta_1 + j\Delta\omega_1)^2 + m^2(p_1 + \beta_1 + j\Delta\omega_1) + m^2}H(t)$$
$$= \varepsilon^{-\beta_1\tau}\varepsilon^{-j\Delta\omega_1\tau}\left(\frac{m^2p_1}{p_1^2 + m^2p_1 + m^2} \times \frac{p_1}{p_1 - \beta_1 - j\Delta\omega_1}\right)H(t)$$
$$= \varepsilon^{-\beta_1\tau}\varepsilon^{-j\Delta\omega_1\tau}\left(\frac{Ap_1^2 + Bp_1}{p_1^2 + m^2p_1 + m^2} + \frac{Cp_1}{p_1 - \beta_1 - j\Delta\omega_1}\right)H(t)$$
$$. \quad . \quad . \quad . \quad (50)$$

where A, B, C are determined by conventional partial fraction analysis and are given in eqn. (27).

Rearranging eqn. (50) gives

$$\varepsilon^{-\beta_1\tau}\varepsilon^{-j\Delta\omega_1\tau}\left[\frac{Ap_1^2+Bp_1}{(p_1+\alpha)^2+\omega^2}+\frac{Cp_1}{p_1-\beta_1-j\Delta\omega_1}\right]\mathrm{H}(t),$$

$$=\varepsilon^{-\beta_1\tau}\varepsilon^{-j\Delta\omega_1\tau}\left[\varepsilon^{-\alpha\tau}A\cos\omega\tau+\frac{B-\alpha A}{\omega}\sin\omega\tau\right.$$

$$\left.+C\varepsilon^{\beta_1\tau}\varepsilon^{j\Delta\omega_1\tau}\right] \quad =C+\varepsilon^{-(\alpha+\beta_1)\tau}(\cos\Delta\omega_1\tau-j\sin\Delta\omega_1\tau)$$

$$\left[\mathscr{R}A\cos\omega\tau+\frac{\mathscr{R}B-\alpha\mathscr{R}A}{\omega}\sin\omega\tau\right.$$

$$\left.+j\left(\mathscr{I}A\cos\omega\tau+\frac{\mathscr{I}B-\alpha\mathscr{I}A}{\omega}\sin\omega\tau\right)\right]$$

$$=C_R+\varepsilon^{-(\alpha+\beta_1)\tau}\left[\cos\Delta\omega_1\tau\left(\mathscr{R}A\cos\omega\tau\right.\right.$$

$$\left.+\frac{\mathscr{R}B-\alpha\mathscr{R}A}{\omega}\sin\omega\tau\right)+\sin\Delta\omega_1\tau\left(\mathscr{I}A\cos\omega\tau\right.$$

$$\left.\left.+\frac{\mathscr{I}B-\alpha\mathscr{I}A}{\omega}\sin\omega\tau\right)\right]+j\left\{\mathscr{I}C+\varepsilon^{-(\alpha+\beta_1)\tau}\right.$$

$$\left[-\sin\Delta\omega_1\tau\left(\mathscr{R}A\cos\omega\tau+\frac{\mathscr{R}B-\alpha\mathscr{R}A}{\omega}\sin\omega\tau\right)\right.$$

$$\left.\left.+\cos\Delta\omega_1\tau\left(\mathscr{I}A\cos\omega\tau+\frac{\mathscr{I}B-\alpha\mathscr{I}A}{\omega}\sin\omega\tau\right)\right]\right\}$$

$$=\mathrm{a}_2(t)+j\mathrm{b}_2(t) \quad . \quad . \quad . \quad . \quad . \quad . \quad . \quad . \quad . \quad . \quad (51)$$

where $\alpha=m^2/2$ and $\omega=m\sqrt{(1-m^2/4)}$

The full solution is therefore

$$\mathrm{g}(t)=\frac{E}{2R_0}[\mathrm{a}(t)+j\mathrm{b}(t)] \quad . \quad . \quad . \quad . \quad (52)$$

where: $\mathrm{a}(t)=\mathrm{a}_1(t)-\mathrm{a}_2(t)$, $\mathrm{b}(t)=\mathrm{b}_1(t)-\mathrm{b}_2(t)$, and $\mathrm{a}_1(t)$, $\mathrm{a}_2(t)$, $\mathrm{b}_1(t)$.$\mathrm{b}_2(t)$, are obtained from eqns. (49), and (51) and are given in eqn. (27).

621.372.622

The Institution of Electrical Engineers
Monograph No. 332 E
Apr. 1959

THE EFFICIENCY OF A FERRITE AS A MICROWAVE MIXER

By L. LEWIN, Associate Member.

(*The paper was first received* 3rd *September*, 1958, *and in revised form* 24th *January*, 1959. *It was published as an* INSTITUTION MONOGRAPH *in April*, 1959.)

SUMMARY

A method proposed by the Services Electronics Research Laboratory is analysed in detail, and expressions are derived for the efficiency under a variety of conditions. It is shown that, subject to reasonable limitations on the intermediate-frequency spacing, a polycrystalline ferrite should behave in many ways like a single crystal sample and that the S.E.R.L. measurements on magnetization can be explained by assuming a basic line width of a few gauss and a spread in resonant fields from point to point in heterogeneous samples. Owing to a remarkable property of the structure of the formulae, this spread in resonance does not degrade the effective permeability, although the measured value is reduced by a factor of about a hundred.

On the figures presented, the tentative conclusion is reached that the conversion efficiency is some 14 dB worse than acceptable conventional crystals will give, although the figures may be capable of improvement. No calculations are made on noise figure.

LIST OF PRINCIPAL SYMBOLS

A = Cross-sectional area of ferrite, cm^2.
$B = \beta(n - r)$.
C = Constant related to the magnetic field in a polycrystalline sample.
V_c = Voltage induced in a coil, volts.
f = Radio frequency, c/s.
f_i = Intermediate frequency, c/s.
$f(\mu)$ = Function of the permeability which determines the local field in a polycrystalline sample.
H_0 = Static applied magnetic field within the ferrite sample, oersteds.
H = R.F. magnetic field.
H_n = R.F. magnetic field in the nth crystallite.
l = Length of ferrite rod, cm.
L = R.F. to i.f. loss factor.
M = R.F. magnetization, gauss. Subscripts 1 and 2 denote local-oscillator and signal frequency.
M_i = I.F. magnetization.
M_s = Saturation magnetization.
N_i = Number of turns in i.f. coil.
N_{iu} = Number of turns per unit length in coil.
n = Integer indicating nth crystallite.
s = Total number of crystallites in ferrite sample.
P = R.F. power, watts. Subscripts 1 and 2 denote local-oscillator and signal frequencies. Subscript n denotes power absorbed in nth crystallite.
P_i = Power available at intermediate frequency from i.f. coil.
r = Parameter determining r.f. mistuning.
R = I.F. coil resistance, i.f. load resistance, ohms.
v = Volume of ferrite, cm^3.
v_n = Volume of nth crystallite.
$y = 2r/s$. A parameter determining r.f. tuning.
$z, z_r = -j\beta s\mu_r/\mu_p$. A quantity related to the permeability.
α = Attenuation coefficient.
β, ρ = Parameters determining the shape of the permeability curve.
$\gamma = 2{\cdot}8$ Mc/gauss.
ϵ = Dielectric constant of ferrite.
λ = R.F. wavelength (free space), cm.
μ = R.F. permeability to circularly polarized waves (unity for free space).
μ_m = Measured permeability of ferrite.
μ_p = Peak permeability for ferrite single crystal.
$\bar{\mu}$ = Effective permeability.
μ_n = R.F. permeability of nth crystallite.
μ_0 = Composite permeability of polycrystalline ferrite.
μ_r = Value of μ_0 at a frequency determined by r.
$\phi_{1,2}$ = Phase of r.f. magnetizations.
Φ = Flux parameter for ferrite sample, maxwells per watt.
θ = Angle of deviation of total magnetization.
ω = R.F. angular frequency, rad/s. Subscripts 1 and 2 denote local-oscillator and signal frequencies.
ω_i = I.F. angular frequency.

(1) INTRODUCTION

A method of utilizing the non-linear properties of ferrites to replace the usual crystal element of a microwave mixer has been suggested by the Services Electronics Research Laboratory, where some preliminary measurements have been made suggesting that usable efficiencies could be obtained at 3 cm wavelength. The purpose of the paper is to examine the theoretical properties which might be expected and to compare the predictions with measured values.

(2) METHOD OF USE

The intended method of using the ferrite is to insert a rod in a rectangular waveguide perpendicular to the guide axis (see Fig. 1). The rod is placed in a static field sufficient to cause

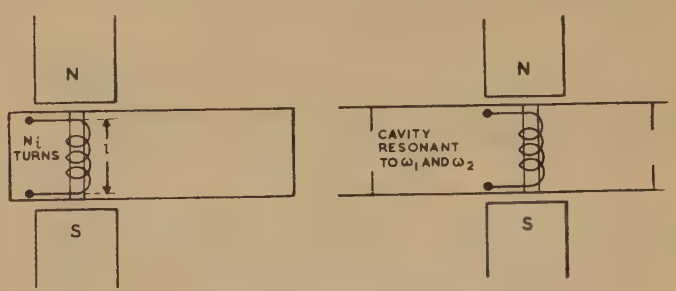

Fig. 1.—Ferrite rod and i.f. coil in microwave cavity.

resonance at the microwave frequencies used and also to saturate the material. Tuning elements in the guide are arranged so that, both at signal and local-oscillator frequencies, all the incident microwave power is absorbed by the ferrite (which is so lossy at resonance that losses in the guide walls can be neglected). A variable component of axial magnetization in the rod appears at

Correspondence on Monographs is invited for consideration with a view to publication.
Mr. Lewin is with Standard Telecommunication Laboratories, Ltd.

the intermediate frequency and can be picked up by a suitable coil surrounding the rod.

The paper is concerned with a ferrite near resonance. If the field is resolved into two components of opposite sense of circular polarization the ferrite appears resonant to only one of them. To the other the material is far off resonance, and that set of components will henceforth be ignored. The following symbols are used for magnetization in the ferrite.

M_s = Saturation magnetization (nearly axial).
$M_i \cos \omega_i t$ = Intermediate-frequency magnetization (axial).
$M_1 \exp(j\omega_1 t)$ = Local-oscillator magnetization (transverse circularly polarized).
$M_2 \exp(j\omega_2 t)$ = Signal-frequency magnetization (transverse circularly polarized).

M_s is of constant length, and is swung off the axis by an angle θ through the application perpendicular to the axis of the micro-

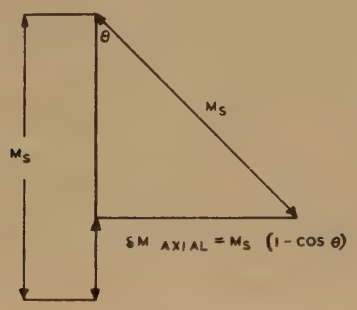

Fig. 2.—Magnetization vector.

wave magnetization $|M_1 \exp(j\omega_1 t) + M_2 \exp(j\omega_2 t)|$ (see Fig. 2). θ is determined by

$$\theta \simeq \sin\theta = \sqrt{(M_1^2 + M_2^2 + 2M_1 M_2 \cos \omega_i t)}/M_s \quad . \quad (1)$$

The axial component of magnetization under these circumstances is $M_s \cos\theta$, and the change is given by

$$\delta M_{axial} = M_s(1 - \cos\theta) \simeq \tfrac{1}{2} M_s \theta^2$$

Substituting for θ from eqn. (1), we get

$$\delta M_{axial} = \frac{1}{2M_s}(M_1^2 + M_2^2 + 2M_1 M_2 \cos \omega_i t) \quad . \quad (2)$$

Extracting the i.f. magnetization term, we get

$$M_i = M_1 M_2 / M_s \quad . \quad . \quad . \quad . \quad . \quad . \quad (3)$$

In the absence of the r.f. signal there is a d.c. change in magnetization due to the local oscillator only. This quantity, which has been measured at S.E.R.L. is given from eqn. (2) by

$$\delta M_{L0} = M_1^2 / 2M_s \quad . \quad . \quad . \quad . \quad . \quad . \quad (4)$$

The variable axial magnetization at intermediate frequency gives rise to a voltage, V_c, in the coil, of resistance R wound round the ferrite. The available power P_i from the coil, considered as a generator of internal resistance R working into an external load of the same resistance, is

$$P_i = \tfrac{1}{2} V_c^2 / 4R \quad . \quad . \quad . \quad . \quad . \quad . \quad . \quad (5)$$

V_c is given by $10^{-8} N_i A d M_i/dt = 10^{-8} N_i A \omega_i M_i$. In terms of v, l and N_{iu} we have $N_i A = N_i v/l = N_{iu} v$.

Inserting in eqn. (5) we get

$$P_i = N_{iu}^2 v^2 \omega_i^2 M_i^2 \times 10^{-16}/8R \quad . \quad . \quad . \quad (6)$$

In order to express this in terms of other physical quantities through eqn. (3), it is necessary to digress a little to relate the r.f. power absorbed in the ferrite with the r.f. magnetization produced.

(3) ABSORPTION IN A FERRITE

The aim is to obtain an expression similar to the familiar equation relating stored energy per unit volume and magnetic field, but here involving power absorbed rather than that stored. The permeability of a ferrite is a tensor

$$[\mu] = \begin{Bmatrix} \mu, & j\kappa, & 0 \\ -j\kappa, & \mu, & 0 \\ 0, & 0, & 1 \end{Bmatrix}$$

but if a circularly polarized component is considered, the permeability becomes a scalar $\mu \pm \kappa$. This latter term will henceforth be denoted by μ. Since the ferrite is near resonance for one sense of circular polarization only, only the components of the field for that sense will be involved and the components for the contrary sense, which will be far off resonance, will be ignored.

To investigate the power flow in an infinite block of material, we consider a section of area A and small thickness t. The peak circularly polarized magnetic field is H, to which the electric field is related by $E = 300\sqrt{(\mu/\epsilon)}H$. The input Poynting flux is

$$P_{in} = \mathscr{R}\frac{10}{4\pi} AE \times H^* = \frac{3000}{4\pi}|H|^2 A \mathscr{R}\sqrt{\frac{\mu}{\epsilon}} \quad . \quad (7)$$

The output flow is given by $P_{out} = P_{in} \exp(-2\alpha t) = P_{in}(1 - 2\alpha t)$ where $\alpha = \mathscr{I}\frac{2\pi}{\lambda}\sqrt{(\mu\epsilon)}$.

Hence

$$P = P_{in} - P_{out} = P_{in} 2\alpha t = \frac{3000}{\lambda}|H|^2 A t \mathscr{R}\sqrt{\frac{\mu}{\epsilon}}\mathscr{I}\sqrt{(\mu\epsilon)}$$

Putting $At = v$, and assuming that the major loss arises from μ, so that ϵ can be taken as real,

$$\mathscr{R}(\sqrt{\mu})\mathscr{I}\sqrt{\mu} = \sqrt{|\mu|}\cos(\tfrac{1}{2}\phi)\sqrt{|\mu|}\sin(\tfrac{1}{2}\phi)$$
$$= \tfrac{1}{2}|\mu|\sin\phi = \tfrac{1}{2}\mathscr{I}\mu$$

where $\mu = |\mu|\varepsilon^{j\phi}$.

Hence
$$P = \frac{3000}{2\lambda} v |H|^2 \mathscr{I}\mu \quad . \quad . \quad . \quad . \quad . \quad (8)$$

This equation relates the power lost per unit volume to the field developed in the sample.

(4) SINGLE-CRYSTAL FERRITE

For a single crystal the permeability will be high at or near resonance, and the approximation $M \simeq \mu H$ can be made as the relation between magnetization and field.* Using subscripts 1 and 2 for local-oscillator and signal frequencies it is found from eqn. (8) that

$$|M_1|^2 = \frac{2\lambda_1 P_1}{3000 v}\frac{|\mu_1|^2}{\mathscr{I}\mu_1} \quad . \quad . \quad . \quad . \quad (9)$$

with a similar equation for M_2. It will not, in general, be necessary to distinguish between λ_1 and λ_2, and they will both be denoted by λ.

* μ and $\mu - 1$ will be used indifferently when μ is large. This does not affect the results of this Section since $\mathscr{I}(\mu) = \mathscr{I}(\mu - 1)$ and in eqn. (12) an expression is used which equals $\mu - 1$ rather than μ. It is only in Section 6 that the approximation enters into the determination of the local distribution of magnetic field.

Using eqns. (3), (6) and (9) we get

$$P_i = \frac{N_{iu}^2\lambda^2\omega_i^2P_1P_2}{9\times10^{22}2R}\times\frac{|\mu_1|^2|\mu_2|^2}{\mathscr{I}(\mu_1)\mathscr{I}(\mu_2)}\frac{1}{M_s^2} \quad . \quad (10)$$

Define the conversion loss by $L = P_i/P_2$. Introducing the microwave frequency f and the intermediate frequency f_i, eqn. (10) becomes

$$L = \frac{\pi^2}{50}\frac{N_{iu}^2P_1}{R}\left(\frac{f_i}{f}\right)^2\left[\frac{|\mu_1|^2|\mu_2|^2}{\mathscr{I}(\mu_1)\mathscr{I}(\mu_2)}\frac{1}{M_s^2}\right] \quad . \quad (11)$$

This equation gives the loss in terms of μ and M_s. When the permeability is given by an equation of the form

$$\mu_1 \simeq \mu_1 - 1 = \frac{\gamma M_s}{\gamma H_0 - \omega_1 + j\rho} \quad . \quad . \quad (12)$$

where γ is the gyromagnetic ratio, H_0 is the internal static field and ρ is a parameter which determines the resonance width, it is found simply that

$$|\mu_1|^2/\mathscr{I}(\mu_1) = \gamma M_s/\rho$$

independently of the resonant frequency. Hence eqn. (11) can be written

$$L = \frac{\pi^2}{50}\frac{N_{iu}^2P_1}{R}\left(\frac{f_i}{f}\right)^2\left(\frac{|\mu|}{M_s}\right)^2 \quad . \quad . \quad . \quad (13)$$

since $|\mu| = \mathscr{I}(\mu)$ at resonance.

Although this equation does not exhibit any effect from the ferrite resonance, it is implied that all the incident power is absorbed in the sample, so that not only must the cavity be matched off frequency but the wall losses must still be negligible compared with the ferrite losses. This limits the frequency mistuning permissible in practice.

Put this equation in terms of other measured quantities obtained from the case in which only the local oscillator is used. From eqn. (4), $\delta M = M_1^2/2M_s$ which gives, using eqn. (8),

$$A\delta M = \frac{A\lambda P_1|\mu|}{M_s\times3\,000v} = \frac{\lambda P_1|\mu|}{3\,000lM_s} \quad . \quad . \quad . \quad (14)$$

Let Φ be the change of flux for a power of 1 watt absorbed in the ferrite. Then $A\delta M = P_1\Phi$, so that

$$\Phi = \frac{\lambda|\mu|}{3\,000lM_s}$$

Substituting for $|\mu|/M_s$ in eqn. (13), we get

$$L = \frac{10^{-16}N_i^2\omega_i^2P_1}{2R}\Phi^2 \quad . \quad . \quad . \quad . \quad (15)$$

In this formula some figures provided by S.E.R.L. can be inserted. The value of Φ is measured as 0·0003 for a polycrystalline sample, but reasons are given later for using it here also for the single-crystal ferrite. $N_i = 70$ turns, $P_1 = 10$ watts, $\omega_i = 2\pi\times6\times10^7$. The circuit resistance was 30 ohms, which was several times the coil resistance. Eqn. (15) is derived from eqn. (5) in which the coefficient 1/4 comes from the assumed matching of circuit and coil. If the circuit resistance is much larger than the coil resistance the coefficient 1/4 is not needed. This amounts to taking $R = 30/4$ in eqn. (15), leading to $L = 4\times10^{-3} \equiv -24$ dB, compared with the conversion loss in conventional crystal mixers of the order of 10 dB or less. To achieve useful results both lower coil resistances and materials with larger values of Φ are therefore necessary. Even so, 10 watts local oscillator power is rather high.

To give $\Phi = 0{\cdot}0003$ with $M_s = 3000$ gauss, $\lambda = 3$ cm and $l = 1$ cm, the above equations require $|\mu| = 900$, which is about 100 times the measured value for polycrystalline samples, but which might be appropriate to a single-crystal sample. Reasons will be given later for linking the value of Φ measured for a polycrystalline sample with that for a single-crystal ferrite. The discrepancy in μ would then be resolved if one were to assume

(*a*) That the single-crystal line width is of the order of several gauss, giving a permeability of about 1 000 at resonance.
(*b*) There is a spread in the internal static field in a polycrystalline sample—possibly due to anisotropy fields—which causes only a degraded average value to appear in permeability *measurements* of polycrystalline samples.

It is accordingly necessary to amend the various formulae in the polycrystalline case in order to take account of such spread in characteristics from one part of the sample to another.

(5) POLYCRYSTALLINE FERRITE SAMPLE

The first question to be resolved is the distribution of the r.f. field in a heterogeneous sample. In the simple extreme case, in which all the grains are in the form of discs having as a common axis the applied static field, continuity at the boundaries requires that the transverse field be the same throughout the sample. At the other extreme, if the grains were of the form of concentric cylindrical shells, the boundary conditions would require continuity of $B = \mu H$ so that H would vary inversely as the local permeability. Between these two extremes, for a random sample, we expect to find H varying as a function both of the local and average value of μ, and we take $H_n \propto f(\mu_n)$, with f yet to be determined, for the field in the nth grain.

The most plausible function to take for $f(\mu)$ can be found from a consideration of the results of Kerner's paper* on the conductivity of composite media, where a similar problem occurs. His eqn. (9) for the conductivity of an assortment of conducting grains of different properties leads, in the magnetic case, to the conclusion that the quantity which is constant from grain to grain is the product $H_n(\mu_n + 2\mu_0)$. μ_0 is determined by

$$\sum_n v_n\frac{\mu_0 - \mu_n}{2\mu_0 + \mu_n} = 0 \quad . \quad . \quad . \quad . \quad . \quad . \quad (16)$$

where v_n is the volume of the nth grain. It is convenient to assume that all the grains have equal volume v/s.

Assume $H_n = Cf(\mu_n)$ where f = 1, $1/\mu$ or $1/(\mu + 2\mu_0)$ in the three cases considered. To calculate C we use eqn. (8) in the form of the power P_n absorbed in the nth grain

$$P_n = \frac{3\,000}{2\lambda}v_n|C^2f^2(\mu_n)|\mathscr{I}\mu_n \quad . \quad . \quad . \quad (17)$$

Summing eqn. (17) gives

$$P = \sum_1^s P_n = \frac{3\,000}{2\lambda}\frac{v}{s}\sum_1^s|f(\mu_n)|^2\mathscr{I}(\mu_n)C^2 \quad . \quad . \quad (18)$$

Hence, after solving eqn. (18) for C, we get

$$H_n = Cf(\mu_n) = \sqrt{\frac{2\lambda P}{3\,000v}}\frac{f(\mu_n)}{\sqrt{\left[\frac{1}{s}\sum_1^s\mathscr{I}(\mu_n)|f(\mu_n)|^2\right]}} \quad (19)$$

This replaces eqn. (8). The magnetization in the nth grain is $M_n = (\mu_n - 1)H_n \simeq \mu_nH_n$.

Eqn. (3) needs to be modified to take into account the phase difference in the r.f. magnetizations. If $M\exp j(\omega t + \phi)$ is taken as the form for the magnetization it is seen that the i.f.

* KERNER, E. H.: 'The Electrical Conductivity of Composite Media', *Proceedings of the Physical Society*, B, 1956, p. 802.

magnetization is $(M_1M_2/M_s)\cos(\omega_i t + \phi_1 - \phi_2)$, so that eqn. (3) is modified to

$$M_i = (M_1M_2/M_s)\exp j(\phi_1 - \phi_2) \quad . \quad . \quad . \quad (20)$$

Since $M \simeq \mu H$, the angle ϕ comprises two parts: the angle of μ and the angle of $f(\mu)$, which relates H to the power by means of eqn. (19). If the average magnetization of the grains is now calculated, and the derivation leading to eqn. (11) is repeated, it is seen that the permeability factor involved is

$$|\bar{\mu}|^2 = \frac{\left|\sum_1^s \mu_{n1}\mu_{n2}^* f(\mu_{n1}) f(\mu_{n2})^*\right|^2}{\sum_1^s \mathscr{I}(\mu_{n1})|f(\mu_{n1})|^2 \sum_1^s \mathscr{I}(\mu_{n2})|f(\mu_{n2})|^2} \quad (21)$$

This replaces $|\mu|^2$ in eqn. (13). (The asterisk denotes the complex conjugate.)

(6) THE FORM FOR μ

Take $\mu_n \simeq \mu_n - 1 = \gamma M_s/(\gamma H_{0n} - \omega + j\rho)$ where H_{0n} differs from grain to grain, giving a spread in values. It is necessary to assume something about the range and distribution of H_{0n}, the simplest being a rectangular distribution centred on a mean value. Although not very realistic, this form, which leads to some simplification in the mathematics, will be pursued in this Section. A triangular or other distribution could be used later as a refinement if the analysis seemed to justify it.

The equation for the permeability of the nth grain can thus be put in the form

$$\mu_n = \frac{\mu_p}{1 + j\beta(n - r)} \quad . \quad . \quad . \quad . \quad (22)$$

μ_p (negative imaginary) is the peak value reached when $\omega = \gamma H_{0n}$ in a single crystal. β is a measure of the spread and is related to the number of grains, whilst n now runs from $-\frac{1}{2}s$ to $+\frac{1}{2}s$. The number, r, indicates the position of the r.f. tuning in the bulk material. As can be seen from eqn. (22) if r lies within the region defined by the spread in magnetic fields there will be some grains at (or very near) to resonance. The calculations will be confined to Kerner's function $1/(\mu + 2\mu_0)$, ignoring the disc and cylinder arrangements as too idealistic.

The measured permeability μ_m is determined by the average magnetization divided by the average field

$$\mu_m = \frac{\sum_n \mu_n H_n}{\sum_n H_n} = \frac{\sum_n \mu_n/(2\mu_0 + \mu_n)}{\sum_n 1/(2\mu_0 + \mu_n)} \quad . \quad . \quad (23)$$

from eqn. (19)

Hence $$\sum_n \frac{\mu_m - \mu_n}{2\mu_0 + \mu_n} = 0$$

Comparing this with eqn. (16) it is seen that $\mu_n = \mu_0$, so that the composite permeability μ_0 appearing in eqn. (16) is simply the permeability of the bulk material which appears from straightforward measurements. However, it is seen to be a function of r, or frequency, and to emphasize this fact it will be written μ_r.

On replacing the summations in eqn. (23) by integrations, an approximate though adequate formula for μ_r is obtained:

$$\mu_r \simeq \int_{-s/2}^{s/2} \frac{dn}{1 + [1 + j\beta(n-r)]2\mu_r/\mu_p} \Big/ \int_{-s/2}^{s/2} \frac{[1 + j\beta(n-r)]dn/\mu_p}{1 + [1 + j\beta(n-r)]2\mu_r/\mu_p}$$

The integrations are quite straightforward. If we define an auxiliary quantity z by

$$z = -j\beta s\mu_r/\mu_p \quad . \quad . \quad . \quad . \quad . \quad (24)$$

z then satisfies the transcendental equation

$$z = \frac{3}{2}\log\frac{1 + z(1 + y) + 2z/j\beta s}{1 - z(1 - y) + 2z/j\beta s} \quad . \quad . \quad . \quad (25)$$

where $y = 2r/s$ is a measure of the r.f. tuning.

(It may sometimes be convenient to stress the dependence of z on r by writing it z_r.)

From eqn. (24)

$$\mu_r = \mu_p(-z/j\beta s) \quad . \quad . \quad . \quad . \quad . \quad (26)$$

and since it is anticipated that the values of μ_r will be appreciably less than μ_p, the quantity βs must (subject to later confirmation) be presumed to be large. The quantity z is complex with a magnitude of the order of 4, so that $2z/j\beta s$ is a small quantity and may be ignored in eqn. (25), leading to the modified equation

$$z = \frac{3}{2}\log\frac{1 + z(1 + y)}{1 - z(1 - y)} \quad . \quad . \quad . \quad . \quad (27)$$

From this equation, which can also be written in the form

$$y = \coth(z/3) - 1/z \quad . \quad . \quad . \quad . \quad (28)$$

it is seen that z is real for large values of y and possesses the asymptotic expansion

$$z \sim 2/y \qquad y \gg 1 \quad . \quad . \quad . \quad . \quad (29)$$

As y decreases a value is reached ($y = 0{\cdot}87$) at which z becomes complex. For $y = 0$ the value of z is imaginary. A semi-empirical relation in this complex region is

$$z \simeq \frac{3{\cdot}436y}{\sqrt{(1 - 0{\cdot}936y^2)}} - j3{\cdot}972\sqrt{\frac{1 - 1{\cdot}320y^2}{1 - 1{\cdot}038y^2}} \qquad 0 < y < 0{\cdot}87$$

. . . . (30)

For $y > 1$ a similar relation is

$$z \simeq \frac{2}{\sqrt{(y^2 - 0{\cdot}51)}} \quad . \quad . \quad . \quad . \quad (31)$$

A plot of the real and imaginary parts of z and $|z|$ is given in Fig. 3. The shape is rather different from the usual response

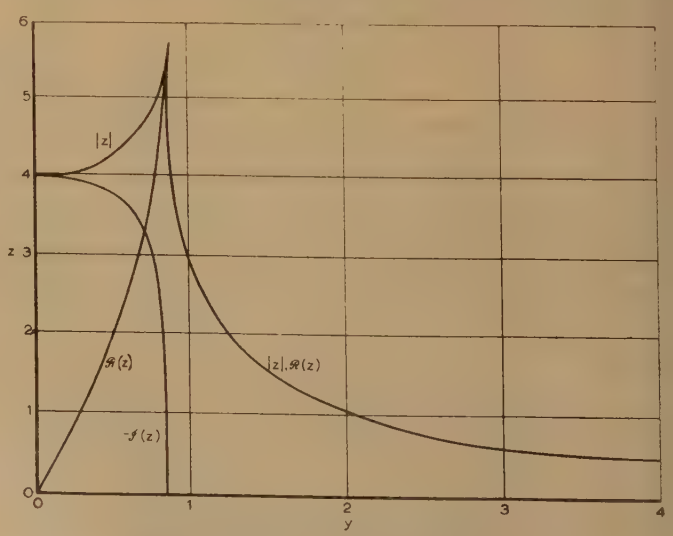

Fig. 3.—Curve of z plotted against y.

of measured materials, but this is a consequence of the rectangular distribution assumed for H_{0n}. (A tapered distribution, giving a concentration of internal fields around a central value, would be more realistic and would lead to a rounded top to the curve.) It is seen that $y = 1$ gives the value of r.f. tuning at which $|z|$ has fallen to 0·707 of its central value, the quantity by which the line width is usually measured. The value of $|z|$ at tuning is approximately 4, leading to

$$\mu_{r=0} = 4\mu_p/\beta s \quad . \quad . \quad . \quad . \quad . \quad (32)$$

In Section 4 a peak value for μ of about 100 times the measured value was required. If the explanation of this factor is given correctly by the present analysis, it is seen from eqn. (32) that $\beta s \simeq 400$, justifying the statement that βs is large. It remains to be shown that the present analysis also leads to a value of $\bar{\mu}$ in eqn. (21) which is *not* degraded, as is the measured permeability, by a factor of this order.

Since μ_p is imaginary,

$$\mathscr{I}(\mu) = \frac{|\mu_p|}{1 + \beta^2(n-r)^2} = \frac{|\mu_p|}{(1+jB)(1-jB)} \text{ where } B = \beta(n-r) \quad . \quad . \quad . \quad . \quad (33)$$

Hence

$$\mathscr{I}(\mu)|f(\mu)|^2 = \frac{\mathscr{I}(\mu)}{(2\mu_r + \mu)(2\mu_r^* + \mu^*)} = \frac{\beta^2 s^2/|\mu_p|}{4zz^*(1 + jB - j\beta s/2z)(1 - jB + j\beta s/2z^*)}$$

on substituting for μ_r and μ from eqns. (22) and (24).

This expression can be put into partial fractions, and on replacing B by $\beta(n-r)$ and integrating, there is found (*inter alia*) the difference between the logarithmic term of eqn. (25) and its complex conjugate. Using eqn. (25) to express this more simply as $\frac{2}{3}(z - z^*)$ it is found that

$$\mathscr{I}(\mu)|f(\mu)|^2 = \frac{(\beta s)^2}{3\beta|\mu_p|} \frac{z - z^*}{\beta s(z - z^*) - 4jzz^*}$$

Consistent with the approximation in going from eqn. (25) to (27), the second term in the denominator can be ignored, giving

$$\mathscr{I}(\mu)|f(\mu)|^2 = \frac{s}{3|\mu_p|} \quad . \quad . \quad . \quad . \quad (34)$$

This is independent of the position of the r.f. tuning. On substituting eqn. (34) in the denominator of eqn. (21) it is therefore not necessary to take note of the subscripts 1 and 2, which may accordingly be dropped. Hence eqn. (21) becomes

$$|\bar{\mu}| = \frac{3|\mu_p|}{s}\left|\sum_1^s \mu_{n1}\mu_{n2}^* f(\mu_{n1}) f(\mu_{n2})^*\right| \quad . \quad . \quad (35)$$

The expressions involved, after substituting for μ_n and μ_r at the two respective frequencies, are substantially the same as those involved in reaching eqn. (34). The result of the integrations gives $\frac{2}{3}(z_0 - z_r^*)$, where z_0 is the value of z_r at $r = 0$ (the ferrite being on tune at the signal frequency).

The following form is obtained

$$|\bar{\mu}| = |\mu_p|\left|\frac{z_0 - z_r^*}{z_0 - z_r^* + yz_0z_r^*}\right| = \left|\frac{|\mu_p|}{1 + y\left(\frac{1}{z_r^*} - \frac{1}{z_0}\right)}\right| \quad (36)$$

Near $y = 0$, $z = -j3{\cdot}97 + 3{\cdot}44y$, from eqn. (30). Substituting in eqn. (36), we get, for values of y less than about 0·5,

$$|\bar{\mu}| \simeq |\mu_p|/\sqrt{(1 + 0{\cdot}689y^2)} \quad . \quad . \quad . \quad (37)$$

Since $y = 1$ corresponds to the half-width tuning of the *measured* permeability μ_r, it is seen that, qualitatively, $|\bar{\mu}|$ possess the peak permeability of the single grain but the broader tuning curve of the bulk polycrystalline material. This mirrors for the bulk material the property evident in eqn. (13), wherein the tuning of the ferrite is shown to be without direct effect. It also justifies the claim that the permeability for the single crystal may also be used for the polycrystalline ferrite, and suggests that no direct advantage (in the present device) is likely to arise from the use of a single-crystal sample, since the peak permeability is already realized in the polycrystalline medium whose broader tuning curve is obviously better suited for matching the power into the ferrite.

(7) CONCLUSIONS

The S.E.R.L. magnetization measurements can be explained, at least as far as order of magnitude is concerned, on the assumption that the basic permeability line width is of the order of only a few gauss. In polycrystalline samples, a spread of the local internal field, caused perhaps by anisotropy forces, debases the measured permeability by a factor of the order of 100. Nevertheless, and rather surprisingly perhaps, it is the peak value which appears in the formulae, provided that the local-oscillator and signal frequencies are not too far removed from the nominal resonance. In the single-crystal case the frequency placing with respect to the resonance does not seem to be of any direct consequence, although there may be difficulties in matching all the power into the ferrite, especially over a very broad signal band. However, the efficiency of the process, on the data used, appears to be about 14 dB lower than that obtainable from a conventional crystal mixer. Unless this figure can be improved appreciably, the practical application of the device is likely to be severely circumscribed.

Of considerable interest is the way in which μ enters the formulae. The structure is such that, although the average measured value of μ can be debased by a large factor, the effective value arises from a peculiar type of mean which is not degraded in the same way. In particular, the form $\mathscr{I}(\mu)/|\mu|^2$ is quite unaffected by the averaging process, the two factors giving complete mutual cancellation. This must surely be one of those rare cases in which nature has failed to take advantage of an averaging process and has left us with a product with peak performance.

621.313.013.23

The Institution of Electrical Engineers
Monograph No. 333
May 1959

THE CALCULATION OF THE MAGNETIC FIELD OF ROTATING MACHINES

Part 1.—The Field of a Tubular Current

By P. HAMMOND, M.A., Associate Member.

(*The paper was first received 6th October*, 1958, *and in revised form 2nd February*, 1959. *It was published as an* INSTITUTION MONOGRAPH *in May*, 1959.)

SUMMARY

An outline is given of a method for calculating the magnetic field of rotating machines. As a first stage in this work the field of a tubular current has been calculated, and curves are given for a particular example of such a current.

LIST OF SYMBOLS

A, A_r, A_θ, A_z = Vector potentials.
$a = \omega/c$.
$a''^2 = b^2 - a^2$.
$b = \pi/g$.
c = Velocity of light.
$2d$ = Axial length of end-ring.
g = Spacing between centres of successive tubes.
H, H_r, H_θ, H_z = Magnetic field strengths.
i_r, i_θ, i_z = Current line densities.
$\hat{i}_r$, $\hat{i}_\theta$, $\hat{i}_z$ = Maximum values of current line densities.
I_p, I_p' = Modified Bessel function and derivative of modified Bessel functions of the first kind and order p.
K_p, K_p' = Modified Bessel function and derivative of modified Bessel functions of the second kind and order p.
$2l$ = Axial length of tube.
L = Self-inductance.
m = A number.
N = Number of turns.
p = Number of pole pairs of current distribution.
r = Radius, co-ordinate.
s = An odd number.
t = Time.
x = A variable.
z = Length, co-ordinate.
α = An angle.
$\beta = 1/b^2r^2$.
$\gamma = R/r$.
$\delta = l/r$.
$\varepsilon = z/r$.
θ = An angle, co-ordinate.
λ = Electrical wavelength.
μ_0 = Magnetic constant.
ρ = A length.
ω = Angular frequency.

(1) INTRODUCTION

The continuing increase in the rating of generating plant is forcing manufacturers to work to extremely close tolerances in the design of a.c. generators. As a result, the magnetic field of such machines is being more closely examined than ever before. In such a programme of examination and research full-scale and model tests play an important part, but it is also of great interest to derive analytical solutions of the fields of certain idealized current distributions. Such solutions can offer general guidance to the designer, and they are helpful in opening up further avenues for experimental investigation. The paper contains the first stage of an analytical investigation carried out in the framework of a general research programme into the behaviour and design of rotating machines.

(2) GENERAL CONSIDERATIONS

(2.1) Statement of the Problem

An immense amount of work has been done since the end of the last century in examining the magnetic field of rotating machines, but this work has been almost exclusively concentrated on the 2-dimensional field of the slot portion. This region is undoubtedly the most important part of the machine, and a number of valuable mathematical tools have been developed to deal with its field. Conformal transformations, relaxation methods and series solutions of Laplace's equation have all been used with good effect: in such methods, the a.c. field is described by a scalar potential function, so that a.c. machines are dealt with by extrapolation from the d.c. case. While this is a perfectly satisfactory approach in the derivation of numerical solutions, it is an approach which turns its back on Maxwell's electromagnetic theory and thus sacrifices much of the understanding of problems involving energy transfer by electromagnetic induction. Moreover, the methods which are so successful in dealing with the 2-dimensional field of the slot portion fail when they are applied to the field of the end-windings. Here a 3-dimensional approach is essential, but the writer is not aware of any successful attempt at solving this problem. Generally, the end-windings are dismissed in some remarks of a qualitative nature. Until recently, such a general discussion may have been satisfactory, but it is quite insufficient if information is sought for the design of end-windings which shall give rise to the smallest possible eddy losses in the core end-plates and associated metal structures.

The difficulties in the path of anybody trying to derive an analytical solution of the magnetic field of an alternator end-winding are considerable. It is true that all the conductors are usually of the same shape, but this shape is not at all amenable to mathematical treatment. To add to the difficulties there are iron masses of various shapes near the conductors. A close examination of turbo-alternator end-windings may well give the impression that a solution of the problem is impossible by analytical methods. Such an impression is strictly correct, but it is not therefore correct to abandon analytical methods: electrical-engineering practice abounds in impossible problems. The general method of attack is to replace the actual physical structure by an idealized one which is amenable to analysis. The practical designer can then use the idealized solution to give him general guidance on the problem he has in hand.

(2.2) Proposed Method of Attack

For the alternator end-winding we propose three simplifications, namely

(*a*) The actual conductor currents are to be replaced by current sheets.
(*b*) The current sheets are to be of simple geometrical shape.
(*c*) There shall be no iron in the vicinity of the current sheets.

Correspondence on Monographs is invited for consideration with a view to publication.
Mr. Hammond is in the Department of Engineering, University of Cambridge.

The first simplification does not greatly depart from reality, and is equivalent to the simplification which divides the air-gap flux into a series of harmonic components. The magnetic field of a suitable arrangement of current sheets can correctly describe the magnetic field of the conductor currents, except in the immediate vicinity of the conductors. More specifically, it will be sufficient to use a current sheet with simple harmonic variation of current density along it to describe the fundamental space component of the magnetic field of the conductor currents. The second simplification is imposed at this stage of the work in order to avoid complications. It is hoped that it will be possible to remove it gradually by the superposition of certain simple standard current distributions, when these have been analysed. The third simplification is a drastic one. But before the effect of iron can be included in the problem it is in any case necessary to calculate the magnetizing field. Thus the solutions here set out are incomplete as they stand. It should be kept in mind, however, that not all coils have iron cores. The solutions derived in the paper do not give a complete description of the field of rotating machines: they are only the first stage of such a work, but they stand in their own right as the solution of the field of a certain current distribution and they are likely to find application in other branches of electrical engineering. It is hoped to include the effect of iron when the magnetizing field of various current distributions has been fully investigated.

Whereas the three simplifications cause the present work to depart to some extent from actual engineering practice, there is one aspect of the treatment which is a decided advance on previous methods. We propose to describe the magnetic field in terms of Maxwell's complete theory by means of a vector potential and not a scalar potential. Thus the alternating currents will no longer be treated as modifications of direct currents. The proposed method enables us to deal with alternating currents of any frequency, and there are considerable incidental advantages, which are set out in Section 3.2. The general subject of energy transfer has been discussed in a previous paper.[1] It is hoped to consider it in more detail at a later date when eddy-current losses are to be considered. It is worth noting here that the existence of eddy currents depends on alternating magnetic fields and that the logical approach must be through the general equations of electromagnetism. This is the approach adopted here.

Having now stated the problem in general terms, we propose to devote the rest of the paper to the detailed discussion of a particular example.

(3) THE MAGNETIC FIELD OF A TUBULAR CURRENT DISTRIBUTION

(3.1) Description

The general symmetry of rotating machines is cylindrical and we propose to consider cylindrical current sheets. Fig. 1(*a*) shows such a current sheet in which the current flow is axial and is designated i_z. The question of continuity of current flow is discussed in Sections 3.2 and 3.3, but at this stage the current sheet should be regarded merely as a current-element, i.e. as an incomplete portion of a current circuit. It will be noted that the line density of the current varies around the tube. This variation is supposed to be of the form $\hat{\imath}_z \sin p\theta$ and thus to represent a winding with $2p$ poles.

Consider now Fig. 1(*b*), which shows a circumferential current sheet i_θ also arranged in $2p$ poles. Here the line density varies as $-\hat{\imath}_\theta \cos p\theta$.

Fig. 1(*c*) shows the radial component of current, i_r. Again the distribution around the tubular sheet is polar and the density varies as $\hat{\imath}_r \sin p\theta$. The current sheet i_r is introduced for the sake of completeness, but is not discussed further. It is clear that any current distribution can be built up by the superposition of the three types of current-element shown.

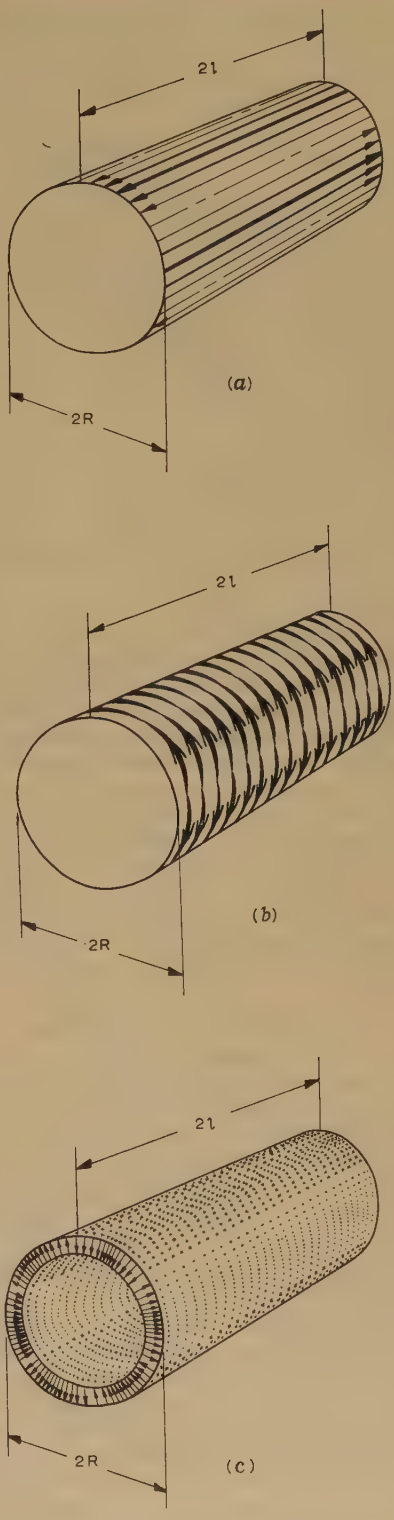

Fig. 1.—Axial (*a*), circumferential (*b*) and radial (*c*) tubular current sheets.

Fig. 2 shows a combination of axial and circumferential

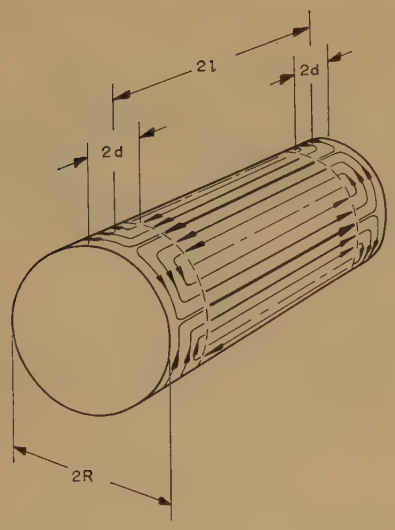

Fig. 2.—A tubular current made up of an axial section and two end-rings.

current sheets resembling the current distribution in the rotor of a squirrel-cage induction motor. The axial current sheet represents the slot portion and the circumferential sheets the end-rings of the induction motor. The problem is to find the magnetic field of this postulated current distribution, and we do not discuss how such a current could be caused to flow in a certain conducting material. For convenience in calculation the current sheets are assumed to be infinitesimally thin. The radius of the tubular sheets is R, the axial length of the axial current sheet is $2l$ and the axial length of each end-ring is $2d$. Cylindrical co-ordinates r, θ and z are chosen, the origin of co-ordinates being on the axis of the tube half-way along it. The positive direction of z is from left to right and θ is therefore measured clockwise in a right-handed system of axes.

(3.2) The Field of the End-Rings

It has been stated in Section 2.1 that we are particularly anxious to calculate the magnetic field of the end-windings. In the tubular current distribution shown in Fig. 2 these end-windings take the form of rings, and it would be very desirable to calculate the field of these rings by themselves. If the current were of constant strength in the θ-direction, the magnetic field could be described by means of Legendre functions. Since there is a variation along the θ-direction [see Figs. 1(*b*) and 2], the obvious first choice is to use tesseral harmonics, i.e. Legendre functions which have a θ-variation. However, it was found that a solution in terms of these functions was not obtainable. This is not surprising, when it is remembered that the basis of such a solution is the replacement of the current distribution by a magnetic-dipole layer on the surface of a sphere. The method uses a scalar magnetic potential and is strictly applicable to problems involving only direct-current flow. But isolated end-rings carrying direct currents of varying strengths in the θ-direction are a physical impossibility. The mathematical failure arises directly from this physical impossibility. The current has to be fed into the end-rings, and it is impossible to obtain the field of the end-rings by themselves if the current is unidirectional.

This objection falls away if the current is alternating. The continuity of such a current can be assured by the provision of additional finite distributions of electric charge such that the divergence of current is equal to the rate of decrease of charge. The magnetic field will depend only on the current, and hence it is possible in principle to calculate the magnetic field of the end-rings quite apart from that of the axial current flow. Similarly, it is possible to calculate the magnetic field of the axial current flow by itself. A scalar magnetic potential is not applicable to the a.c. case and a vector potential will have to be used. This has already been mentioned in Section 2.2.

(3.3) The Form of the Solution

Because of the cylindrical symmetry of the structure, it is convenient to use Bessel functions in the analysis. The treatment is an extension of that given by Moullin,[2] who employed Bessel functions in the calculation of the self-inductance of single-layer solenoids. We first obtain the vector potential $\boldsymbol{A}$ of the current distribution and thence by the relationship $\mu_0 \boldsymbol{H} = \text{curl}\, \boldsymbol{A}$ the magnetic field strength $\boldsymbol{H}$.

The charge distributions mentioned in Section 3.2 can be dispensed with if the current flow is made continuous. Thus the end-rings could be placed over the ends of the axial current sheet in such a way that the axial current diminished towards the ends while the circumferential flow increased. A possible distribution of current would be a constant circumferential current density over the width $2d$ of the end-rings with a corresponding linear decrease of axial current flow over the distance $l - d < z < l + d$ at the ends of the tubular flow. Here the treatment is somewhat simplified by the assumptions that $2d \ll l$ and that the current changes direction at $z = \pm l$. It will be noted that the restriction of the solution to a.c. problems does not apply if the current flow is made continuous; but in such cases the axial and circumferential currents cannot be treated in isolation.

In order to deal with the finite length of the current sheets, use is made of Fourier series. The single isolated tubular current is replaced by an infinite coaxial succession of equal and oppositely directed current sheets spaced at a distance of g between adjacent sheets (see Figs. 3 and 4). It is clear that for

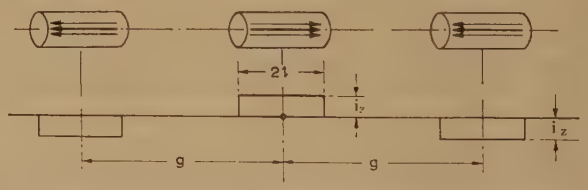

Fig. 3.—Infinite succession of equal and oppositely directed axial current sheets.

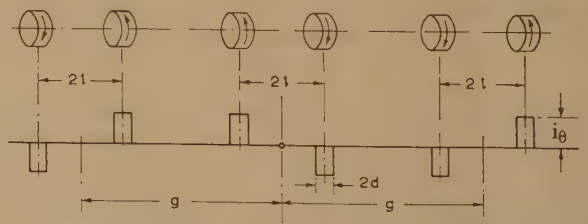

Fig. 4.—Infinite succession of pairs of equal and oppositely directed circumferential current sheets.

$g \gg 2l$ the solution will be very near to that of an isolated tube. This assumption is examined more closely in Section 3.4.

The method of obtaining the solution is competent to deal with currents of any frequency, but in order to keep the present account as short as possible, our treatment is restricted to wavelengths such that $\lambda \gg 2g$. This means that the solution is expressed in terms of modified Bessel functions of argument substantially independent of the frequency (see Appendix).

The three components of the magnetic field have been derived in the Appendix. Rationalized units have been used. If $r > R$,

$$H_r = \frac{4}{\pi}\frac{\hat{\imath}_z R^2 b^2}{p}\cos p\theta \sin \omega t \sum_{s=1}^{\infty} sK_p'(sbr)I_p'(sbR)\sin sbl \cos sbz \quad . \quad (1)$$

$$H_\theta = \frac{4}{\pi}\frac{\hat{\imath}_z R^2 b}{r}\sin p\theta \sin \omega t \sum_{s=1}^{\infty} K_p(sbr)I_p'(sbR)\sin sbl \cos sbz \quad . \quad (2)$$

$$H_z = \frac{4}{\pi}\frac{\hat{\imath}_z R^2 b^2}{p}\cos p\theta \sin \omega t \sum_{s=1}^{\infty} sK_p(sbr)I_p'(sbR)\sin sbl \sin sbz \quad . \quad (3)$$

If $r < R$,

$$H_r = \frac{4}{\pi}\frac{\hat{\imath}_z R^2 b^2}{p}\cos p\theta \sin \omega t \sum_{s=1}^{\infty} sI_p'(sbr)K_p'(sbR)\sin sbl \cos sbz \quad . \quad (4)$$

$$H_\theta = \frac{4}{\pi}\frac{\hat{\imath}_z R^2 b}{r}\sin p\theta \sin \omega t \sum_{s=1}^{\infty} I_p(sbr)K_p'(sbR)\sin sbl \cos sbz \quad . \quad (5)$$

$$H_z = \frac{4}{\pi}\frac{\hat{\imath}_z R^2 b^2}{p}\cos p\theta \sin \omega t \sum_{s=1}^{\infty} sI_p(sbr)K_p'(sbR)\sin sbl \sin sbz \quad . \quad (6)$$

where $\hat{\imath}_z$ is the maximum line density of axial current, $b = \pi/g$, ω is the angular frequency, and s is restricted to odd numbers. It will be noted that the series are convergent everywhere except at $r = R$. Here H_r and H_z oscillate finitely except at $z = \pm l$, where H_z diverges to infinity. This lack of convergency is a result of making $2d \ll l$ and will disappear if this simplification is abandoned.

The above series have been used to calculate the field of tubular currents for which $l = 2R$ and $g = 4(l + R) = 12R$, and $p = 1$ and 2. The results are shown in Figs. 5 and 6 and merit close study. Of particular interest is the remarkable difference in the internal field between the 2-pole case ($p = 1$) shown in Fig. 5 and the 4-pole case ($p = 2$) shown in Fig. 6. It appears that H_r and H_θ vary as r^{p-1}, whereas H_z varies as r^p. This follows from the behaviour of the Bessel function I_p near the origin of co-ordinates. Thus the stator iron-loss of turbo-alternators is likely to be greater than that of multi-polar machines because a greater amount of iron surface, particularly at the end-plates, lies in a strong magnetic field. It will be noted that Figs. 5 and 6 are given in non-dimensional form.

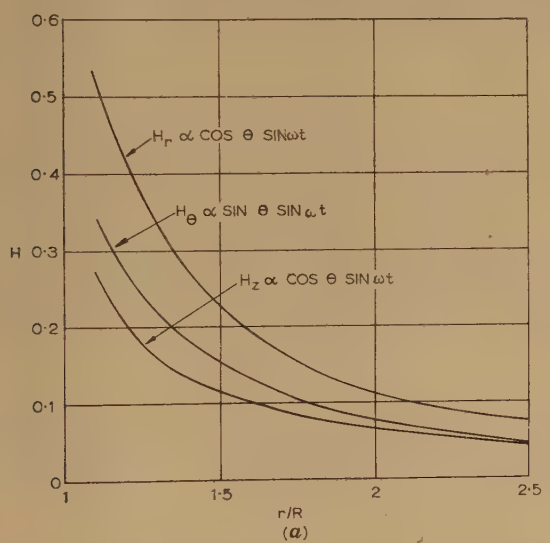

(a)

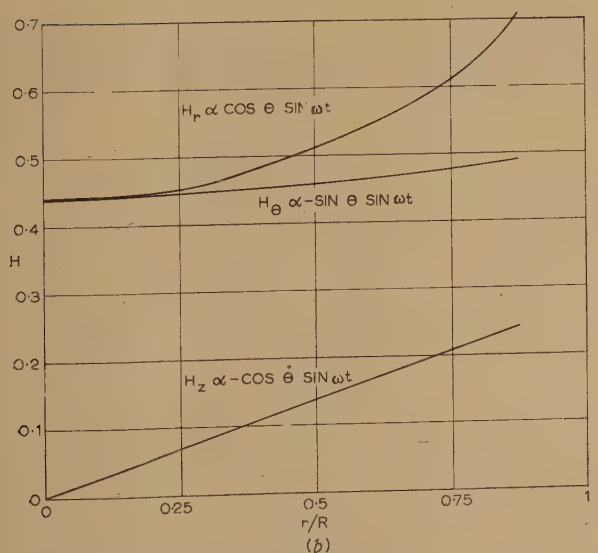

(b)

Fig. 5.—Magnetic fields for 2-pole tubular current.
(a) $r > R$.
(b) $r < R$.

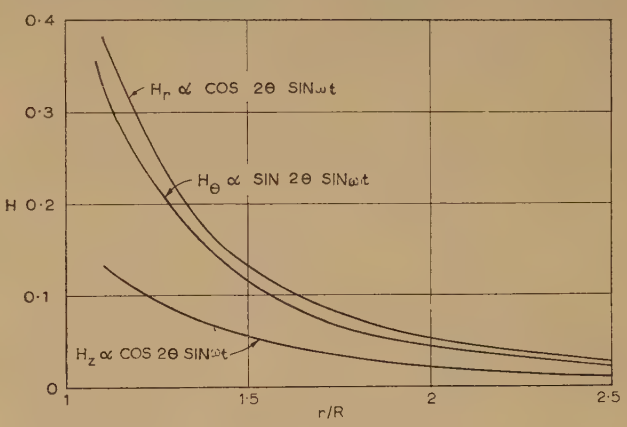

(a)

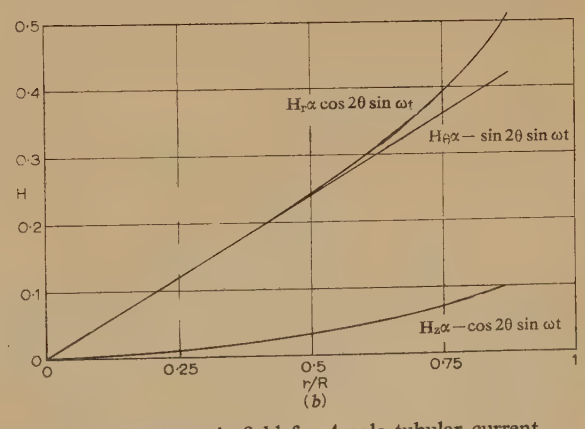

(b)

Fig. 6.—Magnetic field for 4-pole tubular current.
(a) $r > R$.
(b) $r < R$.

It is very important to realize explicitly that the order of the Bessel functions is linked to the order of the circular functions. Thus I_p, I_p', K_p and K_p' are linked to sin $p\theta$ and cos $p\theta$. It is clear that a change in the number of pole pairs must produce a different polar distribution of the magnetic field in the θ-direction, but it is not immediately obvious whether there would be a corresponding change in the r-direction. This question is answered when the relationship between Bessel functions and circular functions is taken into account. Thus formulae (2)–(6) enable one to see at a glance how the number of pole pairs affects the magnetic field in both the θ- and r-directions.

(3.4) The Limiting Case of an Isolated Tubular Current

It was stated in Section 3.3 that the solution obtained applies strictly to an infinite succession of tubular currents on a common axis. In order to obtain the solution for a single isolated tube, we must make g very large in comparison with the dimensions of the tube. In the limit, the infinite series will become infinite integrals and we shall have expressions of the type

$$-H_r = \frac{4}{\pi}\frac{\hat{\imath}_z R^2 b^2}{p}\cos p\theta \sin \omega t \int_0^\infty \beta x K_p'(x) I_p'(\gamma x) \sin \delta x \cos \varepsilon x dx$$

Such infinite integrals are likely to be exceedingly cumbersome in computation and it is highly desirable to retain the simplicity of the series solutions, especially since the series are rapidly convergent, if g is not very large. The question arises as to the choice of g. In effect we must choose g so that the mutual inductance of adjacent tubes is negligible. This provides a useful check, since both the series solution and the integral solution for the self-inductance of a single-layer solenoid are available.[2] Fig. 7 shows the self-inductance of solenoids for

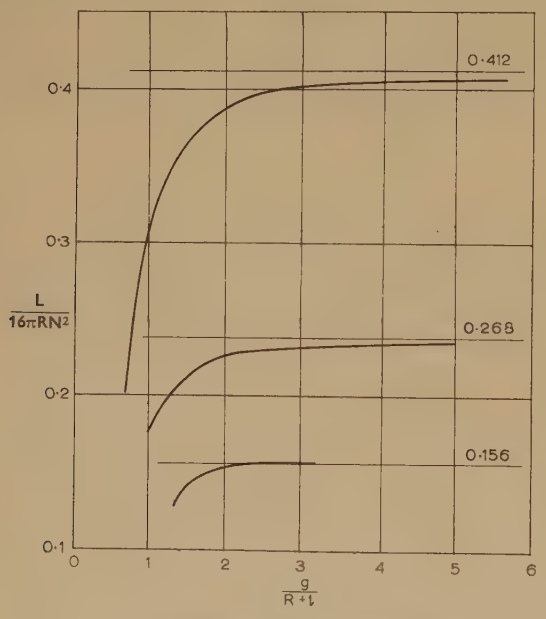

Fig. 7.—Self-inductance of single-layer solenoids.

which $l = 2R$, $l = R$, and $l = \frac{1}{2}R$. It will be seen that the series solution in each case tends rapidly to the asymptotic value obtained by means of an infinite integral. If $l = 2R$, it is seen that, even if g has the smallest possible value of $g = 2l$, i.e. if there is no gap between successive solenoids, the self-inductance is already within 18% of that of an isolated solenoid. With our value of $g = 4(R + l)$ there is no difference between the series and the integral solutions. With very short tubes of large diameter the approach to the asymptotic value is not so rapid, but it is clear that with the choice of a suitable g the series solution can be employed without appreciable loss of accuracy.

(4) ACKNOWLEDGMENTS

The author wishes to acknowledge the encouragement given to him by Sir Willis Jackson, Director of Research of the Metropolitan-Vickers Electrical Co., Ltd. Thanks are also due to Mr. S. Neville of that Company for many stimulating discussions and to Professor E. B. Moullin for advice throughout the course of the work.

(5) REFERENCES

(1) HAMMOND, P.: 'Electromagnetic Energy Transfer', *Proceedings I.E.E.*, Monograph No. 286, February, 1958 (**105** C, p. 352).
(2) MOULLIN, E. B.: 'The Use of Bessel Functions for Calculating the Self-Inductance of Single-Layer Solenoids', *ibid.*, 1949, **96**, Part III, p. 133.
(3) MOULLIN, E. B.: 'Radio Aerials' (Clarendon Press, 1949), p. 42.
(4) WATSON, G. N.: 'Theory of Bessel Functions' (University Press, Cambridge, 1944), p. 361.
(5) MOULLIN, E. B.: 'Radio Aerials' (Clarendon Press, 1949), p. 44.

(6) APPENDIX

(6.1) The Vector Potential of a Tubular Current

(6.1.1) The Vector Potential of an Axial Current of Line Density $\hat{\imath}_z \sin p\alpha \sin \omega t$ distributed around the Surface of a Tube of Radius R.

Refer to Fig. 8 and consider the vector potential at P due to a filament of current at Q. The filament is assumed to be infinitely

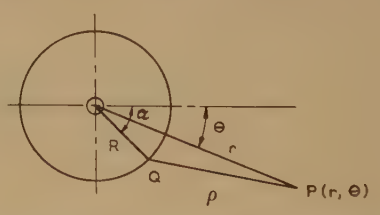

Fig. 8.—Relating to the vector potential of a tubular current.

long and the magnitude of the current varies as cos bz along the filament. Then it can be shown[3] that

$$\frac{2\pi\delta A_z}{\mu_0 \hat{\imath}_z R \cos bz \sin \omega t} = K_0(a''\rho) \sin p\alpha d\alpha \quad . \quad . \quad . \quad (7)$$

where ρ is the distance QP and

$$\text{where} \quad a''^2 = b^2 - a^2 = \left(\frac{\pi}{g}\right)^2 - \left(\frac{\omega}{c}\right)^2 = \left(\frac{\pi}{g}\right)^2 - \left(\frac{2\pi}{\lambda}\right)^2$$

$$\text{But } K_0(a''\rho) = \sum_{m=-\infty}^{+\infty} K_m(a''r) I_m(a''R) \cos m(\alpha - \theta) \text{ (Ref. 4)} \quad (8)$$

Hence the vector potential A_z at P due to the tubular current is given by

$$\frac{2\pi A_z}{\mu_0 \hat{\imath}_z R \cos bz \sin \omega t} = \int_0^{2\pi} \left[\sum_{-\infty}^{+\infty} K_m(a''r) I_m(a''R)(\cos m\alpha \cos m\theta + \sin m\alpha \sin m\theta) \sin p\alpha d\alpha \right] = 2\pi K_p(a''r) I_p(a''R) \sin p\theta \quad . \quad (9)$$

$$\text{Hence} \quad A_z = \mu_0 \hat{\imath}_z R K_p(a''r) I_p(a''R) \sin p\theta \cos bz \sin \omega t \quad . \quad (10)$$

This is the result for $r > R$. If $r < R$ we have

$$A_z = \mu_0 \hat{\imath}_z R \mathrm{I}_p(a''r)\mathrm{K}_p(a''R) \sin p\theta \cos bz \sin \omega t \quad . \quad (11)$$

In order to deal with the finite length of the tube we shall make use of a Fourier series. Referring to Fig. 3 we can write the current line density as

$$i_z = \frac{4}{\pi}\hat{\imath}_z \sum_{s=1}^{\infty} \frac{1}{s} \sin sbl \cos sbz \quad . \quad . \quad . \quad . \quad (12)$$

when s is odd. If now $a''^2 \simeq b^2$, because $g \ll \lambda/2$, the expressions for the vector potential become, if $r > R$

$$A_z = \frac{4}{\pi}\mu_0 \hat{\imath}_z R \sin p\theta \sin \omega t \sum_{s=1}^{\infty} \frac{1}{s}\mathrm{K}_p(sbr)\mathrm{I}_p(sbR) \sin sbl \cos sbz \quad (13)$$

and if $r < R$,

$$A_z = \frac{4}{\pi}\mu_0 \hat{\imath}_z R \sin p\theta \sin \omega t \sum_{s=1}^{\infty} \frac{1}{s}\mathrm{I}_p(sbr)\mathrm{K}_p(sbR) \sin sbl \cos sbz \quad (14)$$

s being restricted to odd numbers.

It will be noted that A_z satisfies Bessel's equation in that Bessel functions of order p are associated with circular functions of order p.

(6.1.2) The Vector Potential of a Circumferential Current of Line Density $-\hat{\imath}_\theta \cos p\alpha \sin \omega t$ distributed around the Surface of a Tube of Radius R.

Refer to Fig. 8 and note that the current now flows around the circumference of the tube. Consider first the vector potential at P due to a blade of current[5] at Q. By a 'blade of current' is meant a narrow strip of infinite length with current flowing transversely to the length. The magnitude of the current varies as sin bz along the axial length of the tube. The vector potential at P will have a radial and a tangential component. Let these be denoted by A_r and A_θ, respectively. Then, if $r > R$,

$$\frac{2\pi\delta A_r}{\mu_0 \hat{\imath}_\theta R \sin bz \sin \omega t} = \mathrm{K}_0(a''\rho) \sin(\alpha - \theta) \cos p\alpha d\alpha$$

$$= \tfrac{1}{2}\mathrm{K}_0(a''\rho)\{\sin[(p+1)\alpha - \theta] - \sin[(p-1)\alpha - \theta]\}d\alpha$$

$$= \tfrac{1}{2}\mathrm{K}_0(a''\rho)[\sin(p+1)\alpha \cos\theta - \cos(p+1)\alpha \sin\theta - \sin(p-1)\alpha \cos\theta - \cos(p-1)\alpha \sin\theta]d\alpha \quad (15)$$

Also

$$\mathrm{K}_0(a''\rho) = \sum_{m=-\infty}^{+\infty} \mathrm{K}_m(a''r)\mathrm{I}_m(a''R)(\cos m\alpha \cos m\theta + \sin m\alpha \sin m\theta) \quad . \quad . \quad . \quad . \quad (16)$$

Hence

$$\frac{-2A_r}{\mu_0 \hat{\imath}_\theta R \sin bz \sin \omega t} = \mathrm{K}_{p+1}(a''r)\mathrm{I}_{p+1}(a''R)[\cos(p+1)\theta \sin\theta - \sin(p+1)\theta \cos\theta] + \mathrm{K}_{p-1}(a''r)\mathrm{I}_{p-1}(a''R)[\cos(p-1)\theta \sin\theta + \sin(p-1)\theta \cos\theta]$$

$$-A_r = \tfrac{1}{2}\mu_0 \hat{\imath}_\theta R[\mathrm{K}_{p-1}(a''r)\mathrm{I}_{p-1}(a''R) - \mathrm{K}_{p+1}(a''r)\mathrm{I}_{p+1}(a''R)] \sin p\theta \sin bz \sin \omega t \quad . \quad (17)$$

Similarly,

$$-A_\theta = \tfrac{1}{2}\mu_0 \hat{\imath}_\theta R[\mathrm{K}_{p-1}(a''r)\mathrm{I}_{p-1}(a''R) + \mathrm{K}_{p+1}(a''r)\mathrm{I}_{p+1}(a''R)] \cos p\theta \sin bz \sin \omega t \quad . \quad (18)$$

If $r < R$,

$$-A_r = \tfrac{1}{2}\mu_0 \hat{\imath}_\theta R[\mathrm{I}_{p-1}(a''r)\mathrm{K}_{p-1}(a''R) - \mathrm{I}_{p+1}(a''r)\mathrm{K}_{p+1}(a''R)] \sin p\theta \sin bz \sin \omega t \quad . \quad (19)$$

$$-A_\theta = \tfrac{1}{2}\mu_0 \hat{\imath}_\theta R[\mathrm{I}_{p-1}(a''r)\mathrm{K}_{p-1}(a''R) + \mathrm{I}_{p+1}(a''r)\mathrm{K}_{p+1}(a''R)] \cos p\theta \sin bz \sin \omega t \quad . \quad (20)$$

In order to deal with the finite length of the tube we shall make use of a Fourier series. Referring to Fig. 4, we can write the current density as

$$i_\theta = \frac{8}{\pi}\hat{\imath}_\theta \sum_{s=1}^{\infty} \frac{1}{s} \sin sbl \sin sbd \sin sbz \quad . \quad . \quad . \quad (21)$$

when s is odd.

If $a'' \simeq b$, the expressions for the vector potential can be expressed as infinite series similar to the series obtained for A_z.

(6.1.3) The Divergence of the Vector Potential.

If the current flow is continuous there need be no electric-charge distributions; hence the vector potential must have no divergence. The calculation of this divergence thus serves as a useful check.

$$\operatorname{div} A = \frac{\partial A_z}{\partial z} + \frac{\partial A_r}{\partial r} + \frac{A_r}{r} + \frac{1}{r}\frac{\partial A_\theta}{\partial \theta} \quad . \quad . \quad (22)$$

Consider the case $r > R$ and take a typical term of the Fourier series.

$$\frac{\operatorname{div} A}{\mu_0 \sin \omega t} = -\frac{4}{\pi}\hat{\imath}_z Rb\mathrm{K}_p(sbr)\mathrm{I}_p(sbR) \sin sbl \sin sbz \sin p\theta$$

$$-\frac{4}{\pi}\frac{\hat{\imath}_\theta R}{rs}\{[sbr\,\mathrm{K}'_{p-1}(sbr) + \mathrm{K}_{p-1}(sbr)]\mathrm{I}_{p-1}(sbR) - [sbr\mathrm{K}'_{p+1}(sbr) + \mathrm{K}_{p+1}(sbr)]\mathrm{I}_{p+1}(sbR)\} \sin p\theta \sin sbl \sin sbd \sin sbz$$

$$+\frac{4}{\pi}\frac{\hat{\imath}_z Rp}{rs}[\mathrm{K}_{p-1}(sbr)\mathrm{I}_{p-1}(sbR) + \mathrm{K}_{p+1}(sbr)\mathrm{I}_{p+1}(sbR)] \sin p\theta \sin sbl \sin sbd \sin sbz \quad . \quad (23)$$

$$= -\frac{4}{\pi} R \sin p\theta \sin sbl \sin sbz \mathrm{K}_p(sbr)\mathrm{I}_p sbR\left[\hat{\imath}_z b - \frac{2\hat{\imath}_\theta \sin(sbd)p}{Rs}\right] \quad . \quad . \quad . \quad . \quad (24)$$

But in order to make the current continuous,

$$\tfrac{1}{2}\int_0^{\pi/p} \hat{\imath}_z \sin p\theta \, Rd\theta = 2\hat{\imath}_\theta d \quad . \quad . \quad . \quad . \quad (25)$$

Therefore

$$\frac{\hat{\imath}_z R}{p} = 2\hat{\imath}_\theta d \quad . \quad . \quad . \quad . \quad . \quad . \quad (26)$$

Also, if $d \ll g$, $\sin sbd \to sbd$

Hence

$$2\hat{\imath}_\theta \frac{\sin(sbd)p}{R_s} \simeq \frac{\hat{\imath}_z R}{pd}\frac{sbdp}{Rs} = \hat{\imath}_z b$$

and

$$\operatorname{div} A = 0$$

(6.2) The Magnetic Field of a Tubular Current

(6.2.1) The Axial Component H_z.

$$\mu_0 H_z = \frac{A_\theta}{r} + \frac{\partial A_\theta}{\partial r} - \frac{1}{r}\frac{\partial A_r}{\partial \theta} \quad . \quad . \quad . \quad (27)$$

Consider first an infinitely long tube of current varying as sin bz. Then, for $r > R$,

$$-\mu_0 H_z = \tfrac{1}{2}\mu_0 \frac{\hat{\imath}_\theta R}{r} \cos p\theta \sin bz \sin \omega t\{[\mathrm{K}_{p-1}(a''r)\mathrm{I}_{p-1}(a''R) + \mathrm{K}_{p+1}(a''r)\mathrm{I}_{p+1}(a''R)] + a''r[\mathrm{K}'_{p-1}(a''r)\mathrm{I}_{p-1}(a''R) + \mathrm{K}'_{p+1}(a''r)\mathrm{I}_{p+1}(a''R)] - p[\mathrm{K}_{p-1}(a''r)\mathrm{I}_{p-1}(a''R) - \mathrm{K}_{p+1}(a''r)\mathrm{I}_{p+1}(a''R)]\} \quad (28)$$

Hence

$$-H_z = \hat{\imath}_\theta R \cos p\theta \sin bz \sin \omega t[-a''rK_p(a''r)I_{p-1}(a''R) - a''rK_p(a''r)I_{p+1}a''R] \quad . \quad (29)$$

$$H_z = \tfrac{1}{2}\hat{\imath}_\theta \frac{R}{2r} \cos p\theta \sin bz \sin \omega t\, 2a''K_p(a''r)I'_p(a''R) \quad . \quad (30)$$

If $a'' \simeq b$ and instead of $\hat{\imath}_\theta \sin bz$ we have

$$\frac{8}{\pi}\hat{\imath}_\theta \sum_{s=1}^{\infty} \frac{1}{s} \sin sbl \sin sbd \sin sbz, \text{ and if } \hat{\imath}_\theta = \hat{\imath}_z R/2pd,$$

$$H_z = \frac{4}{\pi}\frac{\hat{\imath}_z R^2 b}{pd} \cos p\theta \sin \omega t \sum_{s=1}^{\infty} K_p(sbr)I'_p(sbR) \sin sbl \sin sbd \sin sbz \quad . \quad (31)$$

If $\sin sbd \to sbd$

$$H_z = \frac{4}{\pi}\frac{\hat{\imath}_z R^2 b^2}{p} \cos p\theta \sin \omega t \sum_{s=1}^{\infty} sK_p(sbr)I'_p(sbR) \sin sbl \sin sbz \quad . \quad . \quad . \quad . \quad (3)$$

If $r < R$,

$$H_z = \frac{4}{\pi}\frac{\hat{\imath}_z R^2 b^2}{p} \cos p\theta \sin \omega t \sum_{s=1}^{\infty} sI_p(sbr)K'_p(sbR) \sin sbl \sin sbz \quad . \quad . \quad . \quad . \quad (6)$$

It will be noted that H_z satisfies Bessel's equation, as it must.

(6.2.2) **The Radial Component H_r.**

$$\mu_0 H_r = \frac{1}{r}\frac{\partial A_z}{\partial \theta} - \frac{\partial A_\theta}{\partial z} \quad . \quad . \quad . \quad . \quad (32)$$

By the method given in Section 6.2.1, for $r > R$,

$$-H_r = \frac{4}{\pi}\frac{\hat{\imath}_z R^2 b^2}{p} \cos p\theta \sin \omega t \sum_{s=1}^{\infty} sK'_p(sbr)I'_p(sbR) \sin sbl \cos sbz \quad . \quad . \quad . \quad . \quad (1)$$

and if $r < R$,

$$-H_r = \frac{4}{\pi}\frac{\hat{\imath}_z R^2 b^2}{p} \cos p\theta \sin \omega t \sum_{s=1}^{\infty} sI'_p(sbr)K'_p(sbR) \sin sbl \cos sbz \quad . \quad . \quad . \quad . \quad (4)$$

(6.2.3) **The Tangential Component H_θ.**

$$\mu_0 H_\theta = \frac{\partial A_r}{\partial z} - \frac{\partial A_z}{\partial r} \quad . \quad . \quad . \quad . \quad (33)$$

By the method given in Section 6.2.1, for $r > R$,

$$H_\theta = \frac{4}{\pi}\frac{\hat{\imath}_z R^2 b}{r} \sin p\theta \sin \omega t \sum_{s=1}^{\infty} K_p(sbr)I'_p(sbR) \sin sbl \cos sbz \quad (2)$$

and if $r < R$,

$$H_\theta = \frac{4}{\pi}\frac{\hat{\imath}_z R^2 b}{r} \sin p\theta \sin \omega t \sum_{s=1}^{\infty} I_p(sbr)K'_p(sbR) \sin sbl \cos sbz \quad (5)$$

(6.2.4) **The Magnetic Field at the Surface of the Tubular Current.**

A useful check on the accuracy of the expressions for the magnetic field is given by examining whether the magnetic field gives the correct current distribution by using the equation

$$\text{curl } \boldsymbol{H} = \boldsymbol{J} \quad . \quad . \quad . \quad . \quad . \quad . \quad . \quad (34)$$

From Section 6.2.1. we have, at $r = R$,

$$H_{z\,outside} - H_{z\,inside} = \frac{4}{\pi}\frac{\hat{\imath}_z R^2 b}{pd} \cos p\theta \sin \omega t \sum [K_p(sbR)I'_p(sbR) - K'_p(sbR)I_p(sbR)] \sin sbl \sin sbd \sin sbz \quad . \quad (35)$$

But

$$K_p(z)I'_p(z) - K'_p(z)I_p(z) = \frac{1}{z} \quad . \quad . \quad . \quad . \quad (36)$$

Hence

$$H_{z\,outside} - H_{z\,inside} = \frac{4}{\pi}\frac{\hat{\imath}_z R}{p} \cos p\theta \sin \omega t \sum \frac{\sin sbl \sin sbd \sin sbz}{s}$$
$$= i_\theta \cos p\theta \sin \omega t \quad . \quad . \quad . \quad . \quad . \quad . \quad . \quad (37)$$

which is the assigned circumferential current density.

From Section 6.2.2 we have, at $r = R$,

$$H_{r\,inside} = H_{r\,outside} \quad . \quad . \quad . \quad . \quad . \quad . \quad (38)$$

as it should.

From Section 6.2.3 we have, at $r = R$,

$$H_{\theta\,outside} - H_{\theta\,inside} = \frac{4}{\pi}\frac{\hat{\imath}_z R^2 b}{R} \sin p\theta \sin \omega t$$
$$\sum [K_p(sbR)I'_p(sbR) - K'_p(sbR)I_p(sbR)] \sin sbl \cos sbz$$
$$= \frac{4}{\pi}\hat{\imath}_z \sin p\theta \sin \omega t \sum \frac{1}{s} \sin sbl \cos sbz = i_z \sin p\theta \sin \omega t \quad (39)$$

which is the assigned current density.

621.375.9:621.372.85

The Institution of Electrical Engineers
Monograph No. 334 E
May 1959

THE GAIN OF TRAVELLING-WAVE FERROMAGNETIC AMPLIFIERS

By P. J. B. CLARRICOATS, B.Sc.(Eng.), Ph.D.

(*The paper was first received* 23*rd December*, 1958, *and in revised form* 13*th February*, 1959. *It was published as an* INSTITUTION MONOGRAPH *in May*, 1959.)

SUMMARY

The paper describes a general perturbation method for determining the gain of travelling-wave ferromagnetic amplifiers. By use of the method, the gain is determined for an amplifier employing a circular waveguide and an axial ferrite rod of small cross-section. The efficiency of such an amplifier is shown to be low, and a practical version would demand the use of larger rod cross-section and/or a slow-wave structure. Other possible waveguide configurations for amplifiers are briefly mentioned, together with certain practical aspects of construction.

LIST OF PRINCIPAL SYMBOLS

Numbers refer to the equations in which a symbol first appears. Suffixes 1 and 2 refer to signal and idler frequencies ω_1 and ω_2.

a_{1n}, b_{1n}, a_{2n}, b_{2n} = Amplitude coefficients appearing in expansion of the perturbed fields. (7), (8).

A_{1n}, B_{1n}, A_{2n}, B_{2n} = Amplitude coefficients related to a_{1n}, b_{1n}, etc. (36), (37).

$E_{t1,2}$, $E_{z1,2}$ = Transverse and longitudinal components of electric field. (1).

$\bar{E}_{t1,2}$, $\bar{E}_{z1,2}$ = Transverse and longitudinal components of electric field external to ferrite. (31)–(33).

F_{mn}, $m = 1, 2, 3, 4$ = Integrals defined by eqns. (38) and (39).

f_1, f_2 = Integrals defined by eqns. (62) and (63).

G_{mn}, $m = 1, 2, 3, 4$ = Integrals defined by eqns. (38) and (39).

g = Gain of amplifier. (74).

$H_{t1,2}$, $H_{z1,2}$ = Transverse and longitudinal components of magnetic field. (1).

H_p = Magnetic field at pump frequency ω. (26).

H_0 = Static magnetic field. (26).

I_{mn}, $m = 1, 2, 3, 4$ = Integrals obtained by replacing the suffix 1 by 2, and vice versa, in eqn. (54).

$K_{1,2}$ = Wavenumbers in unperturbed waveguide. (65), (66).

$M_{t1,2}$, $M_{z1,2}$ = Transverse and longitudinal components of magnetization. (3), (5).

M_p = Magnetization at pump frequency ω. (26).

M_0 = Static magnetization. (26).

m_{0x}, m_{0z} = Component of pump magnetization divided by the static magnetization M_0. (27)–(29).

$N_{x,y,z}$ = Demagnetizing and depolarizing factors. (27)–(29).

$P_{t1,2}$, $P_{z1,2}$ = Transverse and longitudinal components of polarization. (4), (6).

r_1, r_0 = Radius of rod and waveguide. (69).

S', S = Cross-sectional area of ferrite and waveguide. (15).

α, α_1, α_2 = Attenuation coefficients of perturbed mode and unperturbed modes at frequencies ω_1 and ω_2. (36), (45), (54).

β, β_1, β_2, β_{1n}, β_{2n} = Phase-change coefficients of pump, signal, idler and unperturbed modes. (39), (36), (37), (7), (8).

Δ_{1m}, Δ_{2m} = Integrals representing total power flow in unperturbed modes. (21), (22).

η_{xx}, η_{xy}, etc. = Coefficients relating the polarization to the external electric field by eqns. (31)–(33).

$\theta_p = |\gamma|H_p/\Delta\omega$. (78).

λ = Damping coefficient. (26).

$\rho_{1,2}$ = Functions defined by eqn. (57).

$\phi_{1,2}$ = Solutions of the growth equation. (57).

x_{xx}, x_{xy}, etc. = Coefficients relating the magnetization to the external magnetic field by eqns. (27)–(29).

ω_p, ω_1, ω_2 = Pump, signal and idler frequencies.

$\bar{\omega}_0 = |\gamma|H_a$, where H_a is the applied static magnetic field. (26).

$\omega_M = |\gamma|M_0/\mu_0$, where M_0 is the static magnetization. (26).

ω_R = Ferromagnetic resonance frequency. (26).

$\Delta\omega$ = Frequency line width of ferromagnetic resonance. (27)–(29).

(1) INTRODUCTION

In a recent article, Tien and Suhl[1] describe the principles underlying the operation of a travelling-wave ferromagnetic amplifier. They first treat the general case of a pair of coupled transmission lines with time-varying coupling, similar to the suggestion of Cullen.[2] Secondly, they consider as a specific microwave model a pair of transmission lines embedded in a ferrite-filled circular waveguide. The maximum gain of their model amplifier is found to be 1 dB/in.

The main purpose of this paper is to develop a theory which enables the gain of a more physically realizable amplifier to be determined. This theory is then used to calculate the gain in a specific case. Although the result indicates that the particular configuration chosen is unsuitable as a practical amplifier, a number of ways for improving performance are revealed. If these improvements were to be embodied, a practical travelling-wave ferromagnetic amplifier could be built. The paper concludes with a brief discussion of two other travelling-wave amplifier configurations, together with certain practical aspects of construction.

(2) GENERAL PERTURBATION METHOD FOR DETERMINING AMPLIFIER GAIN

(2.1) Outline of the Method

The basic principles underlying the operation of ferromagnetic amplifiers have been previously described by Suhl.[3] He has

Correspondence on Monographs is invited for consideration with a view to publication.

The paper is a communication from the Staff of the Applied Electronics Laboratories of The General Electric Company Limited, Stanmore, England. Dr. Clarricoats is now in the Department of Light Electrical Engineering, The Queen's University of Belfast.

shown that amplification arises from a regenerative action involving components of the r.f. magnetization at the signal frequency ω_1 and idler frequency ω_2. The magnetization must be driven in a state of uniform precession at a frequency $\omega_p = \omega_1 + \omega_2$, henceforth referred to as the pump frequency. In order to determine the oscillation threshold or gain of a ferromagnetic amplifier, expressions must be obtained which relate the amplitudes of the signal and idler modes. For sufficiently simple structures these expressions can be derived from solutions of the equation of motion of the magnetization and of Maxwell's equations. An example of this kind is to be found in the paper by Tien and Suhl,[1] on travelling-wave ferromagnetic amplifiers. For more complicated structures the expressions can be derived using perturbation theory. Suhl[3] has described in detail such an analysis for an amplifier employing an ellipsoidal ferrite in a resonant cavity. The present paper provides a perturbation method which enables the gain of travelling-wave amplifiers to be determined.

The method is similar to that employed by Suhl and Walker[4] in their treatment of conventional propagation problems involving ferrites in waveguides. The essential differences between the two methods spring from the present use of transverse magnetization and the appearance of additional components of magnetization at frequency ω_1, arising from fields at frequency ω_2, and vice versa. In the absence of the pump, the analysis merely leads to expressions for the attenuation and phase-change coefficients of waves at frequencies ω_1 and ω_2. The introduction of the pump couples the signal and idler waves, giving rise to a pair of generalized modes. Each such mode is comprised of joint signal and idler fields in a definite ratio. As the pump power is increased, the attenuation coefficient of one of these modes decreases to zero. A further increase in pump power then causes the amplitude of the mode to increase with distance along the waveguide. The stages in the analysis are summarized below:

(*a*) Statement of Maxwell's equations for signal and idler fields within the ferrite, written in a form where the perturbation terms are separate.
(*b*) Expansion of signal and idler fields in terms of the normal mode fields of the unperturbed structure.
(*c*) Formulation of equations which enable the amplitudes of these normal mode fields to be determined.
(*d*) Formulation of expressions for the magnetization and polarization in terms of the normal mode fields.
(*e*) Formulation of the equation for the growth factor of the joint signal and idler modes.

(2.2) Perturbation Expression for the Amplifier Gain

(2.2.1) Statement of Maxwell's Equations for Signal and Idler Modes.

The waveguide configuration under discussion is shown in Fig. 1. The ferrite is magnetized in a direction transverse to that of propagation of the signal, idler and pump modes, which have frequencies ω_1, ω_2 and ω_p respectively. For the signal mode Maxwell's equations can be written in terms of the transverse and longitudinal parts as follows:

$$\left(\nabla_t + \boldsymbol{i}_z \frac{d}{d_z}\right) \times (\boldsymbol{E}_{t1} + \boldsymbol{E}_{z1}) = -j\omega_1[(\mu_0 \boldsymbol{H}_{t1} + \boldsymbol{M}_{t1}) + (\mu_0 \boldsymbol{H}_{z1} + \boldsymbol{M}_{z1})] \quad (1)$$

$$\left(\nabla_t + \boldsymbol{i}_z \frac{d}{d_z}\right) \times (\boldsymbol{H}_{t1} + \boldsymbol{H}_{z1}) = j\omega_1[(\epsilon_0 \boldsymbol{E}_{t1} + \boldsymbol{P}_{t1}) + (\epsilon_0 \boldsymbol{E}_{z1} + \boldsymbol{P}_{z1})] \quad (2)$$

On separation into longitudinal and transverse components,

$$\nabla_t \times \boldsymbol{E}_{z1} + \boldsymbol{i}_z \times \frac{d}{d_z}\boldsymbol{E}_{t1} + j\omega_1\mu_0 \boldsymbol{H}_{t1} = -j\omega_1 \boldsymbol{M}_{t1} \quad (3)$$

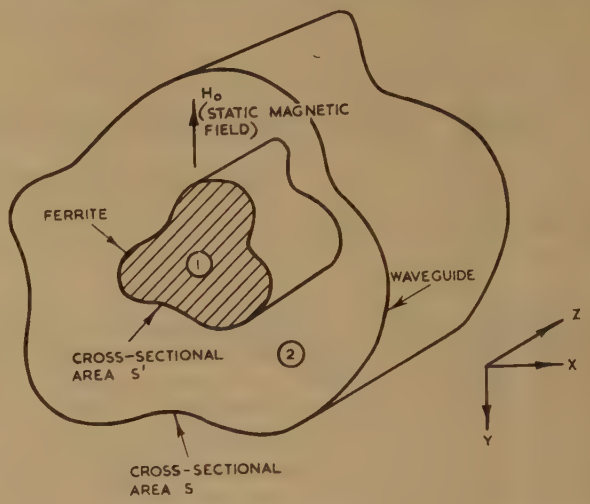

Fig. 1.—General waveguide arrangement for transverse-field ferrite amplifier.

$$\nabla_t \times \boldsymbol{H}_{z1} + \boldsymbol{i}_z \times \frac{d}{d_z}\boldsymbol{H}_{t1} - j\omega_1\epsilon_0 \boldsymbol{E}_{t1} = j\omega_1 \boldsymbol{P}_{t1} \quad (4)$$

$$\nabla_t \times \boldsymbol{E}_{t1} + j\omega_1\mu_0 \boldsymbol{H}_{z1} = -j\omega_1 \boldsymbol{M}_{z1} \quad (5)$$

$$\nabla_t \times \boldsymbol{H}_{t1} - j\omega_1\epsilon_0 \boldsymbol{E}_{z1} = j\omega_1 \boldsymbol{P}_{z1} \quad (6)$$

A similar set of equations can be formed for the idler fields merely by transposing the suffixes 1 and 2 throughout.

(2.2.2) Expansion of Perturbed Fields.

It can be seen that eqns. (3)–(6) are written so that their right-hand sides contain magnetization and polarization terms which represent the perturbation caused by the introduction of the ferrite into region (1) of Fig. 1. The left-hand sides contain the perturbed fields. These fields can now be expanded in terms of the normal mode fields of the unperturbed structure. The normal mode fields $\boldsymbol{E}_{1n}\varepsilon^{-j\beta_{1n}z}$, $\boldsymbol{H}_{1n}\varepsilon^{-j\beta_{1n}z}$, satisfy the unperturbed forms of eqns. (3)–(6), i.e. when their right-hand sides are zero:

$$\boldsymbol{E}_{t1} = \sum_n a_{1n}(z)\boldsymbol{E}_{t1n}(x, y) \quad (7)$$

$$\boldsymbol{H}_{t1} = \sum_n b_{1n}(z)\boldsymbol{H}_{t1n}(x, y) \quad (8)$$

Similarly for $\boldsymbol{E}_{t2}$ and $\boldsymbol{H}_{t2}$.

(2.2.3) Formation of Equations for Amplitudes a_{1n}, b_{1n}, a_{2n}, b_{2n}.

$\boldsymbol{E}_{z1}$ and $\boldsymbol{H}_{z1}$ can be eliminated from eqns. (3) and (4) by substitution from eqns. (5) and (6):

$$\frac{\nabla_t \times (\nabla_t \times \boldsymbol{H}_{t1} - j\omega_1 \boldsymbol{P}_{z1})}{j\omega_1\varepsilon_0} + \boldsymbol{i}_z \times \frac{d}{d_z}\boldsymbol{E}_{t1} + j\omega_1\mu_0 \boldsymbol{H}_{t1} = -j\omega_1 \boldsymbol{M}_{t1} \quad (9)$$

$$\frac{-\nabla_t \times (\nabla_t \times \boldsymbol{E}_{t1} + j\omega_1 \boldsymbol{M}_{z1})}{j\omega_1\mu_0} + \boldsymbol{i}_z \times \frac{d}{d_z}\boldsymbol{H}_{t1} - j\omega_1\epsilon_0 \boldsymbol{E}_{t1} = j\omega_1 \boldsymbol{P}_{t1} \quad (10)$$

Also, for the nth normal mode,

$$\frac{\nabla_t \times (\nabla_t \times \boldsymbol{H}_{t1n})}{j\omega_1\epsilon_0} - j\beta_{1n}\boldsymbol{i}_z \times \boldsymbol{E}_{t1n} + j\omega_1\mu_0 \boldsymbol{H}_{t1n} = 0 \quad (11)$$

$$\frac{-\nabla_t \times (\nabla_t \times \boldsymbol{E}_{t1n})}{j\omega_1\mu_0} - j\beta_{1n}\boldsymbol{i}_z \times \boldsymbol{H}_{t1n} - j\omega_1\epsilon_0 \boldsymbol{E}_{t1n} = 0 \quad (12)$$

where β_{1n} is the propagation coefficient of this mode.

On substituting eqns. (7), (8), (11) and (12) into eqns. (9) and (10),

$$\sum_n \left(j\beta_{1n}b_{1n}+\frac{d}{d_z}a_{1n}\right)\boldsymbol{i}_z\times\boldsymbol{E}_{t1n}=-j\omega_1\boldsymbol{M}_{t1}+\frac{\nabla_t\times\boldsymbol{P}_{z1}}{\epsilon_0} \quad (13)$$

$$\sum_n \left(j\beta_{1n}a_{1n}+\frac{d}{d_z}b_{1n}\right)\boldsymbol{i}_z\times\boldsymbol{H}_{t1n}=j\omega_1\boldsymbol{P}_{t1}+\frac{\nabla_t\times\boldsymbol{M}_{z1}}{\mu_0} \quad (14)$$

The orthogonality condition

$$\int_S \boldsymbol{i}_z\cdot\boldsymbol{E}_{t1m}\times\boldsymbol{H}^*_{t1n}dS=\left\{\begin{array}{l}0,\ (m\neq n);\\ \Delta_{1n},\ (m=n),\ (\text{real})\end{array}\right\}$$

may now be applied to eqns. (13) and (14) as follows. Scalar multiply eqn. (13) by $\boldsymbol{H}^*_{t1m}$ and the complex conjugate of eqn. (14) by $\boldsymbol{E}_{t1m}$ and integrate over the waveguide cross-section S. Then, if S' is the ferrite cross-section,

$$\sum_n \left(j\beta_{1n}b_{1n}+\frac{d}{d_z}a_{1n}\right)\int_S \boldsymbol{i}_z\cdot\boldsymbol{E}_{t1n}\times\boldsymbol{H}^*_{t1m}dS$$

$$=-j\omega_1\int_{S'}\boldsymbol{H}^*_{t1m}\cdot\boldsymbol{M}_{t1}dS+\int_{S'}\boldsymbol{H}^*_{t1m}\cdot\frac{\nabla_t\times\boldsymbol{P}_{z1}}{\epsilon_0}dS \quad (15)$$

$$\sum_n \left(-j\beta_{1n}a^*_{1n}+\frac{d}{d_z}b^*_{1n}\right)\int_S \boldsymbol{i}_z\cdot\boldsymbol{E}_{t1m}\times\boldsymbol{H}^*_{t1n}dS$$

$$=j\omega_1\int_{S'}\boldsymbol{E}_{t1m}\cdot\boldsymbol{P}^*_{t1}dS-\int_{S'}\boldsymbol{E}_{t1m}\cdot\frac{\nabla_t\times\boldsymbol{M}^*_{z1}}{\mu_0}dS \quad (16)$$

$$\left(j\beta_{1n}b_{1n}+\frac{d}{d_z}a_{1n}\right)=\frac{-j\omega_1\int_{S'}\boldsymbol{H}^*_{t1n}\cdot\boldsymbol{M}_1dS+\int_{S'}\frac{\boldsymbol{H}^*_{t1n}\cdot\nabla_t\times\boldsymbol{P}_{z1}}{\epsilon_0}}{\Delta_{1n}} \quad . \quad . \quad . \quad . \quad (17)$$

$$\left(-j\beta_{1n}a^*_{1n}+\frac{d}{d_z}b^*_{1n}\right)=\frac{j\omega_1\int_{S'}\boldsymbol{E}_{t1n}\cdot\boldsymbol{P}^*_{t1}dS-\int_{S'}\frac{\boldsymbol{E}_{t1n}\cdot\nabla_t\times\boldsymbol{M}^*_{z1}dS}{\mu_0}}{\Delta_{1n}} \quad . \quad . \quad . \quad . \quad (18)$$

By use of the identity

$$\int_{S_0}\boldsymbol{G}_T\cdot\nabla_t\times\boldsymbol{F}i_z dS=\int_{S_0}\boldsymbol{F}i_z\cdot\nabla_t\times\boldsymbol{G}_T dS-\oint\boldsymbol{F}G_T\cdot\boldsymbol{i}_z ds$$

where the line integral is taken over the boundary of the surface S_0 (which lies in the transverse plane), it follows that

$$\int_{S'}\boldsymbol{H}^*_{t1n}\cdot\nabla_t\times\boldsymbol{P}_{z1}dS=\int_{S'}\boldsymbol{P}_{z1}\cdot\nabla_t\times\boldsymbol{H}^*_{t1n}dS-\oint\boldsymbol{P}_{z1}\boldsymbol{H}^*_{t1n}\cdot\boldsymbol{ds}$$

$$=\int_{S'}\boldsymbol{P}_{z1}\cdot\nabla_t\times\boldsymbol{H}^*_{t1n}dS$$

since $\boldsymbol{P}_{z1}=0$ outside the ferrite.† If S' and S coincide, the equation still holds since $E_z=0$ on the waveguide periphery.

Now $\nabla_t\times\boldsymbol{H}^*_{t1n}=-j\omega_1\epsilon_0\boldsymbol{E}^*_{z1n}\boldsymbol{i}_z$ from Maxwell's equations; therefore

$$\int_{S'}\frac{\boldsymbol{H}^*_{t1n}\cdot\nabla_t\times\boldsymbol{P}_{z1}}{\epsilon_0}dS=-j\omega_1\int_{S'}\boldsymbol{P}_{z1}\boldsymbol{E}^*_{z1n}dS \quad . \quad (19)$$

† The surface of integration in eqns. (15)–(18) is that of the waveguide cross-section; thus the boundary for the line integral is the waveguide periphery.

Similarly it can be shown that

$$\int_{S'}\frac{\boldsymbol{E}_{t1n}\cdot\nabla_t\times\boldsymbol{M}^*_{z1}}{\mu_0}dS=-j\omega_1\int_{S'}\boldsymbol{M}^*_{z1}\boldsymbol{H}_{z1n}dS \quad . \quad (20)$$

Eqns. (17) and (18) then become

$$j\beta_{1n}b_{1n}+\frac{d}{d_z}a_{1n}=-\frac{j\omega_1}{\Delta_{1n}}\left[\int_{S'}(\boldsymbol{H}^*_{t1n}\cdot\boldsymbol{M}_{t1}+\boldsymbol{E}^*_{z1n}\boldsymbol{P}_{z1})dS\right] \quad (21)$$

and

$$-j\beta_{1n}a^*_{1n}+\frac{d}{d_z}b^*_{1n}=\frac{j\omega_1}{\Delta_{1n}}\left[\int_{S'}(\boldsymbol{E}_{t1n}\cdot\boldsymbol{P}^*_{t1}+\boldsymbol{H}_{z1n}\boldsymbol{M}^*_{z1})dS\right] \quad (22)$$

Since Δ_{1n} is real, the complex conjugate of eqn. (22) is given by

$$j\beta_{1n}a_{1n}+\frac{d}{d_z}b_{1n}=-\frac{j\omega_1}{\Delta_{1n}}\left[\int_{S'}(\boldsymbol{E}^*_{t1n}\cdot\boldsymbol{P}_{t1}+\boldsymbol{H}^*_{z1n}\boldsymbol{M}_{z1})dS\right] \quad (23)$$

Now, although eqns. (21) and (23) (and a similar pair for the idler mode) are exact, they still contain the unknown magnetization and polarization. To determine a_{1n} and b_{1n} from the above equations these unknown quantities must first be expressed in terms of the fields external to the ferrite. Then, provided that the ferrite only slightly perturbs the field in the empty waveguide, the external fields can be represented by the first term in the normal-mode field expansions of eqns. (7) and (8). In this way eqns. (21) and (23) can be written solely in terms of a_{1n}, b_{1n} and the known normal-mode fields.

(2.2.4) Expressions for the Magnetization and Polarization in Terms of the Normal-Mode Fields.

Provided that the unperturbed field is almost uniform over the region S' and that transverse propagation effects within the ferrite are negligible, a simple quasi-static method may be employed in the evaluation of the magnetization and polarization. Under the above conditions the internal fields H_{ij} and E_{ij} can be related to the external fields H_{ej} and E_{ej} by the equations

$$H_{ij}=H_{ej}-\frac{N_jM_j}{\mu_0} \quad . \quad . \quad . \quad . \quad . \quad . \quad (24)$$

and

$$E_{ij}=E_{ej}-\frac{N_jP_j}{\varepsilon_0} \quad . \quad . \quad . \quad . \quad . \quad . \quad (25)$$

$j=x, y, z$, and N_j is a factor which depends only on the ferrite geometry. The transverse magnetization $\boldsymbol{M}_{t1,2}$ is assumed to be related to the internal magnetic fields at frequencies ω_1, ω_2 and ω through the equation

$$\frac{d\boldsymbol{M}_t}{dt}=\gamma(\boldsymbol{M}\times\boldsymbol{H})-\lambda\boldsymbol{M}_t \quad . \quad . \quad . \quad (26)$$

where $\boldsymbol{M}=\boldsymbol{M}_0+\boldsymbol{M}(z,\omega)+\boldsymbol{M}(z,\omega_1)+\boldsymbol{M}(z,\omega_2)$

$$\boldsymbol{H}=\boldsymbol{H}_0+\boldsymbol{H}(z,\omega)+\boldsymbol{H}(z,\omega_1)+\boldsymbol{H}(z,\omega_2)$$

and all time-dependent quantities have the form $\mathrm{F}(\omega)=\mathrm{F}\varepsilon^{j\omega t}+F^*\varepsilon^{-j\omega t}$. Also, if the conservation condition $M_0^2=M_x^2+M_y^2+M_z^2$ is assumed to be satisfied throughout the motion of the magnetization, it is readily established (see Appendix 7.1) that

$$M_{x1}=\chi_{xx1}\bar{H}_{x1}+\chi_{xy1}\bar{H}^*_{y2}+\chi_{xz1}\bar{H}_{z1} \quad . \quad (27)$$

$$M_{y1}=\chi_{xy2}\bar{H}^*_{x2}+\chi_{zy2}\bar{H}^*_{z2} \quad . \quad . \quad . \quad . \quad . \quad (28)$$

$$M_{z1}=-\chi_{xz1}\bar{H}_{x1}+\chi_{zy1}\bar{H}_{y2}+\chi_{zz1}\bar{H}_{z1} \quad . \quad (29)$$

The bar over a field component denotes external field and the coefficients χ_{xx1}, etc., are given by

$$\frac{\chi_{xx1}}{\mu_0} = \frac{\omega_M\bar{\omega}_0 + \omega_M^2(N_z - N_y)}{\omega_R^2 - \omega_1^2 + 2j\lambda\omega_1}, \quad \frac{\chi_{xz1}}{\mu_0} = \frac{j\omega_M(\omega_1 - j\lambda)}{\omega_R^2 - \omega_1^2 + 2j\lambda\omega_1}$$

$$\frac{\chi_{zz1}}{\mu_0} = \frac{\omega_M\bar{\omega}_0 + \omega_M^2(N_x - N_y)}{\omega_R^2 - \omega_1^2 + 2j\lambda\omega_1},$$

$$\frac{\chi_{xy1}}{\mu_0} = \frac{m_{0x}\omega_M[\bar{\omega}_0 + \omega_M(N_z - N_y)] + jm_{0z}\omega_M(\omega_1 - j\lambda)}{\omega_R^2 - \omega_1^2 + 2j\lambda\omega_1}$$

$$\frac{\chi_{zy1}}{\mu_0} = \frac{m_{0z}\omega_M[\bar{\omega}_0 + \omega_M(N_x - N_y)] - jm_{0x}\omega_M(\omega_1 - j\lambda)}{\omega_R^2 - \omega_1^2 + 2j\lambda\omega_1}$$

$$m_{0x} = \frac{\gamma H_p}{\Delta\omega}\,\frac{[j\bar{\omega}_0 + \omega_M(N_z - N_y)\cos\alpha - \sin\alpha]}{\omega_R}$$

$$m_{0z} = \frac{\gamma H_p}{\Delta\omega}\,\frac{[j\bar{\omega}_0 + \omega_M(N_x - N_y)\sin\alpha + \cos\alpha]}{\omega_R}$$

$$\omega_R^2 = [\bar{\omega}_0 + (N_z - N_y)\omega_M][\bar{\omega}_0 + (N_z - N_y)\omega_M], \quad \bar{\omega}_0 = |\gamma|H_a$$

where $\alpha = \text{arc tan}\,(H_{pz}/H_{px})$

$$H_p = (H_{px}^2 + H_{pz}^2)^{1/2}$$

$\omega_1 + \omega_2 = \omega_p = \omega_R$ (i.e. the static field is adjusted so that the resonance frequency ω_R coincides with the pump frequency ω_p). If damping is neglected at the signal and idler frequencies, i.e. $\lambda = 0$, the coefficients χ_{xy2}/μ_0 and χ_{zy2}/μ_0 are obtained on replacing ω_1 and ω_2 in χ_{xy1}/μ_0 and χ_{zy1}/μ_0 respectively. This simplification is permissible since it is assumed that $\omega_R^2 - \omega_{1,2}^2 \gg 2\lambda\omega_{1,2}$—i.e. neither the signal nor the idler frequency is close to the resonance frequency. The equations corresponding to (27)–(29) for the idler magnetization components are obtained transposing the suffixes 1 and 2 throughout.

The polarization components can also be written in terms of the external electric field components by using eqn. (25) together with the equation

$$P_j = (\epsilon - \epsilon_0)E_{ij} \quad . \quad . \quad . \quad . \quad . \quad (30)$$

Then

$$P_{x1,2} = \eta_{xx}\bar{E}_{x1,2} \quad . \quad . \quad . \quad . \quad . \quad . \quad (31)$$

$$P_{y1,2} = \eta_{yy}\bar{E}_{y1,2} \quad . \quad . \quad . \quad . \quad . \quad . \quad (32)$$

$$P_{z1,2} = \eta_{zz}\bar{E}_{z1,2} \quad . \quad . \quad . \quad . \quad . \quad . \quad (33)$$

where

$$\eta_{jj} = \frac{\epsilon - \epsilon_0}{1 + \dfrac{\epsilon - \epsilon_0}{\epsilon_0}N_j} \quad (j = x, y, z)$$

As the magnetization and polarization appear in eqns. (21) and (23) in perturbation terms, it suffices in their determination to approximate the external fields $\bar{E}_{t1}$, $\bar{E}_{z1}$, $\bar{H}_{t1}$ and $\bar{H}_{z1}$ by the dominant normal mode fields, using eqns. (7) and (8). Thus, on retaining just the term $n = 1$ in the expansions,

$$\bar{E}_{t1} = a_{11}E_{t11}, \; \bar{E}_{z1} = b_{11}E_{z11} \quad . \quad . \quad . \quad (34)$$

and

$$H_{t1} = b_{11}H_{t11}, \; \bar{H}_{z1} = a_{11}H_{z11} \quad . \quad . \quad . \quad (35)$$

In general, the coefficients a_{1n} and b_{1n} have z dependence expressed by

$$a_{1n}(z) = \sum_{\alpha} A_{1n}\varepsilon^{-(\alpha + j\beta_1)z} \quad . \quad . \quad . \quad . \quad (36)$$

$$b_{1n}(z) = \sum_{\alpha} B_{1n}\varepsilon^{-(\alpha + j\beta_1)z} \quad . \quad . \quad . \quad . \quad (37)$$

and similarly for $a_{2n}(z)$, $b_{2n}(z)$ with the same values of α as above though with phase-change coefficient β_2. The summation refers to different solutions of the characteristic equation (57), which determines the possible values of α common to $a_{1n}(z)$, $b_{1n}(z)$, $a_{2n}(z)$ and $b_{2n}(z)$. By using eqns. (34) and (35), the magnetization and polarization components in eqns. (27)–(29) and (31)–(33) can be expressed in terms of the normal-mode field functions and the coefficient A_{11}, B_{11}, etc. Finally, on substitution for M_{t1}, M_{z1}, P_{t1} and P_{z1}, eqns. (21) and (23) become

$$j\beta_{1n}B_{1n} - (\alpha + j\beta_1)A_{1n} = -\frac{j\omega_1}{\Delta_{1n}}\int_{S'}[(\chi_{xx1}B_{11}H_{z11} + \chi_{xy1}B_{21}^*H_{y21}^* + \chi_{xz1}A_{11}H_{z11})H_{x1n}^* + (\chi_{xy2}B_{21}^*H_{x21} + \chi_{zy2}A_{21}^*H_{z21}^*)H_{y1n}^* + \eta_{zz}B_{11}E_{z11}E_{z1n}^*]dS \quad (38)$$

$$j\beta_{1n}A_{1n} - (\alpha + j\beta_1)B_{1n} = -\frac{j\omega_1}{\Delta_{1n}}\int_{S'}[\eta_{xx}A_{11}E_{x11}E_{x1n}^* + \eta_{yy}A_{11}E_{y11}E_{y1n}^* + (-\chi_{xz1}B_{11}H_{x11} + \chi_{zy1}B_{21}^*H_{y21}^* + \chi_{zz1}A_{11}H_{z11})H_{z1n}^*]dS \quad (39)$$

In expressing eqns. (38) and (39) it has been assumed that the attenuation coefficient of the pump is zero and the phase-change coefficient satisfies the relation $\beta = \beta_1 + \beta_2$. Then since the coefficients $\chi_{xy1,2}\chi_{zy1,2}$ contain a dependence $\varepsilon^{-j\beta z}$ arising from the pump field H_p, terms such as $\chi_{xy2}\bar{H}_{x2}^*$ contain a z-dependence factor $\varepsilon^{-j(\beta-\beta_2)z} = \varepsilon^{-j\beta_1 z}$. In this way all terms in eqns. (21) and (23) have a dependence $\varepsilon^{-j\beta_1 z}$. Although Tien[5] has discussed in general the performance of travelling-wave amplifiers in which $\beta = \beta_1 + \beta_2 + \Delta\beta$, the above restriction is an optimum one and should not be difficult to satisfy in practice.

Before continuing with the analysis, it is appropriate to examine the significance of eqns. (37) and (38). When the pump is absent, those terms vanish, in the above equations, which contain the dominant normal-mode components of the idler field, H_{x21}, H_{y21} and H_{z21}. This follows from the dependence of the cross-coupling susceptibility coefficients χ_{xy1}, χ_{xy2}, etc., on the existence of the pump. These equations then enable the small change in the propagation coefficient of the signal mode, caused by the introduction of the ferrite into the waveguide, to be determined. The slight change in the relative amplitudes of the normal-mode electric and magnetic field components A_{11}/B_{11} can also be obtained. A pair of equations similar to eqns. (38) and (39) allow corresponding information to be determined for the idler mode. This use of perturbation methods for evaluating the propagation coefficients of waveguides containing ferrites has been extensively described by Suhl and Walker[4] and by the author.[7, 10] When the pump is applied at a frequency $\omega_p = \omega_1 + \omega_2$ (which is also equal to the ferromagnetic resonance frequency ω_R) cross-coupling between signal and idler fields occurs. The amplitude of the field at frequency ω_1 is dependent upon that of the field at ω_2, and vice versa. Furthermore, if the condition $\beta_1 + \beta_2 = \beta$ is satisfied, the contribution to the magnetization at frequency ω_1 which arises from idler fields at frequency ω_2, remains in phase for all values of z with that which arises from the signal. It transpires that the signal and idler fields jointly form a pair of modes. The attenuation coefficients of these modes, ϕ_1 and ϕ_2, can be determined from eqns. (38) and (39), together with the corresponding equations for the idler. In the limit of vanishing pump, these coefficients correspond to α_1 and α_2 and are appropriate to the signal and idler modes alone. When the pump power is small, only a small proportion of the field at frequency ω_2 has an attenuation coefficient ϕ_1 (which is then nearly equal to α_1), and vice versa. As the pump power increases the smaller of the attenuation coefficients ϕ_1, ϕ_2 decreases while the other increases. In general the relative proportions of the

fields at frequencies ω_1 and ω_2 which have attenuation coefficients ϕ_1 or ϕ_2 are determined uniquely by the above equations. It is the purpose of the next Section to establish expressions for ϕ_1 and ϕ_2 in terms of the ferrite and waveguide geometry, the intrinsic properties of the ferrite and the frequencies ω_1 and ω_2.

(2.2.5) Formation of the Equation for the Growth of the Signal and Idler Modes.

Eqns. (38) and (39) can be rewritten in a more compact form:

$$j\beta_{1n}B_{1n} - (\alpha + j\beta_1)A_{1n} = jF_{1n}B_{11} + jF_{2n}A_{11} + jG_{1n}B_{21}^* + jG_{2n}A_{21}^* \quad (40)$$

$$j\beta_{1n}A_{1n} - (\alpha + j\beta_1)B_{1n} = jF_{3n}B_{11} + jF_{4n}A_{11} + jG_{3n}B_{21}^* \quad (41)$$

where the integrals F_{1n}, F_{2n}, etc., G_{1n}, G_{2n}, G_{3n} are defined by eqns. (38) and (39). A similar pair of equations for the idler mode is obtained by transposing the suffixes 1 by 2 appropriately. If the pump is absent, the above equations reduce to

$$j\beta_{1n}B_{1n} - (\alpha + j\beta_1)A_{1n} = jF_{1n}B_{11} + jF_{2n}A_{11} \quad . \quad (42)$$

$$j\beta_{1n}A_{1n} - (\alpha + j\beta_1)B_{1n} = jF_{3n}B_{11} + jF_{4n}A_{11} \quad . \quad (43)$$

On putting $n = 1$ and neglecting second-order quantities, it can readily be shown that

$$\beta_1 - \beta_{11} = -\tfrac{1}{2}\mathscr{R}(F_{11} + F_{21} + F_{31} + F_{41}) \quad . \quad (44)$$

$$\alpha = \alpha_1 = \tfrac{1}{2}\mathscr{I}(F_{11} + F_{21} + F_{31} + F_{41}) \quad (45)$$

$$\frac{A_{11}}{B_{11}} = 1 + \frac{(F_{31} + F_{41}) - (F_{11} + F_{21})}{2\beta_{11}} \quad . \quad (46)$$

Since in eqns. (40) and (41) F_{1n}, F_{2n}, etc., G_{1n}, G_{2n}, G_{3n} are small, eqn. (46) enables one to write $A_{11} = B_{11}$ and similarly $A_{21}^* = B_{21}^*$, on the right-hand sides of those equations. Then if $n = 1$, and for convenience, the additional suffix is dropped:

$$j\beta_{11}B_1 - (\alpha + j\beta_1)A_1 = j(F_1 + F_2)B_1 + j(G_1 + G_2)B_2^* \quad (47)$$

$$j\beta_{11}A_1 - (\alpha + j\beta_1)B_1 = j(F_3 + F_4)B_1 + jG_3B_2^* \quad . \quad . \quad (48)$$

On multiplying eqn. (47) by $(\alpha + j\beta_1)$ and eqn. (48) by $j\beta_{11}$, adding and neglecting second-order quantities,

$$-\beta_{11}^2 - (\alpha + j\beta_1)^2 = j\beta_{11}\left[j(F_1 + F_2 + F_3 + F_4) + j(G_1 + G_2 + G_3)\frac{B_2^*}{B_1}\right] \quad (49)$$

Eqn. (49) can be rearranged and simplified using eqns. (44) and (45) as follows:

$$\beta_1^2 - \beta_{11}^2 - 2j\alpha\beta_1 \simeq 2\beta_{11}(\beta_1 - \beta_{11}) - 2j\alpha\beta_{11} \quad (50)$$

Then

$$2\beta_{11}(\beta_1 - \beta_{11}) - 2j\alpha\beta_{11} + \beta_{11}(F_1 + F_2 + F_3 + F_4) = -\beta_{11}(G_1 + G_2 + G_3)\frac{B_2^*}{B_1} \quad (51)$$

$$2j\alpha_1\beta_{11} - 2j\alpha\beta_{11} = -\beta_{11}(G_1 + G_2 + G_3)\frac{B_2^*}{B_1} \quad (52)$$

$$2(\alpha_1 - \alpha) = j(G_1 + G_2 + G_3)\frac{B_2^*}{B_1} \quad . \quad . \quad (53)$$

Similarly from the corresponding equations for the idler mode:

$$2(\alpha_2 - \alpha) = j(I_1 + I_2 + I_3)\frac{B_1^*}{B_2} \quad . \quad . \quad . \quad (54)$$

where the functions I_1, I_2, I_3, are obtained by transposing suffixes 1 and 2 in G_1, G_2, G_3. Eqns. (53) and (54) enable the attenuation coefficient α, to be determined together with B_1/B_2.

Thus $$\frac{B_2^*}{B_1} = \frac{2(\alpha_1 - \alpha)}{j(G_1 + G_2 + G_3)} = \frac{-j(I_1^* + I_2^* + I_3^*)}{2(\alpha_2 - \alpha)} \quad (55)$$

whereby

$$4(\alpha_1 - \alpha)(\alpha_2 - \alpha) = (G_1 + G_2 + G_3)(I_1^* + I_2^* + I_3^*) \quad (56)$$

Eqn. (56) can be rewritten as

$$\alpha^2 - (\alpha_1 + \alpha_2)\alpha + \alpha_1\alpha_2 - \rho_1\rho_2^* = 0 \quad . \quad . \quad (57)$$

where

$$\rho_1 = \tfrac{1}{2}(G_1 + G_2 + G_3)$$

$$\rho_2 = \tfrac{1}{2}(I_1 + I_2 + I_3)$$

Eqn. (57) has two roots ϕ_1, ϕ_2, which, in the absence of the pump, correspond to α_1 and α_2. When the pump is introduced the mode corresponding to the attenuation coefficient ϕ_1 comprises a joint signal and idler field in the ratio given by eqn. (55) when $\alpha = \phi_1$; and similarly for the other mode. In general, both modes exist, so that the signal and idler fields both have parts with attenuation coefficients ϕ_1 and ϕ_2. For example, in the region exterior to the ferrite,

$$H_{t1} = [B_{1(\phi 1)}\varepsilon^{-(\phi_1 + j\beta_1)z} + B_{1(\phi 2)}\varepsilon^{-(\phi_2 + j\beta_1)z}]H_{t11} \quad (58)$$

$$H_{t2} = [B_{2(\phi 1)}\varepsilon^{-(\phi_1 + j\beta_2)z} + B_{2(\phi 2)}\varepsilon^{-(\phi_2 + j\beta_2)z}]H_{t21} \quad (59)$$

where $$\frac{B_{2(\phi 1)}^*}{B_{1(\phi 1)}} = \frac{2(\alpha_1 - \phi_1)}{j(G_1 + G_2 + G_3)} = \frac{-j(I_1^* + I_2^* + I_3^*)}{2(\alpha_2 - \phi_1)}$$

$$\frac{B_{2(\phi 2)}^*}{B_{1(\phi 2)}} = \frac{2(\alpha_1 - \phi_2)}{j(G_1 + G_2 + G_3)} = \frac{-j(I_1^* + I_2^* + I_3^*)}{2(\alpha_2 - \phi_2)}$$

As the pump field is increased, the smaller of the attenuation coefficients decreases and the other increases. Finally, a slight increase in pump field causes the former coefficient to change sign; then one part of the joint signal and idler field grows with distance. It is only this part which is important in travelling-wave amplifiers. The condition for growth is that

$$\rho_1\rho_2^* > \alpha_1\alpha_2 \quad . \quad . \quad . \quad . \quad . \quad . \quad . \quad (60)$$

This condition may be compared with that for oscillation in a cavity-type ferromagnetic amplifier.[3] There the inequality is given by

$$\bar{\rho}_1\bar{\rho}_2^* > \frac{\omega_1}{Q_1}\frac{\omega_2}{Q_2} \quad . \quad . \quad . \quad . \quad . \quad . \quad (61)$$

$\bar{\rho}_1$ and $\bar{\rho}_2$ are similar to ρ_1 and ρ_2 in eqn. (60); also as $\omega_1/2Q_1$ and $\omega_2/2Q_2$ are the decay coefficients (with time) of the fields in the cavity when the pump is absent, the comparison is close.

(3) GAIN OF FERROMAGNETIC AMPLIFIER EMPLOYING THIN FERRITE ROD IN CIRCULAR WAVEGUIDE

The particular amplifier configuration whose properties are now to be discussed is shown in Fig. 2. Pump, signal and idler modes are assumed to be of the modified H_{11} type. The pump and signal modes are polarized, so that the transverse r.f. magnetic field on axis has only an x-component, while the idler mode has only a y-component. The ferrite cross-section is assumed to be sufficiently small for transverse propagation effects within the ferrite to be neglected. Also, the integrals G_1, G_2, etc., I_1, I_2, etc., can then be replaced by the values of their respective integrands on axis, multiplied by the cross-sectional area of the ferrite. For the signal mode, H_{y11}, H_{z11}, E_{x11}, E_{z11} are assumed zero in that region of the unperturbed structure which the ferrite occupies when the rest of the structure is per-

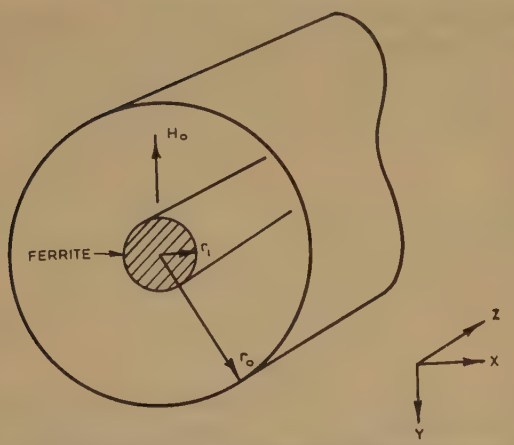

Fig. 2.—Transverse-field ferrite amplifier employing thin ferrite rod in circular waveguide.

turbed. In a similar manner, H_{x21}, H_{z21}, E_{y21} and E_{z21} are assumed zero for the idler mode. Under these conditions only G_1 and I_1 are non-zero and are given by†

$$G_1 = -\chi_{xy1}\frac{\omega_1}{\Delta_{11}}\int_{S'} H^*_{y21}H^*_{x11}dS$$

$$= -\chi_{xy1}\omega_1 f_1 \quad . \quad . \quad . \quad . \quad . \quad . \quad (62)$$

$$I_1 = -\chi_{xy1}\frac{\omega_2}{\Delta_{21}}\int_{S'} H^*_{y21}H^*_{x11}dS$$

$$= -\chi_{xy1}\omega_2 f_2 \quad . \quad . \quad . \quad . \quad . \quad . \quad (63)$$

whence $$\rho_1\rho_2^* = \tfrac{1}{4}|\chi_{xy1}|^2\omega_1\omega_2 f_1 f_2^* \quad . \quad . \quad . \quad . \quad (64)$$

It is shown in Appendix 7.2 that

$$\Delta_{11} = \int_S (E_{t11} \times H^*_{t11}) \,.\, i_z dS = \frac{\pi\beta_{11}\omega_1\mu_0(u_1^2 - 1)J_1^2(u_1)}{K_1^4} \quad (65)$$

where $$J_1'(u_1) = 0$$

$$K_1^2 = \omega_1^2\epsilon_0\mu_0 - \beta_{11}^2 = \frac{u_1^2}{r_0^2}$$

Similarly, $$\Delta_{21} = \frac{\pi\beta_{21}\omega_2\mu_0(u_1^2 - 1)J_1^2(\mu_1)}{K_2^4} \quad . \quad . \quad (66)$$

where $$K_2^2 = \omega_2^2\epsilon_0\mu_0 - \beta_{21}^2 = \frac{u_1^2}{r_0^2}$$

Now, on the waveguide axis, the signal and idler fields can be written

$$H_{x11} = \frac{\beta_{11}}{2K_1} \quad . \quad . \quad . \quad . \quad . \quad . \quad (67)$$

$$H_{y21} = \frac{\beta_{21}}{2K_2} \quad . \quad . \quad . \quad . \quad . \quad . \quad (68)$$

Then $$f_1 = \frac{1}{4}\frac{\beta_{21}}{\omega_1\mu_0}\left(\frac{r_1}{r_0}\right)^2\frac{u_1^2}{(u_1^2 - 1)J_1^2(u_1)} \quad . \quad . \quad . \quad (69)$$

$$f_2 = \frac{1}{4}\frac{\beta_{11}}{\omega_2\mu_0}\left(\frac{r_1}{r_0}\right)^2\frac{u_1^2}{(u_1^2 - 1)J_1^2(u_1)} \quad . \quad . \quad . \quad (70)$$

† For the purpose of the present analysis there is no virtue in writing H_{x11}, H_{y21} as complex quantities since they are components of linearly polarized fields. However, the more general form chosen is helpful in understanding qualitatively the behaviour of travelling-wave amplifiers employing longitudinal magnetization and circularly polarized pump, signal and idler waves. A perturbation method similar to that just described could in fact be used to determine quantitatively the gain of such an amplifier.

and $$\rho_1\rho_2^* = \frac{1}{64}\left|\frac{\chi_{xy1}}{\mu_0}\right|^2\beta_{11}\beta_{21}\left(\frac{r_1}{r_0}\right)^2\left[\frac{u_1^2}{(u_1^2 - 1)J_1^2(u_1)}\right]^2 \quad . \quad (71)$$

If $\alpha_1 \simeq \alpha_2$ and $(\rho_1\rho_2^*) \geqslant \frac{1}{4}(\alpha_1 - \alpha_2)^2$

$$\phi_1 \simeq (\alpha_1\alpha_2)^{1/2} - (\rho_1\rho_2^*)^{1/2} \quad . \quad . \quad . \quad . \quad (72)$$

$$\phi_2 \simeq (\alpha_1\alpha_2)^{1/2} + (\rho_1\rho_2^*)^{1/2} \quad . \quad . \quad . \quad . \quad (73)$$

For gain, $\rho_1\rho_2^* > \alpha_1\alpha_2$, ϕ_1 is negative and the signal and idler grow with distance. The gain in nepers per unit length, g, is given by

$$g = (\rho_1\rho_2^*)^{1/2} - (\alpha_1\alpha_2)^{1/2} \quad . \quad . \quad . \quad . \quad (74)$$

$$= \frac{1}{8}\frac{|\chi_{xy1}|}{\mu_0}\left(\frac{\beta_{11}\beta_{21}}{\omega_1\omega_2}\right)^{1/2}\left(\frac{r_1}{r_0}\right)^2\frac{u_1^2}{(u_1^2 - 1)J_1^2(u_1)} - (\alpha_1\alpha_2)^{1/2} \quad (75)$$

If the pump field has $H_{pz} = 0$ in the neighbourhood of the ferrite,

$$m_{0x} = \frac{j\gamma H_{px}}{\Delta\omega}\frac{\bar{\omega}_0 + \omega_M(N_z - N_y)}{\omega_R} \quad . \quad . \quad (76)$$

$$m_{0z} = \frac{\gamma H_{px}}{\Delta\omega} \quad . \quad . \quad . \quad . \quad . \quad . \quad . \quad . \quad . \quad (77)$$

On putting $\lambda = 0$, and substituting for m_{0x} and m_{0z} in χ_{xy1}/μ_0,

$$\frac{\chi_{xy1}}{\mu_0} = \frac{j\gamma H_{px}}{\Delta\omega}\omega_M\frac{\left\{\frac{[\bar{\omega}_0 + \omega_M(N_z - N_y)]^2}{\omega_R} + \omega_1\right\}}{\omega_R^2\omega_1^2} \quad (78)$$

if $$\frac{|\gamma|H_{px}}{\Delta\omega} = \theta_p$$

$$\frac{|\chi_{xy1}|}{\mu_0} = \theta_p\omega_M\frac{[\bar{\omega}_0 + \omega_M(N_z - N_y)]^2 + \omega_1\omega_R}{\omega_2 - \omega_1^2} \quad (79)\dagger$$

Finally the expression for gain becomes

$$g = \frac{1}{8}\theta_p\omega_M\frac{[\bar{\omega}_0 + \omega_M(N_z - N_y)]^2 + \omega_1\omega_R}{(\omega_R^2 - \omega_1^2)\omega_R}$$

$$(\beta_{11}\beta_{21})^{1/2}\left(\frac{r_1}{r_0}\right)^2\frac{u_1^2}{(u_1^2 - 1)J_1^2(u_1)} - (\alpha_1\alpha_2)^{1/2} \quad (80)$$

For the structure of Fig. 2, $N_z = 0$, $N_y = \frac{1}{2}$ and $\omega_R^2 = \bar{\omega}_0(\bar{\omega}_0 - \omega_M/2)$. Furthermore, if $\omega_1 = \omega_2$, then $\alpha_1 = \alpha_2$ and

$$g = \theta_p\frac{\omega_M}{\omega_R}\frac{3\bar{\omega}_0 - \omega_M}{12\bar{\omega}_0}\beta_{11}\left(\frac{r_1}{r_0}\right)^2\frac{u_1^2}{(u_1^2 - 1)J_1^2(u_1)} - \alpha_1 \quad (81)$$

Eqn. (80) can be compared with eqn. (48) of Reference 1, where an expression is given for the gain of a travelling-wave ferrite amplifier of a more simple although less realistic kind (see Fig. 3 of Reference 1). This gain expression is reproduced below:

$$g = \theta_p\frac{\omega_M}{\omega_2}(\beta_{11}\beta_{21})^{1/2} - (\alpha_1\alpha_2)^{1/2} \quad . \quad . \quad (82)$$

The essential differences between eqns. (80) and (82) are attributed to two causes:

(*a*) The appearance in eqn. (80) of a factor which expresses the reduced energy density in the ferrite, characterized principally by the term $(r_1/r_0)^2$.

(*b*) The appearance of a factor which arises from the r.f. demagnetizing fields at the pump, signal and idler frequencies. In their analysis, Tien and Suhl[1] neglected these effects and assumed that the induced pump magnetization was circularly polarized.

† Because the magnetization is not circularly polarized θ_p only provides a measure of the mean precession angle.

In both cases the gain increases with θ_p, ω_M and the product $\beta_{11}\beta_{21}$. Although at first sight it might appear that θ_p could be indefinitely increased either by increasing the pump field or by reducing the linewidth $\Delta\omega$, this is in fact not so. Suhl[6] has shown that when

$$\theta_p = 2\left(\frac{\Delta\omega}{\omega_M}\right)^{1/2} \quad . \quad . \quad . \quad . \quad . \quad (83)\dagger$$

an instability of the magnetization occurs which prevents any further increase in θ_p and thus imposes a ceiling on the gain. In determining this gain ceiling, one can substitute for θ_p from eqn. (83) directly into eqns. (80)–(81). However, it is important to note that the gain can be limited for a different reason, which must be borne in mind when making such a substitution. This is the limitation due to heating of the ferrite. Since the power dissipated in the ferrite under the above conditions is proportional to $\Delta\omega^2$, it is clear that the gain cannot be indefinitely increased by increasing the ferrite linewidth. In fact, for polycrystalline ferrites (which have linewidths of the order of 100 oersteds) the limitation due to saturation of the resonance will not be reached because of ferrite heating. It is important to note that eqn. (83) imposes a fundamental limitation on the gain, while the heating problem merely imposes a technological limitation. Clearly the degree to which the gain ceiling due to pump saturation can be approached depends on the amount of cooling which exists as well as on the actual sample linewidth.

While, in principle, the gain could be increased by increasing ω_M, i.e. by increasing the saturation magnetization, in practice ω_M and $\Delta\omega$ are not independent parameters and in fact increase together. Thus, in choosing a particular ferrite for a travelling-wave amplifier, both ω_M and $\Delta\omega$ must be considered. In passing, it may be noted that there is some evidence suggesting that for certain ferrites ω_M and $\Delta\omega$ are proportional.

The factors which appear to offer the greatest possibility for improving the gain of the amplifier are the product $\beta_{11}\beta_{21}$, together with the energy density factor, which for thin rods is characterized by the term $(r_1/r_0)^2$. The first of these factors is common to Tien and Suhl's model and that of the present configuration. If a slow-wave structure could be employed in place of the circular waveguide, an improvement in gain of the order of 10 should be quite readily attained. There is substantial evidence elsewhere[7] which shows that, for other than thin rods, the energy density does not depend on r_1/r_0 through a square-law factor. In fact for most ferrites, when $r_1/r_0 \simeq 0{\cdot}35$, and if $r_0/\lambda_0 \simeq 0{\cdot}5$, nearly all the energy flows through the rod. Thus a gain comparable with that of the simple Tien and Suhl model should be achieved without using a waveguide filled with ferrite.

To complete the discussion of this Section the gain ceiling of the amplifier of Fig. 2 is approximately determined using eqns. (81) and (83). The following parameters are assumed, and for convenience in interpretation the C.G.S. system of units is employed:

$\omega_R/2\pi = 9\,\text{Gc/s}$, $\omega_M/2\pi = 11{\cdot}2\,\text{Gc/s}$ ($M_0 = 4000$ gauss), $\bar{\omega}_0/2\pi = 12{\cdot}2\,\text{Gc/s}$ ($H_a = 4350$ oersteds), $\Delta\omega/2\pi = 0{\cdot}36\,\text{Gc/s}$ ($\Delta H \simeq 130$ oersteds), $\epsilon''/\epsilon' = 0{\cdot}001$, $r_1/r_0 = 0{\cdot}2$ (which about represents the limit of accuracy of the perturbation method), $2r_0 = 0{\cdot}875$ in: whereby $\beta_{11} \simeq 1$ radian/cm, $(3\bar{\omega}_0 - \omega_M)/12\bar{\omega}_0 \simeq 0{\cdot}17$, $\theta_p = 0{\cdot}36$ [from eqn. (83)], $\omega_M/\omega_R = 0{\cdot}92$.

If losses in the absence of the pump are assumed to be of dielectric origin only, $\alpha_1 = 0{\cdot}001$ neper/cm. The gain ceiling is then $(0{\cdot}0085 - 0{\cdot}001)$ neper/cm, or, expressed in practical terms, 0·16 dB/in. Although this amount of gain is too low to be useful, it is stressed that by increasing the rod diameter by a factor of 2 the gain in decibels will increase by a factor of about 20. Moreover, if a further factor of 10 could be obtained by using a slow-wave structure, a gain ceiling of about 30 dB/in would be finally achieved. However, it must be pointed out that, for the above ferrite, the gain ceiling could not be usefully realized because of heating. An approximate calculation[8] based on a mean power dissipation of 200 W/cm^3 shows that a duty factor of 1 : 50000 would be required for a gain of 30 dB/in. On reducing the above value of θ_p by a factor of 10, i.e. by reducing the pump power by a factor of 100, a gain of 3 dB/in could be realized. With the same maximum power dissipation as above, a duty factor of 1 : 500 would be required.

† The expression quoted by Suhl in Reference 6, refers to a circularly polarized pump field; this accounts for the factor 2 in eqn. (83). Also, Suhl uses ΔH as the half-linewidth.

(4) OTHER WAVEGUIDE CONFIGURATIONS FOR AMPLIFIERS AND PRACTICAL CONSIDERATIONS

Fig. 3 shows two further configurations for microwave amplification.

In the configuration of Fig. 3(*a*) the signal and idler modes are circularly polarized H_{11}-type coupled by the uniform precession.

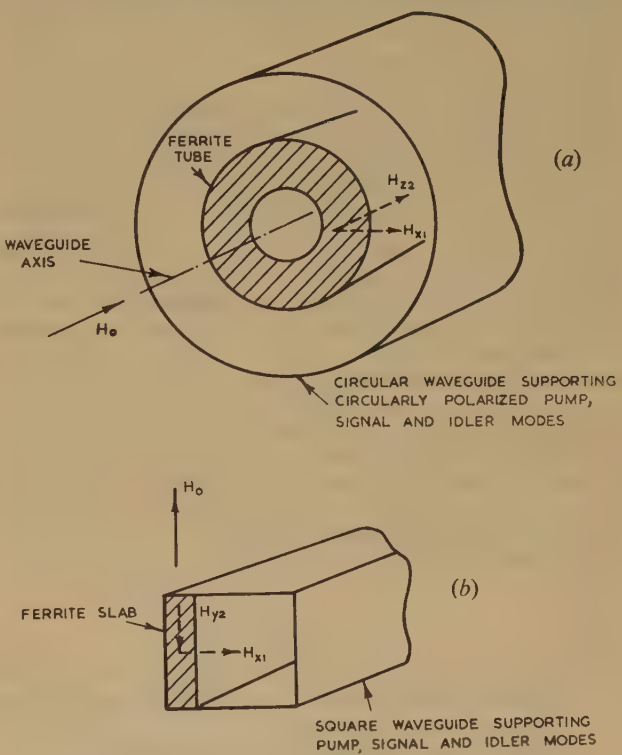

Fig. 3.—Alternative ferrite amplifier configurations.

This is excited by another circularly polarized H_{11}-type mode at frequency $\omega_1 + \omega_2$. Also, from a study of eqns. (38) and (39), it appears that signal and idler will have opposite senses of polarization. The amplifier operation relies on the existence of longitudinal and transverse components of r.f. magnetic field within the ferrite at frequencies ω_1 and ω_2. For this reason the tubular structure may be more advantageous than the rod, in which the longitudinal r.f. magnetic field is reduced.[9] Also, if the tube is in contact with the waveguide wall, the heating problem will be lessened.

In the configuration of Fig. 3(*b*), the signal and idler modes are of the H_{01} and HE_{11}-type, with the pump excited by an H_{01}-mode at frequency $\omega_1 + \omega_2$. If the ferrite represents only a small perturbation of the structure at the idler frequency, the mode is only slightly hybrid and strongly resembles the H_{10} mode. The gain of such a structure could be determined using the

method of Section 2. By placing the ferrite against the waveguide wall, the heating factor would again be reduced.

From a practical standpoint, it is essential that the amplifier should be short in length, since with a pump frequency of 9 Gc/s, a static magnetic field of about 4000 oersteds must be maintained accurate to within $\pm 1\%$, over this length. As there seems no immediate question of using single-crystal ferrites for travelling-wave amplifiers of the present type, the ferrite length is not a limiting factor. In the example discussed in Section 3, the linewidth chosen corresponds to that of polycrystalline nickel-zinc ferrite. The narrowest linewidth measured for a polycrystalline garnet is about half the above value, i.e. 60 oersteds.

(5) CONCLUSIONS

The analysis in Section 2 has enabled the gain of a physically realizable microwave amplifier to be determined, as in Section 3. Although the maximum gain of this amplifier is too low to be of practical importance, there are three ways in which the performance could be improved. These are summarized below:

(*a*) Use of a slow-wave structure, e.g. corrugated waveguide or helix surrounding the ferrite.

(*b*) Use of a ferrite or garnet rod of larger diameter. The only reason for specifying a thin rod in the calculation of Section 3 was in order that the theory should be valid and the result meaningful.

(*c*) Use of a ferrite with large linewidth. A restriction is imposed by the need to dissipate the pump power in the ferrite (which is proportional to the square of the linewidth) without undue heating.

Finally, it can be stated that travelling-wave ferrite amplifiers of the above type will necessarily remain pulse devices. Compared with cavity-type ferromagnetic amplifiers, the signal and idler energy densities in the ferrite are so low that, for appreciable gain, high pump powers are needed. Since only a certain amount of heat can be dissipated within the ferrite (depending on the thermal configuration), the maximum mean power per unit length of the amplifier is limited to about 20 W/in;[8] therefore the duty ratio will of necessity be of the order of 100. However, the advantage of the travelling-wave type of amplifier over the cavity type is the wide bandwidth of operation. Bandwidths of the order of 100 Mc/s should easily be obtained; such figures compare with 1 Mc/s for a cavity amplifier.

(6) REFERENCES

(1) TIEN, P. K., and SUHL, H.: 'A Travelling Wave Ferromagnetic Amplifier', *Proceedings of the Institute of Radio Engineers*, 1958, **44**, p. 100.

(2) CULLEN, A. L.: 'A Travelling Wave Parametric Amplifier', *Nature*, 1958, **181**, p. 332.

(3) SUHL, H.: 'Theory of the Ferromagnetic Microwave Amplifier', *Journal of Applied Physics*, 1957, **28**, p. 1225.

(4) SUHL, H., and WALKER, L. R.: 'Topics in Guided Wave Propagation through Gyromagnetic Media: Pt. III', *Bell System Technical Journal*, 1954, **33**, p. 1133.

(5) TIEN, P. K.: 'Parametric Amplification and Frequency Mixing in Propagating Circuits', *Journal of Applied Physics*, 1958, **29**, p. 1347.

(6) SUHL, H.: 'The Non-Linear Behaviour of Ferrites at High Microwave Signal Levels', *Proceedings of the Institute of Radio Engineers*, 1956, **42**, p. 1270.

(7) CLARRICOATS, P. J. B.: 'Properties of Circular Waveguides containing Ferrites', Ph.D. Thesis, University of London, 1958.

(8) CLAVIN, A.: 'High-Power Ferrite Load Isolators', *Transactions of the Institute of Radio Engineers*, 1955, *M.T.T.*, p. 38.

(9) TOMPKINS, J. E.: 'Energy Distribution in Partially Filled Waveguides', *Journal of Applied Physics*, 1958, **29**, p. 399. See also, paper presented at Brussels Conference 1958 (to be published).

(10) CLARRICOATS, P. J. B.: 'A Perturbation Method for Circular Waveguides Containing Ferrites', *Proceedings I.E.E.*, Paper No. 2796 E, May, 1959 (**106** B, p. 335).

(7) APPENDIX

(7.1) The External Susceptibility of an Ellipsoidal Ferrite

Consider the equation of motion [eqn. (84)] of the transverse component $\boldsymbol{M}_T$ of the magnetization $\boldsymbol{M}$, under the influence of a static field H_0 (assumed to be z-directed), a pump field H_p, a signal field H_1, and an idler field H_2.†

$$\frac{d\boldsymbol{M}_T}{dt} = \gamma(\boldsymbol{M} \times \boldsymbol{H}) - \lambda \boldsymbol{M}_T \quad . \quad . \quad . \quad (84)$$

where

$$M(\omega_{1,2}) = M_{1,2}\varepsilon^{j\omega_{1,2}t} + M^*_{1,2}\varepsilon^{-j\omega_{1,2}t}$$

$$H(\omega_{1,2}) = H_{1,2}\varepsilon^{j\omega_{1,2}t} + H^*_{1,2}\varepsilon^{-j\omega_{1,2}t}, \ \omega_1 + \omega_2 = \omega_p$$

If terms with time dependence $\varepsilon^{j\omega_1 t}$ are selected from eqn. (84) and M_z made equal to M_0 (static magnetization), i.e. terms such as M_{zp}, M^*_{z2} neglected, then

$$(\lambda + j\omega_1)M_{x1} = \gamma \left[M_{y1}\left(H_0 - N_z\frac{M_0}{\mu_0}\right) + M_{yp}H^*_{z2} - \left(H_{y1} - N_y\frac{M_{y1}}{\mu_0}\right)M_{z0} \right]$$

$$= -\bar{\omega}_0 M_{y1} + \omega_M N_z M_{y1} + \gamma M_{yp}H^*_{z2} + \omega_M \mu_0 H_{y1} - \omega_M N_y M_{y1} \quad (85)$$

where $$\bar{\omega}_0 = |\gamma|H_0, \ \omega_M = |\gamma|\frac{M_0}{\mu_0}$$

On collecting terms and putting $m_{0y} = \dfrac{M_{yp}}{M_0}$

$$(\lambda + j\omega_1)M_{x1} + \omega_M M_{y1}(N_y - N_z) + \bar{\omega}_0 M_{y1} = -\omega_M \mu_0 m_{0y}H^*_{z2} + \omega_M \mu_0 H_{y1} \quad (86)$$

Similarly,

$$(\lambda + j\omega_1)M_{y1} - \omega_M M_{y1}(N_x - N_z) - \bar{\omega}_0 N_{x1} = +\omega_M \mu_0 m^*_{0x} - \omega_M \mu_0 H_{x1} \quad (87)$$

On writing

$$\omega_a = \bar{\omega}_0 + \omega_M(N_y - N_z), \ \omega_b = \bar{\omega}_0 + \omega_M(N_x - N_z)$$

$$\omega_M \mu_0 = \bar{\omega}_M$$

eqns. (86) and (87) become

$$(\lambda + j\omega_1)M_{x1} + \omega_a M_{y1} = -\bar{\omega}_M m_{0y}H^*_{z2} + \bar{\omega}_M H_{y1} \quad (88)$$

$$(\lambda + j\omega_1)M_{y1} + \omega_b M_{x1} = \bar{\omega}_M m_{0x}H^*_{z2} - \bar{\omega}_M H_{x1} \quad (89)$$

On solving for M_{x1} and M_{y1},

$$M_{x1} = \chi_{xx1}H_{x1} + \chi_{xy1}H_{y1} - \chi_{xz1}H^*_{z2} \quad . \quad . \quad . \quad . \quad (90)$$

$$M_{y1} = -\chi_{xy1}H_{x1} + \chi_{yy1}H_{y1} - \chi_{yz1}H^*_{z2} \quad . \quad . \quad . \quad (91)$$

† H_0, H_p, H_1, H_2 are fields external to the ferrite. The bar previously used to denote an external field is discarded. Also, the static field is chosen to be z-directed, since this is the form most generally taken. The transformation to the co-ordinates employed in the main text will be made at the end of this Appendix.

where

$$\frac{\chi_{xx1}}{\mu_0} = \frac{\omega_M\bar{\omega}_0 + \omega_M^2(N_y - N_z)}{\omega_R^2 - \omega_1^2 + 2j\lambda\omega_1}, \quad \frac{\chi_{yy1}}{\mu_0} = \frac{\omega_M\bar{\omega}_0 + \omega_M^2(N_x - N_z)}{\omega_R^2 - \omega_1^2 + 2j\lambda\omega_1}$$

$$\frac{\chi_{xy1}}{\mu_0} = \frac{j\omega_M(\omega_1 - j\lambda)}{\omega_R^2 - \omega_1^2 + 2j\lambda\omega_1},$$

$$\frac{\chi_{xz1}}{\mu_0} = \left\{\frac{m_{0x}\omega_M[\bar{\omega}_0 + \omega_M(N_y - N_z)] + jm_{0y}\omega_M(\omega_1 - j\lambda)}{\omega_R^2 - \omega_1^2 + 2j\lambda\omega_1}\right\}$$

$$\frac{\chi_{yz1}}{\mu_0} = \left\{\frac{m_{0y}\omega_M[\bar{\omega}_0 + \omega_M(N_x - N_z)] - jm_{0x}\omega_M(\omega_1 - j\lambda)}{\omega_R^2 - \omega_1^2 + 2j\lambda\omega_1}\right\}$$

$$\omega_R^2 = \omega_a\omega_b = [\bar{\omega}_0 + \omega_M(N_y - N_z)][\bar{\omega}_0 + \omega_M(N_x - N_z)]$$

By virtue of the conservation condition,

$$M_z = (M_0^2 - M_{x,y}^2)^{1/2}$$

$$M_{z1} = (m_{0x}M_{x2}^* + m_{0y}M_{y2}^*)$$

$$= -\left\{\frac{m_{0x}[\omega_M\bar{\omega}_0 + \omega_M^2(N_y - N_z)] + jm_{0y}\omega_M(\omega_2 + j\lambda)}{\omega_R^2 - \omega_2^2 - 2j\lambda\omega_2}H_{x2}^*\right.$$

$$\left. + \frac{m_{0y}[\omega_M\bar{\omega}_0 + \omega_M^2(N_x - N_z)] - jm_{0x}\omega_M(\omega_2 + j\lambda)}{\omega_R^2 - \omega_2^2 - 2j\lambda\omega_2}H_{y2}^*\right\} \quad (92)$$

If $\lambda = 0$, eqn. (92) reduces to

$$M_{z1} = -(\chi_{xz2}H_{x2}^* + \chi_{yz2}H_{y2}^*) \quad . \quad . \quad . \quad (93)$$

where χ_{xz2} and χ_{yz2} are obtained from χ_{xz1} and χ_{yz1} on replacing ω_1 by ω_2.

Finally, if the following transformations are introduced, eqns. (27)–(29) are obtained:

$H_x \to H_x$, $H_y \to H_z$, $H_z \to -H_y$, $M_x \to M_x$, $M_y \to M_z$, $M_z \to -M_y$, $N_x \to N_x$, $N_y \to N_z$, $N_z \to N_y$, $\chi_{xx} \to \chi_{xx}$, $\chi_{yy} \to \chi_{zz}$, $\chi_{xy} \to \chi_{xz}$, $\chi_{xz} \to \chi_{xy}$, $\chi_{yz} \to \chi_{zy}$.

(7.2) Evaluation of $\int_S E_t \times H_t^* \cdot i_z dS$

From Maxwell's equations, if $E_z = 0$,

$$E_t = \frac{-j\omega\mu_0}{K^2}\nabla_t H_z \times i_z \quad . \quad . \quad . \quad . \quad . \quad (94)$$

$$H_t = \frac{-\gamma}{K^2}\nabla_t H_z \quad . \quad . \quad . \quad . \quad . \quad . \quad . \quad (95)$$

A solution of the wave equation in cylindrical co-ordinates yields

$$H_z(r, \theta) = J_n(Kr)\varepsilon^{jn\theta} \quad \text{where } K^2 = \frac{u_n^2}{r_0^2}$$

Thus $E_t \times H_t^* = \left[K^2J_n'^2(Kr) + n^2\frac{J_n^2(Kr)}{r^2}\right]i_z\frac{\beta\omega\mu_0}{K^4}$

$$\int_S E_t \times H_t^* \cdot i_z dS = \int_0^{2\pi}\int_0^{r_0} K^2\left[J_n^{2\prime}(Kr) + \frac{J_n^2(Kr)}{(Kr)^2}\right]rdrd\theta\frac{\beta\omega\mu_0}{K^4}$$

$$= 2\pi\int_0^{u_n}\left[J_n^{2\prime}(x) + n^2\frac{J_n^2(x)}{x^2}\right]xdx\frac{\beta\omega\mu_0}{K^4}$$

If $n = 1$, $\int_S E_t \times H_t^* \cdot i_z dS = \frac{\pi\beta\omega\mu_0(u_1^2 - 1)J_1^2(u_1)}{K^4}$

$$\Delta_{11} = \frac{\pi\beta_{11}\omega_1\mu_0(u_1^2 - 1)J_1^2(u_1)}{K_1^4}$$

and

$$\Delta_{21} = \frac{\pi\beta_{21}\omega_2\mu_0(u_1^2 - 1)J_1^2(u_1)}{K_2^4}$$

621.372.6

The Institution of Electrical Engineers
Monograph No. 335 E
June 1959

THE ORDER OF COMPLEXITY OF ELECTRICAL NETWORKS

By P. R. BRYANT, M.A., M.Sc.

(*The paper was first received* 3rd *December*, 1958, *and in revised form* 11*th February*, 1959. *It was published as an* INSTITUTION MONOGRAPH *in June*, 1959.)

SUMMARY

The natural frequencies of an electrical network are defined, and the number of these natural frequencies is called the *order of complexity* of the network. *RLC* networks are considered, and the order of complexity, σ, is shown to be given by

$$\sigma = B_L + N + S - S_C - S_{CR}$$

Here B_L is the number of inductors in the network, N is the number of nodes, S, S_C and S_{CR} are the connectivities, i.e. the number of separate parts of, respectively, the given network and those sub-networks formed of the capacitors only and of the capacitors and resistors only. Other expressions for σ are also obtained.

It is shown that this order of complexity is also the number of arbitrary integration constants in the complete solution of the network equations, and the number of dynamically-independent network variables. Complete sets of such dynamically-independent variables are obtained by a process of elimination from the network equations. A particular type of complete set is classified topologically, such sets being made up of voltages across capacitors forming a forest of the capacitor-only network obtained by open-circuiting all the resistors and inductors, together with the currents through inductors forming a set of chords of the inductor-only network obtained by short-circuiting all the capacitors and resistors.

LIST OF PRINCIPAL SYMBOLS

A_a = Incidence matrix.
A = Reduced incidence matrix.
A' = Transpose of A.
B = Chord-loop matrix.
B = Number of branches in a network $\mathcal{N}$.
B_C = Number of capacitors in $\mathcal{N}$.
= Number of capacitors in $\mathcal{N}_C$.
B_L = Number of inductors in $\mathcal{N}$.
= Number of inductors in $\mathcal{N}_L$.
B_R = Number of resistors in $\mathcal{N}$.
= Number of resistors in $\mathcal{N}_R$.
$DC_{\alpha\alpha}$ = Diagonal sub-matrix of $Y_C(D)$ corresponding to the capacitive chords of the tree $\mathcal{T}$.
$DC_{\delta\delta}$ = Diagonal sub-matrix of $Y_C(D)$ corresponding to the capacitor branches in the tree $\mathcal{T}$.
D = Differential operator, d/dt.
$e_k(t)$ = kth branch voltage generator.
$\boldsymbol{e}(t)$ = Branch voltage generator vector.
$E(t)$ = Loop voltage generator vector.
F = Columns of B corresponding to a set of chords.
$F_{\alpha\delta}, \ldots,$ etc. = Sub-matrices of F.
$\mathcal{F}_C, \mathcal{F}_{CR}$ = Forests of $\mathcal{N}_C, \mathcal{N}_{CR}$.
$H(D)$ = $2B \times 2B$ branch-equation matrix.
Adj $H(\lambda)$ = Adjugate or adjoint of the matrix $H(\lambda)$.
$[\text{Adj } H(\lambda_s)]^{(p)} = \left\{\frac{d^p}{d\lambda^p}[\text{Adj } H(\lambda)]\right\}_{\lambda=\lambda_s}$
det $H(D)$ = Determinant of $H(D)$.
$i_k(t)$ = kth branch current.
$\boldsymbol{i}(t)$ = Branch-current vector.
$\boldsymbol{i}_\alpha, \boldsymbol{i}_\beta, \ldots,$ etc. = Sub-vectors of $\boldsymbol{i}$.
$j_k(t)$ = kth branch current generator.
$\boldsymbol{j}(t)$ = Branch current generator vector.
$\boldsymbol{J}(t)$ = Nodal current generator vector.
K = Columns of A corresponding to a tree.
$DL_{\gamma\gamma}$ = Diagonal sub-matrix of $Z_{LR}(D)$ corresponding to the inductive chords of the tree $\mathcal{T}$.
$DL_{\zeta\zeta}$ = Diagonal sub-matrix of $Z_{LR}(D)$ corresponding to the inductor branches in the tree $\mathcal{T}$.
M = Number of independent loops in a network $\mathcal{N}$.
$M_C, M_{CR}, M_L^*,$ etc. = Number of independent loops in the networks $\mathcal{N}_C, \mathcal{N}_{CR}, \mathcal{N}_L^*,$ etc.
N = Number of nodes in a network $\mathcal{N}$.
$N_C, N_{CR}, N_L^*,$ etc. = Number of nodes in the networks $\mathcal{N}_C$, $\mathcal{N}_{CR}, \mathcal{N}_L^*,$ etc.
$\mathcal{N}$ = Typical *RLC* network.
$\mathcal{N}_C, \mathcal{N}_{CR},$ etc. = Networks formed from $\mathcal{N}$ by substituting open-circuits for those elements not denoted by the suffixes.
$\mathcal{N}_C^*, \mathcal{N}_{CR}^*,$ etc. = Networks formed from $\mathcal{N}$ by substituting short-circuits for those elements not denoted by the suffixes.
$P(\lambda)$ = Nodal-admittance matrix.
$R_{\beta\beta}$ = Diagonal sub-matrix of $Z_{LR}(D)$ corresponding to resistive chords of the tree $\mathcal{T}$.
$R_{\epsilon\epsilon}$ = Diagonal sub-matrix of $Z_{LR}(D)$ corresponding to resistor branches in the tree $\mathcal{T}$.
S = Connectivity of a network $\mathcal{N}$.
$S_C, S_{CR}, S_L^*,$ etc. = Connectivities of the networks $\mathcal{N}_C, \mathcal{N}_{CR}, \mathcal{N}_L^*,$ etc.
S = $B \times B$ matrix defined in Section 6.1.
t = Time.
T = Number of trees in a network $\mathcal{N}$.
T = $B \times B$ matrix defined in Section 6.1; also, in Section 6.2, the cut-set current generator vector, $K^{-1}J$.
$\mathcal{T}$ = A tree of a network $\mathcal{N}$, constructed as described in Section 6.2.
$v_k(t)$ = kth branch voltage.
$\boldsymbol{v}(t)$ = Branch-voltage vector.
$\boldsymbol{v}_\alpha, \boldsymbol{v}_\beta, \ldots,$ etc. = Sub-vectors of $\boldsymbol{v}(t)$.
X = Columns of A corresponding to a set of chords.
$Y_C(D)$ = $B \times B$ operator matrix.
$Z_{LR}(D)$ = $B \times B$ operator matrix.

Correspondence on Monographs is invited for consideration with a view to publication.

Mr. Bryant is the holder of a G.E.C. Scholarship in the Department of Engineering, University of Cambridge.

$\alpha, \beta, \gamma, \delta, \epsilon, \zeta$ = Suffixes denoting the classification of network branches.
σ = Order of complexity of a network $\mathcal{N}$.
λ = Complex-frequency variable.
$\mathbf{1}_\sigma$ = Unit matrix of order σ.
$\mathbf{1}_{\alpha\alpha}, \ldots$, etc. = Unit matrices corresponding to the branches $\alpha, \ldots$, etc.

(1) INTRODUCTION

The concept of the 'natural frequencies' of an electrical network arises from consideration of its transient behaviour. It is well known[5] that the solution of the network equations for any prescribed forcing function involves a particular integral and the complementary function. The complementary function will be made up of a number of exponential terms, the complex exponents of which are the natural frequencies. From the method of obtaining this complementary function[4] we may obtain the well-known result that the natural frequencies are the roots of the determinant of the operator matrix of the network equations. The network equations usually considered are either the nodal-voltage equations or the loop-current equations, with the result that it is the roots of the determinants associated with them which have often been defined to be the natural frequencies of the network (see, for example, Chapter 5 of Reference 5). For the purpose of obtaining an accurate definition of the natural frequencies, it seems reasonable to consider equations whose variables are such that a knowledge of their instantaneous values enables the instantaneous values of all the currents and voltages in the network to be calculated. This is not the case with either the nodal voltages or the loop currents. It is thus necessary first to frame the network equations in a form which involves all the network currents and voltages as dependent variables. In order to apply well-understood theory,[4] it is desirable to express these equations as a set of simultaneous differential equations, rather than in an integro-differential form so often used. Provided that these equations are of the lowest possible order, the roots of the associated determinant will be a set of natural frequencies which gives complete knowledge of the transient behaviour of the network.

Because of the existence of algebraic relations between certain of the currents and voltages, e.g. the Kirchhoff constraints, it is not necessary in general to use a set of equations having all of the currents and voltages as dependent variables. We return to this later.

In this paper we consider networks made up entirely of resistors, self-inductors and capacitors, i.e. *RLC* networks. We define a *branch* of such a network to be a single element: a resistor, an inductor or a capacitor. Then the branch currents and voltages form a complete set of currents and voltages of the network. We show that the network equations in terms of the branch currents and voltages may be expressed as a set of first-order differential equations, and so we get:

Definition 1.—The *natural frequencies* of an *RLC* network are defined to be the roots of the determinant polynomial of the operator matrix of the network equations when these are framed as a set of first-order differential equations for the branch currents and voltages. The number of these natural frequencies is called the *order of complexity* of the network and is denoted by σ.

In using the term 'order of complexity' we are following Reza.[12] In the past the term 'number of degrees of freedom' has been rather loosely used.[5,6] This term originates in the study of mechanical systems[8,14] and has meaning only if any significance can be attached to the term 'position' or 'configuration' of the system. This is not easy to do in the case of electrical networks, and we prefer not to use the term.

It is well known[4] that the number of arbitrary constants involved in the solution of a set of linear differential equations is given by the degree of the determinant polynomial of the operator matrix of the equations. From Definition 1 it is thus obvious that for the set of branch equations of an *RLC* network this number will be the same as the order of complexity, σ. By considering this degree, we obtain in Section 2 an expression for σ in terms of the network topology.

In Section 3 we consider sets of 'dynamically-independent network variables'. These are discussed by Guillemin in Section 2, Chapter 5, of Reference 6.† We define them as follows: Let us call the set of instantaneous values of all the branch currents and voltages the instantaneous 'state' of the network. Hence a knowledge of the instantaneous values of all of these variables determines this instantaneous state. Some of the branch variables, however, are connected by algebraic relations rather than differential relations. This means that it is not necessary to know all of their instantaneous values; some can be calculated from others. For example the instantaneous value of a resistor voltage can be obtained from the instantaneous value of the corresponding resistor current. We thus obtain our second definition:

Definition 2.—A minimal set of branch currents and voltages whose instantaneous values are sufficient to determine completely the instantaneous state of the network is called a 'complete set of dynamically-independent network variables'.

In Section 3 we show how to obtain such sets, and show that the number of variables in such a set is, as might be expected, the same as the order of complexity. The results obtained in this Section are compared in Appendix 6.3 with similar results obtained by Bashkow[2] in an earlier paper.

Throughout the paper we shall use the *RLC* network shown in Fig. 1 as an illustrative example.

(2) THE NATURAL FREQUENCIES AND ARBITRARY INTEGRATION CONSTANTS

(2.1) Introduction

In order to obtain an expression for the number of natural frequencies and the number of arbitrary integration constants, it is necessary to study the network equations. As we have discussed in Section 1, instead of choosing the nodal-voltage equations or the loop-current equations, we choose the more fundamental equations in terms of the branch‡ currents and voltages. If these branch equations are obtained in the form of a set of linear differential equations, rather than integro-differential equations, then the well-known theory of such equations[4] tells us how to determine the number of natural frequencies of the network. If multiple zeros§ are counted according to multiplicity, this number will be the degree of the determinant polynomial of the equation matrix. Considerations of a previous paper[3] enable us to obtain this degree, which will also give the number of arbitrary constants in the solution of the equations.[4]

(2.2) Preliminary Definitions and Results

Before we can write down the network branch equations we need a certain amount of preliminary work. We denote a typical electrical network made up entirely of resistors, self-inductors and capacitors (i.e. an *RLC* network) by $\mathcal{N}$. We define a *branch* of the network to be a single electrical element: a resistor, a self-inductor or a capacitor. We suppose the

† It should be noticed that our results differ from those of Guillemin, who also only considers the *LC* case.

‡ Throughout this paper, a *branch* of the *RLC* network is taken to be a single element: resistor, self-inductor or capacitor.

§ The form taken by the complementary function when multiple zeros are present is discussed in Section 2.8.

network to contain B such branches, namely B_R resistors, B_L inductors and B_C capacitors, where $B_L + B_C + B_R = B$. The branches are connected together at nodes, and we suppose $\mathcal{N}$ to contain N nodes. We arbitrarily number the nodes from 0 to $(N-1)$, and the branches from 1 to B; in a later Section a particular ordering of the branches will be used. The branches are further assumed to be arbitrarily oriented.[10] We denote by S the connectivity, i.e. the number of separate parts[7] of $\mathcal{N}$; if $S = 1$ we say that $\mathcal{N}$ is *connected*. We shall assume at first that $\mathcal{N}$ is connected. The extension to networks having $S > 1$ is indicated in Section 2.5.

Example of Fig. 1.—For the network of Fig. 1 we have

$$B = 6$$
$$N = 4$$
$$S = 1$$

The network with arbitrary node numbering and arbitrary branch numbering and orientation is shown in Fig. 2.

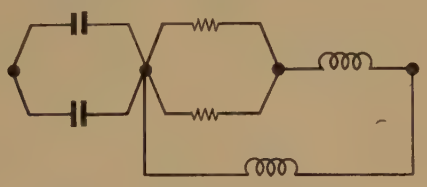

Fig. 1.—A typical *RLC* network $\mathcal{N}$.

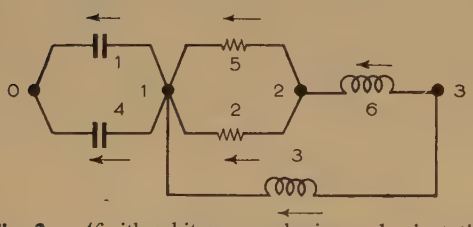

Fig. 2.—$\mathcal{N}$ with arbitrary numbering and orientations.

Denote by A_a the $N \times B$ *incidence matrix*[9,10] or *vertex matrix* of $\mathcal{N}$. We take node 0 to be the reference node, and denote by A the corresponding *reduced incidence matrix*, i.e. the matrix obtained from A_a by deleting the row corresponding to node 0. A is of order $(N-1) \times B$.

Example of Fig. 1.—From Fig. 2 we get:

$$A_a = \begin{bmatrix} -1 & 0 & 0 & -1 & 0 & 0 \\ +1 & -1 & -1 & +1 & -1 & 0 \\ 0 & +1 & 0 & 0 & +1 & -1 \\ 0 & 0 & +1 & 0 & 0 & +1 \end{bmatrix}$$

$$A = \begin{bmatrix} +1 & -1 & -1 & +1 & -1 & 0 \\ 0 & +1 & 0 & 0 & +1 & -1 \\ 0 & 0 & +1 & 0 & 0 & +1 \end{bmatrix}$$

Assume that a tree[3,7,9,10] of the network has been selected (in a later Section we specify a particular tree to be used). Let the corresponding set of chord loops or circuits[10] (or fundamental loops or circuits[9]) be specified by the $M \times B$ chord-loop matrix[10] $\boldsymbol{B}$.† Here M is the number of independent loops in the network $\mathcal{N}$ and is given by[10]

$$M = B - N + 1 \quad . \quad . \quad . \quad . \quad . \quad . \quad . \quad (1)$$

Example of Fig. 1.—Let us select the tree shown in Fig. 3. We have $M = 3$, and the set of chord-loops defined by this tree is shown in Fig. 4. $\boldsymbol{B}$ is given by

$$\boldsymbol{B} = \begin{bmatrix} +1 & 0 & 0 & -1 & 0 & 0 \\ 0 & +1 & 0 & 0 & -1 & 0 \\ 0 & 0 & +1 & 0 & -1 & -1 \end{bmatrix}$$

† The notation used in Reference 10 is B_c. As we later use subscripts to denote sub-matrices, and as we consider no loop matrices other than chord-loop matrices, we drop the subscript.

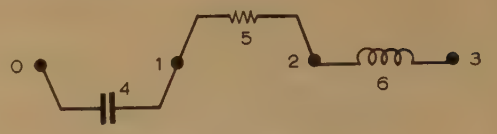

Fig. 3.—A tree of $\mathcal{N}$.

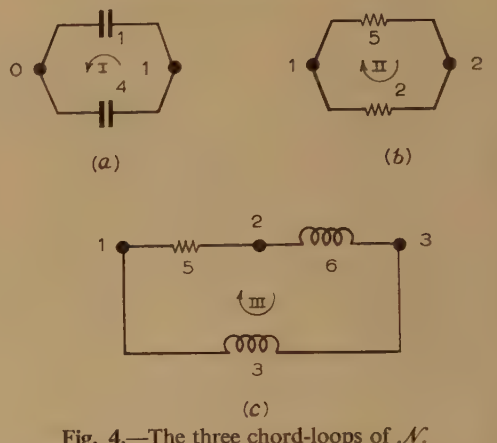

Fig. 4.—The three chord-loops of $\mathcal{N}$.

The network $\mathcal{N}$ has so far been assumed to contain no generators. However, ideal current and voltage generators may be applied to $\mathcal{N}$, provided that current generators are inserted only across nodes while voltage generators are inserted only into branches. A complete knowledge of these generators is assumed as part of the network. We shall be general and suppose that every branch of $\mathcal{N}$ has connected across it an ideal current generator and inserted into it an ideal voltage generator. The kth branch current generator, which will be some function of the time t, is denoted by $j_k(t)$, its voltage generator by $e_k(t)$; the potential across the kth passive branch is denoted by $v_k(t)$ and the current through it by $i_k(t)$. The relative positions and orientations of these currents and potentials for a general kth branch are shown in Fig. 5.† We define the various $B \times 1$

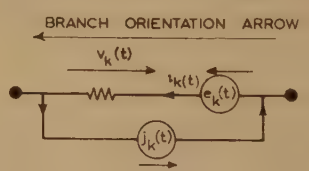

Fig. 5.—A typical active branch.

column vectors $\boldsymbol{j}(t)$, $\boldsymbol{e}(t)$, $\boldsymbol{v}(t)$, and $\boldsymbol{i}(t)$ in the obvious way. We shall often drop the explicit inclusion of the time variable t in our later work.

Example of Fig. 1.—Our network together with all its branch generators and branch potentials and currents is shown in Fig. 6.

Although we are now in a position to write down the network equations, we shall give first a few further definitions, some of which we need in Section 2.4. The notation is slightly different from that used in our earlier paper.[3] We denote by $\mathcal{N}_C$, $\mathcal{N}_L$, $\mathcal{N}_{CR}$ etc., those networks obtained from $\mathcal{N}$ by substituting *open* circuits for those elements *not* denoted by the suffixes. The numbers of nodes, branches, loops and separate parts of these networks we shall denote by the obvious notation N_C, B_C, M_C, S_C, N_L, B_L, etc. Notice that this definition of B_C, B_L and B_R

† It is assumed that the arrows indicating potentials point towards the higher potential.

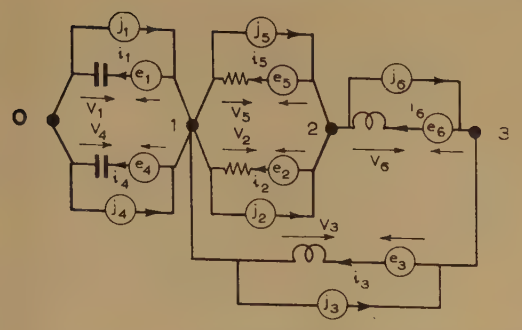

Fig. 6.—$\mathcal{N}$, together with its branch generators and variables.

does not conflict with that previously given, i.e. as the number of capacitors, inductors and resistors in $\mathcal{N}$. We denote by $\mathcal{N}_C^*$, $\mathcal{N}_L^*$, $\mathcal{N}_{CR}^*$, etc., the networks obtained from $\mathcal{N}$ by substituting *short*-circuits for those elements *not* denoted by the suffixes. The numbers of nodes, branches, etc., are denoted by N_C^*, B_C^*, etc.

It should be especially noted that if a network should contain any isolated nodes, then each such node is considered to be a separate part of the network and should be counted when determining the network connectivity.

Example of Fig. 1.—As examples we show $\mathcal{N}_C$, $\mathcal{N}_{CR}$ and $\mathcal{N}_L^*$ in Fig. 7. We have from the figure:

$$\begin{aligned} N_C &= 4 \\ B_C &= 2 \\ M_C &= 1 \\ S_C &= 3 \end{aligned}$$

$$\begin{aligned} N_{CR} &= 4 \\ B_{CR} &= 4 \\ M_{CR} &= 2 \\ S_{CR} &= 2 \end{aligned}$$

$$\begin{aligned} N_L^* &= 2 \\ B_L^* &= 2 \\ M_L^* &= 1 \\ S_L^* &= 1 \end{aligned}$$

We shall now define one further term which we use in later Sections. We recall[3,7,9,10] that a tree of a connected network is a connected set of $(N-1)$ branches containing no loops.

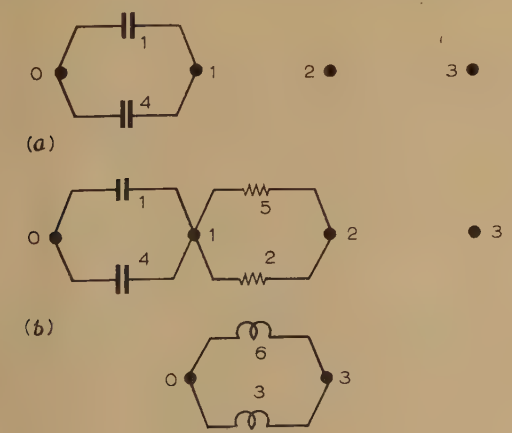

Fig. 7.—$\mathcal{N}_C$, $\mathcal{N}_{CR}$ and $\mathcal{N}_L^*$.

(*a*) $\mathcal{N}_C$.

(*b*) $\mathcal{N}_{CR}$.

(*c*) $\mathcal{N}_L^*$.

If the network is not connected it can contain no trees. However, each of the S separate parts is by definition connected, and so each will contain a tree; the collection of the S trees so obtained we call a *forest*[3] of $\mathcal{N}$. A forest will obviously contain $(N-S)$ branches. If any of the separate parts of the network consist of isolated nodes, then, by definition, these isolated nodes shall be included as part of any forest. This is slightly different from the definition given in Reference 3.

(2.3) The Network Branch Equations

We may now write down the network branch equations, which are the Kirchhoff current and voltage laws, and the generalized Ohm's law applied to each branch.

Kirchhoff's current law becomes[9]

$$\boldsymbol{A}(\boldsymbol{i}-\boldsymbol{j}) = \boldsymbol{0} \quad . \quad . \quad . \quad . \quad . \quad . \quad . \quad (2)$$

and Kirchhoff's voltage law becomes[9]

$$\boldsymbol{B}(\boldsymbol{v}-\boldsymbol{e}) = \boldsymbol{0} \quad . \quad . \quad . \quad . \quad . \quad . \quad . \quad (3)$$

Example of Fig. 1.—Written out in full, and taking 'generator terms' over to the right-hand side, eqns. (2) and (3) become:

$$\left.\begin{aligned} +i_1 - i_2 - i_3 + i_4 - i_5 &= +j_1 - j_2 - j_3 + j_4 - j_5 \\ +i_2 + i_5 - i_6 &= +j_2 + j_5 - j_6 \\ +i_3 + i_6 &= +j_3 + j_6 \end{aligned}\right\} \quad (2')\dagger$$

$$\left.\begin{aligned} +v_1 - v_4 &= +e_1 - e_4 \\ +v_2 - v_5 &= +e_2 - e_5 \\ +v_3 - v_5 + v_6 &= +e_3 - e_5 - e_6 \end{aligned}\right\} \quad (3')$$

Consider the generalized Ohm's law:

A capacitor branch obeys a differential equation like

$$i(t) = C\frac{dv(t)}{dt} \quad . \quad . \quad . \quad . \quad . \quad . \quad . \quad (4)$$

An inductor branch obeys a differential equation like

$$v(t) = L\frac{di(t)}{dt} \quad . \quad . \quad . \quad . \quad . \quad . \quad . \quad (5)$$

while a resistor branch obeys an algebraic equation like

$$v(t) = Ri(t) \quad . \quad . \quad . \quad . \quad . \quad . \quad . \quad (6)$$

Let us denote the differential operator d/dt by D; then eqns. (4), (5) and (6) may be combined into one matrix equation of differential form:

$$\boldsymbol{Y}_C(D)\boldsymbol{v}(t) = \boldsymbol{Z}_{LR}(D)\boldsymbol{i}(t) \quad . \quad . \quad . \quad . \quad (7)$$

Here the matrix $\boldsymbol{Y}_C(D)$ is $B \times B$ diagonal, has units in those diagonal elements corresponding to inductive or resistive branches, and a term of the form CD corresponding to a capacitive branch. Similarly $\boldsymbol{Z}_{LR}(D)$ is $B \times B$ diagonal, has units corresponding to capacitive branches, a term of the form LD corresponding to an inductive branch, and a term of the form R corresponding to a resistive branch.

Note that eqns. (7) are a set of first-order differential equations, not integro-differential equations.

Example of Fig. 1. We shall have

$$\boldsymbol{Y}_C(D) = \begin{bmatrix} C_1D & . & . & . & . \\ . & 1 & . & . & . \\ . & . & 1 & . & . \\ . & . & . & C_4D & . \\ . & . & . & . & 1 \end{bmatrix}; \quad \boldsymbol{Z}_{LR}(D) = \begin{bmatrix} 1 & . & . & . & . \\ . & R_2 & . & . & . \\ . & . & L_3D & . & . \\ . & . & . & 1 & . \\ . & . & . & . & R_5 \end{bmatrix}$$

† To assist the reader, equation numbers in the running example are primed, indicating that the equation is the particular case of the corresponding unprimed equation of the general discussion.

and eqns. (7) written out in full become

$$\left.\begin{aligned} C_1\frac{dv_1}{dt} &= i_1 \\ v_2 &= R_2 i_2 \\ v_3 &= L_3\frac{di_3}{dt} \\ C_4\frac{dv_4}{dt} &= i_4 \\ v_5 &= R_5 i_5 \\ v_6 &= L_6\frac{di_6}{dt} \end{aligned}\right\} \quad \ldots\ldots\ldots \quad (7')$$

Eqns. (2), (3) and (7) may be written as a single matrix equation:

$$\left[\begin{array}{c|c} \mathbf{0} & \boldsymbol{B} \\ \boldsymbol{A} & \mathbf{0} \\ \hline \boldsymbol{Z}_{LR}(D) & -\boldsymbol{Y}_C(D) \end{array}\right]\left[\begin{array}{c} \boldsymbol{i} \\ \hline \boldsymbol{v} \end{array}\right] = \left[\begin{array}{c} \boldsymbol{Be} \\ \boldsymbol{Aj} \\ \hline \mathbf{0} \end{array}\right] \quad \ldots \quad (8)$$

Here we have shown by dotted lines the partitioning of the matrices and vectors concerned into $B \times B$ sub-matrices and $B \times 1$ sub-vectors.

Concerning the vector on the right-hand side of eqn. (8), the $(N-1) \times 1$ column vector $\boldsymbol{Aj}$ we denote by $\boldsymbol{J}$ and call the nodal current-generator vector, while the $M \times 1$ column vector $\boldsymbol{Be}$ we denote by $\boldsymbol{E}$ and call the loop voltage-generator vector. These vectors form the *forcing functions of* eqn. (8).

We further put

$$\left[\begin{array}{cc} \mathbf{0} & \boldsymbol{B} \\ \boldsymbol{A} & \mathbf{0} \\ \boldsymbol{Z}_{LR}(D) & -\boldsymbol{Y}_C(D) \end{array}\right] \equiv \boldsymbol{H}(D) \quad \ldots \quad (9)$$

Eqn. (8) now becomes

$$\boldsymbol{H}(D)\left[\begin{array}{c} \boldsymbol{i} \\ \hline \boldsymbol{v} \end{array}\right] = \left[\begin{array}{c} \boldsymbol{E} \\ \boldsymbol{J} \\ \hline \mathbf{0} \end{array}\right] \quad \ldots\ldots \quad (10)$$

which are the network branch equations.

Example of Fig. 1.—We shall have:

$$\boldsymbol{J} = \begin{bmatrix} (j_1 - j_2 - j_3 + j_4 - j_5) \\ (j_2 + j_5 - j_6) \\ (j_3 + j_6) \end{bmatrix}$$

$$\boldsymbol{E} = \begin{bmatrix} (e_1 - e_4) \\ (e_2 - e_5) \\ (e_3 - e_5 - e_6) \end{bmatrix}$$

$$\boldsymbol{H}(D) = \left[\begin{array}{cccccc|cccccc} \cdot & \cdot & \cdot & \cdot & \cdot & \cdot & 1 & 0 & 0 & -1 & 0 & 0 \\ \cdot & \cdot & \cdot & \cdot & \cdot & \cdot & 0 & 1 & 0 & 0 & -1 & 0 \\ \cdot & \cdot & \cdot & \cdot & \cdot & \cdot & 0 & 0 & 1 & 0 & -1 & -1 \\ 1 & -1 & -1 & 1 & -1 & 0 & \cdot & \cdot & \cdot & \cdot & \cdot & \cdot \\ 0 & 1 & 0 & 0 & 1 & -1 & \cdot & \cdot & \cdot & \cdot & \cdot & \cdot \\ 0 & 0 & 1 & 0 & 0 & 1 & \cdot & \cdot & \cdot & \cdot & \cdot & \cdot \\ \hline 1 & \cdot & \cdot & \cdot & \cdot & \cdot & -C_1D & \cdot & \cdot & \cdot & \cdot & \cdot \\ \cdot & R_2 & \cdot & \cdot & \cdot & \cdot & \cdot & -1 & \cdot & \cdot & \cdot & \cdot \\ \cdot & \cdot & L_3D & \cdot & \cdot & \cdot & \cdot & \cdot & -1 & \cdot & \cdot & \cdot \\ \cdot & \cdot & \cdot & 1 & \cdot & \cdot & \cdot & \cdot & \cdot & -C_4D & \cdot & \cdot \\ \cdot & \cdot & \cdot & \cdot & R_5 & \cdot & \cdot & \cdot & \cdot & \cdot & -1 & \cdot \\ \cdot & \cdot & \cdot & \cdot & \cdot & L_6D & \cdot & \cdot & \cdot & \cdot & \cdot & -1 \end{array}\right]$$

$$\ldots\ldots \quad (9')$$

Note that in $\boldsymbol{H}(D)$ we have used dots in place of zeros whenever these occur in whole blocks. This has been done so as to show up the form of construction of the matrix.

(2.4) The Natural Frequencies

The natural frequencies of the network $\mathcal{N}$ are, by Definition 1, the roots of the polynomial $\det \boldsymbol{H}(\lambda)$, where λ is the complex frequency variable, and $\boldsymbol{H}(D)$ is the operator matrix of eqns. (9) and (10).

We thus wish to expand $\det \boldsymbol{H}(\lambda)$. This expansion is obtained in Appendix 6.1, where it is shown that if $\boldsymbol{P}(\lambda)$ denotes the well-known nodal-admittance matrix of $\mathcal{N}$, then

$$\det \boldsymbol{H}(\lambda) = \pm \binom{\text{product of all}}{\text{inductors}}\binom{\text{product of all}}{\text{resistors}}\lambda^{B_L} \det \boldsymbol{P}(\lambda) \quad \ldots\ldots \quad (11)$$

Example of Fig. 1.—From Fig. 2 we have

$$\boldsymbol{P}(\lambda) = \left[\begin{array}{ccc} \left(\lambda C_1 + \lambda C_4 + \frac{1}{R_2} + \frac{1}{R_5} + \frac{1}{\lambda L_3}\right) & -\left(\frac{1}{R_2} + \frac{1}{R_5}\right) & -\frac{1}{\lambda L_3} \\ -\left(\frac{1}{R_2} + \frac{1}{R_5}\right) & \left(\frac{1}{R_2} + \frac{1}{R_5} + \frac{1}{\lambda L_6}\right) & -\frac{1}{\lambda L_6} \\ -\frac{1}{\lambda L_3} & -\frac{1}{\lambda L_6} & \left(\frac{1}{\lambda L_3} + \frac{1}{\lambda L_6}\right) \end{array}\right]$$

If we expand $\det \boldsymbol{P}(\lambda)$ we obtain

$$\det \boldsymbol{P}(\lambda) = \frac{(C_1 + C_4)(R_2 + R_5)(L_3 + L_6)\lambda + R_2R_5(C_1 + C_4)}{R_2R_5L_3L_6\lambda}$$

Hence from eqn. (11)

$$\begin{aligned} \det \boldsymbol{H}(\lambda) &= \pm (R_2R_5)(L_3L_6)\lambda^2 \det \boldsymbol{P}(\lambda) \\ &= \pm (C_1 + C_4)\lambda[(L_3 + L_6)(R_2 + R_5)\lambda + R_2R_5] \quad \ldots \quad (11') \end{aligned}$$

Hence the natural frequencies of $\mathcal{N}$ are given by

$$\lambda = 0$$

and

$$\lambda = -R_2R_5/(L_3 + L_6)(R_2 + R_5)$$

Notice that $\lambda = 0$ is *not* a root of $\det \boldsymbol{P}(\lambda) = 0$ (cf. Lemma 1 below).

In Reference 3, we have shown that

$$\det \boldsymbol{P}(\lambda) = \frac{\left[\begin{array}{c}\text{Polynomial in } \lambda \text{ containing a constant and of} \\ \text{degree } (2N + 2 - S_C - S_{CR} - S_L - S_{LR})\end{array}\right]}{\lambda^{N+1-S_L-S_{LR}}} \quad \ldots\ldots \quad (12)$$

where the connectivities S_C, S_{CR}, etc., are defined in Section 2.2. Hence

$$\det \boldsymbol{H}(\lambda) = \left[\begin{array}{c}\text{Polynomial in } \lambda \text{ of degree} \\ (2N + 2 - S_C - S_{CR} - S_L - S_{LR})\end{array}\right]\lambda^{(B_L+S_L+S_{LR}-N-1)} \quad \ldots\ldots \quad (13)$$

Now

$$B_L + S_L + S_{LR} - N - 1 \geqslant 0 \quad \ldots \quad (14)$$

for

$$B_L - N + S_L = M_L \geqslant 0 \quad \ldots\ldots \quad (15)$$

and

$$S_{LR} - 1 \geqslant 0 \quad \ldots\ldots \quad (16)$$

Hence, as we would expect, $\det \boldsymbol{H}(\lambda)$ is a polynomial, and its degree, σ, is given by

$$\begin{aligned} \sigma &= (2N + 2 - S_C - S_{CR} - S_L - S_{LR}) \\ &\quad + (B_L + S_L + S_{LR} - N - 1) \quad \ldots \quad (17) \end{aligned}$$

i.e.

$$\sigma = B_L + N + 1 - S_C - S_{CR} \quad \ldots \quad (18)$$

It is of interest to note that from eqn. (11) we obtain the following Lemma:

Lemma 1.—The non-zero natural frequencies of $\mathcal{N}$ are the finite non-zero roots of $\det \boldsymbol{P}(\lambda)$ (cf. Reference 3, footnote on p. 1).

Example of Fig. 1.—For Fig. 1 we have

$$B_L = 2$$
$$N = 4$$
$$S_C = 3$$
$$S_{CR} = 2$$

giving

$$\sigma = 2$$

This agrees with the expansion (11′).

(2.5) The Extension to Non-Connected Networks

If $\mathcal{N}$ is not connected, i.e. if $S > 1$, the above considerations may be applied to each part separately. The order of complexity for the whole network will then be the sum of the orders of complexity of each part.

Hence we obtain the following theorem:

Theorem 1.—In the notation of this Section, the order of complexity σ of an *RLC* network is given by

$$\sigma = B_L + N + S - S_C - S_{CR} \quad . \quad . \quad . \quad (19)$$

(2.6) The Arbitrary Integration Constants

As is well known,[4] the number of arbitrary constants involved in the solution of eqns. (10) will be given by the degree in λ of det $H(\lambda)$. Hence their number is also σ, the order of complexity of $\mathcal{N}$. Eqns. (10) are a system of first-order linear differential equations and these arbitrary constants may be taken to be the initial values of σ of the variables $v_k(t)$, $i_k(t)$. Precisely which of these variables may be chosen is discussed in Section 3.1.

(2.7) Some Other Expressions for σ

By application of eqn. (1) to the various networks $\mathcal{N}_C$, $\mathcal{N}_{CR}$, $\mathcal{N}_L^*$, etc., and use of the following results, which are proved in Reference 3,

$$(a)\ S_{CR} = N_L^*$$
$$(b)\ S_L^* = S$$
$$(c)\ N_C = N_{CR} = N$$

the following alternative expressions for σ may be obtained:

$$\sigma = B_L + N + S - S_C - S_{CR} \quad . \quad . \quad . \quad (20)$$
$$= B_L + B_C - M_C - (N_L^* - S_L^*) \quad . \quad . \quad (21)$$
$$= B_C + M - M_C - M_{CR} \quad . \quad . \quad . \quad . \quad (22)$$

The notation used here was explained in Section 2.2.

Now a *cut-set* of a network is a set of network branches whose removal increases the connectivity of the network by one provided that, if one or more branches of the set are omitted, the remaining branches in the set do not have this property. The number of independent cut-sets in $\mathcal{N}$ may be shown[11] to be given by $(N - S)$. Thus $(N_L^* - S_L^*)$ is the number of independent cut-sets in $\mathcal{N}_L^*$. From Lemma 11 (Section 6.3), we see that this is also the number of independent inductor-only cut-sets in $\mathcal{N}$. Thus eqn. (21) may be put into words as: 'The order of complexity of an *RLC* network is given by the number of reactive elements less the number of independent capacitor-only loops, less the number of independent inductor-only cut-sets'.

This statement takes on a physical meaning when considered in the light of the elimination process used to obtain a set of dynamically-independent network variables described in Section 6.2.

(2.8) Multiple Zeros of det $H(\lambda)$

When det $H(\lambda)$ contains multiple zeros, the form of the complementary function is interesting. We first point out that eqn. (10) represents a set of simultaneous equations involving $2B$ dependent variables. The form of the complementary function when multiple zeros occur is, in this case, often different from the well-known form obtained when only one equation for one dependent variable is under consideration. In this latter case, if λ_s, say, is a root of multiplicity $m > 1$, then the corresponding part of the complementary function is well known to be

$$[A_0 + A_1 t + \ldots + A_{m-1} t^{m-1}] e^{\lambda_s t} \quad . \quad . \quad . \quad (23)$$

where the A_i are a set of arbitrary constants. The corresponding form for the case of a set of simultaneous equations does not appear to be quite so well known by electrical engineers. A full discussion of this is given in Section 5.7 of Reference 4, and we give here the results.

Let λ_s be a root of det $H(\lambda)$ of multiplicity $m > 1$. Denote by Adj $H(\lambda)$ the adjugate or adjoint,[1,4] matrix of $H(\lambda)$, and denote $\left[\frac{d^p}{d\lambda^p} \text{Adj } H(\lambda)\right]_{\lambda=\lambda_s}$ by $[\text{Adj } H(\lambda_s)]^{(p)}$. Then it can be shown[4] that m independent solutions of $H(D)x(t) = \mathbf{0}$ will be contained amongst the $2Bm$ columns of the following m matrices:

$$\text{Adj } H(\lambda_s) e^{\lambda_s t}$$

$$[\text{Adj } H(\lambda_s)]^{(1)} + t \text{ Adj } H(\lambda_s) e^{\lambda_s t}$$

$$\vdots$$

$$\left\{[\text{Adj } H(\lambda_s)]^{(p)} + pt[\text{Adj } H(\lambda_s)]^{(p-1)} + \binom{p}{2} t^2 [\text{Adj } H(\lambda_s)]^{(p-2)} + \ldots + t^p \text{ Adj } H(\lambda_s)\right\} e^{\lambda_s t}$$

$$\vdots$$

$$\left\{[\text{Adj } H(\lambda_s)]^{(m-1)} + (m-1)t[\text{Adj } H(\lambda_s)]^{(m-2)} + \binom{m-1}{2} t^2 [\text{Adj } H(\lambda_s)]^{(m-3)} + \ldots + t^{m-1} \text{Adj } H(\lambda_s)\right\} e^{\lambda_s t} \quad (24)$$

An important point to notice about eqn. (24) is that if

$$[\text{Adj } H(\lambda_s)]^{(m-2)} = [\text{Adj } H(\lambda_s)]^{(m-3)} = \ldots = \text{Adj } H(\lambda_s) = \mathbf{0} \quad . \quad . \quad . \quad . \quad (25)$$

then no columns containing powers of t will be present. In this case, $[\text{Adj } H(\lambda_s)]^{(m-1)}$ will contain m independent columns, and if we denote them by $\boldsymbol{h}_1(\lambda_s)$, $\boldsymbol{h}_2(\lambda_s)$, . . ., $\boldsymbol{h}_m(\lambda_s)$, then that part of the complementary function corresponding to λ_s is

$$[A_1 \boldsymbol{h}_1(\lambda_s) + A_2 \boldsymbol{h}_2(\lambda_s) + \ldots + A_m \boldsymbol{h}_m(\lambda_s)] e^{\lambda_s t} \quad . \quad (26)$$

where the A_i are arbitrary constants. Notice that eqn. (25) holds only when $(\lambda - \lambda_s)^{m-1}$ is a factor of every element of Adj $H(\lambda)$.

Consider now the stability of the transient behaviour of the network. The complementary function in the solution of eqn. (10) must obviously have no columns containing powers of t arising from a multiple zero of det $H(\lambda)$ on the imaginary λ-axis, i.e. corresponding to a real frequency. For such a root then, eqn. (25) must hold. Hence if λ_s is an mth order pure imaginary root of det $H(\lambda)$, then $(\lambda - \lambda_s)^{m-1}$ must be a factor of every element of Adj $H(\lambda)$. From this we may obtain the well-known property of various network functions—that they have only simple poles on the imaginary λ-axis.

(3) COMPLETE SETS OF DYNAMICALLY-INDEPENDENT VARIABLES

(3.1) Introduction

In Section 1, Definition 2, we defined a complete set of dynamically-independent network variables as a minimal set whose instantaneous values are sufficient to determine com-

pletely the instantaneous state of the network. Since the set is minimal, it follows that there exist no algebraic equations between them, while since it is sufficient, all other of the network variables are expressible in terms of this set by unique algebraic equations. This indicates a method of obtaining such a complete set. Starting from the network branch equations, and using all explicit and implicit algebraic relations, variables are eliminated until a complete set of dynamically-independent variables is obtained. Before proceeding to do this, we give first a further discussion of the arbitrary integration constants which shows that a complete set of dynamically-independent variables contains precisely σ such variables, where σ is the order of complexity. We pointed out in Section 2.6 that the σ arbitrary integration constants may be taken to be the initial values of σ of the branch variables $v_k(t)$, $i_k(t)$. However, not *any* set of σ of these variables may be given arbitrary instantaneous values, owing to the possibility of the existence of algebraic relations between them. We have just pointed out, however, that a complete set of dynamically-independent variables have no such algebraic relations between them, while all other of the network variables are algebraically expressible in terms of the complete set. Hence such a complete set is capable of taking arbitrary instantaneous values, i.e. their initial values may be taken to be a complete set of arbitrary integration constants. We thus obtain Theorem 2:

Theorem 2.—A complete set of dynamically-independent network variables will contain σ of the variables $i_k(t)$, $v_k(t)$, where σ is the order of complexity of the network, and their initial values may be taken to be a set of arbitrary integration constants.

(3.2) Elimination

The process of elimination we use to arrive at a complete set of dynamically-independent network variables depends upon forming our branch equations in a particular form. This form involves the classification of the network branches into six groups, and hence the branch variables into twelve groups, i.e. a set of voltages and currents for each group. Our elimination process then involves expressing ten of these groups algebraically in terms of the remaining two groups, which are shown to contain between them σ variables. These two groups will thus together form a complete set of dynamically-independent variables as required. The classification of the variables, and also the particular form of the branch equations, is obtained by using a particular tree of the network. The construction of this tree, and the resulting process of elimination, is given in detail in Appendix 6.2, whence we obtain Theorem 3:

Theorem 3.—The voltages across $(N - S_C)$ capacitors forming a forest† of $\mathcal{N}_C$ and the currents through $(B_L + S - S_{CR})$ inductors forming a set of chords‡ to a forest of $\mathcal{N}_L^*$ together make up a complete set of dynamically-independent variables of an *RLC* network $\mathcal{N}$ of connectivity S.

The proof of Theorem 3 is contained in Section 6.2.

Definition 3.—We call a set of σ network elements made up of $(N - S_C)$ capacitors forming a forest of $\mathcal{N}_C$ and $(B_L + S - S_{CR})$ inductors forming a set of chords of $\mathcal{N}_L^*$ a 'fundamental set of elements'. The voltages across these capacitors and the currents through these inductors we call a 'fundamental complete set of dynamically-independent network variables'.

Example of Fig. 1.—Any one of the two capacitors of $\mathcal{N}$ forms a forest of $\mathcal{N}_C$, and any one of the two inductors forms a set of chords of $\mathcal{N}_L^*$; see Figs. 7(*a*) and (*c*). Hence, for example, i_3 and v_4 form a fundamental complete set of dynamically-independent network variables.

† The term 'forest' is defined in Section 2.2.

‡ Although $\mathcal{N}_L^*$ will have connectivity S, and so not be connected in general, we define a set of chords as being the complement of a forest.

A process of elimination amongst network variables has been described in an earlier paper by Bashkow.[2] His results are expressed, however, rather differently from ours. We discuss them in Appendix 6.3 and show that they coincide with ours.

(3.3) Independent Points of Energy Storage

The energy-storage elements of an *RLC* network $\mathcal{N}$ are, of course, the reactive elements, i.e. the inductors and capacitors. Now the instantaneous stored energy in a capacitor at time t is $\frac{1}{2}C[v(t)]^2$, while that in an inductor is $\frac{1}{2}L[i(t)]^2$. Hence the instantaneous values of the fundamental complete set of variables fixes the instantaneous energy stored in the fundamental set of elements. But the instantaneous values of all the other network variables are completely determined by those of the fundamental complete set, and so the instantaneous energy stored in the whole network is also so fixed. Hence the fundamental set of elements forms a set of independent points of energy storage.

(3.4) Other Complete Sets

It may be asked what other sets of σ network variables form complete sets of dynamically-independent variables besides the fundamental complete sets.

That such other complete sets can exist is shown by the following trivial example. Consider the network of a resistor and capacitor connected in parallel:

$$\left.\begin{aligned} B_L &= 0 \\ N &= 2 \\ S &= 1 \\ S_C &= 1 \\ S_{CR} &= 1 \end{aligned}\right\} \quad \text{Hence } \sigma = 1$$

There is only one fundamental dynamically-independent variable, and that is the capacitor voltage. However, it is obvious that either the voltage across or the current through the resistor may be taken as a dynamically-independent variable instead. Neither of these variables is a fundamental variable.

Let us consider the general case. Denote the set of $2B$ network variables by the $2B \times 1$ vector $\boldsymbol{z}$; denote a fundamental set of independent variables by the $\sigma \times 1$ vector $\boldsymbol{y}$, and the other $(2B - \sigma)$ variables by the $(2B - \sigma) \times 1$ vector $\boldsymbol{x}$. Assume

$$\boldsymbol{z} = \begin{bmatrix} \boldsymbol{x} \\ \boldsymbol{y} \end{bmatrix} \quad . \quad . \quad . \quad . \quad . \quad . \quad . \quad (27)$$

Let us assume that the algebraic relation between $\boldsymbol{x}$ and $\boldsymbol{y}$, which will also involve the various network generators, is written in the form

$$\boldsymbol{x} = \boldsymbol{M}\boldsymbol{y} + \boldsymbol{g} \quad . \quad . \quad . \quad . \quad . \quad . \quad . \quad (28)$$

where $\boldsymbol{M}$ is a $(2B - \sigma) \times \sigma$ matrix and $\boldsymbol{g}$ is the vector involving the network generators. Eqn. (28) may also be written as

$$\boldsymbol{z} = \begin{bmatrix} \boldsymbol{M} \\ \mathbf{1}_\sigma \end{bmatrix} \boldsymbol{y} + \boldsymbol{g} \quad . \quad . \quad . \quad . \quad . \quad . \quad (29)$$

where an obvious slight modification in the definition of $\boldsymbol{g}$ is required. Let us put

$$\begin{bmatrix} \boldsymbol{M} \\ \mathbf{1}_\sigma \end{bmatrix} \equiv \boldsymbol{N} \quad . \quad . \quad . \quad . \quad . \quad . \quad . \quad (30)$$

Then eqn. (29) becomes

$$\boldsymbol{z} = \boldsymbol{N}\boldsymbol{y} + \boldsymbol{g} \quad . \quad . \quad . \quad . \quad . \quad . \quad . \quad (31)$$

and $\boldsymbol{N}$ is obviously of rank σ from eqn. (30).

We now show the following theorem:

Theorem 4.—A set of σ network variables forms a complete

set of dynamically-independent variables if and only if the corresponding set of σ rows from the matrix N of eqn. (31) defines a non-singular $\sigma \times \sigma$ matrix.

Proof.—Sufficiency: Denote the $\sigma \times \sigma$ non-singular sub-matrix of N by W, and the corresponding set of σ variables by w. Then from eqn. (31), if we write h for that part of g corresponding to w, we obtain

$$w = Wy + h \quad . \quad . \quad . \quad . \quad . \quad . \quad . \quad (32)$$

i.e.

$$y = W^{-1}w + W^{-1}h \quad . \quad . \quad . \quad . \quad . \quad (33)$$

Hence the σ variables w may take arbitrary instantaneous values, and so they form a complete set of dynamically-independent variables.

Necessity: Denote the complete set of dynamically-independent variables by the $\sigma \times 1$ vector w, and the corresponding sub-matrix of N by W. Again from eqn. (31)

$$w = Wy + h \quad . \quad . \quad . \quad . \quad . \quad . \quad . \quad (34)$$

Since w forms a complete set of dynamically-independent variables, eqn. (34) must have a solution for y for *any* w. Hence the columns of N must be linearly independent, and so W is non-singular. Hence the theorem.

Example of Fig. 1.—Let us choose v_4 and i_3 as our fundamental complete set (cf. Section 3.2).

Then

$$y = \begin{bmatrix} i_3 \\ v_4 \end{bmatrix}$$

$$x = \begin{bmatrix} i_1 \\ i_2 \\ i_4 \\ i_5 \\ i_6 \\ v_1 \\ v_2 \\ v_3 \\ v_5 \\ v_6 \end{bmatrix} \text{ and } z = \begin{bmatrix} i_1 \\ i_2 \\ i_4 \\ i_5 \\ i_6 \\ v_1 \\ v_2 \\ v_3 \\ v_5 \\ v_6 \\ i_3 \\ v_4 \end{bmatrix}$$

From Appendix 6.2, eqn. (94′), we have

$$N = \begin{bmatrix} 0 & 0 \\ -R_5/(R_2+R_5) & 0 \\ 0 & 0 \\ -R_2/(R_2+R_5) & 0 \\ -1 & 0 \\ 0 & 1 \\ -R_2R_5/(R_2+R_5) & 0 \\ -L_3R_2R_5/(R_2+R_5)(L_3+L_6) & 0 \\ -R_2R_5/(R_2+R_5) & 0 \\ L_6R_2R_5/(R_2+R_5)(L_3+L_6) & 0 \\ 1 & 0 \\ 0 & 1 \end{bmatrix}$$

Hence, by Theorem 4, one variable of the complete set must be either v_1 or v_4 (but not both), and the other can be any other voltage or any current except i_1 and i_4.

(4) ACKNOWLEDGMENTS

The author is indebted to The General Electric Company Limited for the award of a G.E.C. Scholarship and for permission to publish the paper; also to Dr. K. F. Sander and Mr. A. T. Fuller, both of the Department of Engineering, University of Cambridge, for valuable discussions.

(5) REFERENCES

(1) AITKEN, A. C.: 'Determinants and Matrices' (Oliver and Boyd, 2nd Edition, 1942).

(2) BASHKOW, T. R.: 'The A Matrix, New Network Description', *Transactions of the Institute of Radio Engineers on Circuit Theory*, 1957, **CT-4**, p. 117.

(3) BRYANT, P. R.: 'A Topological Investigation of Network Determinants', *Proceedings I.E.E.*, Monograph No. 312 R, September, 1958 (**106** C, p. 16).

(4) FRAZER, R. A., DUNCAN, N. J., and COLLAR, A. R.: 'Elementary Matrices' (Cambridge University Press, 1938).

(5) GUILLEMIN, E. A.: 'Communication Networks', Vol. I (Wiley, 1931).

(6) GUILLEMIN, E. A.: 'Synthesis of Passive Networks' (Wiley, 1958).

(7) INSTITUTE OF RADIO ENGINEERS: 'Definitions of Terms in Network Topology', *Proceedings of the Institute of Radio Engineers*, 1951, **39**, p. 27.

(8) LANCZOS, C.: 'The Variational Principles of Mechanics', Chapter 1 (University of Toronto Press, 1949).

(9) MAYEDA, W., and SESHU, S.: 'Topological Formulas for Network Functions', *University of Illinois Engineering Experiment Station Bulletin No. 446*, 1957.

(10) REED, M. B., and SESHU, S.: 'On Topology and Network Theory' (Proceedings of the Symposium on Circuit Analysis, University of Illinois, 1955).

(11) REED, M. B., and SESHU, S.: 'On Cut Sets of Electrical Networks' (presented at the Symposium on Circuit Theory, E. Lansing, Michigan, December, 1956).

(12) REZA, F. M.: 'Order of Complexity and Minimal Structures in Network Analysis' (Proceedings of the Symposium on Circuit Analysis, University of Illinois, 1955).

(13) TRENT, H. M.: 'A Note on the Enumeration and Listing of all Possible Trees of a Connected Linear Graph', *Proceedings of the National Academy of Sciences, U.S.A.*, 1954, **40**(B), p. 1004.

(14) WHITTAKER, E. T.: 'A Treatise on the Analytical Dynamics of Particles and Rigid Bodies', Chapter 2 (Cambridge University Press, 4th Edition, 1937).

(6) APPENDICES

(6.1) The Expansion of det $H(\lambda)$

In this Appendix the relationship between det $H(\lambda)$ and det $P(\lambda)$ given in eqn. (11) of Section 2.4 is obtained. The notation and terminology is as in Section 2. $\mathcal{N}$ is assumed to be connected throughout Section 6.1. We need the following lemmas and definitions. Lemmas 2 and 4 are proved in Reference 10; Lemmas 3 and 5 in Reference 9.

Lemma 2.[10]—An $(N-1)$-minor of A is non-singular if, and only if, the $(N-1)$ columns forming that minor correspond to a set of branches of $\mathcal{N}$ forming a tree.

Lemma 3.[9]—A non-singular $(N-1)$-minor of A has value $+1$ or -1.

Lemma 4.[10]—An M-minor of B is non-singular if, and only if, the M columns forming that minor correspond to a set of chords of a tree of $\mathcal{N}$.

Lemma 5.[9]—If B is a *chord*-loop matrix, a non-singular M-minor of B has value $+1$ or -1.

Definition 4.—We shall say that a non-zero $(N-1)$-minor of A and a non-zero M-minor of B *correspond* if, and only if, the chords defining the minor of B are chords of the tree defining the minor of A.

Definition 5.—We call the sign of the product of two corresponding minors of A and B, which is either $+1$ or -1, the *tree-chord sign.*

Lemma 6.—The tree-chord signs of $\mathcal{N}$ are such that the terms in the Laplace expansion of det $\begin{bmatrix} A \\ B \end{bmatrix}$ are either all positive or all negative.

Proof.—Define the two $(B \times B)$ matrices S and T as follows:

$$S \equiv \begin{bmatrix} A \\ [BB']^{-1}B \end{bmatrix} \quad . \quad . \quad . \quad . \quad . \quad . \quad (37)$$

$$T \equiv [A'[AA']^{-1}; B'] \quad . \quad . \quad . \quad . \quad . \quad (38)$$

Consider the product

$$\boldsymbol{ST} = \begin{bmatrix} (\boldsymbol{AA'})(\boldsymbol{AA'})^{-1}, & \boldsymbol{AB'} \\ (\boldsymbol{BB'})^{-1}\boldsymbol{BA'}(\boldsymbol{AA'})^{-1}, & (\boldsymbol{BB'})^{-1}(\boldsymbol{BB'}) \end{bmatrix} \quad . \quad . \quad (39)$$

$$= \begin{bmatrix} \mathbf{1}_{N-1} & \mathbf{0} \\ \mathbf{0} & \mathbf{1}_M \end{bmatrix}, \text{ (since}^{10}\ \boldsymbol{AB'} = \mathbf{0}) \quad . \quad . \quad . \quad . \quad (40)$$

$$= \mathbf{1}_B \quad . \quad . \quad . \quad . \quad . \quad . \quad . \quad . \quad . \quad . \quad . \quad (41)$$

Hence $$(\det \boldsymbol{S})(\det \boldsymbol{T}) = 1 \quad . \quad . \quad . \quad . \quad . \quad . \quad (42)$$

Now $$\det \boldsymbol{S} = \det (\boldsymbol{BB'})^{-1} \det \begin{bmatrix} \boldsymbol{A} \\ \boldsymbol{B} \end{bmatrix} \quad . \quad . \quad . \quad . \quad (43)$$

and $$\det \boldsymbol{T} = \det (\boldsymbol{AA'})^{-1} \det \begin{bmatrix} \boldsymbol{A} \\ \boldsymbol{B} \end{bmatrix} \quad . \quad . \quad . \quad . \quad (44)$$

Further[13] $$\det (\boldsymbol{BB'}) = \det (\boldsymbol{AA'}) = \text{number of trees in } \mathscr{N}$$
$$= T \text{ (say)} \quad . \quad . \quad . \quad . \quad . \quad . \quad . \quad . \quad . \quad (45)$$

Hence, from eqns. (43), (44) and (45),

$$(\det \boldsymbol{S})(\det \boldsymbol{T}) = \frac{1}{T^2}\left\{ \det \begin{bmatrix} \boldsymbol{A} \\ \boldsymbol{B} \end{bmatrix} \right\}^2$$
$$= 1 \text{ from eqn. (42)} \quad . \quad . \quad . \quad (46)$$

Hence $$\det \begin{bmatrix} \boldsymbol{A} \\ \boldsymbol{B} \end{bmatrix} = \pm T \quad . \quad . \quad . \quad . \quad . \quad . \quad (47)$$

Consideration of a Laplace expansion[1] of $\det \begin{bmatrix} \boldsymbol{A} \\ \boldsymbol{B} \end{bmatrix}$ by the first $(N-1)$ rows, and use of Lemmas 2, 3, 4 and 5, shows that eqn. (47) can be true if, and only if, all the terms in that expansion are of the same sign, i.e. either all positive, giving $+T$ in eqn. (47), or all negative, giving $-T$ in eqn. (47). Hence the lemma is established.

We are now in a position to expand $\det \boldsymbol{H}(\lambda)$.

Lemma 7.—In the notation of Section 2,

$$\det \boldsymbol{H}(\lambda) = \pm \begin{pmatrix} \text{product of all} \\ \text{inductors} \end{pmatrix} \begin{pmatrix} \text{product of all} \\ \text{resistors} \end{pmatrix} \lambda^{B_L} \det \boldsymbol{P}(\lambda)$$
$$. \quad . \quad . \quad . \quad (48)$$

where $\boldsymbol{P}(\lambda)$ is the well-known nodal-admittance matrix of $\mathscr{N}$.

Proof.—Expand the determinant by a Laplace expansion of the first B rows.[1] From Lemmas 2 and 4, a set of B columns from these first B rows will form a non-zero minor if, and only if, $(N-1)$ columns come from $\begin{bmatrix} \mathbf{0} \\ \boldsymbol{A} \end{bmatrix}$ and correspond to a tree, while the other M columns come from $\begin{bmatrix} \boldsymbol{B} \\ \mathbf{0} \end{bmatrix}$ and correspond to a set of chords.

Consideration of the complementary set of columns from the last B rows, remembering that $\boldsymbol{Z}_{LR}(\lambda)$ and $\boldsymbol{Y}_C(\lambda)$ are both $B \times B$ diagonal, shows that we will get a non-zero complementary minor from these last B rows if, and only if, the minors of $\boldsymbol{A}$ and $\boldsymbol{B}$ correspond (Definition 4). We then obtain as a single term in the Laplace expansion:

$$\pm \begin{pmatrix} \text{capacitor tree-branch} \\ \text{admittance product} \end{pmatrix} \times \begin{pmatrix} \text{inductor chord} \\ \text{impedance product} \end{pmatrix}$$
$$\times \begin{pmatrix} \text{resistor chord} \\ \text{impedance product} \end{pmatrix} \quad . \quad (49)$$

From Lemma 6 we see that when we obtain all the terms in the Laplace expansion, they will all be of the same sign, and so we obtain

$$\det \boldsymbol{H}(\lambda) = \pm \sum_{\substack{\text{(all} \\ \text{trees)}}} \begin{pmatrix} \text{capacitor tree-branch} \\ \text{admittance product} \end{pmatrix} \begin{pmatrix} \text{inductor chord} \\ \text{impedance product} \end{pmatrix}$$
$$\times \begin{pmatrix} \text{resistor chord} \\ \text{impedance product} \end{pmatrix} \quad . \quad (50)$$

Now

$$\begin{pmatrix} \text{inductor chord} \\ \text{impedance product} \end{pmatrix} = \begin{pmatrix} \text{product of} \\ \text{all inductors} \end{pmatrix} \lambda^{B_L} \begin{pmatrix} \text{inductor tree-branch} \\ \text{admittance product} \end{pmatrix}$$
$$. \quad . \quad . \quad . \quad (51)$$

and

$$\begin{pmatrix} \text{resistor chord} \\ \text{impedance product} \end{pmatrix} = \begin{pmatrix} \text{product of} \\ \text{all resistors} \end{pmatrix} \begin{pmatrix} \text{resistor tree-branch} \\ \text{admittance product} \end{pmatrix}$$
$$. \quad . \quad . \quad . \quad (52)$$

Hence we obtain

$\det \boldsymbol{H}(\lambda) =$

$$\pm \begin{pmatrix} \text{product of} \\ \text{all inductors} \end{pmatrix} \begin{pmatrix} \text{product of} \\ \text{all resistors} \end{pmatrix} \lambda^{B_L} \sum_{\substack{\text{(all} \\ \text{trees)}}} \begin{pmatrix} \text{tree-branch} \\ \text{admittance product} \end{pmatrix}$$
$$. \quad . \quad . \quad (53)$$

But[3,9] $$\sum_{\substack{\text{(all} \\ \text{trees)}}} \begin{pmatrix} \text{tree-branch} \\ \text{admittance product} \end{pmatrix} = \det \boldsymbol{P}(\lambda) \quad . \quad . \quad . \quad (54)$$

where $\boldsymbol{P}(\lambda)$ is the nodal-admittance matrix. Hence the lemma is established.

(6.2) The Elimination Process

As mentioned in Section 3.2, our elimination process involves expressing the branch equations in a special form by the use of a particular tree construction. This construction is as follows, where we have assumed that $\mathscr{N}$ is connected.

First choose any forest† $\mathscr{F}_C$ in $\mathscr{N}_C$. $\mathscr{F}_C$ will contain $(N-S_C)$ capacitors.[3] If $\mathscr{N}_C$ is connected, $\mathscr{F}_C$ will be a tree of $\mathscr{N}$, and will be the tree we require. If $\mathscr{N}_C$ is not connected, we consider $\mathscr{N}_{CR}$. If the connectivity of $\mathscr{N}_{CR}$ is the same as that of $\mathscr{N}_C$, then $\mathscr{F}_C$ is also a forest of $\mathscr{N}_{CR}$. If not we may add resistors to $\mathscr{F}_C$ to form a forest $\mathscr{F}_{CR}$ in $\mathscr{N}_{CR}$. $\mathscr{F}_{CR}$ will contain $(N-S_{CR})$ capacitors and resistors. If $\mathscr{N}_{CR}$ is connected, then $\mathscr{F}_{CR}$ will be a tree of $\mathscr{N}$ and will be the tree we require. If $\mathscr{N}_{CR}$ is not connected, then since $\mathscr{N}$ is connected, we may add inductors to $\mathscr{F}_{CR}$ to form a tree $\mathscr{T}$ in $\mathscr{N}$; $\mathscr{T}$ will be the tree of $\mathscr{N}$ which we require.

It should be noted that the inductive branches of our tree $\mathscr{T}$ are in fact a tree in $\mathscr{N}_L^*$.

We now number our network branches as follows. We number the capacitive chords first, from 1 to M_C. Next we number the resistive chords, from (M_C+1) to M_{CR}, and then the inductive chords from $(M_{CR}+1)$ to M. Turning now to the tree, we number the capacitive tree branches from $(M+1)$ to $(M+N-S_C)$, the resistive tree branches from $(M+N-S_C+1)$ to $(M+N-S_{CR})$ and finally the inductive tree branches we number from $(M+N-S_{CR}+1)$ to $B \equiv (M+N-1)$.

In general the tree $\mathscr{T}$ obtained by the construction described above is not unique, and so neither is the branch ordering.

Fig. 8.—The tree $\mathscr{T}$ of $\mathscr{N}$.

However, any one of the possible trees and the consequent branch numbering will do.

Example of Fig. 1.—As the tree $\mathscr{T}$ we shall use that shown in Fig. 8. In order that no confusion should arise at this stage between two different schemes of branch numbering, the 'arbitrary' branch numbering previously chosen in Section 2.2 was made to coincide with that which we obtain from this tree. Our numbering is thus still as shown in Fig. 2. It should be remembered, however, that if a change did occur, then the matrices $\boldsymbol{A}$, $\boldsymbol{B}$, $\boldsymbol{Z}_{LR}(D)$ and $\boldsymbol{Y}_C(D)$ would also have to be changed.

† Defined in Section 2.2.

Consider the branch numbering. It will be seen that the branches have been classified into six groups; we number these groups $\alpha, \beta, \gamma, \delta, \epsilon, \zeta$ as follows:†

(α) capacitive chords;
(β) resistive chords;
(γ) inductive chords;
(δ) capacitive tree branches;
(ϵ) resistive tree branches;
(ζ) inductive tree branches.

We use this branch classification to partition our various network vectors and matrices into sub-vectors and sub-matrices. Thus we put

$$\boldsymbol{i} = \begin{bmatrix} \boldsymbol{i}_\alpha \\ \boldsymbol{i}_\beta \\ \boldsymbol{i}_\gamma \\ \boldsymbol{i}_\delta \\ \boldsymbol{i}_\epsilon \\ \boldsymbol{i}_\zeta \end{bmatrix}; \quad \boldsymbol{v} = \begin{bmatrix} \boldsymbol{v}_\alpha \\ \boldsymbol{v}_\beta \\ \boldsymbol{v}_\gamma \\ \boldsymbol{v}_\delta \\ \boldsymbol{v}_\epsilon \\ \boldsymbol{v}_\zeta \end{bmatrix} \quad . \quad . \quad . \quad . \quad . \quad . \quad (55)$$

The reduced incidence matrix $\boldsymbol{A}$, and the chord-loop matrix $\boldsymbol{B}$ we first partition according to chords and tree branches as follows:

$$\boldsymbol{A} = [\boldsymbol{X}, \boldsymbol{K}]; \quad \boldsymbol{B} = [\mathbf{1}_M, \boldsymbol{F}] \quad . \quad . \quad . \quad . \quad (56)$$

Note that the relation[10]

$$\boldsymbol{A}\boldsymbol{B}' = \mathbf{0} \quad . \quad . \quad . \quad . \quad . \quad . \quad . \quad (57)$$

gives

$$-\boldsymbol{F}' = \boldsymbol{K}^{-1}\boldsymbol{X} \quad . \quad . \quad . \quad . \quad . \quad . \quad (58)$$

$\boldsymbol{B}$ may be further partitioned as follows: the columns, corresponding to the branches, into the six groups α to ζ, and the rows, corresponding to the chord loops, and so to the chords, into the three groups α, β and γ. If we denote the corresponding unit matrices by the obvious notation of $\mathbf{1}_{\alpha\alpha}$, etc., and the sub-matrices of $\boldsymbol{F}$ similarly, we get

$$\boldsymbol{B} = \begin{bmatrix} \mathbf{1}_{\alpha\alpha} & \mathbf{0} & \mathbf{0} & \boldsymbol{F}_{\alpha\delta} & \boldsymbol{F}_{\alpha\epsilon} & \boldsymbol{F}_{\alpha\zeta} \\ \mathbf{0} & \mathbf{1}_{\beta\beta} & \mathbf{0} & \boldsymbol{F}_{\beta\delta} & \boldsymbol{F}_{\beta\epsilon} & \boldsymbol{F}_{\beta\zeta} \\ \mathbf{0} & \mathbf{0} & \mathbf{1}_{\gamma\gamma} & \boldsymbol{F}_{\gamma\delta} & \boldsymbol{F}_{\gamma\epsilon} & \boldsymbol{F}_{\gamma\zeta} \end{bmatrix} \quad . \quad . \quad . \quad (59)$$

The matrices $\boldsymbol{Y}_C(D)$ and $\boldsymbol{Z}_{LR}(D)$ are also partitioned; thus we put

$$\boldsymbol{Y}_C(D) = \begin{bmatrix} D\boldsymbol{C}_{\alpha\alpha} & \mathbf{0} & \mathbf{0} & \mathbf{0} & \mathbf{0} & \mathbf{0} \\ \mathbf{0} & \mathbf{1}_{\beta\beta} & \mathbf{0} & \mathbf{0} & \mathbf{0} & \mathbf{0} \\ \mathbf{0} & \mathbf{0} & \mathbf{1}_{\gamma\gamma} & \mathbf{0} & \mathbf{0} & \mathbf{0} \\ \mathbf{0} & \mathbf{0} & \mathbf{0} & D\boldsymbol{C}_{\delta\delta} & \mathbf{0} & \mathbf{0} \\ \mathbf{0} & \mathbf{0} & \mathbf{0} & \mathbf{0} & \mathbf{1}_{\epsilon\epsilon} & \mathbf{0} \\ \mathbf{0} & \mathbf{0} & \mathbf{0} & \mathbf{0} & \mathbf{0} & \mathbf{1}_{\zeta\zeta} \end{bmatrix} \quad . \quad (60)$$

and

$$\boldsymbol{Z}_{LR}(D) = \begin{bmatrix} \mathbf{1}_{\alpha\alpha} & \mathbf{0} & \mathbf{0} & \mathbf{0} & \mathbf{0} & \mathbf{0} \\ \mathbf{0} & \boldsymbol{R}_{\beta\beta} & \mathbf{0} & \mathbf{0} & \mathbf{0} & \mathbf{0} \\ \mathbf{0} & \mathbf{0} & D\boldsymbol{L}_{\gamma\gamma} & \mathbf{0} & \mathbf{0} & \mathbf{0} \\ \mathbf{0} & \mathbf{0} & \mathbf{0} & \mathbf{1}_{\delta\delta} & \mathbf{0} & \mathbf{0} \\ \mathbf{0} & \mathbf{0} & \mathbf{0} & \mathbf{0} & \boldsymbol{R}_{\epsilon\epsilon} & \mathbf{0} \\ \mathbf{0} & \mathbf{0} & \mathbf{0} & \mathbf{0} & \mathbf{0} & D\boldsymbol{L}_{\zeta\zeta} \end{bmatrix} \quad . \quad (61)$$

Example of Fig. 1.—Our various sub-vectors and sub-matrices become

$$\left.\begin{array}{l} \boldsymbol{i}_\alpha = [i_1] \\ \boldsymbol{i}_\beta = [i_2] \\ \quad . \\ \quad . \\ \quad . \\ \boldsymbol{i}_\zeta = [i_6] \\ \boldsymbol{v}_\alpha = [v_1] \\ \boldsymbol{v}_\beta = [v_2] \\ \quad . \\ \quad . \\ \quad . \\ \boldsymbol{v}_\zeta = [v_6] \end{array}\right\} \quad . \quad . \quad . \quad . \quad . \quad . \quad . \quad . \quad (55')$$

† It may, of course, happen that in a particular case, one or more of these groups is empty, i.e. non-existent.

$$\boldsymbol{X} = \begin{bmatrix} 1 & -1 & -1 \\ 0 & 1 & 0 \\ 0 & 0 & 1 \end{bmatrix}$$

$$\boldsymbol{K} = \begin{bmatrix} 1 & -1 & 0 \\ 0 & 1 & -1 \\ 0 & 0 & 1 \end{bmatrix}$$

$$\boldsymbol{F} = \left[\begin{array}{c|c|c} -1 & 0 & 0 \\ \hline 0 & -1 & 0 \\ \hline 0 & -1 & -1 \end{array}\right]$$

where the partitioning shows the sub-matrices of $\boldsymbol{F}$, as in eqn. (59). Similarly, using partitioning we get

$$\boldsymbol{Y}_C(D) = \left[\begin{array}{c|c|c|c|c|c} C_1D & . & . & . & . & . \\ \hline . & 1 & . & . & . & . \\ \hline . & . & 1 & . & . & . \\ \hline . & . & . & C_4D & . & . \\ \hline . & . & . & . & 1 & . \\ \hline . & . & . & . & . & 1 \end{array}\right] \quad . \quad . \quad (60')$$

$$\boldsymbol{Z}_{LR}(D) = \left[\begin{array}{c|c|c|c|c|c} 1 & . & . & . & . & . \\ \hline . & R_2 & . & . & . & . \\ \hline . & . & L_3D & . & . & . \\ \hline . & . & . & 1 & . & . \\ \hline . & . & . & . & R_5 & . \\ \hline . & . & . & . & . & L_6D \end{array}\right] \quad . \quad . \quad (61')$$

An important lemma concerning $\boldsymbol{B}$ follows from the way in which our tree was constructed and our branches were numbered:

Lemma 8.—Let $\boldsymbol{B}$ be a chord-loop matrix corresponding to a tree constructed as described. Then if $\boldsymbol{B}$ is partitioned as in eqn. (59), we shall have

$$\left.\begin{array}{l} \boldsymbol{F}_{\alpha\epsilon} = \mathbf{0} \\ \boldsymbol{F}_{\alpha\zeta} = \mathbf{0} \\ \boldsymbol{F}_{\beta\zeta} = \mathbf{0} \end{array}\right\} \quad . \quad . \quad . \quad . \quad . \quad . \quad . \quad (62)$$

Proof.—By the tree construction, the loops defined by the capacitive chords must be purely capacitive. Hence

$$\boldsymbol{F}_{\alpha\epsilon} = \mathbf{0}$$

and

$$\boldsymbol{F}_{\alpha\zeta} = \mathbf{0}$$

Further, the loops defined by the resistive chords can contain no inductors. Hence

$$\boldsymbol{F}_{\beta\zeta} = \mathbf{0}$$

and so the lemma follows.

Before carrying on with the elimination process, we shall state and prove a lemma concerning our tree construction.

Lemma 9.—If a tree $\mathscr{T}$ is constructed as described above,

(*a*) the capacitive chords, i.e. the branches α, define a complete set of independent capacitor-only loops;

(*b*) the inductive tree-branches, i.e. the branches ζ, define a complete set of independent inductor-only cut-sets.†

Proof.—(*a*) Self-evident.

(*b*) It has been pointed out that the inductive tree branches form a tree of $\mathscr{N}_L^*$. Hence they define a complete set of independent cut-sets in $\mathscr{N}_L^*$.[11] Thus, by Lemma 11 (Section 6.3) they define a complete set of independent inductor-only cut-sets in $\mathscr{N}$.

† A cut-set is defined in Section 2.7.

*

We may now carry out our elimination process, which consists of showing that

$$i_\alpha, i_\beta, i_\delta, i_\epsilon, i_\zeta, v_\alpha, v_\beta, v_\gamma, v_\epsilon \text{ and } v_\zeta$$

can all be expressed algebraically in terms of i_γ and v_δ, together with the various network generators and their differentials.

We recall the network branch equations (10):

$$\left[\begin{array}{c|c} 0 & B \\ A & 0 \\ \hline Z_{LR}(D) & -Y_C(D) \end{array}\right]\left[\begin{array}{c} i(t) \\ \hline v(t) \end{array}\right] = \left[\begin{array}{c} E(t) \\ J(t) \\ \hline 0 \end{array}\right] \quad . \quad (63)$$

Our elimination takes place in three stages:

(*a*) Using Kirchhoff's laws.
(*b*) Using Ohm's law applied to resistive branches.
(*c*) Using capacitor-only loops and inductor-only cut-sets.

(*a*) *Elimination by Kirchhoff's Laws.*—From eqn. (63) the Kirchhoff equations are

$$Bv = E \quad . \quad . \quad . \quad . \quad . \quad . \quad . \quad (64)$$

$$Ai = J \quad . \quad . \quad . \quad . \quad . \quad . \quad . \quad (65)$$

Using eqns. (55) and (56), and conformably partitioning E, we get from eqn. (64)

$$\begin{bmatrix} v_\alpha \\ v_\beta \\ v_\gamma \end{bmatrix} = -F\begin{bmatrix} v_\delta \\ v_\epsilon \\ v_\zeta \end{bmatrix} + \begin{bmatrix} E_\alpha \\ E_\beta \\ E_\gamma \end{bmatrix} \quad . \quad . \quad . \quad . \quad (66)$$

Hence, using eqns. (59) and (62),

$$\begin{bmatrix} v_\alpha \\ v_\beta \\ v_\gamma \end{bmatrix} = -\begin{bmatrix} F_{\alpha\delta} & 0 & 0 \\ F_{\beta\delta} & F_{\beta\epsilon} & 0 \\ F_{\gamma\delta} & F_{\gamma\epsilon} & F_{\gamma\zeta} \end{bmatrix}\begin{bmatrix} v_\delta \\ v_\epsilon \\ v_\zeta \end{bmatrix} + \begin{bmatrix} E_\alpha \\ E_\beta \\ E_\gamma \end{bmatrix} \quad . \quad . \quad (67)$$

which are the elimination equations obtained from Kirchhoff's voltage law. From Kirchhoff's current law, eqn. (65), we get, using eqns. (55) and (56) and conformably partitioning J:

$$X\begin{bmatrix} i_\alpha \\ i_\beta \\ i_\gamma \end{bmatrix} + K\begin{bmatrix} i_\delta \\ i_\epsilon \\ i_\zeta \end{bmatrix} = \begin{bmatrix} J_\delta \\ J_\epsilon \\ J_\zeta \end{bmatrix} \quad . \quad . \quad . \quad . \quad . \quad (68)$$

From Lemma 2, K is non-singular. Hence

$$\begin{bmatrix} i_\delta \\ i_\epsilon \\ i_\zeta \end{bmatrix} = -K^{-1}X\begin{bmatrix} i_\alpha \\ i_\beta \\ i_\gamma \end{bmatrix} + K^{-1}\begin{bmatrix} J_\delta \\ J_\epsilon \\ J_\zeta \end{bmatrix} \quad . \quad . \quad . \quad (69)$$

Putting $K^{-1}J \equiv T$, which we conformably partition, and using eqn. (58), we obtain

$$\begin{bmatrix} i_\delta \\ i_\epsilon \\ i_\zeta \end{bmatrix} = F'\begin{bmatrix} i_\alpha \\ i_\beta \\ i_\gamma \end{bmatrix} + \begin{bmatrix} T_\delta \\ T_\epsilon \\ T_\zeta \end{bmatrix} \quad . \quad . \quad . \quad . \quad (70)$$

Hence, using eqns. (59) and (62),

$$\begin{bmatrix} i_\delta \\ i_\epsilon \\ i_\zeta \end{bmatrix} = \begin{bmatrix} F'_{\alpha\delta} & F'_{\beta\delta} & F'_{\gamma\delta} \\ 0 & F'_{\beta\epsilon} & F'_{\gamma\epsilon} \\ 0 & 0 & F'_{\gamma\zeta} \end{bmatrix}\begin{bmatrix} i_\alpha \\ i_\beta \\ i_\gamma \end{bmatrix} + \begin{bmatrix} T_\delta \\ T_\epsilon \\ T_\zeta \end{bmatrix} \quad . \quad . \quad (71)$$

which are the elimination equations obtained from Kirchhoff's current law.

(*b*) *Elimination from Ohm's Law applied to Resistors.*—From eqn. (63), using eqns. (60) and (61), the equations giving Ohm's law applied to the resistors are

$$v_\beta = R_{\beta\beta}i_\beta \quad . \quad . \quad . \quad . \quad . \quad . \quad . \quad (72)$$

$$v_\epsilon = R_{\epsilon\epsilon}i_\epsilon \quad . \quad . \quad . \quad . \quad . \quad . \quad . \quad (73)$$

Using eqn. (67), we get from eqn. (72)

$$i_\beta = -R_{\beta\beta}^{-1}[F_{\beta\delta}v_\delta + F_{\beta\epsilon}v_\epsilon - E_\beta] \quad . \quad . \quad . \quad (74)$$

i.e.

$$i_\beta + R_{\beta\beta}^{-1}F_{\beta\epsilon}v_\epsilon = -R_{\beta\beta}^{-1}F_{\beta\delta}v_\delta + R_{\beta\beta}^{-1}E_\beta \quad . \quad . \quad (75)$$

Similarly, using eqn. (71), we obtain from eqn. (73)

$$-R_{\epsilon\epsilon}F'_{\beta\epsilon}i_\beta + v_\epsilon = +R_{\epsilon\epsilon}F'_{\gamma\epsilon}i_\gamma + R_{\epsilon\epsilon}T_\epsilon \quad . \quad . \quad (76)$$

Combining eqns. (75) and (76) into one equation:

$$\begin{bmatrix} 1_{\beta\beta}, & R_{\beta\beta}^{-1}F_{\beta\epsilon} \\ -R_{\epsilon\epsilon}F'_{\beta\epsilon}, & 1_{\epsilon\epsilon} \end{bmatrix}\begin{bmatrix} i_\beta \\ v_\epsilon \end{bmatrix} = \begin{bmatrix} -R_{\beta\beta}^{-1}F_{\beta\delta}, & 0 \\ 0, & +R_{\epsilon\epsilon}F'_{\gamma\epsilon} \end{bmatrix}\begin{bmatrix} v_\delta \\ i_\gamma \end{bmatrix} + \begin{bmatrix} R_{\beta\beta}^{-1}E_\beta \\ R_{\epsilon\epsilon}T_\epsilon \end{bmatrix} \quad . \quad (77)$$

In Lemma 17, Appendix 6.4, we show that the matrix

$$\begin{bmatrix} 1_{\beta\beta}, & R_{\beta\beta}^{-1}F_{\beta\epsilon} \\ -R_{\epsilon\epsilon}F'_{\beta\epsilon}, & 1_{\epsilon\epsilon} \end{bmatrix}$$

is non-singular, and that its inverse is

$$\begin{bmatrix} [1_{\beta\beta} + R_{\beta\beta}^{-1}F_{\beta\epsilon}R_{\epsilon\epsilon}F'_{\beta\epsilon}]^{-1}, & -R_{\beta\beta}^{-1}F_{\beta\epsilon}[1_{\epsilon\epsilon} + R_{\epsilon\epsilon}F'_{\beta\epsilon}R_{\beta\beta}^{-1}F_{\beta\epsilon}]^{-1} \\ R_{\epsilon\epsilon}F'_{\beta\epsilon}[1_{\beta\beta} + R_{\beta\beta}^{-1}F_{\beta\epsilon}R_{\epsilon\epsilon}F'_{\beta\epsilon}]^{-1}, & [1_{\epsilon\epsilon} + R_{\epsilon\epsilon}F_{\beta\epsilon}R_{\beta\beta}^{-1}F_{\beta\epsilon}]^{-1} \end{bmatrix} \quad . \quad . \quad . \quad . \quad (78)$$

Hence eqn. (77) may be solved for i_β and v_ϵ in terms of v_δ and i_γ (and E_β and T_ϵ). Further this solution may be substituted back into eqns. (67) and (71) to obtain

$$\left.\begin{array}{ll} v_\alpha \text{ in terms of } v_\delta & (\text{and } E_\alpha) \\ v_\beta \text{ in terms of } v_\delta \text{ and } i_\gamma & (\text{and } E_\beta \text{ and } T_\epsilon) \\ v_\gamma \text{ in terms of } v_\delta, v_\zeta \text{ and } i_\gamma & (\text{and } E_\beta, E_\gamma \text{ and } T_\epsilon) \\ v_\epsilon \text{ in terms of } v_\delta \text{ and } i_\gamma & (\text{and } E_\beta \text{ and } T_\epsilon) \\ i_\beta \text{ in terms of } v_\delta \text{ and } i_\gamma & (\text{and } E_\beta \text{ and } T_\epsilon) \\ i_\delta \text{ in terms of } v_\delta, i_\alpha \text{ and } i_\gamma & (\text{and } E_\beta, T_\delta \text{ and } T_\epsilon) \\ i_\epsilon \text{ in terms of } v_\delta \text{ and } i_\gamma & (\text{and } E_\beta \text{ and } T_\epsilon) \\ i_\zeta \text{ in terms of } i_\gamma & (\text{and } T_\zeta) \end{array}\right\} \quad . \quad (79)$$

(*c*) *Elimination from Capacitor-only Loops and Inductor-only Cut-sets.*—From Lemma 9 and eqns. (67) and (71), we obtain as the equations to be considered:

$$v_\alpha(t) + F_{\alpha\delta}v_\delta(t) = E_\alpha(t) \quad . \quad . \quad . \quad . \quad (80)$$

$$i_\zeta(t) - F'_{\gamma\zeta}i_\gamma(t) = T_\zeta(t) \quad . \quad . \quad . \quad . \quad (81)$$

Differentiate each of these with respect to time, t, using a dot to denote this differentiation:

$$\dot{v}_\alpha(t) + F_{\alpha\delta}\dot{v}_\delta(t) = \dot{E}_\alpha(t) \quad . \quad . \quad . \quad . \quad (82)$$

$$\dot{i}_\zeta(t) - F'_{\gamma\zeta}\dot{i}_\gamma(t) = \dot{T}_\zeta(t) \quad . \quad . \quad . \quad . \quad (83)$$

From eqns. (60), (61) and (63),

$$\left.\begin{array}{l} i_\alpha = C_{\alpha\alpha}\dot{v}_\alpha \\ i_\delta = C_{\delta\delta}\dot{v}_\delta \\ v_\gamma = L_{\gamma\gamma}\dot{i}_\gamma \\ v_\zeta = L_{\zeta\zeta}\dot{i}_\zeta \end{array}\right\} \quad . \quad . \quad . \quad . \quad . \quad . \quad (84)$$

Putting these into eqns. (82) and (83) we obtain

$$i_\alpha = -C_{\alpha\alpha}F_{\alpha\delta}C^{-1}i_\delta + C_{\alpha\alpha}\dot{E}_\alpha \quad . \quad . \quad . \quad (85)$$

$$v_\zeta = L_{\zeta\zeta}F'_{\gamma\zeta}L_{\gamma\gamma}^{-1}v_\gamma + L_{\zeta\zeta}\dot{T}_\zeta \quad . \quad . \quad . \quad . \quad (86)$$

Consider eqn. (85) first. From eqn. (79) we have i_δ in terms of i_α, i_γ and v_δ. Hence, if we are to obtain i_α and i_δ each in terms of v_δ and i_γ, we must solve an equation. The form of the eqn. (79) for i_δ is

$$i_\delta = F'_{\alpha\delta}i_\alpha + [\text{terms in } v_\delta, i_\gamma, E_\beta, T_\delta \text{ and } T_\epsilon] \quad . \quad (87)$$

Hence, from eqn. (85),

$$\boldsymbol{i}_\alpha = -\,\boldsymbol{C}_{\alpha\alpha}\boldsymbol{F}_{\alpha\delta}\boldsymbol{C}_{\delta\delta}^{-1}\boldsymbol{F}'_{\alpha\delta}\dot{\boldsymbol{i}}_\alpha + [\text{terms in } \boldsymbol{v}_\delta, \boldsymbol{i}_\gamma, \boldsymbol{E}_\beta, \boldsymbol{T}_\delta, \boldsymbol{T}_\epsilon \text{ and } \dot{\boldsymbol{E}}_\alpha] \quad . \quad . \quad . \quad . \quad . \quad (88)$$

i.e. $\dot{\boldsymbol{i}}_\alpha[\mathbf{1}_{\alpha\alpha} + \boldsymbol{C}_{\alpha\alpha}\boldsymbol{F}_{\alpha\delta}\boldsymbol{C}_{\delta\delta}^{-1}\boldsymbol{F}'_{\alpha\delta}] = [\text{terms in } \boldsymbol{v}_\delta, \boldsymbol{i}_\gamma, \boldsymbol{E}_\beta, \boldsymbol{T}_\delta, \boldsymbol{T}_\epsilon \text{ and } \dot{\boldsymbol{E}}_\alpha]$ . . . . . (89)

To show that we may solve eqn. (89) for $\boldsymbol{i}_\alpha$ we must show that the matrix

$$[\mathbf{1}_{\alpha\alpha} + \boldsymbol{C}_{\alpha\alpha}\boldsymbol{F}_{\alpha\delta}\boldsymbol{C}_{\delta\delta}^{-1}\boldsymbol{F}'_{\alpha\delta}] \quad . \quad . \quad . \quad . \quad (90)$$

is non-singular.

We have as an identity

$$[\mathbf{1}_{\alpha\alpha} + \boldsymbol{C}_{\alpha\alpha}\boldsymbol{F}_{\alpha\delta}\boldsymbol{C}_{\delta\delta}^{-1}\boldsymbol{F}'_{\alpha\delta}] = \boldsymbol{C}_{\alpha\alpha}[\boldsymbol{F}_{\alpha\delta}, \mathbf{1}_{\alpha\alpha}]\begin{bmatrix}\boldsymbol{C}_{\delta\delta}^{-1} & 0 \\ 0 & \boldsymbol{C}_{\alpha\alpha}^{-1}\end{bmatrix}\begin{bmatrix}\boldsymbol{F}'_{\alpha\delta} \\ \mathbf{1}_{\alpha\alpha}\end{bmatrix} \quad . \quad (91)$$

from which we see that the matrix (90) is non-singular. Hence we may solve eqn. (89) for

$$\dot{\boldsymbol{i}}_\alpha \text{ in terms of } \boldsymbol{v}_\delta, \boldsymbol{i}_\gamma, \boldsymbol{E}_\beta, \boldsymbol{T}_\delta, \boldsymbol{T}_\epsilon \text{ and } \dot{\boldsymbol{E}}_\alpha \quad . \quad . \quad (92)$$

Similarly we may obtain from eqns. (86) and (79)

$$\dot{\boldsymbol{v}}_\zeta \text{ in terms of } \boldsymbol{v}_\delta, \boldsymbol{i}_\gamma, \boldsymbol{E}_\beta, \boldsymbol{E}_\gamma, \boldsymbol{T}_\epsilon \text{ and } \dot{\boldsymbol{T}}_\zeta \quad . \quad . \quad (93)$$

Substituting eqns. (92) and (93) into eqn. (79) we finally obtain

$$\left.\begin{array}{ll}
\boldsymbol{v}_\alpha \text{ in terms of } \boldsymbol{v}_\delta & (\text{and } \boldsymbol{E}_\alpha) \\
\boldsymbol{v}_\beta \text{ in terms of } \boldsymbol{v}_\delta \text{ and } \boldsymbol{i}_\gamma & (\text{and } \boldsymbol{E}_\beta \text{ and } \boldsymbol{T}_\epsilon) \\
\boldsymbol{v}_\gamma \text{ in terms of } \boldsymbol{v}_\delta \text{ and } \boldsymbol{i}_\gamma & (\text{and } \boldsymbol{E}_\beta, \boldsymbol{E}_\gamma, \boldsymbol{T}_\epsilon \text{ and } \dot{\boldsymbol{T}}_\zeta) \\
\boldsymbol{v}_\epsilon \text{ in terms of } \boldsymbol{v}_\delta \text{ and } \boldsymbol{i}_\gamma & (\text{and } \boldsymbol{E}_\beta \text{ and } \boldsymbol{T}_\epsilon) \\
\boldsymbol{v}_\zeta \text{ in terms of } \boldsymbol{v}_\delta \text{ and } \boldsymbol{i}_\gamma & (\text{and } \boldsymbol{E}_\beta, \boldsymbol{E}_\gamma, \boldsymbol{T}_\epsilon \text{ and } \dot{\boldsymbol{T}}_\zeta) \\
\boldsymbol{i}_\alpha \text{ in terms of } \boldsymbol{v}_\delta \text{ and } \boldsymbol{i}_\gamma & (\text{and } \boldsymbol{E}_\beta, \boldsymbol{T}_\delta, \boldsymbol{T}_\epsilon \text{ and } \dot{\boldsymbol{E}}_\alpha) \\
\boldsymbol{i}_\beta \text{ in terms of } \boldsymbol{v}_\delta \text{ and } \boldsymbol{i}_\gamma & (\text{and } \boldsymbol{E}_\beta \text{ and } \boldsymbol{T}_\epsilon) \\
\boldsymbol{i}_\delta \text{ in terms of } \boldsymbol{v}_\delta \text{ and } \boldsymbol{i}_\gamma & (\text{and } \boldsymbol{E}_\beta, \boldsymbol{T}_\delta, \boldsymbol{T}_\epsilon \text{ and } \dot{\boldsymbol{E}}_\alpha) \\
\boldsymbol{i}_\epsilon \text{ in terms of } \boldsymbol{v}_\delta \text{ and } \boldsymbol{i}_\gamma & (\text{and } \boldsymbol{E}_\beta \text{ and } \boldsymbol{T}_\epsilon) \\
\boldsymbol{i}_\zeta \text{ in terms of } \boldsymbol{i}_\gamma & (\text{and } \boldsymbol{T}_\zeta)
\end{array}\right\} \quad . \quad (94)$$

Note the 'mirror symmetry' of these expressions.

From the construction of the tree $\mathscr{T}$, we see that the variables $\boldsymbol{v}_\delta$ and $\boldsymbol{i}_\gamma$ are, respectively, the voltages across the capacitors forming a forest of $\mathscr{N}_C$, and the currents through the inductors forming a set of chords of $\mathscr{N}_L^*$. Now a forest of $\mathscr{N}_C$ will contain $(N_C - S_C)$ capacitors, and since $N_C = N$ (see Reference 3, Lemma 2), we thus have $(N - S_C)$ capacitor voltages. Further, a tree of $\mathscr{N}_L^*$ will contain $(N_L^* - 1)$ inductors, and so a set of chords of $\mathscr{N}_L^*$ will contain $(B_L^* - N_L^* + 1)$ inductors. Now $N_L^* = S_{CR}$ (proved in Reference 3, Lemma 14), and $B_L^* = B_L$; hence we have $(B_L - S_{CR} + 1)$ inductor currents.

If $\mathscr{N}$ is not connected, as we have assumed above, then the considerations of this Section may be applied to each part of $\mathscr{N}$ separately. Provided we modify our definition of a set of chords of $\mathscr{N}_L^*$ (which may no longer be connected) to being the complement of a *forest* rather than of a tree, the results still hold, except that we now obtain $(B_L - S_{CR} + S)$ inductors and inductor currents. We have thus proved Theorem 3 of Section 3.2.

It may be shown that the remaining equations for $\boldsymbol{v}_\delta$ and $\boldsymbol{i}_\gamma$ are a set of σ first-order linear differential equations. Thus, if we write

$$\boldsymbol{y} = \begin{bmatrix}\boldsymbol{i}_\gamma \\ \boldsymbol{v}_\delta\end{bmatrix} \quad . \quad . \quad . \quad . \quad . \quad . \quad . \quad (95)$$

the differential equation for $\boldsymbol{y}$ may be obtained in the form

$$\boldsymbol{u} + \frac{d\boldsymbol{y}}{dt} = \boldsymbol{U}\boldsymbol{y} \quad . \quad . \quad . \quad . \quad . \quad . \quad (96)$$

where $\boldsymbol{u}$ denotes the 'forcing function vector', involving the network generators and their differentials, and $\boldsymbol{U}$ is a $\sigma \times \sigma$ matrix in terms of the various network matrices $\boldsymbol{F}$, $\boldsymbol{C}_{\alpha\alpha}$, $\boldsymbol{R}_{\beta\beta}$, etc. Eqn. (96) is the equivalent of Bashkow's 'A equation'.[2]

Example of Fig. 1.—Our equations are

$$\left.\begin{array}{lr}
+v_1 - v_4 & = E_1 \\
+v_2 - v_5 & = E_2 \\
+v_3 - v_5 - v_6 & = E_3 \\
+i_1 - i_2 - i_3 + i_4 - i_5 & = J_1 \\
+i_2 + i_5 - i_6 & = J_2 \\
+i_3 + i_6 & = J_3 \\
+i_1 - C_1\dfrac{dv_1}{dt} & = 0 \\
R_2 i_2 - v_2 & = 0 \\
L_3\dfrac{di_3}{dt} - v_3 & = 0 \\
+i_4 - C_4\dfrac{dv_4}{dt} & = 0 \\
R_5 i_5 - v_5 & = 0 \\
L_6\dfrac{di_6}{dt} - v_6 & = 0
\end{array}\right\} (63')$$

Our three stages of elimination become:

(*a*) *Using Kirchhoff's Laws.*

$$\left.\begin{array}{l}
v_1 = v_4 + E_1 \\
v_2 = v_5 + E_2 \\
v_3 = v_5 + v_6 + E_3
\end{array}\right\} \quad . \quad . \quad . \quad . \quad (67')$$

$$\left.\begin{array}{l}
i_4 = -i_1 + T_4 \\
i_5 = -i_2 - i_3 + T_5 \\
i_6 = -i_3 + T_6
\end{array}\right\} \quad . \quad . \quad . \quad (71')$$

where

$$\begin{array}{l}
T_4 \equiv J_1 + J_2 + J_3 \\
T_5 \equiv J_2 + J_3 \\
T_6 \equiv J_3
\end{array}$$

(*b*) *Using Ohm's Law applied to Resistors.*

$$v_2 = R_2 i_2 \quad . \quad . \quad . \quad . \quad . \quad . \quad . \quad . \quad (72')$$

$$v_5 = R_5 i_5 \quad . \quad . \quad . \quad . \quad . \quad . \quad . \quad . \quad (73')$$

Writing G_2 for $1/R_2$ we get, using eqns. (67′) and (71′),

$$\left.\begin{array}{l}
i_2 - G_2 v_5 = +G_2 E_2 \\
R_5 i_2 + v_5 = -R_5 i_3 + R_5 T_5
\end{array}\right\} \quad . \quad . \quad . \quad (77')$$

Hence, using eqn. (78) to invert (77′),

$$i_2 = \frac{-G_2R_5}{(1+G_2R_5)}i_3 + \frac{G_2}{(1+G_2R_5)}E_2 + \frac{G_2R_5}{(1+G_2R_5)}T_5$$

and

$$v_5 = \frac{-R_5}{(1+G_2R_5)}i_3 - \frac{G_2R_5}{(1+G_2R_5)}E_2 + \frac{R_5}{(1+G_2R_5)}T_5$$

Thus, using eqns. (67′) and (71′), we get

$$\left.\begin{array}{l}
v_1 = v_4 + E_1 \\
v_2 = \dfrac{-R_5}{(1+G_2R_5)}i_3 + \dfrac{1}{(1+G_2R_5)}E_2 + \dfrac{R_5}{(1+G_2R_5)}T_5 \\
v_3 = \dfrac{-R_5}{(1+G_2R_5)}i_3 + v_6 - \dfrac{G_2R_5}{(1+G_2R_5)}E_2 + E_3 + \dfrac{R_5}{(1+G_2R_5)}T_5 \\
v_5 = \dfrac{-R_5}{(1+G_2R_5)}i_3 - \dfrac{G_2R_5}{(1+G_2R_5)}E_2 + \dfrac{R_5}{(1+G_2R_5)}T_5 \\
i_2 = \dfrac{-G_2R_5}{(1+G_2R_5)}i_3 + \dfrac{G_2}{(1+G_2R_5)}E_2 + \dfrac{G_2R_5}{(1+G_2R_5)}T_5 \\
i_4 = -i_1 + T_4 \\
i_5 = \dfrac{-1}{(1+G_2R_5)}i_3 - \dfrac{G_2}{(1+G_2R_5)}E_2 + \dfrac{1}{(1+G_2R_5)}T_5 \\
i_6 = -i_3 + T_6
\end{array}\right\} (79')$$

(*c*) *Using Capacitor-only Loops and Inductor-only Cut-sets.*

$$v_1 - v_4 = E_1 \quad . \quad . \quad . \quad . \quad . \quad . \quad . \quad (80')$$

$$i_3 + i_6 = T_6 \quad . \quad . \quad . \quad . \quad . \quad . \quad . \quad (81')$$

Differentiate each with respect to time:

$$\dot{v}_1 - \dot{v}_4 = \dot{E}_1 \quad . \quad . \quad . \quad . \quad . \quad . \quad (82')$$

$$\dot{i}_3 + \dot{i}_6 = \dot{T}_6 \quad . \quad . \quad . \quad . \quad . \quad . \quad (83')$$

From eqn. (63'),

$$\left.\begin{aligned} C_1\dot{v}_1 &= i_1 \\ C_4\dot{v}_4 &= i_4 \\ L_3\dot{i}_3 &= v_3 \\ L_6\dot{i}_6 &= v_6 \end{aligned}\right\} \quad . \quad . \quad . \quad . \quad . \quad . \quad (84')$$

Putting these into eqns. (82') and (83'),

$$i_1 = (C_1/C_4)i_4 + C_1\dot{E}_1 \quad . \quad . \quad . \quad . \quad . \quad (85')$$

$$v_6 = -(L_6/L_3)v_3 + L_6\dot{T}_6 \quad . \quad . \quad . \quad . \quad (86')$$

From eqns. (85') and (79'),

$$i_1(1 + C_1/C_4) = C_1\dot{E}_1 + (C_1/C_4)T_4$$

i.e.
$$i_1 = \frac{C_4C_1}{(C_1 + C_4)}\dot{E}_1 + \frac{C_1}{C_1 + C_4}T_4$$

From eqns. (86') and (79'),

$$\frac{(L_3 + L_6)}{L_3}v_6 = \frac{L_6R_5}{L_3(1 + G_2R_5)}i_3 + \frac{L_6G_2R_5}{L_3(1 + G_2R_5)}E_2 - \frac{L_6}{L_3}E_3 - \frac{L_6R_5}{L_3(1 + G_2R_5)}T_5 + L_6\dot{T}_6$$

i.e.

$$v_6 = \frac{L_6R_5}{(1 + G_2R_5)(L_3 + L_6)}i_3 + \frac{L_6G_2R_5}{(1 + G_2R_5)(L_3 + L_6)}E_2 - \frac{L_6}{(L_3 + L_6)}E_3 - \frac{L_6R_5}{(1 + G_2R_5)(L_3 + L_6)}T_5 + \frac{L_3L_6}{(L_3 + L_6)}\dot{T}_6$$

Hence we obtain as our elimination equations

$$v_1 = v_4 + E_1$$

$$v_2 = \frac{-R_2R_5}{(R_2 + R_5)}i_3 + \frac{R_2}{(R_2 + R_5)}E_2 + \frac{R_2R_5}{(R_2 + R_5)}T_5$$

$$v_3 = \frac{-L_3R_2R_5}{(R_2 + R_5)(L_3 + L_6)}i_3 + \frac{R_5L_3}{(R_2 + R_5)(L_3 + L_6)}E_2 - \frac{L_3}{(L_3 + L_6)}E_3 - \frac{R_2R_5L_3}{(R_2 + R_5)(L_3 + L_6)}T_5 + \frac{L_3L_6}{(L_3 + L_6)}\dot{T}_6$$

$$v_5 = \frac{-R_2R_5}{(R_2 + R_5)}i_3 - \frac{R_5}{(R_2 + R_5)}E_2 + \frac{R_2R_5}{(R_2 + R_5)}T_5$$

$$v_6 = \frac{L_6R_2R_5}{(R_2 + R_5)(L_3 + L_6)}i_3 + \frac{L_6R_5}{(R_2 + R_5)(L_3 + L_6)}E_2 - \frac{L_6}{(L_3 + L_6)}E_3 - \frac{L_6R_2R_5}{(R_2 + R_5)(L_3 + L_6)}T_5 + \frac{L_3L_6}{(L_3 + L_6)}\dot{T}_6$$

$$i_1 = \frac{C_1}{(C_1 + C_4)}T_4 + \frac{C_1C_4}{(C_1 + C_4)}\dot{E}_1$$

$$i_2 = \frac{-R_5}{(R_2 + R_5)}i_3 + \frac{1}{(R_2 + R_5)}E_2 + \frac{R_5}{(R_2 + R_5)}T_5$$

$$i_4 = \frac{C_4}{(C_1 + C_4)}T_4 - \frac{C_1C_4}{(C_1 + C_4)}\dot{E}_1$$

$$i_5 = \frac{-R_2}{(R_2 + R_5)}i_3 - \frac{1}{(R_2 + R_5)}E_2 + \frac{R_2}{(R_2 + R_5)}T_5$$

$$i_6 = -i_3 + T_6 \quad . \quad . \quad . \quad (94')$$

We obtain the differential equations for i_3 and v_4 as follows: From eqn. (84'),

$$C_4\dot{v}_4 = i_4$$

$$= \frac{-C_1C_4}{(C_1 + C_4)}\dot{E}_1 + \frac{C_4}{(C_1 + C_4)}T_4 \text{ from (94')}$$

Also from eqn. (84'),

$$L_3\dot{i}_3 = v_3$$

i.e., from eqn. (94'),

$$L_3\dot{i}_3 = \frac{-L_3R_2R_5}{(R_2 + R_5)(L_3 + L_6)}i_3 + \frac{R_5L_3}{(R_2 + R_5)}E_2 - \frac{L_3}{(L_3 + L_6)}E_3 - \frac{R_2R_5L_3}{(R_2 + R_5)(L_3 + L_6)}T_5 + \frac{L_3L_6}{(L_3 + L_6)}\dot{T}_6$$

i.e.

$$\begin{bmatrix} \left[\frac{-R_5}{(R_2+R_5)}\dot{E}_2 + \frac{1}{(L_3+L_6)}E_3 + \frac{R_2R_5}{(R_2+R_5)(L_3+L_6)}T_5 - \frac{L_6}{(L_3+L_6)}\dot{T}_6\right] \\ \left[\frac{C_1}{(C_1 + C_4)}\dot{E}_1 - \frac{1}{(C_1 + C_4)}T_4\right] \end{bmatrix} + \frac{d}{dt}\begin{bmatrix} i_3 \\ v_4 \end{bmatrix} = \begin{bmatrix} \frac{-R_2R_5}{(R_2 + R_5)(L_3 + L_6)} & 0 \\ 0 & 0 \end{bmatrix}\begin{bmatrix} i_3 \\ v_4 \end{bmatrix} \quad . \quad . \quad . \quad . \quad (96')$$

Note that the natural frequencies obtained from eqn. (96') are the same as those we obtained in Section 2.4, namely

$$\lambda = 0$$

and
$$\lambda = \frac{-R_2R_5}{(R_2 + R_5)(L_3 + L_6)}$$

(6.3) Comparison with Bashkow

In this Section we compare the results given in Sections 3.2 and 6.2 with those obtained by Bashkow.[2] Before we do this, we give a brief account of Bashkow's paper. We slightly change the terminology in order to agree with ours.

Like us, in order to carry out his elimination, Bashkow finds it convenient to state his network branch equations in terms of a specific tree of the network. To obtain this tree, however, the network has generally to be modified by the addition of extra inductors and capacitors. The effects of this modification are taken care of at the end of his process.

Bashkow first defines a *proper tree* of a network:

Definition 6.—A *proper tree* of a network (assuming that it contains one) is a tree which contains every capacitor and no inductor.

It is obvious that any *RLC* network will not in general contain a proper tree. Its formation can be prevented by the presence of various capacitors and inductors.

Definition 7.—Any capacitor or inductor which prevents the formation of a proper tree is called *excess*.

Example of Fig. 1.—The network of Fig. 1 contains no proper tree. Any one of the two capacitors is an excess capacitor and any one of the two inductors is an excess inductor.

Bashkow points out that, if each excess capacitor has an inductor added in series with it, and if each excess inductor has a capacitor added in parallel, then the modified network will contain a proper tree. Working with this modified network and the associated proper tree, Bashkow shows that some of the network branch variables can be eliminated to obtain a set of independent variables which are the capacitor voltages and the inductor currents. Obtaining his original network $\mathcal{N}$ from his modified network, by letting his added capacitors and inductors vanish, he shows that the excess capacitor voltages and the excess inductor currents can be eliminated, as well as the currents through the added inductors and the voltages across the added capacitors. Hence Bashkow obtains for $\mathcal{N}$ a set of dynamically-independent variables which consists of:

(*a*) the voltages across those capacitors of $\mathcal{N}$ which are not excess, and

(*b*) the currents through those inductors of $\mathcal{N}$ which are not excess.

That these results are equivalent to our results of Section 3.2 will follow from Lemma 13.

We shall need first Lemmas 10, 11, 12.

Lemma 10.—A cut-set of $\mathcal{N}$ contains at least one branch of every tree of $\mathcal{N}$.

Proof.—This lemma is contained in Theorem 2 of Reference 11.

Lemma 11.—A set of inductors of $\mathcal{N}$ form an inductor-only cut-set of $\mathcal{N}$ if and only if they form a cut-set in $\mathcal{N}_L^*$.

Proof.—Sufficiency: We have a cut-set of $\mathcal{N}_L^*$. Hence cutting all the inductors forming this cut-set separates $\mathcal{N}_L^*$ into two parts. If now we restore the resistors and capacitors (in place of the short-circuits substituted in forming $\mathcal{N}_L^*$) the resulting network will still be in two parts. Further, since cutting no sub-set of the cut-set of $\mathcal{N}_L^*$ will separate $\mathcal{N}_L^*$ into two parts, neither will it when the resistors and capacitors are restored. Hence the cut-set of $\mathcal{N}_L^*$ is also a cut-set of $\mathcal{N}$, i.e. it is an inductor-only cut-set of $\mathcal{N}$.

Necessity: We have an inductor-only cut-set of $\mathcal{N}$. A reverse argument to the above shows that it will be a cut-set of $\mathcal{N}_L^*$.

Lemma 12.—(*a*) A capacitor is excess if, and only if, it is part of a capacitor-only loop.

(*b*) An inductor is excess if, and only if, it is part of an inductor-only cut-set.

Proof.—(*a*) *Sufficiency*: Because the capacitor is part of a capacitor-only loop, its presence certainly prevents the formation of a proper tree. Hence it is excess.

Necessity: Because the capacitor is excess, every tree of $\mathcal{N}$ must, because of it, leave out a capacitor. Hence $\mathcal{N}_C$ must contain at least one loop containing this capacitor, and so it is part of this capacitor-only loop.

(*b*) *Sufficiency*: Because the inductor is part of an inductor-only cut-set, then by Lemma 10, every tree of $\mathcal{N}$ must contain an inductor. Hence $\mathcal{N}$ can contain no proper tree, and so the inductor is excess.

Necessity: Because the inductor is excess, every tree of $\mathcal{N}$ must contain an inductor. Hence $\mathcal{N}_L^*$ must contain at least one cut-set containing the inductor; i.e. by Lemma 11, the inductor is part of an inductor-only cut-set of $\mathcal{N}$.

Definition 8.—A set of excess capacitors is called a *complete* set of excess capacitors if by substituting open-circuits for those capacitors in the set we are left with a network containing no excess capacitors, while no proper sub-set† of the set has this property. A set of excess inductors is called a *complete* set of excess inductors if by substituting short-circuits for those inductors in the set we obtain a network containing no excess inductors, while no proper sub-set of the set has this property.

Lemma 13.—(*a*) A set of capacitors of $\mathcal{N}$ are a complete set of excess capacitors if and only if they form a set of chords‡ of a forest in $\mathcal{N}_C$.

(*b*) A set of inductors of $\mathcal{N}$ are a complete set of excess inductors if and only if they form a tree§ of $\mathcal{N}_L^*$.

Proof.—(*a*) *Sufficiency*: Since a complete set of chords in $\mathcal{N}_C$ [i.e. a set of $(B_C - N + S_C)$ chords], defines a complete set of independent capacitor-only loops in $\mathcal{N}$, then, by Lemma 12, these capacitor chords are certainly excess. Further, substituting open-circuits for them, leaves an $\mathcal{N}_C$ containing no loops, while substituting open-circuits for a proper sub-set of them will not. Hence the chords form a complete set of excess capacitors.

Necessity: Substituting open-circuits for our complete set of excess capacitors will, by Definition 8, leave a network containing no excess capacitors, and so, by Lemma 12, containing no capacitor-only loops. Hence the corresponding modified $\mathcal{N}_C$ will contain no loops. Since this property will not hold for any proper sub-set of the complete set of excess capacitors, this complete set must form a set of chords of a forest of $\mathcal{N}_C$.

(*b*) *Sufficiency*: The tree of $\mathcal{N}_L^*$ defines a set of independent cut-sets in $\mathcal{N}_L^*$.[11] Hence, by Lemma 11, the tree branches define a set of independent inductor-only cut-sets. Hence by Lemma 12 they are certainly excess inductors. Further, substituting short-circuits for them leaves an $\mathcal{N}_L^*$ containing only one node, and so no cut-sets, i.e. will leave $\mathcal{N}$ containing no excess inductors. Substituting short-circuits for any proper sub-set of the tree branches will not leave such a network. Hence the tree branches form a complete set of excess inductors.

Necessity: Substituting short-circuits for our complete set of excess inductors will, by Definition 8, leave a network containing no excess inductors. Hence, by Lemma 12, this modified network will not contain any inductor-only cut-sets, and so, by Lemma 11, the corresponding modified $\mathcal{N}_L^*$ will contain no cut-sets, i.e. will contain only one node. Since this property will not hold for any proper sub-set of the complete set of excess inductors, this complete set must form a tree in $\mathcal{N}_L^*$.

From Lemma 13, and its obvious extension to non-connected networks, it follows that Bashkow's results coincide with ours of Theorem 3.

(6.4) Some Matrix Lemmas

In this Section the matrices U and V are general rectangular matrices.

We shall suppose that we have a square matrix which may be partitioned into the form

$$\begin{bmatrix} \mathbf{1} & U \\ V & \mathbf{1} \end{bmatrix}$$

We obtain in Lemma 16 the inverse of such a matrix, and in Lemma 17 apply this to a matrix defined in Section 6.2. We first require Lemmas 14 and 15.

Lemma 14

$$\begin{bmatrix} \mathbf{1} & U \\ V & \mathbf{1} \end{bmatrix} = \begin{bmatrix} \mathbf{1} & \mathbf{0} \\ V & \mathbf{1} \end{bmatrix} \begin{bmatrix} \mathbf{1} & U \\ \mathbf{0} & \mathbf{1} - VU \end{bmatrix}$$

$$= \begin{bmatrix} \mathbf{1} & U \\ \mathbf{0} & \mathbf{1} \end{bmatrix} \begin{bmatrix} \mathbf{1} - UV & \mathbf{0} \\ V & \mathbf{1} \end{bmatrix} \quad . \quad . \quad (97)$$

Proof by carrying out the multiplications.

Lemma 15

$$\det \begin{bmatrix} \mathbf{1} & U \\ V & \mathbf{1} \end{bmatrix} = \det [\mathbf{1} - VU] = \det [\mathbf{1} - UV] \quad . \quad (98)$$

Proof from Lemma 14, using Laplace expansions[1] of the determinants on the right-hand side of eqn. (97).

Lemma 16.—If $\begin{bmatrix} \mathbf{1} & U \\ V & \mathbf{1} \end{bmatrix}$ is non-singular, then

$$\begin{bmatrix} \mathbf{1} & U \\ V & \mathbf{1} \end{bmatrix}^{-1} = \begin{bmatrix} [\mathbf{1} - UV]^{-1} & -U[\mathbf{1} - VU]^{-1} \\ -V[\mathbf{1} - UV]^{-1} & [\mathbf{1} - VU]^{-1} \end{bmatrix} \quad . \quad (99)$$

Proof.—The sub-matrices on the right-hand side exist by Lemma 15. The proof now follows by carrying out matrix multiplication.

We now apply these results to the matrix contained in eqn. (77) of Section 6.2.

Lemma 17.—If $\begin{bmatrix} \mathbf{1}_{\beta\beta} & R_{\beta\beta}^{-1} F_{\beta\epsilon} \\ -R_{\epsilon\epsilon} F'_{\beta\epsilon} & \mathbf{1}_{\epsilon\epsilon} \end{bmatrix}$ is as defined in eqn. (77), it is

† A 'proper' sub-set of a set is any sub-set which is not the complete set itself.

‡ Although $\mathcal{N}_C$ will not in general be connected, we define a set of chords of a forest of $\mathcal{N}_C$ as being the branches of $\mathcal{N}_C$ not contained in that forest.

§ We are assuming that $\mathcal{N}$, and so also $\mathcal{N}_L^*$, is connected. Extension to non-connected networks follows by consideration of each part separately.

non-singular and its inverse is given by

$$\begin{bmatrix} [\mathbf{1}_{\beta\beta} + \boldsymbol{R}_{\beta\beta}^{-1}\boldsymbol{F}_{\beta\epsilon}\boldsymbol{R}_{\epsilon\epsilon}\boldsymbol{F}'_{\beta\epsilon}]^{-1} & -\boldsymbol{R}_{\beta\beta}^{-1}\boldsymbol{F}_{\beta\epsilon}[\mathbf{1}_{\epsilon\epsilon} + \boldsymbol{R}_{\epsilon\epsilon}\boldsymbol{F}'_{\beta\epsilon}\boldsymbol{R}_{\beta\beta}^{-1}\boldsymbol{F}_{\beta\epsilon}]^{-1} \\ \boldsymbol{R}_{\epsilon\epsilon}\boldsymbol{F}'_{\beta\epsilon}[\mathbf{1}_{\beta\beta} + \boldsymbol{R}_{\beta\beta}^{-1}\boldsymbol{F}_{\beta\epsilon}\boldsymbol{R}_{\epsilon\epsilon}\boldsymbol{F}'_{\beta\epsilon}]^{-1} & [\mathbf{1}_{\epsilon\epsilon} + \boldsymbol{R}_{\epsilon\epsilon}\boldsymbol{F}'_{\beta\epsilon}\boldsymbol{R}_{\beta\beta}^{-1}\boldsymbol{F}_{\beta\epsilon}]^{-1} \end{bmatrix} \quad . \quad . \quad . \quad (100)$$

Proof by Lemma 15:

$$\det \begin{bmatrix} \mathbf{1}_{\beta\beta} & \boldsymbol{R}_{\beta\beta}^{-1}\boldsymbol{F}_{\beta\epsilon} \\ -\boldsymbol{R}_{\epsilon\epsilon}\boldsymbol{F}'_{\beta\epsilon} & \mathbf{1}_{\epsilon\epsilon} \end{bmatrix} = \det [\mathbf{1}_{\beta\beta} + \boldsymbol{R}_{\beta\beta}^{-1}\boldsymbol{F}_{\beta\epsilon}\boldsymbol{R}_{\epsilon\epsilon}\boldsymbol{F}'_{\beta\epsilon}] = \det [\mathbf{1}_{\epsilon\epsilon} + \boldsymbol{R}_{\epsilon\epsilon}\boldsymbol{F}'_{\beta\epsilon}\boldsymbol{R}_{\beta\beta}^{-1}\boldsymbol{F}_{\beta\epsilon}] \quad . \quad (101)$$

Now we have as an identity

$$[\mathbf{1}_{\beta\beta} + \boldsymbol{R}_{\beta\beta}^{-1}\boldsymbol{F}_{\beta\epsilon}\boldsymbol{R}_{\epsilon\epsilon}\boldsymbol{F}'_{\beta\epsilon}] = \boldsymbol{R}_{\beta\beta}^{-1}[\boldsymbol{F}_{\beta\epsilon}, \mathbf{1}_{\beta\beta}] \begin{bmatrix} \boldsymbol{R}_{\epsilon\epsilon} & \mathbf{0} \\ \mathbf{0} & \boldsymbol{R}_{\beta\beta} \end{bmatrix} \begin{bmatrix} \boldsymbol{F}'_{\beta\epsilon} \\ \mathbf{1}_{\beta\beta} \end{bmatrix} \quad . \quad (102)$$

from which we see that the matrix

$$[\mathbf{1}_{\beta\beta} + \boldsymbol{R}_{\beta\beta}^{-1}\boldsymbol{F}_{\beta\epsilon}\boldsymbol{R}_{\epsilon\epsilon}\boldsymbol{F}'_{\beta\epsilon}]$$

is non-singular.

Hence, using Lemma 16, the lemma follows.

621.318.424 : 621.313.1

The Institution of Electrical Engineers
Monograph No. 336 U
June 1959

RISE OF FLUX IN SOLID IRON CORE DUE TO IMPACT EXCITATION

By N. KESAVAMURTHY, M.A., B.E., M.Sc.Tech., Graduate, and P. K. RAJAGOPALAN, B.E., M.S.

(*The paper was first received 6th October*, 1958, *and in revised form 27th January*, 1959. *It was published as an* INSTITUTION MONOGRAPH *in June*, 1959.)

SUMMARY

In designing machines and apparatus with solid magnetic circuits, flux/time curves have often to be predetermined to secure a desired rapidity of response. Their prediction has hitherto been uncertain, especially in the presence of saturation.

In the paper, an attempt is made to derive the equations for the rise of flux and current on the basis of a limiting non-linear theory. This results in an original treatment and gives a greater insight into the physical phenomena involved in the magnetization of a core due to impact excitation. The results obtained from these equations compare favourably with test results.

LIST OF PRINCIPAL SYMBOLS

B_s = Final flux density, gauss.
N = Number of turns of the magnetizing winding.
I = Final exciting current, amperes.
i = Instantaneous exciting current, amperes.
R = Resistance of the winding, ohms.
t = Time, seconds.
V = Applied voltage, volts.
i_b = Eddy current in the core at time t.
Φ = Instantaneous flux, maxwells.
ρ = Resistivity of the core material, ohm-cm.
l = Length of flux path in solid iron, centimetres.
b = Width of the rectangular section of the core, centimetres.
d = Depth of the rectangular section of the core, centimetres.

(1) INTRODUCTION

Analytical and graphical methods of determining flux/time curves are available for magnetic circuits in which eddy currents are negligible. There is, however, a need for a precise knowledge of the damping action of eddy currents.

An impact excitation on a solid core of iron of given section and known electric and magnetic properties creates eddy currents in the core whose action is to retard the rise of flux by creating a non-uniform distribution of flux density in any section of the core. The determination of this distribution becomes more complicated owing to the presence of saturation.

The simplest approach to the analysis of the problem is based on the assumption of constant permeability for the iron. Such an assumption leads to the formulation of Poisson's equation, giving the distribution of eddy currents over the section of the core. This method is applicable only when the decay of the flux is of interest, but fails to yield a satisfactory solution for the rise of flux if the resistance of the exciting winding is taken into account.

However, equations for flux and exciting-coil current have been developed by Dunaevskii,[1,2] who considers a magnetic circuit consisting of a solid section, a laminated section and an air-gap in series combination. These equations are derived on the basis of constant permeability of the magnetic circuit. To include the effects of iron saturation, the saturation curve of the material could be approximately represented by several straight lines, and a step-by-step analysis with different flux values and time-constants could be employed. Such an extension of Dunaevskii's method is applied to calculate the voltage response using an experimental cast-steel solid toroid (see Section 4) having the magnetization characteristic of Fig. 1, with the three regions of the saturation curve approximated by straight lines (i), (ii) and (iii). The build-up of the flux is computed and is plotted in Fig. 4.

A graphical method of determining the flux/time curve due to impact excitation has been suggested by Pohl.[4] In this method the graphical construction[5] of the curve for a laminated core is taken as the starting-point. The method is extended to the case of a laminated core having a secondary winding with 100% coupling. Assuming that an unlaminated core is equivalent to a laminated one with a short-circuited secondary having a resistance related to the section and to the electric properties of the materials, it is possible to determine the flux/time curve for a solid core. A comparison with the experimental results does not justify the replacement of the eddy currents by this fictitious damping ring having 100% coupling.

The object of the paper is to calculate from first principles the rise of flux and current in an iron core of given section and known electric and magnetic properties when subjected to an impact excitation, and to prove its agreement with test results. The equations for the rise of flux and current are deduced on the basis of a limiting non-linear theory resulting in an original treatment.

(2) LIMITING NON-LINEAR MAGNETIC CHARACTERISTIC AND ITS IMPLICATIONS

For the development of the theory, the material of magnetic characteristic shown in Fig. 1 is replaced by one having the non-linear magnetic characteristic[3] shown in Fig. 2. This material is magnetized to saturation if the field intensity is different from zero and it is only possible to change the flux density at $H = 0$. This implies that if the flux density is changing, H must be zero. However, the converse statement, that if H is zero the flux density must be changing, is not necessarily true. Thus, it is possible to have regions within the material where H is zero, but where the flux density can have any constant value less than or equal to the saturation induction. The particular constant value would depend upon the state in which the material was left during some previous process.

When the exciting winding of a solid core is subjected to a sudden change of excitation, the magnetization takes place radially inwards, starting from the surface of the core. For the material having the non-linear magnetic characteristic it is obvious that, at any time t prior to complete magnetization, there would be a surface of separation between two states of iron in the core, one saturated to the induction density B_s and the other unmagnetized. In other words, in regions above the surface of separation the magnetizing force H is greater than zero, whilst in regions below the layer of separation, $H = 0$. The magnetization of the core is complete when the surface of

Correspondence on Monographs is invited for consideration with a view to publication.
Prof. Kesavamurthy is Professor of Electrical Engineering, and Mr. Rajagopalan is Lecturer in Electrical Engineering, at the Indian Institute of Technology, Kharagpur.

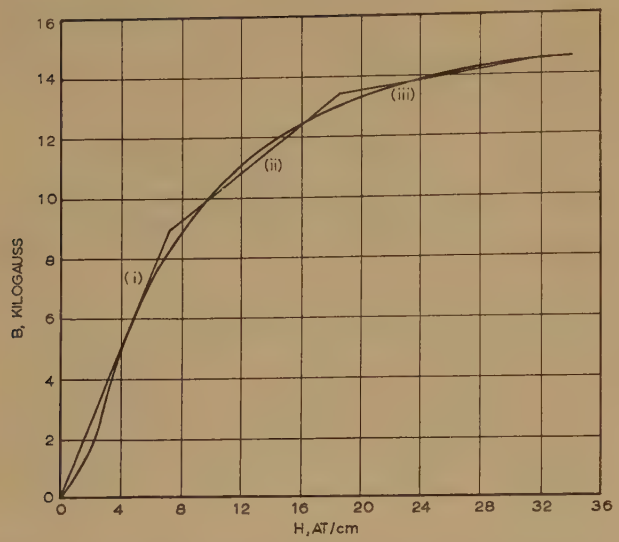

Fig. 1.—Magnetization curve of the experimental solid steel ring.
The straight line approximations are for use in Dunaevskii's equations.

separation moves to the centre of the core. Any change in the position of this surface implies that the layers above it undergo a change in flux linkage, as a consequence of which eddy currents will be induced in this region. Since no magnetizing force exists below the surface of separation, the equivalent ampere-turns due to the eddy currents in the region above the surface of separation will balance the ampere-turns of the exciting winding.

(3) DERIVATION OF EQUATIONS FOR CURRENT AND FLUX ON THE BASIS OF THE LIMITING NON-LINEAR THEORY

Consider a solid magnetic core of length l with a uniformly wound exciting coil of N turns and resistance R ohms. Let the resistivity of the material be ρ and the non-linear characteristic be as shown in Fig. 2. A voltage is suddenly applied to the exciting winding. In the following Sections, the equations for current and flux are derived for various types of iron section.

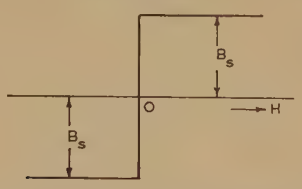

Fig. 2.—Limiting non-linear magnetization curve.

(3.1) Rectangular Section of Depth very small compared with Width

Consider a rectangular section, shown in Fig. 3(*a*), where the depth, $2d$, is small compared with the width, $2b$. At time t after an application of voltage V, let the surface of separation be at a distance x measured from the surface of the core. If, after a small time interval dt, the layer moves inwards by a distance dx, the change in flux linkage is $d\Phi = 2B_s dx$. Hence

$$\frac{d\Phi}{dt} = 2B_s \frac{dx}{dt}$$

The e.m.f. induced in the main winding is

$$v = -2NB_s \frac{dx}{dt} \times 10^{-8}$$

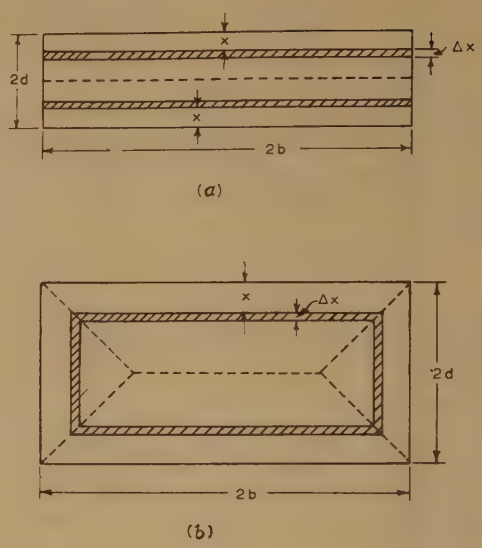

Fig. 3.—Rectangular sections of solid ring showing the eddy-current paths.
(*a*) For depth very small compared to width.
(*b*) For comparable width and depth.

All the layers above the surface of separation undergo the same rate of change of flux linkage and hence the current density is the same in all these layers. The induced e.m.f. for the layers above is $-(d\Phi/dt) \times 10^{-8}$. Hence the total eddy current is

$$i_b = -\frac{B_s}{2b\rho}\frac{dx}{dt} xl \times 10^{-8}$$

If the ampere-turns due to the exciting winding at time t are iN, then $iN + i_b = 0$, or

$$i = \frac{B_s xl}{2Nb\rho}\frac{dx}{dt} \times 10^{-8}$$

The voltage equation for the main winding is $V + v - iR = 0$. Hence

$$\frac{dx}{dt} = \frac{V}{2NB_s\left(1 + \dfrac{Rxl}{4N^2b\rho}\right) \times 10^{-8}}$$

Integrating and using the initial condition $x = 0$ at $t = 0$,

$$Vt = 2NB_s\left(x + \frac{Rx^2l}{8\rho N^2 b}\right) \times 10^{-8} \quad . \quad . \quad . \quad (1)$$

$$i = \frac{V}{4N^2b\rho\left(1 + \dfrac{Rxl}{4N^2b\rho}\right)} \quad . \quad . \quad . \quad . \quad (2)$$

$$\Phi = 4B\,bx \quad . \quad . \quad . \quad . \quad . \quad . \quad (3)$$

Eqns. (1), (2) and (3) are the required current and flux equations.

(3.2) Rectangular Section of Comparable Width and Depth

The surface of separation at any time t has the configuration shown in Fig. 3(*b*). This particular choice of configuration has the advantage that its change has only one degree of freedom. The eddy-current paths are assumed to have a similar configuration. At time t let the surface of separation be at a distance x from the surface of the material. The perimeter a

depth x is $4(b + d - 2x)$ and the change in flux linkage, $d\Phi$, is $4B_s(b + d - 2x)dx$. Hence

$$\frac{d\Phi}{dt} = 4B_s(b + d - 2x)\frac{dx}{dt}$$

and the e.m.f. induced in the main winding is

$$v = -4NB_s(b + d - 2x)\frac{dx}{dt} \times 10^{-8}$$
$$= Nv_b$$

where v_b is the e.m.f. induced in all the eddy-current paths. The resistance of an elemental path of thickness dy situated at depth y from the surface is $4\rho(b + d - 2y)l dy$. Hence the total conductance, G, of the region above the surface of separation is given by

$$G = \int_0^x \frac{l dy}{4\rho(b + d - 2y)} = -\frac{l}{8\rho}\log\frac{b + d - 2x}{b + d}$$

Hence the total eddy current is

$$i_b = -\left(\frac{d\Phi}{dt}\right)G \times 10^{-8}$$

Also $i_b + iN = 0$, and $V = -v + iR$.

Thus

$$\frac{dx}{dt} = \frac{V}{4NB_s\left(1 - \frac{Rl}{8N^2\rho}\log\frac{b + d - 2x}{b + d}\right) \times 10^{-8}}$$

Integration and substitution of initial conditions leads to

$$Vt = 4B_sN\left[1 + \frac{Rl}{8\rho N^2}\log(b + d)\right][(b + d)x - x^2] \times 10^{-8}$$
$$+ \frac{B_sRl}{8\rho N^2}\{(b + d - 2x)^2[\log(b + d - x) - \tfrac{1}{2}]$$
$$- (b + d)^2[\log(b + d) - \tfrac{1}{2}]\} \quad . \quad . \quad . \quad . \quad (4)$$

$$i = \frac{-Vl(b + d - 2x)\log\left(\frac{b + d - 2x}{b + d}\right)}{8\rho N^2\left[1 - \frac{Rl}{8\rho N^2}\log\left(\frac{b + d - 2x}{b + d}\right)\right]} \quad . \quad . \quad (5)$$

and $$\Phi = 4B_s(b + d - x)x \quad . \quad . \quad . \quad . \quad . \quad (6)$$

In a similar manner, the relevant equations for flux and current may be obtained for square and circular sections.

(3.3) Choice of B_s for Computation of Flux/Time and Current/Time Curves

For the actual material, the magnetic characteristic is quite different from the non-linear characteristic shown in Fig. 2. For a proper application of the results of the foregoing Sections it is necessary to choose suitable values of B_s. Also, this choice of induction should be consistent with the nature of the actual B/H curve. It is obvious that the first consideration that should weigh in the choice of B_s is that value of induction which would be established when a current i flows in the main winding. On this basis, the computation of the flux and current curves would be as follows:

(*a*) Determine the current for a specific value of x, using eqn. (5).
(*b*) For this value of current, choose the corresponding value of B_s from the static magnetization curve of the material.
(*c*) Substitute this value of B_s in eqns. (4) and (6) to obtain relationships between x and t, and Φ and t, respectively.
(*d*) Repeat (*a*), (*b*) and (*c*) for different values of x and thus obtain the flux/time and current/time curves.

(4) COMPUTATION OF FLUX/TIME AND CURRENT/TIME CURVES FOR A SOLID STEEL RING AND COMPARISON WITH TEST RESULTS

The above analysis was applied to a magnetic circuit consisting of a solid cast-steel ring without air-gap, of 90·9 cm external

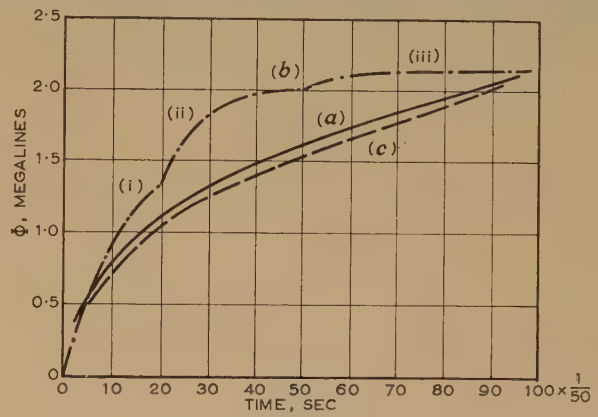

Fig. 4.—Flux/time curves.
(*a*) Experimental results.
(*b*) Curve based on Dunaevskii's equations.
(*c*) Curve based on authors' treatment.

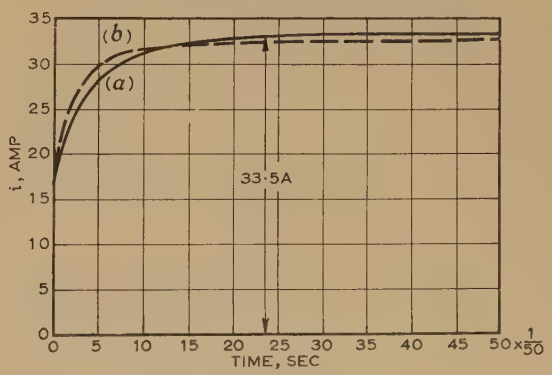

Fig. 5.—Current/time curves.
(*a*) Experimental results.
(*b*) Curve based on authors' treatment.

Table 1

CALCULATIONS FOR THE FLUX/TIME AND CURRENT/TIME CURVES

x	0·05	0·1	0·25	0·5	0·75	1·00	1·25	1·50	1·75	2·00	2·25	2·50	2·75	3·00	3·25	3·50	3·75	4·00	4·5
i	11·63	17·15	24·32	28·28	29·92	30·79	31·37	31·74	32·02	32·24	32·41	32·54	32·66	32·75	32·84	32·90	32·97	33·03	33·12
B_s	9·58	11·70	13·25	13·74	13·90	13·96	14·02	14·06	14·08	14·1	14·1	14·1	14·1	14·1	14·1	14·1	14·1	14·1	14·1
t	0·254	0·3	0·622	2·61	4·82	9·89	12·45	17·34	22·37	29·2	36·05	43·13	51·19	59·07	67·8	76·3	85·5	94·4	112·3
Φ	0·024	0·59	0·165	0·336	0·5	0·655	0·803	0·945	1·08	1·21	1·33	1·44	1·55	1·64	1·73	1·82	1·90	1·99	2·08

x, cm (assumed); i, amp (from eqn. 5); B_s, kilogauss (from B/H curve Fig. 1); t, cycles on a 50 c/s base (from eqn. 4); Φ, megamaxwells (from eqn. 6).

diameter, 69·8 cm internal diameter and 14·8 cm width. Its resistivity was $17{\cdot}48 \times 10^{-6}$ ohm-cm and its magnetization curve is shown in Fig. 1. The uniformly spaced exciting coil had 200 turns and 49 volts were suddenly applied across the winding. The resistance of the exciting winding was 1·464 ohms, giving a final current of 33·45 amp. Table 1 shows the results of the calculations.

Test results for the above magnetic circuit are given by Pohl[5] and are reproduced in Figs. 4 and 5. Unfortunately, facilities are not available for the authors to repeat the experimental work of Pohl. Fig. 4 shows the theoretical flux/time curve on the basis of Dunaevskii's equations, as compared with the curves based on the present theory and also with the experimental ones. Fig. 5 shows a comparison of the calculated current/time curve with experimental results. It is seen that the analysis outlined in the paper yields results in close agreement with the test results, bearing in mind the experimental errors introduced in the oscillographic measurements and the integration for the flux curve, and also the degree of uncertainty as to the magnetic and electric properties of the specimen.

The present theory appears to be a simple approach to the problem of the study of penetration of magnetism into a solid core of magnetic material, taking the non-linearity of the *B/H* curve into consideration. The method is both elegant and simple and yields results accurate enough for design purposes.

(5) ACKNOWLEDGMENT

The authors are grateful to the Director, Indian Institute of Technology, Kharagpur (India) for granting facilities for the work described in the paper.

(6) REFERENCES

(1) DUNAEVSKII, S. I.: 'Effects of Eddy Currents on Magnetic Flux', *Elektrichestvo*, 1951, **8**, Part II, p. 55.

(2) BROCKMAN, J. J., and LINKOUS, C. E.: 'D.C. Machines: Response to Impact Excitation', *Transactions of the American I.E.E.*, 1955, **74**, Part III, p. 500.

(3) MCCONNELL, H. M.: 'Eddy-Current Phenomena in Ferromagnetic Materials', *ibid.*, 1954, **73**, Part I, p. 226.

(4) POHL, R.: 'Impact Exciters', *Elektrotechnik und Maschinenbau*, 1936, **54**, p. 1.

(5) POHL, R.: 'Rise of Flux Due to Impact Excitation: Retardation by Eddy Currents in Solid Parts', *Proceedings I.E.E.*, Paper No. 776 S, February, 1949 (**96**, Part II, p. 57).

621.372.2: 621.372.8

The Institution of Electrical Engineers
Monograph No. 337 E
June 1959

A GUIDE TO THE PRACTICAL APPLICATION OF CHEBŸSHEV FUNCTIONS TO THE DESIGN OF MICROWAVE COMPONENTS

By R. LEVY, M.A.

(*The paper was first received* 3*rd December*, 1958, *and in revised form* 19*th February*, 1959. *It was published as an* INSTITUTION MONOGRAPH *in June*, 1959.)

SUMMARY

The properties of Chebÿshev functions and their application to the design of several types of microwave components are described.

Formulae giving the broadest possible bandwidth in a given physical length are derived for stepped transformers, stepped twists and multi-element directional couplers. These formulae are intended for practical application by the microwave engineer to the design of actual components, and it is suggested that they should be used rather than the conventional 'binomial' formulae, which do not give the optimum or simplest design. Microwave band-pass filters with Chebÿshev equal-ripple characteristics are also described.

(1) INTRODUCTION

A considerable amount of literature has been published on the design of multi-element microwave components. This has mainly dealt with the type of matching procedure giving what is variously known as the binomial, maximally flat, or Butterworth characteristic (e.g. References 1, 2, 13, 14, 16, 24). This method consists in tapering the voltage reflection coefficients of the individual elements to the coefficients of a binomial expansion. However, an improved overall reflection-coefficient/frequency characteristic may be obtained by tapering individual elements to give a characteristic which is a Chebÿshev polynomial of the first kind. Several papers have been published on this method,[3–8] but many of them are mathematically complicated and are applied only to the design of a single type of component. This may partly account for the apparent lack of use of designs based on Chebÿshev functions while the binomial designs are widely used. The object of the paper is to present the design criteria in a simple general form applicable to any type of microwave component. Examples are also given, with experimental results, of the application of Chebÿshev functions to the design of quarter-wave transformers, stepped twists, directional couplers and microwave filters.

(2) PROPERTIES OF CHEBŸSHEV FUNCTIONS

(2.1) Chebÿshev Functions of the First Kind

The Chebÿshev function of the first kind of integral order n is defined as

$$T_n(x) = \begin{cases} \cos(n \arccos x) \ldots & |x| \leqslant 1 \\ \cosh(n \operatorname{arccosh} x) \ldots & |x| \geqslant 1 \end{cases} \quad \ldots \quad (1)$$

In the interval $|x| < 1$ this function oscillates between ± 1 and has $(n - 1)$ equal maxima or minima in the interval. The function also assumes the values ± 1 at $x = \pm 1$. Outside this region the function exceeds unity in value and approaches $\pm\infty$. Diagrams of five Chebÿshev functions in the interval $|x| < 1$ are shown in Fig. 1.

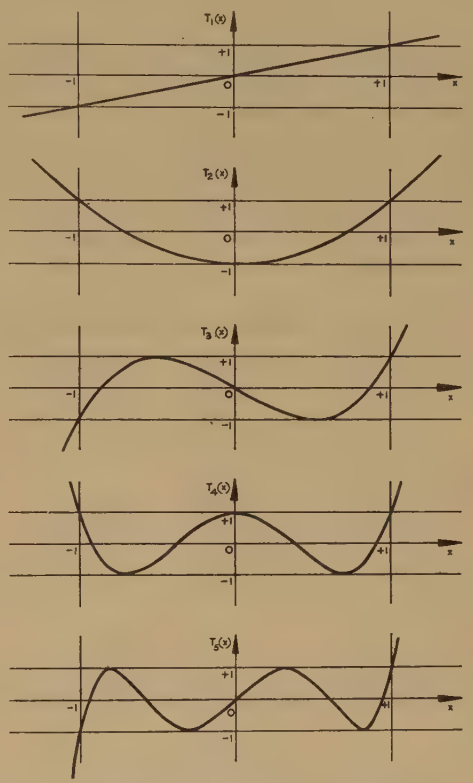

Fig. 1.—Chebÿshev functions of the first kind.

The Chebÿshev functions may be expanded as a power series in x by use of the recurrence formula:

$$T_{n+1}(x) + T_{n-1}(x) = 2xT_n(x) \quad \ldots \quad (2)$$

and the first six Chebÿshev functions expressed as polynomials in x are given in Table 1.

Table 1

CHEBŸSHEV FUNCTIONS OF THE FIRST KIND

n	$T_n(x)$
0	1
1	x
2	$2x^2 - 1$
3	$4x^3 - 3x$
4	$8x^4 - 8x^2 + 1$
5	$16x^5 - 20x^3 + 5x$

These expansions are valid for all values of x.

Correspondence on Monographs is invited for consideration with a view to publication.

The paper is a communication from the Staff of the Applied Electronics Laboratories of The General Electric Company Limited, Stanmore, England.

A general formula for the series expansion of $T_n(x)$ and also its expansion as a finite Fourier series are given by Duhamel.[9]

When a number of obstacles are arranged along a waveguide or transmission line to form a microwave component it is often desirable to obtain a good input v.s.w.r. over a broad band. It can be shown[4, 11] that the optimum result is obtained by spacing and tapering the reflection coefficients of the individual objects along the line so that the modulus of the reflection coefficient ρ as a function of frequency deviation $\Delta\omega$ is proportional to the modulus of a Chebÿshev polynomial of the first kind in a progressive (i.e. increasing or decreasing) function of $\Delta\omega$, i.e.

$$|\rho(\Delta\omega)| = \rho' . |T_n[f(\Delta\omega)]| \quad . \quad . \quad . \quad . \quad (3)$$

Here n is the degree of the polynomial and is one less than the number of obstacles along the line, and ρ' is the maximum value of the input reflection coefficient in the band. Any frequency-dependent variable may be substituted for ω in eqn. (3), i.e. wavelength or its reciprocal, or any progressive function of these variables. Such a substitution will be equivalent to a transformation (or distortion) of the frequency axis, and a Chebÿshev reflection coefficient (i.e. equal ripple) response with frequency will still be obtained.

(2.2) Chebÿshev Functions of the Second Kind

The rationalized Chebÿshev function of the second kind is defined as

$$U_n(x) = \begin{cases} \dfrac{\sin(n \arccos x)}{\sqrt{(1-x^2)}} & \ldots \ |x| \leqslant 1 \\ \dfrac{\sinh(n \operatorname{arc\,cosh} x)}{\sqrt{(x^2-1)}} & \ldots \ |x| \geqslant 1 \end{cases} \quad . \quad . \quad (4)$$

$U_n(x)$ may be expanded in a power series using the same recursion formula as eqn. (2):

$$U_{n+1}(x) + U_{n-1}(x) = 2xU_n(x) \quad . \quad . \quad . \quad (5)$$

The first five functions expressed as polynomials in x are given in Table 2.

Table 2

CHEBŸSHEV FUNCTIONS OF THE SECOND KIND

n	$U_n(x)$
1	1
2	$2x$
3	$4x^2 - 1$
4	$8x^3 - 4x$
5	$16x^4 - 12x^2 + 1$

It can be shown that a formula similar to eqn. (3) may be written:

$$|\rho(\Delta\omega)| = \rho' . |g(\Delta\omega)U_n[f(\Delta\omega)]| \quad . \quad . \quad . \quad (6)$$

and that this represents the case where all the objects along the transmission line are identical. Here ρ' is a constant and the other symbols have the same meaning as in eqn. (3). The maxima of $|U_n(x)|$ are not all equal in the region $|x| \leqslant 1$ but increase as $|x| \to 1$ [note the denominator in eqn. (4)], so that eqn. (6) does not represent an optimum response, which can only be given by eqn. (3). However, $U_n(x)$ is of interest in representing the input reflection coefficient characteristics of a uniform non-tapered multi-element microwave component.[10]

(3) APPLICATION OF CHEBŸSHEV FUNCTIONS TO THE BROAD-BAND DESIGN OF MICROWAVE COMPONENTS

(3.1) Derivation of a Chebÿshev Response

Consider a waveguide with a number of discrete obstacles equi-spaced along it by electrical distances

$$\phi = \frac{2\pi l}{\lambda_g} \quad . \quad . \quad . \quad . \quad . \quad . \quad . \quad (7)$$

where l is the physical spacing of the obstacles and λ_g is the guide wavelength. The reflection coefficients of the obstacles are arranged so that the structure is symmetrical. For example, Fig. 2 shows four obstacles with reflection coefficients of moduli

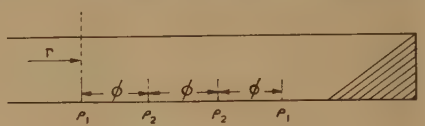

Fig. 2.—Four obstacles in a waveguide.

ρ_1, ρ_2, ρ_2, ρ_1, respectively, in a waveguide terminated by a matched load. It is assumed that the moduli of the reflection coefficients are all small, so that multiple reflections may be ignored, and that the spacing of the obstacles is sufficiently large to prevent the interaction of higher-order evanescent modes on adjacent obstacles. These restrictions are satisfied by a large class of microwave components (Section 4). The case of large reflection coefficients is treated in Section 5.

The input reflection coefficient of the four obstacles shown in Fig. 2 is

$$\Gamma = \rho_1 + \rho_2\varepsilon^{-2j\phi} + \rho_2\varepsilon^{-4j\phi} + \rho_1\varepsilon^{-6j\phi}$$
$$= (2\rho_1 \cos 3\phi + 2\rho_2 \cos\phi)\varepsilon^{-3j\phi} \quad . \quad . \quad . \quad (8)$$

Hence, putting $x = \cos\phi$,

$$|\Gamma| = |2\rho_1 T_3(x) + 2\rho_2 T_1(x)| \quad . \quad . \quad . \quad . \quad (9)$$
$$= |8\rho_1 x^3 - (6\rho_1 - 2\rho_2)x| \quad . \quad . \quad . \quad (10)$$

Here x is a frequency-dependent variable of the kind specified in Section 2.1, and a Chebÿshev response is obtained by putting

$$|\Gamma| = \gamma T_3(tx) \quad . \quad . \quad . \quad . \quad . \quad (11)$$

where γ is a constant equal to the maximum value of $|\Gamma|$ in the band, and t is a scale factor determining the width of the band, the limits being defined as the extreme points where $|\Gamma| = \gamma$. These occur when $tx = \pm 1$, i.e. where ϕ takes the values given by

$$\cos\phi_{lim} = \pm\frac{1}{t}, (t \geqslant 1) \quad . \quad . \quad . \quad . \quad (12)$$

In general, γ and t may be independently assigned.

From eqns. (10) and (11),

$$8\rho_1 x^3 - (6\rho_1 - 2\rho_2)x = \gamma(4t^3x^3 - 3tx)$$

Since coefficients of x and x^3 are independent they may be equated to give

$$\left.\begin{aligned} 8\rho_1 &= \gamma 4t^3 \\ 6\rho_1 - 2\rho_2 &= \gamma 3t \end{aligned}\right\} \quad . \quad . \quad . \quad . \quad (13)$$

i.e.

$$\left.\begin{aligned} \rho_1 &= \tfrac{1}{2}\gamma t^3 \\ \rho_2 &= \tfrac{3}{2}\gamma(t^3 - t) \end{aligned}\right\} \quad . \quad . \quad . \quad . \quad . \quad (14)$$

Now, the sum of the four reflection coefficients is

$$\Sigma\rho_i = 2(\rho_1 + \rho_2) = \gamma(4t^3 - 3t) = \gamma T_3(t)$$

i.e.
$$\gamma = \frac{\Sigma\rho_i}{T_3(t)} \quad . \quad . \quad . \quad . \quad . \quad . \quad (15)$$

Substituting this value of γ in eqn. (14),

$$\left.\begin{aligned} \rho_1 &= \tfrac{1}{2}\Sigma\rho_i \frac{t^3}{T_3(t)} \\ \rho_2 &= \tfrac{3}{2}\Sigma\rho_i \frac{(t^3 - t)}{T_3(t)} \end{aligned}\right\} \quad . \quad . \quad . \quad . \quad (16)$$

For a given value of $\Sigma\rho_i$, eqns. (12) and (15) show the relation between bandwidth and the maximum value of $|\Gamma|$ in that band. The larger the bandwidth, the smaller will be t, and the larger will be the maximum reflection coefficient in the band.

(3.2) Comparison with the Characteristic of the Binomial Design

In the binomial method of design the reflection coefficients are made proportional to the coefficients of the binomial expansion with the same number of coefficients as there are obstacles; e.g. for four obstacles the reflection coefficients would take the values ρ, 3ρ, 3ρ, and ρ, spaced at quarter-wavelength intervals. This is because all zeros of the input reflection coefficient are required to coincide at the mid-band or design frequency. Hence to obtain a binomial response the expression for $|\Gamma|$ given by eqn. (10) must contain only the highest power of x,

i.e.
$$|\Gamma| = |8\rho_1 x^3 - (6\rho_1 - 2\rho_2)x| = \gamma t^3 x^3 \quad . \quad . \quad (17)$$

so that
$$\left.\begin{aligned} \rho_1 &= \tfrac{1}{8}\gamma t^3 \\ \rho_2 &= \tfrac{3}{8}\gamma t^3 \end{aligned}\right\} \quad . \quad . \quad . \quad . \quad . \quad (18)$$

The sum of the four reflection coefficients is

$$\Sigma\rho_i = \gamma t^3$$

so that
$$\gamma = \frac{\Sigma\rho_i}{t^3} \quad . \quad . \quad . \quad . \quad . \quad . \quad (19)$$

The limits of the pass band are defined to the points where $|\Gamma| = \gamma$, i.e. where $tx = \pm 1$, as in the Chebyshev case [eqn. (12)]. Hence for the same bandwidth the ratio of the maximum values of the reflection coefficients in the pass band [see eqns. (15) and (19)] is

$$\frac{\gamma \text{ (Binomial)}}{\gamma \text{ (Chebyshev)}} = \frac{T_3(t)}{t^3} = 4 - 3/t^2, \ (t \geqslant 1) \quad . \quad (20)$$

i.e. the Chebyshev design gives a much smaller maximum reflection coefficient for the same bandwidth since $T_3(t) \geqslant 1$ for $t > 1$. For example, taking $t = 1{\cdot}5$, which is a value that might be used in practice, $T_3(t)/t^3 = 2{\cdot}67$, so that the improvement is considerable. It would mean an improvement from 0·875 v.s.w.r. in the binomial case to 0·95 in the Chebyshev case over the same band. The sum of the individual reflection coefficients is the same in both cases.

With four obstacles designed to give a Chebyshev response, it is seen from eqn. (16) that the individual reflection coefficients are staggered in the ratios

$$1 : 3(1 - 1/t^2) : 3(1 - 1/t^2) : 1 \quad . \quad . \quad . \quad (21)$$

whereas in the binomial case the corresponding ratios are

$$1 : 3 : 3 : 1 \quad . \quad . \quad . \quad . \quad . \quad . \quad (22)$$

Since $t > 1$ the ratio of the inner to the outer reflection coefficient is less in the Chebyshev design than in the binomial. This is true for any number of obstacles. Hence the assumption that the reflection coefficients are all small is more nearly satisfied. The fact that a smaller range of reflection coefficients or obstacles is needed in a Chebyshev design can be of considerable advantage, since it is often difficult to make small obstacles accurately in a waveguide. As an example, difficulty is often experienced in manufacturing the end slots in multi-slot directional couplers (Section 4.3). The advantage of the Chebyshev design is most marked in this respect when the number of obstacles is large, for then the binomial design becomes a very difficult manufacturing problem. For $(n + 1)$ obstacles the second reflection coefficient will be n times the first in the binomial design, and the largest will be greater than the smallest by the factor ${}_nC_{\frac{1}{2}n}$ for n even or ${}_nC_{\frac{1}{2}(n-1)}$ for n odd. These factors are very large for, say, $n = 9$ (9 and 126 respectively). It is obvious, then, that the first and last obstacles contribute very little to the design, since they are 'swamped' by the reflections from all other obstacles. They are required only to satisfy a theoretical formula for the input reflection coefficient. A large number of obstacles are also often required in the design of microwave filters (Section 5), and then there is again a considerable advantage in using the Chebyshev method, since the ratio between the Q-factors of the central and outer cavities becomes more manageable.

A general proof that the Chebyshev design is broader band than the corresponding binomial one has been given by Fano.[11] He has shown that it is not possible to match an arbitrary impedance over the whole frequency spectrum or even to all frequencies within a finite frequency band. The statement of the matching problem must include the maximum tolerance on the match as well as the minimum bandwidth in which the match is to be obtained. For a given initial mismatch and a given final tolerance, there is an upper limit to the bandwidth that can be obtained by means of a physically realizable network. This upper limit could be obtained only by an infinite number of lumped matching elements, and the closest approach to a given tolerance over the band is obtained by means of a Chebyshev function, or alternatively a Jacobian elliptic function. The smaller the initial mismatch, the fewer will be the number of lumped elements required to reach the final tolerance. As the binomial distribution utilizes a discontinuity greater than the corresponding one in the Chebyshev case, and since the remaining discontinuities constitute a matching network, the attainable bandwidth for a given acceptable v.s.w.r. will be less.

(4) EXAMPLES OF CHEBYSHEV DESIGN

(4.1) Quarter-Wave Stepped Transformers

It is often required to make a broad-band transition between two transmission lines or waveguides with different characteristic impedances. One method commonly employed is to use a uniformly tapered transition. However, an equally good transition can be made in a much shorter length by using the Chebyshev method. The only parameter in a uniform taper which can be varied to produce a better match is its length. On the other hand, there is an almost unlimited variety of stepped transitions in a given length and a Chebyshev design may be chosen. In addition, a stepped transition may be simpler to manufacture than a smooth taper.

The stepped transition may be derived using the theory described in Section 3.1 from the additional knowledge of the reflection coefficient at the junction of two waveguides. This may be calculated using Farmer's theory.[12] In the present context the major contribution to the reflection coefficient is

due to the change in characteristic impedance at the junction (lumped impedances being negligible in effect). If the ratio of the characteristic impedances Z_i, Z_{i+1} of any two waveguides is known, the reflection coefficient is given by the formula

$$\rho_i = \frac{Z_i - Z_{i+1}}{Z_i + Z_{i+1}} \quad . \quad . \quad . \quad . \quad . \quad (23)$$

This assumes that the effect of higher-order modes may be neglected at the junction, which is approximately true when the discontinuity is small. The reflection coefficient ρ_i can be written

$$\rho_i = \frac{Z_i - Z_{i+1}}{Z_i + Z_{i+1}} = \frac{\delta Z}{2Z_{av}} = \tfrac{1}{2}\delta\,(\log Z)$$

i.e.
$$\rho_i = \tfrac{1}{2}\,(\log Z_i - \log Z_{i+1})$$

$$= \tfrac{1}{2}\log\frac{Z_i}{Z_{i+1}} \quad . \quad . \quad . \quad . \quad . \quad . \quad . \quad (24)$$

Hence
$$\Sigma\rho_i = \tfrac{1}{2}\log\frac{Z_1}{Z_2} \quad . \quad . \quad . \quad . \quad . \quad . \quad . \quad (25)$$

where Z_1 and Z_2 are the characteristic impedances of the input and output waveguides. This condition states that the algebraic sum of the reflection coefficients at the junctions is equal to that reflection coefficient which would be observed at a direct connection of the input and output waveguides.

The analysis would now proceed as in Section 3.1.

(4.2) Stepped Twists

A uniformly twisted waveguide does not represent the optimum design in a given length for reasons similar to those given in Section 4.1 for the uniformly tapered transformer. A better performance in a shorter length of waveguide can be obtained by varying the rate of twist along its length. In practice this is done by making the twist in the form of a number of steps, the magnitude of which can be varied along the twist. The characteristics of a single-face step twist are given by Wheeler and Schwiebert,[13] who have shown that for small steps the reflection coefficient is proportional to the square of that angle of twist.

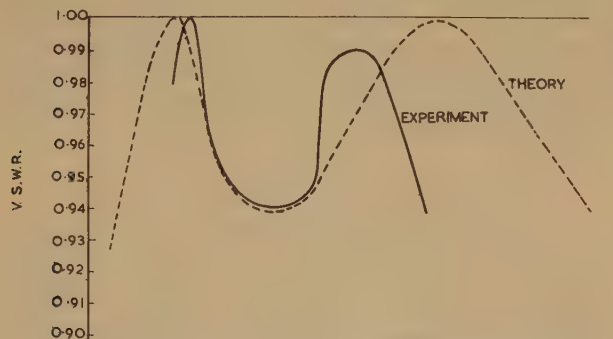

Fig. 3.—V.S.W.R. of a three-face two-step 45° twist.

However, they consider only binomial configurations, and as shown in Section 3.2, a much broader-band device may be obtained by using a Chebyshev form of taper. As a check on the design method, a two-step 45° twist was made of three equal 15°-step faces spaced at quarter-wavelength intervals; the results obtained are plotted in Fig. 3. The general theory of the three-face twist is as follows.

Consider three faces separated by equal electrical distances ϕ. The voltage reflection coefficients of the three faces are ρ_1, ρ_2, ρ_1, respectively, and therefore the input reflection coefficient is

$$\Gamma = \rho_1 + \rho_2\varepsilon^{-2j\phi} + \rho_1\varepsilon^{-4j\phi}$$

i.e.
$$|\Gamma| = |2\rho_1\cos 2\phi + \rho_2|$$
$$= |(\rho_2 - 2\rho_1) + 4\rho_1 x^2| \quad . \quad . \quad . \quad (26)$$

where $x = \cos\phi$.

The condition for Chebyshev response is

$$|\Gamma| = |\gamma T_2(tx)| = |\gamma(2t^2x^2 - 1)| \quad . \quad . \quad . \quad (27)$$

and hence, comparing eqns. (26) and (27),

$$\left.\begin{aligned}\rho_1 &= \tfrac{1}{2}t^2\gamma\\ \rho_2 &= (t^2-1)\gamma\end{aligned}\right\} \quad . \quad . \quad . \quad . \quad . \quad (28)$$

The angles of the step twists are made proportional to the square roots of ρ_1 and ρ_2. For simplicity of construction it is desirable to make all three angles of twist equal, so that in this case $\rho_1 = \rho_2 = \rho$ and $t = \sqrt{2}$, with input reflection coefficient given by

$$|\Gamma| = |\rho(4x^2 - 1)|,\ x = \cos\phi \quad . \quad . \quad . \quad (29)$$

The v.s.w.r. of a single-step twist of 15° angle for a waveguide with an aspect ratio* of 2 : 1 was measured over a 40% band, and was found to vary between 0·93 and 0·95, giving $\rho = 0{\cdot}03$ in eqn. (29). The v.s.w.r. corresponding to this value of $|\Gamma|$ for the three-face 45° twist section is plotted in Fig. 3 as a function of λ_g/λ_{g0}, where λ_{g0} is the guide wavelength at $\phi = \pi/2$, i.e. at a quarter-wavelength. The experimental result, on the same graph, shows fair agreement with theory except at large values of λ_g.

(4.3) Multi-Element Directional Couplers

The design of multi-element directional couplers may be improved by extending the analysis of Harrison[1] to cover the case of Chebyshev equal-ripple responses as well as the conventional binomial response. In the following analysis the case of a five-slot branched guide coupler is considered, although the results are applicable to any type of multi-element coupler.

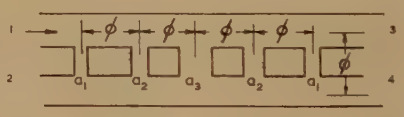

Fig. 4.—Five-slot branched-guide directional coupler.

Fig. 4 shows a five-slot branched-guide directional coupler with symmetrically arranged coupling elements of voltage coupling, a_1, a_2, a_3, a_2, a_1 respectively. The length of each slot and the spacing between adjacent slots is made equal to $\lambda_g/4$ at the design frequency. This is denoted by an electrical length ϕ at any frequency [eqn. (7)]. Following Harrison, for a wave of unit amplitude incident on arm 1 and matched on all other arms, the wave in arm 2 is equal to V, where

$$V = a_1 + a_2\varepsilon^{-2j\phi} + a_3\varepsilon^{-4j\phi} + a_2\varepsilon^{-6j\phi} + a_1\varepsilon^{-8j\phi} \quad (30)$$

i.e.
$$V = (2a_1\cos 4\phi + 2a_2\cos 2\phi + a_3)\varepsilon^{-4j\phi}$$

or
$$|V| = |2a_1\cos 4\phi + 2a_2\cos 2\phi + a_3| \quad . \quad . \quad (31)$$

The analysis now proceeds similarly to that given in Section 3.1 or 3.2. If all the zeros of $|V|$ are to be coincident at the design frequency, a binomial distribution of the a_i results. If a minimum value of $|V|$ over a given band is specified, a Chebyshev

* Ratio of the broad dimension to the narrow dimension of the waveguide.

design is more appropriate and the values of the voltage couplings are given by

$$\left.\begin{aligned} a_1 &= \frac{\Sigma a_i}{T_4(t)}\frac{1}{2}t^4 \\ a_2 &= \frac{\Sigma a_i}{T_4(t)}2(t^4 - t^2) \\ a_3 &= \frac{\Sigma a_i}{T_4(t)}(3t^4 - 4t^2 + 1) \end{aligned}\right\} \quad . \quad . \quad . \quad . \quad (32)$$

where the maximum value of the wave in arm 2 is

$$a_m = \frac{\Sigma a_i}{T_4(t)} \quad . \quad . \quad . \quad . \quad . \quad . \quad (33)$$

as may be seen by putting $x = 1$ in the relation

$$|V| = |2a_1T_4(x) + 2a_2T_2(x) + a_3| \equiv a_mT_4(tx)$$

Now the voltage coupling into arm 4 is equal to V_C, where

$$V_C\varepsilon^{-4j\phi} = \Sigma a_i \quad . \quad . \quad . \quad . \quad . \quad (34)$$

so that the voltage directivity represented by the wave a_m is equal to

$$D_V = \frac{a_m}{|V_C|} = \frac{1}{T_4(t)} \quad . \quad . \quad . \quad . \quad . \quad (35)$$

i.e. the worst directivity value in the band is equal to

$$D_{Ch} = 20 \log_{10} T_4(t) \text{ decibels} \quad . \quad . \quad . \quad (36)$$

The limits of the band are defined in eqn. (12). Taking a value for t of 1·6, these limits are found to be given by

$$\phi_{lim} = 51{\cdot}3° \text{ and } 128{\cdot}7°$$

which represents a guide wavelength variation of 2·5 : 1. Substituting $t = 1{\cdot}6$ in eqn. (12), the minimum directivity over this band is found to be about 30 dB. This may be compared with the theoretical directivity of the binomial coupler at the edges of the same band, which is given by

$$D_{Bin} = 20 \log_{10} (t^4) \text{ decibels} \quad . \quad . \quad . \quad (37)$$

and with $t = 1{\cdot}6$ this is 16·3 dB.

Even though in an actual coupler the theoretical directivity is rarely obtained, the above theory indicates that a Chebyshev design is likely to possess a broader-band performance than the corresponding coupler designed with the conventional binomial response. Another advantage of the Chebyshev design, the smaller ratio of the largest to the smallest coupling slot, was mentioned in Section 3.2. Thus, for five slots the couplings are staggered in the ratio

$$1 : 4\left(1 - \frac{1}{t^2}\right) : 6\left(1 - \frac{4}{3t^2} + \frac{1}{3t^4}\right) : 4\left(1 - \frac{1}{t^2}\right) : 1 \quad (38)$$

which for $t = 1{\cdot}6$ becomes 1 : 2·44 : 3·18 : 2·44 : 1, compared with the binomial distribution of 1 : 4 : 6 : 4 : 1. The ratio of largest to smallest coupling in the Chebyshev design is nearly halved. Thus, the Chebyshev coupler is mechanically easier to manufacture in small waveguides, where for the above design the outer slots are nearly twice as wide as in the corresponding binomial design. This difficulty is mentioned by Lomer and Crompton.[14]

The dimensions and performance of a five-slot 3 dB branched-guide Chebyshev coupler with $t = 1{\cdot}6$ are shown in Fig. 5, and a five-slot binomial coupler is shown in Fig. 6. Modifications to the theoretical design (Fig. 4) have been included to allow

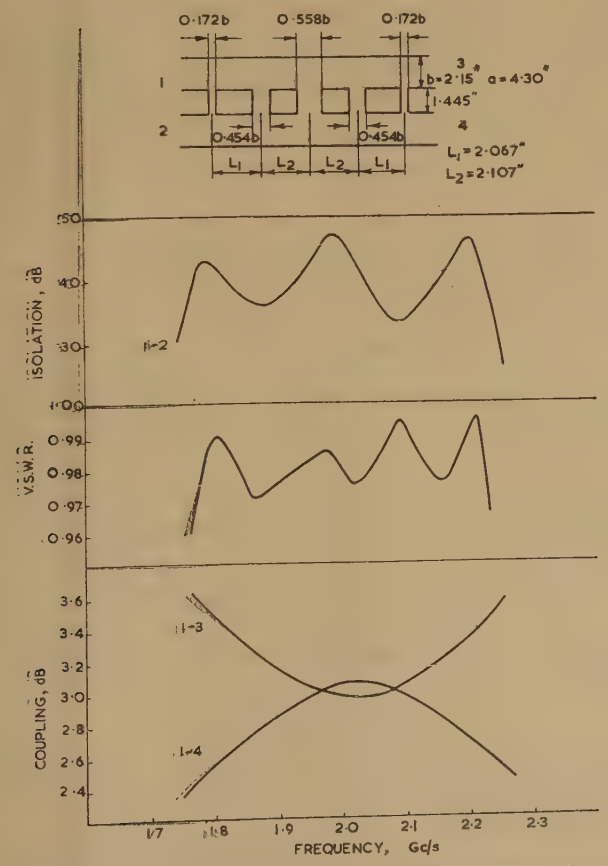

Fig. 5.—Five-slot 3 dB Chebyshev directional coupler in W.G.8.

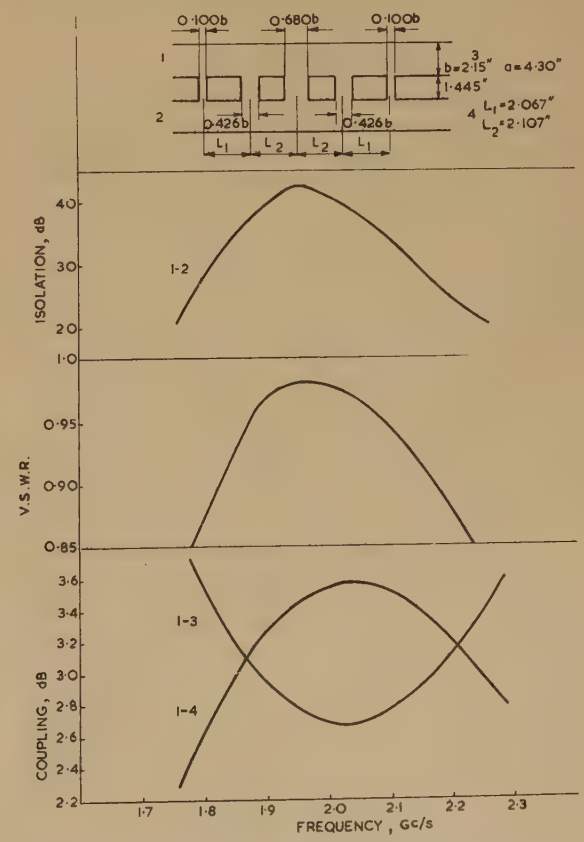

Fig. 6.—Five-slot 3 dB binomial directional coupler in W.G.8.

for end-effects and tight coupling.[1] If equal coupling at the design frequency is taken as the criterion, it is clear that these couplers are not directly comparable, but it is evident that the performance of the Chebŷshev coupler is superior, and if the binomial coupler were optimized for coupling, the Chebŷshev coupler would still possess the better performance.

(5) APPLICATION OF CHEBŸSHEV FUNCTIONS TO THE DESIGN OF MICROWAVE FILTERS

(5.1) Early Design Methods

The design of Chebŷshev filters in the r.f. bands where lumped circuit parameters are used is now well known,[15] but only comparatively recently has the method been extended to waveguide filters[8] owing to the difficulty of calculating the effects of a number of large discontinuities. Previously only two types of waveguide filters had been described. The first is known as the maximally-flat filter[16] and corresponds to a binomial taper design, since the filter is perfectly matched in its pass band only at the design frequency, i.e. the roots of the insertion loss/frequency deviation function are all equal to zero and coincide at the mid-band frequency to which the filter is tuned. This design is achieved by tapering the loaded Q-factors of the cavities according to a sine-law relationship.[16] It may be noted here that in a multi-cavity microwave filter all cavities are tuned to the same frequency in order to obtain minimum pass-band insertion loss and for ease of theoretical calculation. Different filter responses are obtained by varying the loaded Q-factors of the cavities, i.e. the couplings between adjacent cavities.

The second type of filter previously described consists of a number of identical cavities coupled together by either quarter-wave[10] or direct[17] couplings. This has been called a Chebŷshev filter,[10] since the response curve is given by the formula

$$L = 1 + [x\mathrm{U}_n(x)]^2 \quad . \quad . \quad . \quad . \quad . \quad (39)$$

where L is the insertion loss, x is a frequency-dependent variable equal to zero at the design frequency, n is the number of cavities and $\mathrm{U}_n(x)$ is the rationalized Chebŷshev polynomial of the second kind, of degree $(n-1)$ (Section 2.2). However, for $n \geqslant 3$ this response curve always contains two or more insertion-loss peaks in the pass band which rapidly increase in magnitude as n increases. For example, for $n = 4$ they are equal to 0·97 dB, and hence this type of filter is practically useless for a large number of cavities. It is not a true Chebŷshev filter, but may be referred to as the Chebŷshev equal-cavity filter, not to be confused with the Chebŷshev equal-ripple filter.

The equal-cavity filter does possess the advantage that the attenuation outside the pass band increases far more rapidly than in the case of the maximally flat filter, which, however, has the better response in the pass band. A compromise between the two filters is necessary, i.e. one with high attenuation outside the pass band consistent with a tolerably low pass-band insertion loss. A step in this direction was taken by the introduction of the concept of the generalized filter, i.e. one with the Q-factor of the cavities tapered in a quite general way. An analysis of the resulting configuration has been made for filters with six cavities or less, but the results are often complex and the equations become unwieldy for more than four cavities.[17, 18] In addition, for any filter with an even number of cavities, whose response in general may contain a centre-band mismatch, the method applies only to the special case of responses with zero centre-band mismatch. On the other hand, the analysis of the generalized filter is particularly instructive and useful in the case of three cavities, for the resulting design is always a Chebŷshev equal-ripple filter.

(5.2) Cohn's Method for the Equal-Ripple Chebŷshev Response Filter

A narrow-band Chebŷshev equal-ripple filter cannot be designed by the method given in Section 3.1, for the assumption that the reflection coefficients are small is far from true. The individual obstacles may have reflection coefficients which approach unity. The only method is to synthesize the filter from the desired insertion-loss function by the procedure first discovered by Darlington[19] (described briefly in Ragan, Reference 2, p. 580). The results of the method applied to microwave filters are given in a paper by S. B. Cohn.[8] Here, not only are design formulae given for Chebŷshev equal-ripple narrow-band filters, but also equally accurate formulae for comparatively wide-band filters, i.e. those with bandwidths greater than about 1%. Experimentally good agreement has been obtained with direct-coupled filters of up to ten cavities with bandwidths of up to 12%.

It has been found possible to simplify Cohn's formulae to some extent as an aid to computation, and the revised theory for waveguide filters with equal-ripple Chebŷshev characteristics is presented below.

The filter consists of a number of waveguide cavities formed by inductive susceptances, spaced at approximately half-wavelength intervals. The cavities are coupled directly in cascade, so that each susceptance, except the two at the ends of the filter, is common to two cavities. The filter response is symmetrical with respect to guide wavelength λ_g rather than to frequency, and the optimum response is given as a function of λ_g by the formula

$$L = 1 + \frac{(1-s)^2}{4s}\mathrm{T}_n^2\left[\frac{\frac{1}{2}(\lambda_{g1}+\lambda_{g2}) - \lambda_g}{\frac{1}{2}(\lambda_{g1}-\lambda_{g2})}\right] \quad . \quad (40)$$

where L is the insertion loss and n is the number of cavities. The pass band is defined by λ_{g1} and λ_{g2}, the values of λ_g at its edges, and s is the worst v.s.w.r. in this band. From the properties of the Chebŷshev polynomial it can be seen that there will be $(n-1)$ equal ripples in the pass band with the v.s.w.r. varying between unity and a prescribed value of s.

The normalized susceptances in the filter are arranged in the sequence

$$b_{01};\ b_{12};\ b_{23};\ \ldots,\ b_{n-1,n};\ b_{n,n+1} \quad . \quad . \quad (41)$$

and the distance d_i between the susceptances $b_{i-1,i}$ and $b_{i,i+1}$, i.e. the length of the ith cavity is given by

$$\phi_i = \frac{2\pi d_i}{\frac{1}{2}(\lambda_{g1}+\lambda_{g2})} = \frac{1}{2}\left(\arctan\frac{2}{b_{i-1,i}} + \arctan\frac{2}{b_{i,i+1}}\right) \quad (42)$$

Since the susceptances are inductive, b *is* negative and ϕ_i is chosen so that

$$\frac{\pi}{2} < \phi_i < \pi \quad . \quad . \quad . \quad . \quad . \quad (43)$$

To obtain a Chebŷshev response in the given band, the required susceptances are

$$b_{i,i+1} = \frac{g_0}{\sqrt{(g_i g_{i+1})}} - \frac{\sqrt{(g_i g_{i+1})}}{g_0} \quad . \quad . \quad (44)$$

where g_0 is a number dependent on the bandwidth of the filter, i.e.

$$g_0 = \frac{|\lambda_{g1}-\lambda_{g2}|}{\lambda_{g1}+\lambda_{g2}}\pi \quad . \quad . \quad . \quad . \quad . \quad (45)$$

and the response shaping factors g_i, which are dependent on the number of cavities, n, the worst v.s.w.r. in the pass band, s, are given by the formulae

$$g_1 = 2\sin\frac{\pi}{2n} \Big/ \sinh\left(\frac{1}{n}\operatorname{arc\,sinh}\frac{2\sqrt{s}}{1-s}\right) \quad . \quad . \quad (46)$$

$$g_i g_{i+1} = 4 \sin\frac{(2i-1)\pi}{2n} \sin\frac{(2i+1)\pi}{2n} \Big/ \left[\sinh^2\left(\frac{1}{n}\operatorname{arc\,sinh}\frac{2\sqrt{s}}{1-s}\right) + \sin^2\frac{i\pi}{n}\right] \quad i = 1, 2, 3 \ldots (n-1) \quad (47)$$

$$g_{n+1} = \left\{\begin{matrix} g_0 \ldots (n \text{ odd}) \\ g_{0/s} \ldots (n \text{ even}) \end{matrix}\right\} \quad . \quad . \quad . \quad (48)$$

The normal forms of obstacles used in waveguide filters are the inductive post structures[21, 22, 23, 24] and the circular aperture,[25] the former generally being preferred in waveguide for mechanical reasons. Fig. 7 shows the performance of a nine-

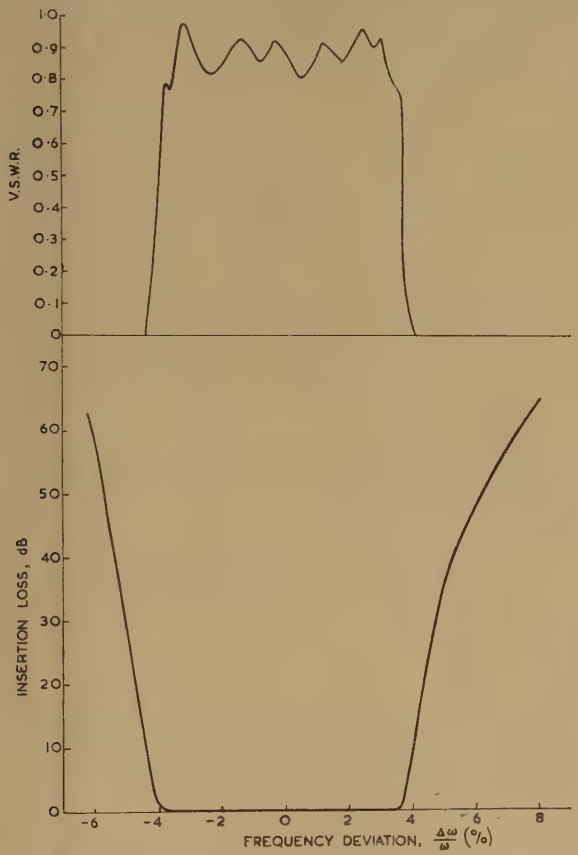

Fig. 7.—Nine-cavity Chebyshev filter.

cavity filter designed to give eight dips of v.s.w.r. 0·85 in the pass band. In practice, some of these are smoothed out by the finite insertion loss in the pass band of about 0·5 dB and by mechanical errors, but the attenuation outside this band is in almost exact agreement with the theoretical value given by eqn. (40). This filter gives an identical performance whether manufactured in brass waveguide with soldered copper posts and a silver-flash finish or in aluminium waveguide using aluminium posts fixed in position by a salt-bath brazing method. It is worthy of note that this filter was designed entirely by theory, with only small experimental corrections to allow for the finite thickness of the inductive obstacles. No tuning screws are required if the tolerances are held to within reasonably close limits.

(6) REFERENCES

(1) HARRISON, R. J.: 'Design Considerations for Directional Couplers', Massachusetts Institute of Technology, Radiation Laboratory Report No. 724.

(2) HALFORD, G. J.: 'A Wide Band Waveguide Phase Shifter', *Proceedings I.E.E.*, Paper No. 1466, May, 1953 (**100**, Part III, p. 117).

(3) DOLPH, C. L.: 'A Current Distribution for Broadside Arrays which Optimises the Relationship between Beam Width and Side-Lobe Level', *Proceedings of the Institute of Radio Engineers*, 1946, **34**, p. 335.

(4) COLLIN, R. E.: 'Theory and Design of Wide-Band Multisection Quarter-Wave Transformers', *ibid.*, 1955, **43**, p. 179.

(5) COHN, S. B.: 'Optimum Design of Stepped Transmission-Line Transformers', *Transactions of the Institute of Radio Engineers*, 1955, **MTT-3**, p. 36.

(6) RIBLET, H. J.: 'General Synthesis of Quarter-Wave Impedance Transformers', *ibid.*, 1957, **MTT-5**, p. 36.

(7) TUROVYER, Y. M., and STRUTINSKY, N. I.: 'The Use of Chebyshev Polynomials for the Design of Stepped Transitions', *Radiotekhnika i Elektronika*, 1956, No. 2, p. 143.

(8) COHN, S. B.: 'Direct-Coupled Resonator Filters', *Proceedings of the Institute of Radio Engineers*, 1957, **45**, p. 187.

(9) DUHAMEL, R. H.: 'Optimum Patterns for Endfire Arrays', *ibid.*, **41**, 1953, p. 653.

(10) PRITCHARD, W. L.: 'Quarter-Wave Coupled Waveguide Filters', *Journal of Applied Physics*, 1947, **18**, p. 862.

(11) FANO, R. M.: 'Theoretical Limitation on the Broad-Band Matching of Arbitrary Impedances', *Journal of the Franklin Institute*, 1950, **249**, pp. 57 and 139.

(12) FARMER, E. D.: 'Junction Admittance between Waveguide of Arbitrary Cross-Sections', *Proceedings I.E.E.*, Monograph No. 148 R, September, 1956 (**103** C, p. 145).

(13) WHEELER, H. A., and SCHWIEBERT, H.: 'Step-Twist Waveguide Components', *Transactions of the Institute of Radio Engineers*, 1955, **MTT-3**, p. 44.

(14) LOMER, P. D., and CROMPTON, J. W.: 'A New Form of Hybrid Junction for Microwave Frequencies', *Proceedings I.E.E.*, Paper No. 2356 R, May, 1957 (**104** B, p. 261).

(15) SKWIRZINSKI, J., and ZDUNEK, J. K.: 'Design Data for Symmetrical Darlington Filters', *Proceedings I.E.E.*, Monograph No. 227 R, September, 1957 (**104** C, p. 366).

(16) MUMFORD, W. W.: 'Maximally Flat Filters in Waveguide', *Bell System Technical Journal*, 1948, **27**, p. 684.

(17) LEVY, R.: 'An Improved Design Procedure for the Multi-Section Generalized Microwave Filter', *Proceedings I.E.E.*, Monograph No. 233 R, September, 1957 (**104** C, p. 173).

(18) POTOCK, M. H. N.: 'The Design of Inductive Post-Type Microwave Filters', *Journal of the British Institution of Radio Engineers*, 1958, **18**, p. 263.

(19) DARLINGTON, S.: 'Synthesis of Reactance Four-Poles which produce Prescribed Insertion Loss Characteristics, including Special Applications to Filter Design', *Journal of Mathematics and Physics*, 1939, **18**, p. 257.

(20) RAGAN, G. L.: 'Microwave Transmission Circuits' (McGraw-Hill, 1958).

(21) MARCUVITZ, N.: 'Waveguide Handbook' (McGraw-Hill, 1951), p. 257.

(22) SIMON, J. C., and BROUSSAUD, G.: 'Les filtres passe-bande en hyperfréquence', *Annales de Radioélectricité*, 1953, **3**, p. 8.

(23) GRUENBERG, H.: 'Symmetrically Placed Inductive Posts in Rectangular Waveguide', *Canadian Journal of Physics*, 1952, **30**, p. 211.

(24) CRAVEN, G., and LEWIN, L.: 'Design of Microwave Filters with Quarter-Wave Couplings', *Proceedings I.E.E.*, Paper No. 2001 R, 1956 (**103** B, p. 173). Discussions, *ibid.* (**103** B, p. 632; **104** B, p. 528; **105** B, p. 395).

(25) SHNURER, F.: 'Design of Aperture-Coupled Filters', *Transactions of the Institute of Radio Engineers*, 1957, **MTT-5**, p. 238.

621.315.14:621.319.7

The Institution of Electrical Engineers
Monograph No. 338 S
June 1959

THE ELECTRIC FIELD NEAR BUNDLE CONDUCTORS

By S.-Y. KING, B.Sc.(Eng.), Ph.D., Associate Member.

(*The paper was first received* 29*th May*, 1958, *and in revised form* 17*th February*, 1959. *It was published as an* INSTITUTION MONOGRAPH *in June*, 1959.)

SUMMARY

The electric field surrounding bundle conductors can be determined by replacing each conductor of the bundle by one of negligible radius displaced slightly from the centre of the original conductor. This is based on the fact that equipotential surfaces near such a thin conductor are nearly cylindrical, so that an actual conductor may be so placed as to take up the position of one of the equipotentials. The accuracy of the method depends on the ratio, D/d, between the diameter of the bundle circle and that of each conductor; the greater the ratio, the more accurate is the method. With the ratios usually found in high-voltage transmission lines, the deviation of the equipotential surface from a true cylinder is small, and it can be arranged that the deviation is zero at the point of maximum surface gradient. Maximum deviation from the surface of a cylinder occurs somewhere between points of maximum and minimum gradients. For example, with a bundle of two conductors and $D/d = 10$, this maximum deviation does not exceed 0·5%; with $D/d = 20$ it is about 0·1%.

The analysis deals with single-phase lines with a bundle of 2, 3 or 4 conductors, but it can be extended to cover any number of conductors in a bundle. For 3-phase lines the resultant field can be found by the principle of superposition when the fields due to the two other phases are taken into consideration. In the latter case, the electric charge per metre of each phase is to be determined with all the three phases and their images involved.

Formulae giving the potential gradient at any point on a conductor surface are developed and compared with those given by Cahen.[1] The method is checked by experimental field mapping using a circular double-layer electrolytic tank.

LIST OF PRINCIPAL SYMBOLS

$d = 2r$ = Diameter of each conductor.
$D = 2R$ = Diameter of bundle circle.
n = Number of conductors in a bundle.
q = Charge per unit length of each conductor.
$E_m = q/\epsilon_0 2\pi r$ = Surface field on conductor of radius r and charge q per unit length, q being uniformly distributed over the conductor.
V = Potential of bundle conductors relative to earth.
H = Height of centre of bundle circle above ground.
δ = Displacement of equivalent conductor from the centre of the original conductor.
r_0 = Radius of equivalent conductor, which is negligibly small compared with r.
$D_0 = D + 2\delta = 2R_0$.
V_0 = Potential of equivalent conductor relative to earth.
AB . . . G . . . N are centres of actual conductors in a bundle.
$A_0B_0 \ldots G_0 \ldots N_0$ are centres of equivalent conductors.

(1) INTRODUCTION

With the expansion of electric power-supply systems, higher transmission voltages, such as 275, 287, 380 and 400 kV, have been introduced for reasons of economy. In order to avoid excessive corona loss, special types of conductor have been designed to reduce the maximum electric field at their surfaces. In one design, each phase employs a bundle of two or more conductors, with a total section equal to the economic section; this arrangement also reduces the line reactance—a desirable feature in long-distance a.c. transmission.

Poritsky[2] and Quilico[3] have analysed the electric field near a bundle of two conductors by means of conformal mapping, while Cahen and Pelissier[1, 4] have deduced a very simple approximate expression for calculating the electric field on a conductor surface in a bundle of any number of conductors. A method is proposed in the paper of calculating the field near bundle conductors based on a simple physical representation. When parallel, thin conductors are placed symmetrically on the periphery of a circle, each carrying an equal charge per unit length, the equipotential surfaces very close to any conductor will be found to be nearly cylindrical. Each equivalent conductor has a very small radius, so that the distribution of charge over its surface will be uniform; at the same time, with a finite radius, the surface potential gradient will be finite, although very high, because of the small radius. The actual bundle conductors are now identified with suitable nearly-cylindrical equipotentials of the thin-wire arrangement.

Throughout the paper, only single-phase lines are considered, with the effect of earth on the distribution of charge over a conductor surface neglected. The information given in the paper would still be useful for 3-phase lines, but with the following additional remarks:

(*a*) The distribution of charge on a conductor surface is assumed to be unaffected by the presence of charges in the other phases.
(*b*) The charge, q, on each conductor is to be determined with all the three phases involved, as well as the effect of earth.
(*c*) The resultant field is, by the principle of superposition, the sum of fields due to all the charges in the three phases.

(2) EQUIPOTENTIAL LINES NEAR A BUNDLE OF VERY SMALL PARALLEL CYLINDERS

Fig. 1 shows a single-phase line with a bundle of n conductors, each of radius r_0 and carrying a positive charge q per unit length, r_0 being negligible compared with R_0. By neglecting the effect of electric images, the potential, V_p, at point P relative to

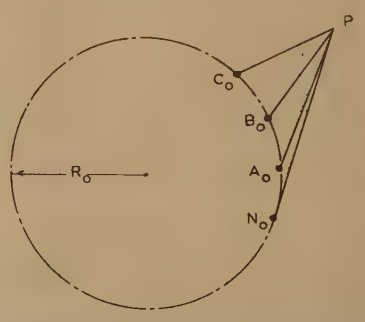

Fig. 1.—A bundle of n conductors whose radii are negligible.

Correspondence on Monographs is invited for consideration with a view to publication.
Dr. King is in the Department of Civil Engineering, University of Hong Kong.

the potential, V_0, of the bundle can be determined in the usual way:

$$V_p - V_0 = -\frac{q}{\epsilon_0 2\pi} \log_e \frac{A_0P \times B_0P \times \ldots \times N_0P}{r_0 \times B_0A_0 \times \ldots \times N_0A_0}$$

Point P will trace an equipotential path if the product $A_0P \times B_0P \times \ldots \times N_0P$ is constant, say equal to $K_nR_0^n$. We can thus define an equipotential line by giving to it a certain value of K_n. Hence

$$V_p - V_0 = -\frac{q}{\epsilon_0 2\pi} \log_e \frac{K_nR_0^n}{r_0 \times B_0A_0 \times \ldots \times N_0A_0} \qquad (1)$$

Fig. 2 shows examples of equipotential lines surrounding bundles of two and three conductors respectively. On account of the

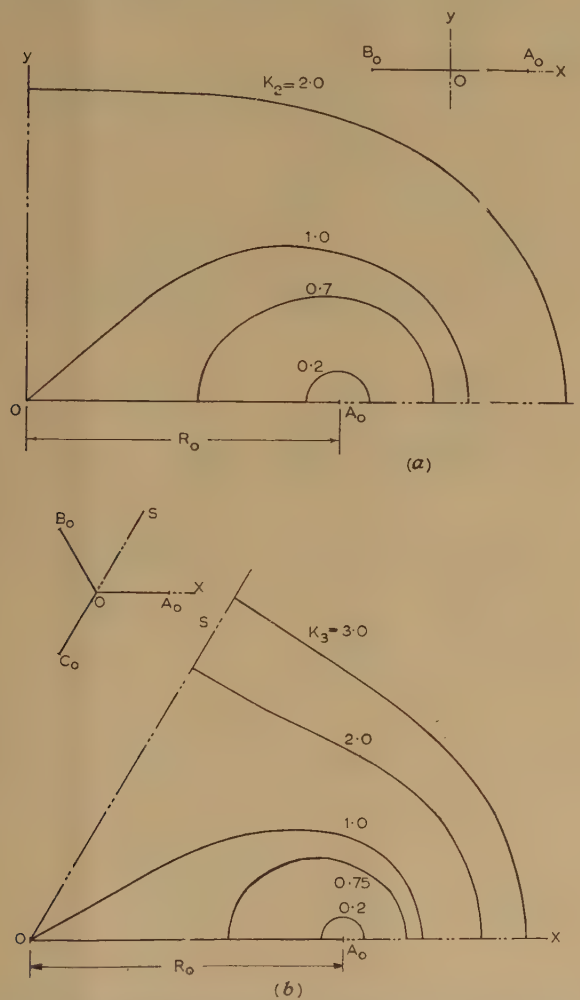

Fig. 2.—Equipotential lines surrounding a bundle of conductors.
(*a*) Two conductors.
(*b*) Three conductors.

symmetry, the field is shown only in part in each case. It can be seen that when K_n is small the locus is nearly a circle.

Section 9.1 explains the construction of equipotential lines in a bundle of two or more conductors.

(3) EQUIPOTENTIAL LINES NEAR A BUNDLE OF PARALLEL CYLINDERS WHOSE RADII ARE NOT NEGLIGIBLE

It has been seen that when K_n is small the equipotential lines near a bundle of very small parallel cylinders are nearly circles. (The deviation of these lines from true circles will be studied in detail in Section 3.2.) On replacing the bundle conductors by a set of such suitable equipotential lines, the electric field near the bundle conductors can be determined, as in Section 2, by substituting for them equivalent conductors each of a very small radius r_0. Thus, the boundaries of the bundle conductors are now circular equipotentials produced by the equivalent conductors which have the same charge per unit length as that of the original conductors. In practice, the ratio of the diameter of the bundle circle to that of each conductor is known. It is necessary to find the value of K_n corresponding to the contours of the bundle conductors.

(3.1) Relation Between D/d and K_n

At values of K_n below about 0·3 the equipotentials can be assumed to be circular in shape, as shown in Fig. 3. A, B, . . . G, . . . N are centres of the actual conductors each of radius r,

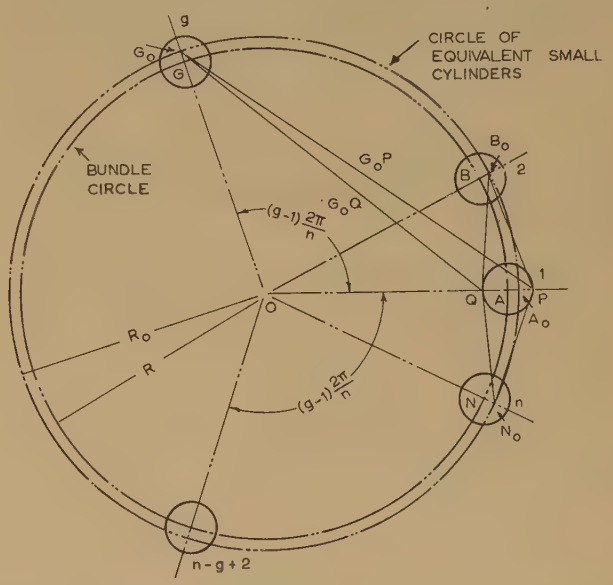

Fig. 3.—A bundle of n conductors whose radii are not negligible.

and $A_0, B_0 \ldots G_0 \ldots N_0$ are the centres of equivalent conductors each of very small radius r_0. Consider a given equipotential surface passing through P and Q and lying on the radial line through the centre of the bundle circle; for point P ($OP = X_1$),

$$A_0P \,.\, B_0P \,.\, C_0P \ldots G_0P \ldots N_0P = K_nR_0^n$$

From symmetry, the product of these lengths is equal to the product of the corresponding vectors. Then, since

$$G_0P = X_1 - R_0\left[\cos\frac{2(g-1)\pi}{n} + j\sin\frac{2(g-1)\pi}{n}\right]$$

we find

$$\prod_{g=1}^{n}\left\{X_1 - R_0\left[\cos\frac{2(g-1)\pi}{n} + j\sin\frac{2(g-1)\pi}{n}\right]\right\} = K_nR_0^n$$

But, by de Moivre's theorem, the above product is the product of all the simple factors of $X_1^n - R_0^n$. Hence

$$X_1^n - R_0^n = K_nR_0^n \quad . \quad . \quad . \quad . \quad . \quad (2)$$

Similarly, for point Q ($OQ = X_2$),

$$A_0Q \,.\, B_0Q \,.\, C_0Q \ldots G_0Q \ldots N_0Q = K_nR_0^n$$

and

$$\prod_{g=1}^{n}\left\{R_0\left[\cos\frac{2(g-1)\pi}{n}+j\sin\frac{2(g-1)\pi}{n}\right]-X_2\right\}=K_nR_0^n$$

i.e.
$$R_0^n-X_2^n=K_nR_0^n \quad . \quad . \quad . \quad . \quad . \quad (3)$$

Solving eqns. (2) and (3) simultaneously gives

$$K_n=\frac{X_1^n-X_2^n}{X_1^n+X_2^n} \text{ and } R_0^n=\tfrac{1}{2}(X_1^n+X_2^n)$$

Replacing X_1 by $\frac{1}{2}(D+d)$ and X_2 by $\frac{1}{2}(D-d)$ gives

$$K_n=\frac{\left(\frac{D}{d}+1\right)^n-\left(\frac{D}{d}-1\right)^n}{\left(\frac{D}{d}+1\right)^n+\left(\frac{D}{d}-1\right)^n} \quad . \quad . \quad . \quad (4)$$

$$R_0^n=\frac{d^n}{2^{n+1}}\left[\left(\frac{D}{d}+1\right)^n+\left(\frac{D}{d}-1\right)^n\right] \quad . \quad . \quad (5)$$

and $\delta = AA_0$ = Displacement of equivalent conductor from the centre of the original conductor.

$$=R_0-R$$

$$=\frac{d}{2}\sqrt{\left\{\frac{1}{2}\left[\left(\frac{D}{d}+1\right)^n+\left(\frac{D}{d}-1\right)^n\right]\right\}}-\frac{D}{2} \quad . \quad (6)$$

Fig. 4 shows the relation between D/d and K_n for $n = 2$, 3 and 4 respectively.

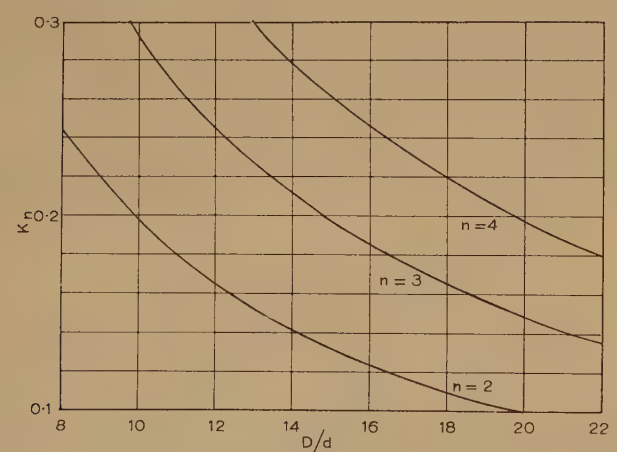

Fig. 4.—Relationship between K_n and D/d.

To determine the electric field around bundle conductors with a known ratio of D/d, it is necessary to find the corresponding value of K_n in order to locate the position of equivalent conductors. K_n can be calculated by eqn. (4) or read directly from Fig. 4.

(3.2) Deviation of Equipotential Lines from True Circles

Consider one of the bundle conductors in Fig. 5 and compare the equipotential passing through P and Q and the circle passing through the same points. The circle, which is the actual conductor periphery, has radius r and centre A as shown in Fig. 5.

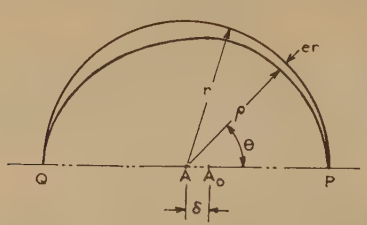

Fig. 5.—Deviation of equipotential line from true circle.

Let (ρ, θ) be the polar co-ordinates of the equipotential with the origin at A, and let e be the deviation of ρ from r per unit of r. Thus $\rho = (1 - e)r$. Section 9.2 gives the derivation of e in terms of θ for $n = 4$. For other values of n the same procedure can be followed:

(*a*) $n = 2$.

$$e=\frac{[1-\sqrt{(1-k_2^2)}]\sin^2\theta}{2\left\{2+K_2\cos\theta-[1-\sqrt{(1-K_2^2)}]\cos^2\theta\right\}} \quad . \quad (7)$$

(*b*) $n = 3$.

$$e=\frac{r^6+A_5r^5+A_4r^4+A_3r^3+A_2r^2+A_1r+A_0}{6r^6+5A_5r^5+4A_4r^4+3A_3r^3+2A_2r^2+A_1r} \quad (8)$$

where $A_5 = 6R\cos\theta$

$A_4 = 3R^2(4\cos^2\theta+1)$

$A_3 = 6(2R^3+R_0^3)\cos\theta-8(R_0^3-R^3)\cos^3\theta$

$A_2 = 3R(R^3+R_0^3)-12(R_0^3-R^3)R\cos^2\theta$

$A_1 = -6(R_0^3-R^3)R^2\cos\theta$

$A_0 = (R_0^3-R^3)^2-K_3^2R_0^6$

(*c*) $n = 4$.

$$e=\frac{r^8+B_7r^7+B_6r^6+B_5r^5+B_4r^4+B_3r^3+B_2r^2+B_1r+B_0}{8r^8+7B_7r^7+6B_6r^6+5B_5r^5+4B_4r^4+3B_3r^3+2B_2r^2+B_1r} \quad . \quad . \quad . \quad . \quad (9)$$

where $B_7 = 8R\cos\theta$

$B_6 = 4R^2(6\cos^2\theta+1)$

$B_5 = 8R^3\cos\theta(3+4\cos^2\theta)$

$B_4 = 6R^4-2R_0^4+16(3R^4+R_0^4)\cos^2\theta+16(R^4-R_0^4)\cos^4\theta$

$B_3 = 8R\cos\theta\,[3(R_0^4+R^4)+4(R^4-R_0^4)\cos^2\theta]$

$B_2 = 24R^2(R^4-R_0^4)\cos^2\theta+4R^2(R^4+3R_0^4)$

$B_1 = 8R^3(R^4-R_0^4)\cos\theta$

$B_0 = (R_0^4-R^4)-K_4^2R_0^8$

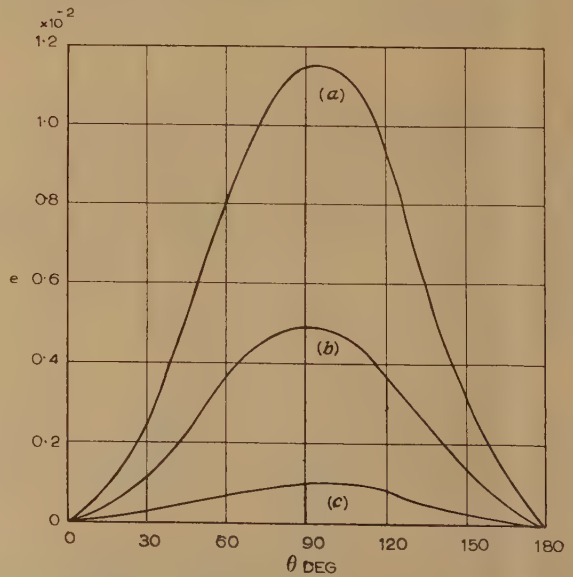

Fig. 6.—Variation of e with θ for $n = 2$.

(*a*) $K_2 = 0{\cdot}3$, $D/d = 6{\cdot}51$.
(*b*) $K_2 = 0{\cdot}2$, $D/d = 9{\cdot}90$.
(*c*) $K_2 = 0{\cdot}1$, $D/d = 19{\cdot}95$.

Fig. 6 shows the variation of e with θ for $n = 2$. Similar curves are obtained for $n = 3$ and $n = 4$. It can be seen that e is zero at $\theta = 0°$ and 180° and the maximum error occurs somewhere near $\theta = 90°$. When $\theta = 0$ we have the position for maximum surface gradient, and the deviation from a true circle in this region is a minimum. This is a desirable feature, since the maximum electric stress is of interest to transmission engineers.

(4) ELECTRIC FIELD AT CONDUCTOR SURFACE

The electric field at any point on a conductor surface is influenced, not only by the charge on this conductor, but also by other charges in the bundle. In the following analysis, $E_m = (q/\epsilon_0 2\pi r)$.

(4.1) Electric Field on Conductor Surface due to its own Charge [Fig. 7(*a*)]

Let ${}_{A_0}E_\theta$ be the electric field at Z due to the equivalent charge at A_0. Then

$$ {}_{A_0}E_\theta = \frac{q\left(\frac{d\beta}{2\pi}\right)}{\epsilon_0 r d\theta \cos(\beta - \theta)} $$

This field is along the direction of A_0Z and hence its normal component to the surface of the conductor, at Z, is given by

$$ {}_{A}E_\theta = {}_{A_0}E_\theta \cos(\beta - \theta) $$

$$ = \frac{q\left(\frac{d\beta}{2\pi}\right)}{\epsilon_0 r d\theta} $$

$$ = E_m r(r - \delta\cos\theta)/(r^2 + \delta^2 - 2r\delta\cos\theta) \quad . \quad (10) $$

(4.2) Electric Field at Conductor Surface due to other Charges in the Bundle

(*a*) $n = 2$ [Fig. 7(*b*)]

${}_{B}E_\theta$ = Electric field at Z due to the equivalent charge at B_0.

$$ = \frac{q}{\epsilon_0 2\pi B_0 Z}\cos \angle B_0 Z A $$

$$ = E_m r \frac{r + (D + \delta)\cos\theta}{(D + \delta)^2 + 2(D + \delta) r\cos\theta + r^2} \quad . \quad . \quad . \quad (11) $$

(*b*) $n = 3$ [Fig. 7(*c*)].

${}_{B}E_\theta + {}_{C}E_\theta$ = Electric field at Z due to equivalent charges at B_0 and C_0 respectively.

$$ = \frac{q}{\epsilon_0 2\pi}\left(\frac{\cos \angle B_0 Z A}{B_0 Z} + \frac{\cos \angle C_0 Z A}{C_0 Z}\right) $$

$$ = E_m\left\{1 - \frac{(\frac{3}{4}D^2 + \frac{3}{2}D\delta + \delta^2 - r^2)[\frac{3}{4}D^2 + \frac{3}{2}D\delta + \delta^2 + r^2 + (\frac{3}{2}D + \delta) r\cos\theta](r^2 - 2r\delta\cos\theta + \delta^2)}{K_3^2 (D/2 + \delta)^6}\right\} \quad . \quad . \quad . \quad (12) $$

(*c*) $n = 4$.

${}_{B}E_\theta + {}_{C}E_\theta + {}_{D}E_\theta$ = Electric field at Z due to equivalent charges at B_0, C_0 and D_0 respectively.

$$ = \frac{q}{\epsilon_0 2\pi}\left(\frac{\cos \angle B_0 Z A}{B_0 Z} + \frac{\cos \angle C_0 Z A}{C_0 Z} + \frac{\cos \angle D_0 Z A}{D_0 Z}\right) $$

$$ = E_m\left\{\frac{r[r + (D + \delta)\cos\theta]}{(D + \delta)^2 + 2(D + \delta) r\cos\theta + r^2}\right. $$

$$ \left. + 1 - \left[\left(\frac{D}{2} + \delta\right)^2 + \left(\frac{D}{2}\right)^2 - r^2\right]\frac{\left[\left(\frac{D}{2}\right)^2 + Dr\cos\theta + r^2 + \left(\frac{D}{2} + \delta\right)^2\right]}{\left[\left(\frac{D}{2}\right)^2 + Dr\cos\theta + r^2 + \left(\frac{D}{2} + \delta\right)^2\right]^2 - 4\left(\frac{D}{2} + \delta\right)^2 r^2 \sin^2\theta}\right\} \quad (13) $$

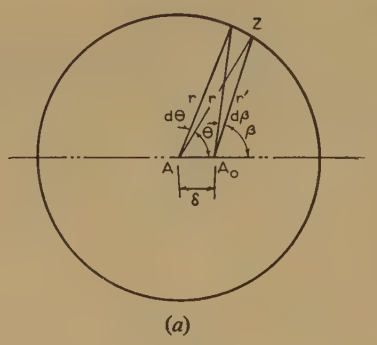

(*a*)

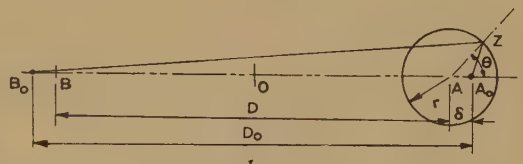

(*b*)

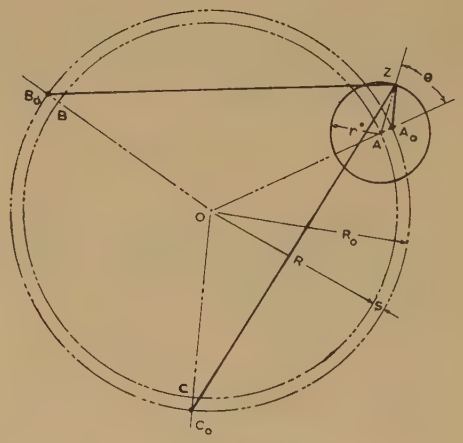

(*c*)

Fig. 7.—Electric field on conductor surface.
(*a*) Due to its own charge.
(*b*) Due to other charges in the bundle for $n = 2$.
(*c*) Due to other charges in the bundle for $n = 3$.

(4.3) Resultant Electric Field at any Point on a Conductor Surface

The resultant field, E_θ, can be calculated by adding the fields due to the different equivalent charges concerned as given by eqns. (10)–(13).

Table 1

VARIATION OF E_θ/E_m with θ

θ	E_θ/E_m					
	$n = 2, \frac{D}{d} = 10$		$n = 3, \frac{D}{d} = 15$		$n = 4, \frac{D}{d} = 15$	
	Eqns. (10) and (11)	Cahen's equation	Eqns. (10) and (12)	Cahen's equation	Eqns. (10) and (13)	Cahen's equation
deg						
0	1·1024	1·1000	1·1346	1·1333	1·2094	1·2000
30	1·0870	1·0866	1·1122	1·1155	1·1770	1·1732
60	1·0498	1·0500	1·0549	1·0667	1·0944	1·1000
90	0·9999	1·0000	0·9849	1·0000	0·9912	1·0000
120	0·9402	0·9500	0·9236	0·9333	0·8967	0·9000
150	0·9131	0·9134	0·8837	0·8845	0·8318	0·8286
180	0·8997	0·9000	0·8702	0·8667	0·8088	0·8000

Table 1 shows the variation of the resultant fields with θ. The values are compared with those calculated by Cahen's approximate equation,[1] namely

$$E_\theta = E_m\left[1 + (n-1)\frac{d}{D}\cos\theta\right]$$

(4.3.1) Maximum Electric Field at the Conductor Surface.

From Figs. 7(*b*) and 7(*c*) the maximum electric field is seen to occur when $\theta = 0$ for a given value of D/d.

For $n = 2$, eqns. (10) and (11),

$$E_0 = E_m(D + 2r)r/(Dr + r^2 - D\delta - \delta^2) \quad . \quad . \quad (14)$$

For $n = 3$ (eqns. (10) and (12),

$$E_0 = E_m\left[\frac{(D_0/2 + D + 2r)}{(D_0/4 + D/2 + r)^2 + \frac{3}{16}D_0^2} + \frac{1}{r - \delta}\right]r \quad (15)$$

For $n = 4$, eqns. (10) and (13),

$$E_0 = \frac{E_m r(D + 2r)^3}{2\left[\left(\frac{D + 2r}{2}\right)^4 - \left(\frac{D_0}{2}\right)^4\right]} \quad . \quad . \quad (16)$$

The variation of E_0/E_m with D/d is shown in Fig. 8. Since D/d will also affect q for a given line voltage, and hence E_m in eqns. (14)–(16), the maximum field, E_0, must be determined in conjunction with E_m, which is a function of H, D and d in a bundle of n conductors.

Consider a bundle of three conductors, with $d = 30$ mm and $H = 25$ m. When the diameter of the bundle circle, D, is varied from 290 to 900 mm, the maximum surface gradient, E_0, in terms of the voltage to earth, V, varies in accordance with the curve shown in Fig. 9. It is seen that the maximum gradient is the least when D lies in the neighbourhood of 500 mm. The values of d and H chosen for this example are very close to those for the 400 kV transmission lines described by Rokotyan and Lebedev,[5] using a bundle of three conductors. It is of interest to note that there the diameter of the bundle circle chosen is $400 \times 2/\sqrt{3}$, or 462 mm.

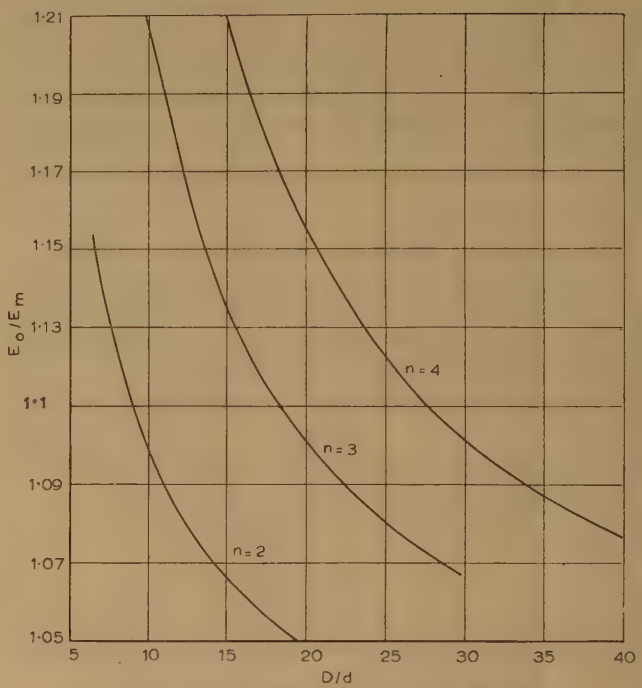

Fig. 8.—Relationship between E_0/E_m and D/d.

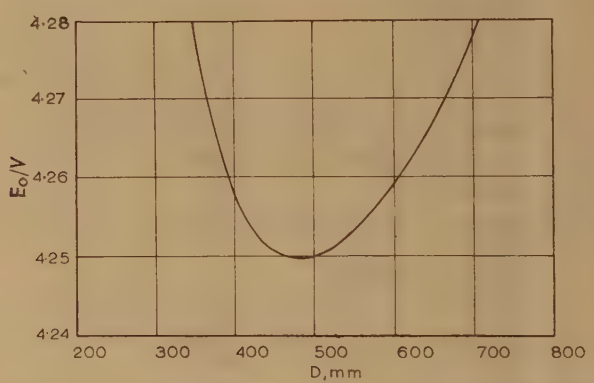

Fig. 9.—Relationship between E_0/V and D for a bundle of three conductors, with $d = 30$ mm and $H = 25$ m.

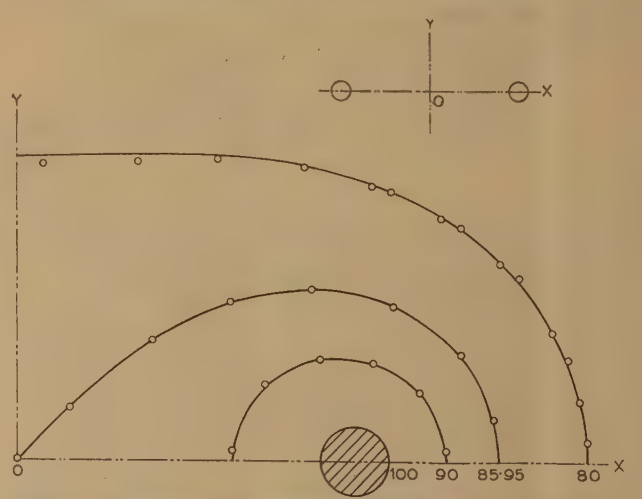

Fig. 10.—Equipotential lines around a bundle of two conductors with $D/d = 10$.

Potential of conductors = 100; potential at infinity = 0.

(5) MAPPING OF ELECTRIC FIELDS NEAR BUNDLE CONDUCTORS IN A DOUBLE-LAYER CIRCULAR TANK[6]

Fig. 10 shows the electric field surrounding a single-phase line consisting of a bundle of two conductors. The solid lines are obtained from theoretical calculations by the method outlined in the paper, and the small circles indicate experimental points. The closeness between the experimental results and the theoretical calculations can be clearly seen. A similar result has been obtained for $n = 3$ and $n = 4$.

(6) CONCLUSIONS

The proposed method of calculating the electric field near bundle conductors is to replace the actual conductors in a bundle of n conductors by n equivalent conductors of very small radius, r_0, which is negligible in comparison with the spacing between the conductors. These equivalent charges are displaced from the centres of the original conductors by such an amount that one set of equipotential points coincides with points of maximum and minimum surface gradient at the conductor surface. This permits of an accurate evaluation of the maximum gradient. The maximum deviation of equipotential surfaces with small values of K_n from true circles occurs at points in the region between maximum and minimum surface gradients, and for D/d ratios used in practice this deviation is well below 1%. Once the positions for equivalent charges are located, the field at any point near the bundle conductors can be determined. The method may be extended to cover 3-phase lines by the principle of superposition.

The advantage of the method therefore lies in the fact that it gives the most accurate evaluation of maximum surface gradients over bundle conductors. With a system of equivalent charges established, the electric field at any point can also be easily computed.

(7) ACKNOWLEDGMENTS

The author wishes to acknowledge his indebtedness to the University of Hong Kong for the research grant he received to enable him to carry out the investigation, the result of which is partly published in the paper. He is grateful to Professor F. Cahen, Directeur-Adjoint des Études et Récherches, l'Électricité de France, for supplying information concerning his previous work on bundle conductors. He also wishes to thank his colleagues, Dr. K. V. Leung and Dr. J. J. Raftery for advice.

(8) REFERENCES

(1) CAHEN, F.: 'The Problems of Power Transmission at Voltages above 225 kV', *Beama Journal*, 1951, **58**, pp. 269, 314, 362 and 385.

(2) PORITSKY, H.: 'The Field due to Two Equally-Charged Parallel Conducting Cylinders', *Journal of Mathematics and Physics*, 1932, **11**, p. 3.

(3) QUILICO, G.: 'On the Equivalent Diameter and the Surface Electric Gradients of Twin Conductors', CIGRÉ, Paris, 1956, Paper No. 214.

(4) CAHEN, F., and PELISSIER, R.: 'L'emploi des conducteurs en faisceaux pour l'armement des lignes à tres haute tension', *Bulletin de la Société Française des Électriciens*, 1948, **8**, p. 111.

(5) ROKOTYAN, S. S., and LEBEDEV, B. P.: '400 kV Transmission Systems in the Soviet Union', *Proceedings I.E.E.*, Paper No. 2400 S, December, 1957 (**104** A, p. 471).

(6) KING, SING-YUI, LUMB, P., and YU, P. K.: 'The Application of the Electrolytic Tank to Engineering Problems', Hong Kong Joint Oversea Group of the Institutions of Civil, Mechanical and Electrical Engineers, 1958, Occasional Paper No. 6.

(9) APPENDICES

(9.1) Construction of Equipotential Lines due to Parallel Conductors of Negligible Radii

For a bundle of two conductors (Fig. 11), the equipotential lines can be determined by

$$C^2 = R_0^2\{\cos 2\phi \pm \sqrt{[\cos^2 2\phi - (1 - K_2^2)]}\}$$

where $C_1C_2 = K_2R_0^2$.

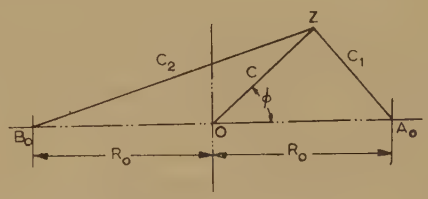

Fig. 11.—A bundle of two thin conductors at A_0 and B_0.

When $K_2 = 1$ the locus becomes the well-known curve of 'lemniscate', for other values of K_2 the loci are known as 'Cassinian ovals'.

For a bundle of more than two conductors, a mathematical determination of the locus of equipotential points is not easy. Consider only one conductor with its centre at A_0 and of a very small radius, r_0, in a bundle of three or four conductors, as shown in Fig. 12, in which point O denotes the centre of the

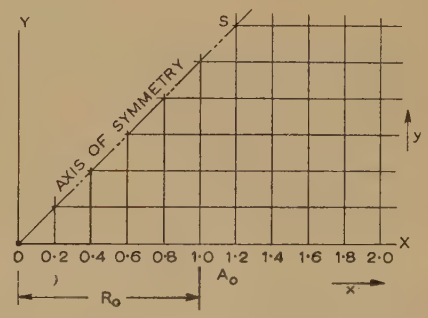

Fig. 12.—Determination of K_n at the corners of small squares.

bundle circle. Subdivide the space in the first sector into squares of sides, say, one-tenth of R_0. Determine the axis of symmetry, OS, which is at 60° with OX for $n = 3$ and 45° for $n = 4$. Compute the values of K_n at the corners of those squares lying between OS and OX. Then plot a set of curves, each showing the relation between K_n and x for a given value of y. These are plotted in Fig. 13 for $n = 3$ and 4 respectively. If necessary, another set of curves may be plotted showing the relation between K_n and y for given values of x. When K_n of an equipotential line is given, the co-ordinates x and y can be found from these curves.

(9.2) Deviation from a True Circle of an Equipotential with a Small Value of K_n

Consider the case of $n = 4$ only (Fig. 14).

Point $Z(x, y)$ is a point on an equipotential line

$$[(x - R_0)^2 + y^2][(x + R_0)^2 + y^2]$$
$$[x^2 + (R_0 - y)^2][x^2 + (R_0 + y)^2] = K_4^2R_0^8 \quad (17)$$

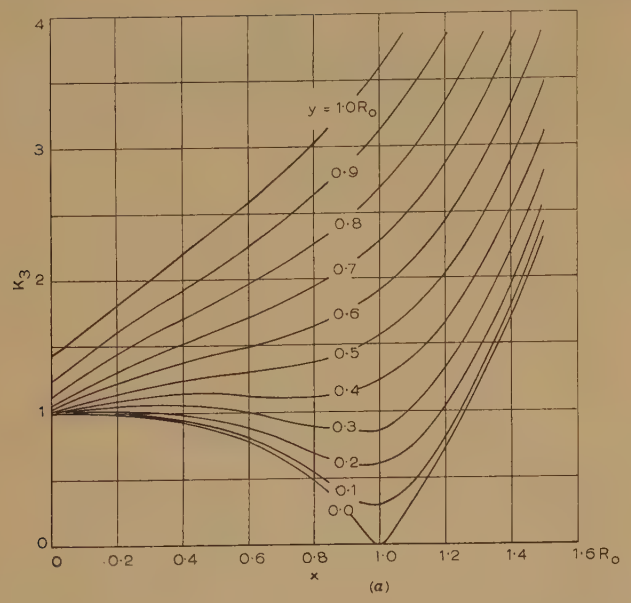

(a)

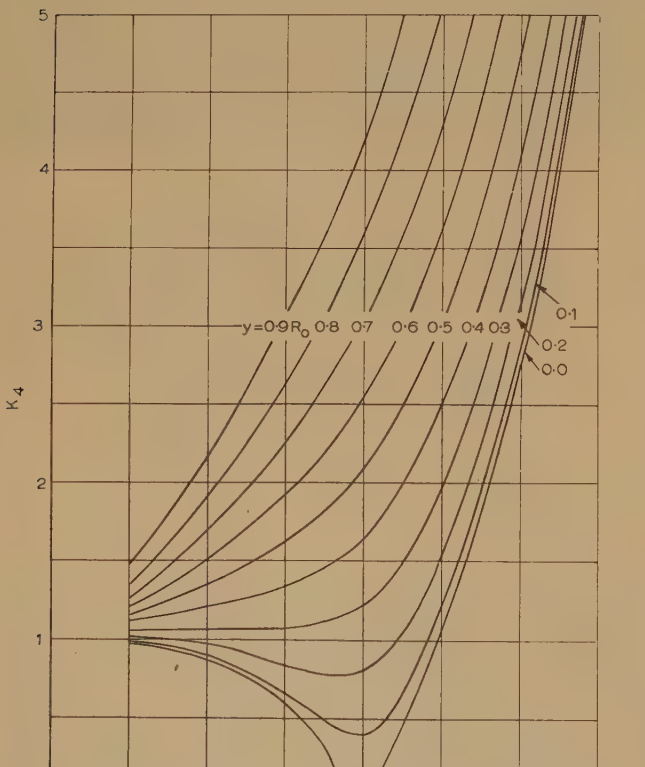

(b)

Fig. 13.—Graphs for determining the equipotential lines of a bundle of conductors.
(*a*) Three conductors.
(*b*) Four conductors.

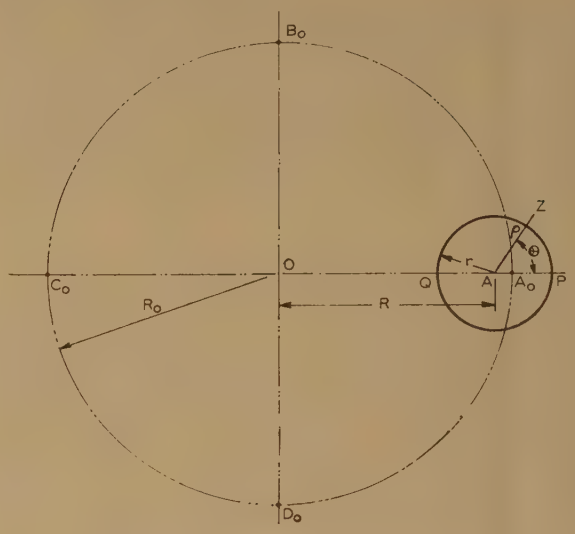

Fig. 14.—A bundle of four conductors.

By shifting the origin from O to A and using polar co-ordinates (ρ, θ) with respect to A, we have the transformation

$$x = R + \rho \cos\theta$$
$$y = \rho \sin\theta$$

Substituting $R + \rho\cos\theta$ and $\rho\sin\theta$ for x and y respectively in eqn. (17) and rearranging the terms gives

$$\rho^8 + B_7\rho^7 + B_6\rho^6 + B_5\rho^5 + B_4\rho^4 + B_3\rho^3 + B_2\rho^2 + B_1\rho + B_0 = 0 \quad (18)$$

where

$$B_7 = 8R\cos\theta$$
$$B_6 = 4R^2(6\cos^2\theta + 1)$$
$$B_5 = 8R^3\cos\theta(3 + 4\cos^2\theta)$$
$$B_4 = 6R^4 - 2R_0^4 + 16(3R^4 + R_0^4)\cos^2\theta + 16(R^4 - R_0^4)\cos^4\theta$$
$$B_3 = 8R\cos\theta[3(R_0^4 + R^4) - 4(R_0^4 - R^4)\cos^2\theta]$$
$$B_2 = -24R^2(R_0^4 - R^4)\cos^2\theta + 4R^2(R^4 + 3R_0^4)$$
$$B_1 = 8R^3(R^4 - R_0^4)\cos\theta$$
$$B_0 = (R_0^4 - R^4)^2 - K_4^2R_0^8$$

Let $\rho = (1 - e)r$. Since the deviation, e, of the equipotential from a true circle is small when K_4 is small (say at values below 0·3), ρ^m in eqn. (18) can be replaced by $(1 - me)r^m$ without appreciable error ($m = 1, 2, \ldots 8$).

Thus

$$e = \frac{r^8 + B_7r^7 + B_6r^6 + B_5r^5 + B_4r^4 + B_3r^3 + B_2r^2 + B_1r + B_0}{8r^8 + 7B_7r^7 + 6B_6r^6 + 5B_5r^5 + 4B_4r^4 + 3B_3r^3 + 2B_2r^2 + B_1r}$$

which is eqn. (9).

621.318.424.014.4

The Institution of Electrical Engineers
Monograph No. 339 U
June 1959

EDDY CURRENTS IN SOLID IRON DUE TO ALTERNATING MAGNETIC FLUX

By N. KESAVAMURTHY, M.A., B.E., M.Sc.Tech., Graduate, and P. K. RAJAGOPALAN, B.E., M.S.

(*The paper was first received 27th October*, 1958, *and in revised form 23rd February*, 1959. *It was published as an* INSTITUTION MONOGRAPH *in June*, 1959.)

SUMMARY

The predetermination of the phenomena connected with the penetration of alternating flux into solid iron due to an alternating magnetic field is a problem of great complexity. The prediction is particularly difficult in the presence of saturation.

The object of the paper is to present a unique graphical construction which would enable the designer to compute readily quantities such as flux, eddy-current loss, etc. This single construction has the merit of suitability for determining the above quantities for any magnetic material over any desired range of frequencies.

A close examination of the geometry of the graphical construction leads to a new method of formulating the basic equations. This method of approach brings out the importance of the law of variation of the magnetizing force with the depth of penetration of the flux for the determination of all other relevant quantities associated with the phenomena. On the basis of the basic differential equations, a law for the field intensity is suggested, to take saturation into account. This law is shown to agree favourably with the results of the graphical construction.

The analysis is applied to two different magnetic materials and is verified experimentally.

LIST OF PRINCIPAL SYMBOLS

h, H = Instantaneous value and amplitude respectively of the magnetizing force at point (x, y, z), AT/cm.
H_0 = Amplitude of the magnetizing force at the surface of the iron, AT/cm.
b, B = Instantaneous value and amplitude respectively of the flux density at the point (x, y, z), gauss.
B_s = Saturation flux density, gauss.
Φ, Φ_0 = Amplitude of the flux at the point (x, y, z) and at the surface respectively, per unit length in the z-direction, maxwells.
μ = Permeability of iron.
ρ = Resistivity, ohm-cm.
θ = Phase shift at (x, y, z) of H or of B.
λ = Phase shift at (x, y, z) of Φ.
ψ = Phase difference at (x, y, z) between H and Φ.
x_0 = Total depth of penetration, cm.
ω = Angular frequency, rad/s.
P_i = Iron loss per surface area, watts/cm^2.

(1) INTRODUCTION

A problem of great practical interest is the complete predetermination of the phenomena connected with the penetration of alternating flux into solid iron due to an alternating or rotating magnetic field. The classical expressions for the flux and current distribution and the iron loss due to an alternating m.m.f. rest on the assumption of constant permeability and, therefore, apply only to low values of flux density. It is now increasingly realized that the saturation of the iron is an important factor, and many authors[1–4] have presented various theories to take saturation into account. Among these, the graphical analysis suggested by Pohl is rigorous in so far as it is a step-by-step solution of a non-linear differential equation which takes into account the exact nature of the magnetization curve of the material. In this method, in order to predetermine the flux, eddy-current loss, etc., for a given material over a particular range of frequencies, a family of curves has to be constructed. Consequently, the method is laborious when the magnetic and electric data of materials vary over a wide range. Hence there is a need for a graphical construction, the results of which could be interpreted for any magnetic material over a wide range of frequencies and resistances. The object of the paper is to present such a method.

Furthermore, a closer examination of the geometry of the graphical construction suggests an alternative formulation of the basic differential equations underlying the phenomena. These equations in turn suggest a law of variation for the magnetizing force with the depth of penetration of alternating flux that is particularly applicable to saturated cores. The validity of the law is examined in the light of the results of the graphical construction and experimental data.

(2) A NON-DIMENSIONAL GRAPHICAL CONSTRUCTION FOR THE DETERMINATION OF Φ AND H CURVES

Consider an infinite half-space of solid iron with its surface on the y, z-plane and excited so that the magnetizing force at the surface is in the y-direction only. The x-direction is normal to the y, z-plane and is measured towards the surface. Clearly, at any point (x, y, z), H_y, B_y and Φ_y alone exist, and each is a function of x only. In what follows, the above quantities are denoted by H, B and Φ respectively and are to be understood as functions of x only.

For the simple case of constant permeability, the effects at depth x produced by the surface magnetizing force, $h_0 = H_0 \cos \omega t$, without regard to hysteresis, may be expressed[4] as

$$\left.\begin{aligned} & h = H_0 \varepsilon^{mx} \cos(\omega t - mx) \\ \text{and} \quad & b = B_0 \varepsilon^{mx} \cos(\omega t - mx) \\ \text{also} \quad & \Phi = \Phi_0 \varepsilon^{mx} \cos(\omega t - mx - \pi/4) \\ \text{where} \quad & m^2 = \frac{\pi f \mu}{\rho} \times 10^{-8} \\ \text{and} \quad & \Phi_0 = \frac{\mu H_0}{\sqrt{(2)} m} \end{aligned}\right\} \quad . \; . \; . \; (1)$$

These equations show that the H-vector leads the Φ-vector by 45°. This phase shift is constant at any value of x. The above rigorous analytical solution is valid for the case of constant permeability, that is, for that part of the magnetization curve below the knee. For the upper part, we shall have to be content at this stage with a graphical construction.

(2.1) Graphical Analysis by Pohl

A graphical treatment to determine the flux and current distributions in solid iron under saturation has been developed by Pohl.[4] This analysis is an extension to a non-linear medium of a method originated by Hay.[5]

Correspondence on Monographs is invited for consideration with a view to publication.
Prof. Kesavamurthy is Professor of Electrical Engineering, and Mr. Rajagopalan is Lecturer in Electrical Engineering, at the Indian Institute of Technology, Kharagpur.

In this step-by-step construction, the values of H and Φ at x (measured from an arbitrary origin) are assumed to be known. The problem is then one of determining graphically the values of $H + \Delta H$, $\Phi + \Delta\Phi$ at an adjacent layer at distance $x + \Delta x$. The flux density at x is known from the assumed value of H at x and from the B/H curve. Also, $\Delta H = (E_z/\rho)\Delta x$ where E_z is the electric force at the layer x, determined by the assumed flux, Φ. Lastly, $\Delta\Phi$ is given by $B\Delta x$. These quantities are added vectorially to give their magnitude and phase at the adjacent layer $x + \Delta x$. The starting-point for H is the point on the B/H curve when linearity terminates, and, by eqns. (1), the magnitude and phase of B and Φ at this point are known. This step-by-step construction is illustrated in Fig. 1.

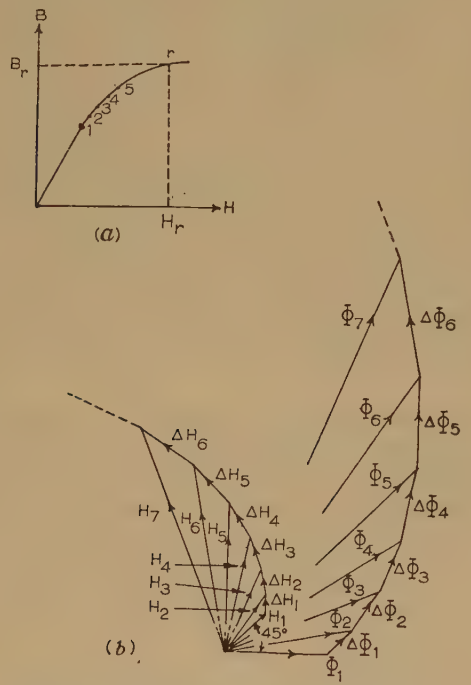

Fig. 1.—Step-by-step graphical construction.
(*a*) B/H curve indicating the flux density at the respective layers.
(*b*) Build-up of Φ- and H-loci. ΔH_n is perpendicular to Φ_n. $\Delta\Phi_n$ is parallel to H_n.

(2.2) A Method of Normalization of the Graphical Construction

An attempt to make the above graphical construction independent of the flux density, angular frequency and resistivity is based on the following considerations:

(*a*) The magnetization curve of the material could be approximated as shown in Fig. 2. This implies that the flux density, B_s, at any layer is independent of the magnetizing force at that layer.

(*b*) The quantities involved in the Φ- and H-loci of the graphical construction outlined in Section 2.1 are the vector quantities ΔH and $\Delta\Phi$. The magnitudes of these for the type of magnetization curve stated in (*a*) would now be

$$\left.\begin{aligned}\Delta H &= \Phi\frac{\omega}{\rho}\Delta x \times 10^{-8}\\ \Delta\Phi &= B_s\Delta x\end{aligned}\right\} \quad . \quad . \quad . \quad . \quad (2)$$

Now let us suppose that the Φ- and H-loci for a particular value of $B_s = B_{s0}$, say, and of $\omega/\rho = 1$ have been drawn. In the general case, the value to start with for H for the graphical construction will be a finite quantity, and that for Φ will be zero. To apply this construction for other values of $B_s = B_{s1}$, say, and of ω/ρ we have only to bear in mind the facts stated in (*b*), namely that the Φ- and H-loci will be magnified by scale factors B_{s1}/B_{s0} and $B_{s1}\omega/B_{s0}\rho$ respectively. In other words, if these two loci have been drawn for $B_{s0} = 10000$ gauss, $\omega/\rho = 1$ and with initial values $H_1 = 1$ and $\Phi_1 = 0$, then the same curve will correspond to $B_{s0} = 20000$ and $\omega/\rho = \frac{1}{2}$ with the same initial values for H_1 and Φ_1.

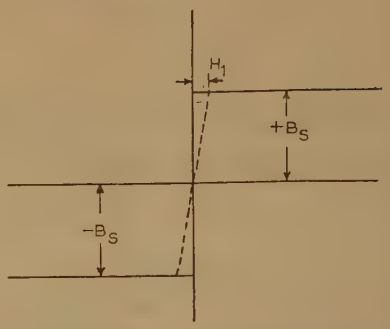

Fig. 2.—Approximation to the magnetization curve.

For the case of an infinite half-space of iron the initial values of H and Φ will be zero at the layer, which could be chosen as the origin of reference. Therefore, the Φ- and H-loci with $H_1 = \Phi_1 = 0$ as the starting value lead to normalized curves that could be adapted for all values of B_s and ω/ρ by suitably altering the scale factors.

(2.3) A Normalized Graphical Construction for the Case of the Infinite Half-Space of Iron

For such a graphical construction, the reference values of $B_s = 10000$ and $B_s(\omega/\rho) \times 10^{-8} = 1$ are chosen. Since both Φ and H start from zero, it becomes difficult to visualize how these loci will build up for successive layers. However, this difficulty could be overcome by a very close approximation to the stepped B/H curve, as shown in Fig. 2. The curve is linear up to H_1, which is a very small quantity, so that $\mu = B_s/H_1$ and $\Phi_1 = \dfrac{B_s}{\sqrt{(2)m}}$

where $$m^2 = \frac{\omega\mu}{2\rho} \times 10^{-8} = \frac{\omega B_s}{2\rho H_1} \times 10^{-8}$$

i.e. $\Phi_1 = B_s\sqrt{H_1}$. Also, the phase angle between Φ_1 and H_1 is 45°.

A step-by-step graphical construction was made with $B_{s0} = 10^4$ gauss and $H_1 = 25 \times 10^{-6}$, a value small enough to approximate very closely to the step curve. To reduce the errors of the graphical construction to a minimum, the thickness Δx of adjacent layers was made 0·001 cm. To cover all cases of practical interest, the Φ- and H-loci were made to cover 1 cm depth of penetration of the flux. To permit ready reference, a summary of the results of the graphical construction is given in Table 1. For any given values of B_s and ω/ρ the scale factors are:

for H, $$B_s\frac{\omega}{\rho} \times 10^{-8}$$

and for Φ, $$\frac{B_s}{B_{s0}} \times 10^{-4}$$

(2.3.1) Choice of B_s.

For the actual material, the magnetic characteristic is quite different from the non-linear characteristic shown in Fig. 2. For a proper application of the results of the graphical construc-

Table 1

DISTRIBUTION OF H' AND Φ' AT VARIOUS LAYERS WHEN $B_s = B_{s0} = 10000$ gauss

Layer No.	H'	Φ'	x_0	Layer No.	H'	Φ'	x_0	Layer No.	H'	Φ'	x_0
	$\times 10^{-6}$		cm $\times 10^{-3}$		$\times 10^{-6}$		cm $\times 10^{-3}$		$\times 10^{-6}$		cm $\times 10^{-3}$
(0)	25	50	0	(47)	1515	480	69	(94)	34200	2235	365
(1)	29	58	1	(48)	1590	492	71	(95)	36000	2295	375
(2)	33	66	2	(49)	1673	504	73	(96)	37950	2355	385
(3)	38	72	3	(50)	1755	516	75	(97)	40000	2415	395
(4)	44	80	4	(51)	1920	541	79	(98)	42600	2475	405
(5)	50	87	5	(52)	2100	565	83	(99)	44700	2535	415
(6)	57	93	6	(53)	2280	588	87	(100)	46800	2595	425
(7)	64·5	100	7	(54)	2470	612	91	(101)	49000	2650	435
(8)	72·5	106	8	(55)	2675	636	95	(102)	51200	2710	445
(9)	81	113	9	(56)	2885	658	99	(103)	53400	2770	455
(10)	90	120	10	(57)	3100	682	103	(104)	55600	2825	465
(11)	99·5	126	11	(58)	3320	705	107	(105)	57900	2880	475
(12)	110	134	12	(59)	3555	728	111	(106)	60300	2940	485
(13)	121	140	13	(60)	3790	752	115	(107)	62800	3000	495
(14)	132·5	146	14	(61)	4030	776	119	(108)	65400	3060	505
(15)	144·5	152	15	(62)	4290	800	123	(109)	67800	3120	515
(16)	157	158	16	(63)	4560	823	127	(110)	70300	3180	525
(17)	171	164	17	(64)	4830	847	131	(111)	73000	3240	535
(18)	184·5	169	18	(65)	5110	870	135	(112)	75600	3295	545
(19)	198	176	19	(66)	5420	890	139	(113)	78000	3350	555
(20)	212·5	181	20	(67)	5700	915	143	(114)	81200	3420	565
(21)	228	187	21	(68)	6020	937·5	147	(115)	84000	3480	575
(22)	244	192	22	(69)	6320	960	151	(116)	86800	3540	585
(23)	260·5	198	23	(70)	6640	985	155	(117)	90000	3600	595
(24)	277·5	205	24	(71)	6970	1010	159	(118)	93400	3660	605
(25)	294·5	210	25	(72)	7300	1030	163	(119)	96800	3720	615
(26)	330	223	27	(73)	7650	1055	167	(120)	99600	3770	625
(27)	365	236	29	(74)	8025	1080	171	(121)	105600	3880	645
(28)	405	247	31	(75)	8375	1103	175	(122)	112000	3990	665
(29)	448	260	33	(76)	9300	1160	185	(123)	118400	4110	685
(30)	488	272	35	(77)	10200	1220	195	(124)	125600	4230	705
(31)	535	285	37	(78)	11250	1278	205	(125)	132200	4340	725
(32)	580	297	39	(79)	12300	1335	215	(126)	139200	4465	745
(33)	630	309	41	(80)	13350	1395	225	(127)	146600	4580	765
(34)	685	321	43	(81)	14475	1453	235	(128)	154000	4700	785
(35)	740	334	45	(82)	15560	1510	245	(129)	161400	4810	805
(36)	793	345	47	(83)	16875	1568	255	(130)	169500	4920	825
(37)	848	357	49	(84)	18150	1625	265	(131)	178000	5040	845
(38)	905	396	51	(85)	19500	1680	275	(132)	186000	5160	865
(39)	960	382	53	(86)	20900	1755	285	(133)	194000	5260	885
(40)	1025	396	55	(87)	22400	1815	295	(134)	202500	5380	905
(41)	1088	407	57	(88)	23950	1880	305	(135)	211500	5490	925
(47)	1155	420	59	(89)	25550	1935	315	(136)	221500	5610	945
(43)	1223	432	61	(90)	27300	1995	325	(137)	230000	5720	965
(44)	1293	444	63	(91)	28900	2055	335	(138)	240000	5830	985
(45)	1365	456	65	(92)	30600	2115	345	(139)	249500	5950	1005
(46)	1440	468	67	(93)	32300	2175	355				

x_0 = depth of penetration. Ψ = phase difference between H' and Φ' = a constant = arc sin 0·816. For any other value of $B_s = B_{s1}$, $H = \left(\frac{B_{s1}}{\rho}\omega \times 10^{-8}\right)H'$ AT/cm and $\Phi = \frac{B_{s1}}{B_{s0}}\Phi'$ maxwells.

tion suitable values of B_s must be chosen and this choice should be consistent with the nature of the actual B/H curve. Consequently, for a known value of H_0 the corresponding value of B_s is chosen from the static magnetization curve of the material.

(2.3.2) Illustrative Example.

As an illustration of the use of Table 1, consider the specific case of an infinite half-space of iron subjected to a pulsating field at 50 c/s having the magnetization curve shown at (*a*) in Fig. 3 and $\rho = 16{\cdot}3 \times 10^{-6}$ ohm-cm. It is required to compute for flux per unit length in the z-direction, the depth of penetration, x_0, and the iron loss for an amplitude of the magnetizing force $H_0 = 100$ AT/cm. From curve (*a*) in Fig. 3, for $H = 100$ AT/cm, B_s is 18300 gauss. The scale factor for H is $B_s\frac{\omega}{\rho} \times 10^{-8} = 3525$. That is, an H_0 of 100 AT/cm at the surface corresponds to 28370×10^{-6} unit in the H-locus. From Table 1, for this value of H the depth of penetration is $x_0 = 0{\cdot}332$ cm and the flux is 2035. Using the scale factor of 1·83 ($=B_s/10000$), the flux per unit length in the z-direction is 3725 maxwells. Also ψ, the phase angle between Φ and H, is 54·75°. Hence, the iron loss per unit surface area (*vide* Section 3) is $\left(\frac{\omega}{2} \times 10^{-8}\right)\Phi H \sin\psi = 0{\cdot}475$ watt.

(2.4) Determination of Flux and Current Distribution and Iron Losses in a Solid Toroid Subjected to an Alternating Field

A problem of practical interest is the determination of fluxes, currents and iron losses in a solid toroid whose winding carries a sinusoidal current. A toroid of solid iron, the dimensions of whose section are large compared with the depth of penetration, can be viewed as a portion of an infinite half-space of iron whose length in the z-direction is equal to the perimeter of the section whose length in the y-direction is the mean circumferential

length of the toroid. The magnetizing force at the surface of the infinite half-space is the same as for the toroid.

Fig. 3 gives the magnetization curves of two specimens. The other relevant dimensions are included in Section 6. For any known frequency and for a given value of H, by using Table 1 as suggested in Section 2.3 we can determine the flux, Φ, and the iron loss, P_i. Knowing Φ and the number of turns of the exciting winding, the induced e.m.f. in the main winding can be calculated. Making suitable allowance for the voltage drop in the winding, the applied voltage across the exciting winding can be computed. Similar computations could be made for other assumed values of H.

Figs. 4 and 5 show the results of the computation for two different toroids compared with test results. In Fig. 6 the curves for the predetermined values of the currents for known applied voltages at frequencies 40 and 60 c/s are shown and compared with test results.

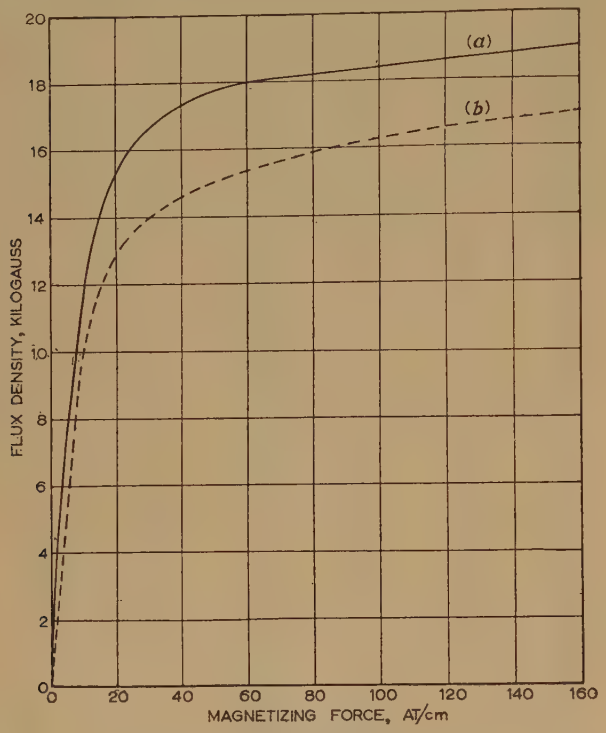

Fig. 3.—Magnetization curves for the two specimens of iron.
(*a*) Toroid 1; $\rho = 16{\cdot}3 \times 10^{-6}$ ohm-cm.
(*b*) Toroid 2; $\rho = 18{\cdot}5 \times 10^{-6}$ ohm-cm.

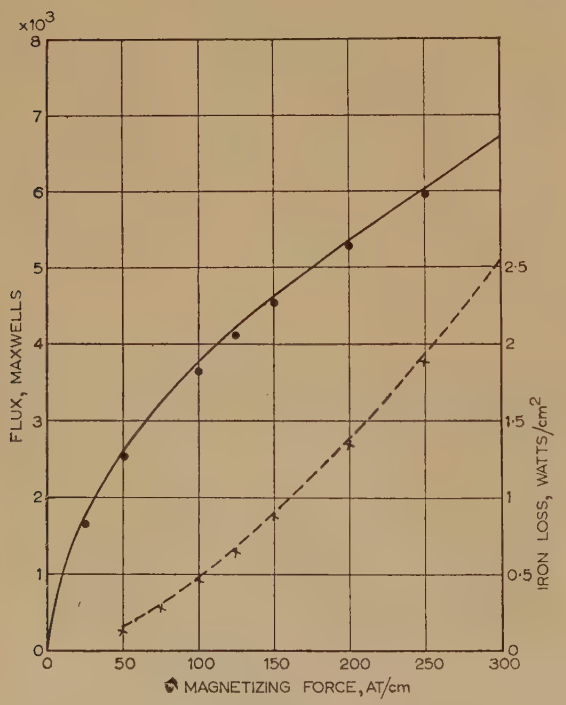

Fig. 4.—Flux and iron-loss curves for toroid 1.
—— Calculated flux.
● Experimental values of flux.
--- Calculated iron loss.
× Experimental values of iron loss.

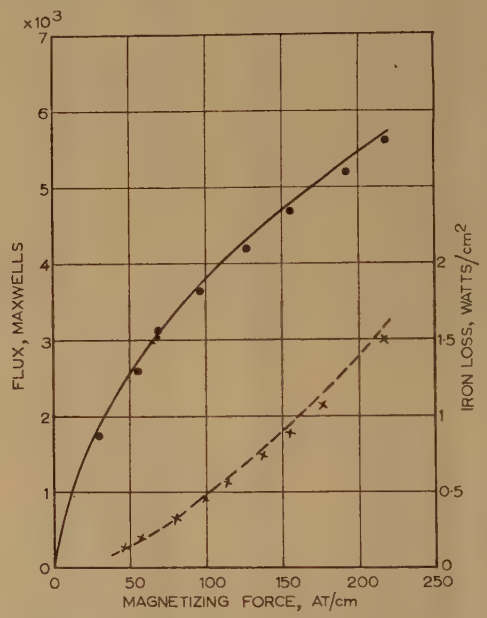

Fig. 5.—Flux and iron-loss curves for toroid 2.
—— Calculated flux.
● Experimental values of flux.
--- Calculated iron loss.
× Experimental values of iron loss.

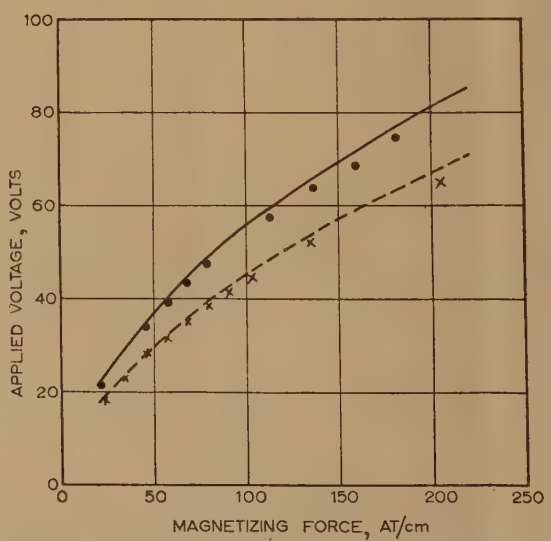

Fig. 6.—Voltage curves at 60 and 40 c/s for toroid 2.
—— Theoretical curve, 60 c/s.
● Experimental values, 60 c/s.
--- Theoretical curve, 40 c/s.
× Experimental values, 40 c/s.

These computations illustrate the scope and elegance of the normalized graphical construction.

(2.5) Limitations of the Graphical Construction

The step-by-step construction outlined by the authors is based on the following simplifying assumptions:

(*a*) The amplitude of the flux density at any layer for a known value of magnetizing force at that layer could be determined from the magnetization curve of the material.
(*b*) The effects of harmonics are ignored.

A further limitation is that the results of Table 1 can be used only for the case of infinite half-space of iron where $H_1 = \Phi_1 = 0$ at the starting-point. However, the construction could be modified to be applicable to iron plates of finite thickness where H is a finite quantity at the centre. In such cases, a family of normalized curves could be drawn to cover a range of initial values of H.

(3) A GEOMETRICAL INTERPRETATION OF THE GRAPHICAL CONSTRUCTION

A critical examination of the graphical construction for the Φ- and H-loci for any given magnetization curve leads to certain interesting interpretations.

(*a*) The tangent to the H-locus at any point is normal to the corresponding radius vector on the Φ-locus (Fig. 7).

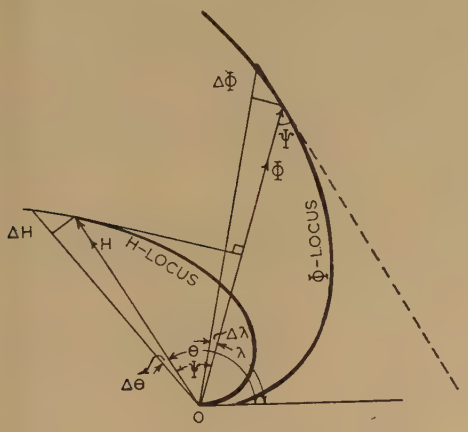

Fig. 7.—The geometry of Φ- and H-loci.

(*b*) The tangent of the Φ-locus at any point is parallel to corresponding radius vector on the H-locus.

(*c*) If O is the origin for both loci (Fig. 7), then

$$\frac{dH}{\sin\psi} = \frac{\omega}{\rho} \times 10^{-8}\Phi dx$$

Also, since the induced e.m.f. per unit axial length is $\omega\Phi \times 10^{-8}$, the current density at the corresponding layer is $\omega\Phi \times 10^{-8}/\rho$. Consequently, the power loss in a layer of thickness Δx and unit width is

$$\tfrac{1}{2}eidx = \tfrac{1}{2}\frac{(\omega \times 10^{-8})^2}{\rho}\Phi^2 dx$$

Hence the total power loss per unit surface area is

$$\tfrac{1}{2}\int_0^X \frac{(\omega \times 10^{-8})^2}{\rho}\Phi^2 dx$$

(*d*) Alternatively, from physical considerations it is obvious that the power loss per unit surface area is $\frac{1}{2}EH\sin\psi$. Making use of the results of (*c*) for $\sin\psi$, the total power loss per unit surface area is

$$\tfrac{1}{2}\rho H\frac{dH}{dx}$$

(*e*) Combining the results of (*c*) and (*d*),

$$\int_0^X \frac{(\omega \times 10^{-8})^2}{\rho}\Phi^2 dx = \rho H\frac{dH}{dx}$$

Differentiating,

$$\Phi = \frac{\rho}{\omega \times 10^{-8}}\left[H\frac{d^2H}{dx^2} + \left(\frac{dH}{dx}\right)^2\right]^{1/2} \quad . \quad . \quad (3)$$

Eqn. (3) is the general expression for the flux below any layer at a depth x.

(*f*) Also from (*c*) and (*e*),

$$\sin\psi = \frac{dH}{dx}\Big/\left[H\frac{d^2H}{dx^2} + \left(\frac{dH}{dx}\right)^2\right]^{1/2} \quad . \quad . \quad . \quad (4)$$

Clearly, $\sin\psi$ signifies the power factor at the layer x.

These results lead to the important conclusion that, if the variation of the amplitude of H as a function of x is known, it is a simple matter to calculate Φ, ψ and the loss at any layer, whether the region is saturated or not.

A further interpretation of the geometry of the graphical construction leads to Maxwell's field equations, as outlined in Section 4.

(4) FORMULATION OF THE BASIC DIFFERENTIAL EQUATIONS FOR AN INFINITE HALF-SPACE

(4.1) Derivation Based on the Geometry of the Graphical Construction

From the geometry of Fig. 7 and the results in Section 3 we have the following equations:

$$\frac{dH}{dx} = k\Phi\sin\psi \quad . \quad . \quad . \quad . \quad . \quad . \quad . \quad (5)$$

$$H\frac{d\theta}{dx} = k\Phi\cos\psi \quad . \quad . \quad . \quad . \quad . \quad . \quad . \quad (6)$$

$$\tan\psi = \Phi\frac{d\lambda}{d\Phi} \quad . \quad . \quad . \quad . \quad . \quad . \quad . \quad . \quad (7)$$

where $$\lambda = \theta - \psi \text{ and } k = \frac{\omega \times 10^{-8}}{\rho} \quad . \quad . \quad . \quad (8)$$

Differentiating eqn. (5) and substituting for ψ from eqns. (6) and (7),

$$\frac{d^2H}{dx^2} = H\frac{d\theta}{dx} \quad . \quad . \quad . \quad . \quad . \quad . \quad . \quad (9)$$

Also, from eqns. (5) and (6),

$$\frac{1}{H}\frac{d}{dx}\left(H^2\frac{d\theta}{dx}\right) = \frac{2dH}{dx}\frac{d\theta}{dx} + H\frac{d^2\theta}{dx^2} = \frac{k}{\sin\psi}\frac{d\lambda}{dx}$$

since $$\sin\psi = \frac{\Phi}{B}\frac{d\lambda}{dx}.$$

Hence $$\frac{1}{H}\frac{d}{dx}\left(H^2\frac{d\theta}{dx}\right) = kB \quad . \quad . \quad . \quad . \quad . \quad (10)$$

Lastly, the property of the material is such that there exists a relationship between B and H at any point x in the form

$$B = \mathrm{F}(H) \quad . \quad . \quad . \quad . \quad . \quad . \quad (11)$$

Eqns. (9), (10) and (11) are the basic differential equations governing the distribution of B, H and the phase shift, θ, at each layer of the material.

(4.2) Alternative Method of Derivation of Equations

An alternative form of deduction of the above equations is based on the facts

$$B_z = B_x = 0$$

$$\frac{\partial^2 h_y}{\partial x^2}(x, t) = \frac{1}{\rho}\left[\frac{\partial b_y}{\partial t}(x, t)\right] \times 10^{-8}$$

For the type of material under investigation $h_y(x, t)$ and $b_y(x, t)$ are always in time phase and hence they could be rewritten as

$$h_y(x, t) = H \cos(\omega t + \theta)$$

and

$$b_y(x, t) = B \cos(\omega t + \theta)$$

H, B and θ being functions of x only. From these equations, on substitution and reduction, we are led to eqns. (9) and (10), where $k = \dfrac{\omega}{\rho} \times 10^{-8}$.

(5) SOLUTION OF EQUATIONS (9), (10), (11)

(5.1) Solution for the Linear Case

Eqns. (9), (10) and (11) are applied to a material of constant permeability, that is, $B = \mu H$. Using the substitutions, $H = \varepsilon^u$, $p = du/dx$ and $q = d\theta/dx$ eqns. (9) and (10) could be rewritten as

$$\frac{dp}{dx} = q^2 - p^2 \text{ and } \frac{dq}{dx} = k\mu - 2pq$$

whence

$$\frac{d}{dx}(p + jq) = \mu jk - (p + jq)^2$$

If

$$Y = p + jq \text{ then } \frac{dY}{dx} = jk\mu - Y^2$$

This yields

$$\exp[u + j\theta - x\sqrt{(jk\mu)}] = A + C\varepsilon^{-2x\sqrt{(jk\mu)}}$$

Or

$$H\varepsilon^{j\theta} = A\varepsilon^{(1+j)x\sqrt{(\frac{1}{2}k\mu)}} + C\varepsilon^{-(1+j)x\sqrt{(\frac{1}{2}k\mu)}}$$

which could be recognized as the classical expression for the linear theory. For the condition of infinite half-space ($H = 0$, $x = -\infty$), we finally have $H\varepsilon^{j\theta} = H_0\varepsilon^{m(1+j)k}$, where H_0 is the magnetizing force at the surface.

(5.2) A Particular Solution when $B = B_s$ = a Constant

It is obvious that for large values of flux density the assumption of constant permeability is not tenable. For the step-magnetization curve for which the normalized graphical construction has been drawn, $B = B_s$, $H = 0$. The field equations would then become

$$\frac{d^2H}{dx^2} - H\left(\frac{d\theta}{dx}\right)^2 = 0$$

$$\frac{1}{H}\frac{d}{dx}\left(H^2\frac{d\theta}{dx}\right) = kB_s$$

If

$$H = kB_sH' = \left(\frac{\omega B_s}{\rho} \times 10^{-8}\right)H' \quad . \quad . \quad . \quad (12)$$

then we have the normalized differential equations

$$\frac{d^2H'}{dx^2} - H'\left(\frac{d\theta}{dx}\right)^2 = 0 \quad . \quad . \quad . \quad . \quad (13)$$

$$\frac{1}{H'}\frac{d}{dx}\left(H^2\frac{d\theta}{dx}\right) = 1 \quad . \quad . \quad . \quad . \quad . \quad (14)$$

The normalized step-by-step graphical construction of Section 2 is in effect the solution of the non-linear simultaneous equations (13) and (14).

There appears to be no general solution with arbitrary constants. However, one could recognize the above equations as analogous to the dynamics of motion of a particle with radial and transverse accelerations. It is a well-known result that, if a particle moves in an equiangular spiral and if the radial acceleration is zero, then the transverse acceleration is proportional to (distance)^2. Stated explicitly, if $H' \propto \varepsilon^{\sqrt{2}\theta}$, then the above equations hold simultaneously.

As a consequence,

$$H' = \frac{1}{3\sqrt{2}}(x + d)^2 \quad . \quad . \quad . \quad . \quad . \quad (15)$$

where d is an arbitrary constant.

The above is the law of variation of H' with x. Strictly speaking, therefore, this law of variation is by no means a general one. However, its acceptance for the specific problem in question rests on the following considerations:

(*a*) The step-by-step normalized graphical construction gives the variation of H' with θ as an equiangular spiral.

(*b*) A complete solution for H' with two arbitrary constants although essential to deal with sheets of finite thickness or with a discontinuous medium, is unnecessary for a problem concerning an infinite half-space of iron for which one of the arbitrary constants must be zero, to satisfy the requirements of a vanishing H' for large values of x.

(*c*) The above postulate concerning the law of variation for H' when applied to specific problems, must yield results sufficiently close to experimental ones to warrant the assumption that the law is, at worst, a very close approximation.

(5.3) Computation of Eddy-Current Loss, Flux, etc., based on $H' \propto x^2$

For the specific case of infinite half-space where the origin is so chosen that $H' = 0$ at $x = 0$, eqn. (15) reduces to

$$H' = \frac{x^2}{3\sqrt{2}}$$

or

$$H = ax^2 \quad \text{where} \quad a = \frac{B_s \times 10^{-8}}{3\sqrt{2}\rho} \quad . \quad . \quad . \quad (16)$$

It has been emphasized in Section 3 that all relevant quantities could be deduced once a law for H as a function of x is known. Making use of the results of Section 3 we finally have:

Loss per unit surface area,

$$P_i = 0{\cdot}485\,4\sqrt{(\rho B_s\omega \times 10^{-8})}H_0^{3/2} \text{ watts} \quad . \quad . \quad (17)$$

Flux per unit length of perimeter,

$$\Phi_0 = 1{\cdot}189\sqrt{\left(\frac{\rho B_s}{\omega \times 10^{-8}}\right)}H_0^{1/2} \text{ maxwells} \quad . \quad . \quad (18)$$

Power factor,

$$\sin\psi_0 = 0{\cdot}816\,5 \quad . \quad . \quad . \quad . \quad (19)$$

Total depth of penetration,

$$x_0 = 2{\cdot}06\sqrt{\left(\frac{\rho}{\omega B_s \times 10^{-8}}\right)}H_0^{1/2} \quad . \quad . \quad . \quad (20)$$

where H_0 is the amplitude of the magnetizing force of the exciting winding. The choice of B_s is as in Section 2.3.1.

(6) EXPERIMENTAL VERIFICATION

The results of the graphical construction and also the expressions deduced in Section 5.3 are simultaneously verified with experimental data on two toroids of different electric and magnetic properties. The details of the toroids are as follows:

	Toroid 1	*Toroid* 2
Material	Mild steel	Mild steel
Resistivity	$16{\cdot}3 \times 10^{-6}$ ohm-cm at 20° C	$18{\cdot}5 \times 10^{-6}$ ohm-cm at 20° C
B/H curve	Fig. 4, curve (*a*)	Fig. 4, curve (*b*)
External diameter ..	34·3 cm	33·66 cm
Internal diameter ..	30·5 cm	29·21 cm
Cross-section	$1{\cdot}9 \times 1{\cdot}9$ cm (corners rounded to 0·32 cm radius)	$2{\cdot}22 \times 1{\cdot}43$ cm (corners rounded to 0·08 cm radius)
Perimeter of section ..	7·08 cm	7·17 cm
Mean circumference ..	101·8 cm	98·7 cm
Number of turns of magnetizing winding	1 000	800
Number of secondary turns (for flux measurement)	500	500

The flux and loss curves under sinusoidal magnetization up to very high values of H_0 are given in Figs. 4 and 5. To avoid an appreciable departure from the desired sinusoidal waveform of current, each of the exciting coils was energized from the 400-volt 50 c/s mains through a large non-inductive resistor. The oscillograms for currents showed no recognizable harmonics. Readings were taken quickly and the temperature was allowed to fall to room temperature after every reading to maintain the resistivity practically constant. A mean-reading voltmeter was connected across the secondary winding for measuring the flux. The test results for toroid 1 have been given by Pohl,[4] and are reproduced in Fig. 4, whilst Fig. 5 gives the results on toroid 2 obtained by the authors. In these Figures are also shown curves computed from Table 1 or from eqn. (18). It is seen that in each case there is agreement within the limits of accuracy of measurements.

Further tests were carried out on toroid 2 at 60 c/s and 40 c/s with a pure sinusoidal applied voltage obtained from a sine-wave generator. Fig. 6 gives the results of measured voltage for currents through the exciting winding (expressed as equivalent ampere-turns per centimetre). Curves obtained from Table 1 or from eqn. (18) are also shown.

(7) CONCLUSIONS

The results of Section 6 justify the conclusion that the normalized graphical construction could be applied to the calculation of all quantities for any given magnetic material over any range of frequencies. The graphical construction in general has the further advantage that a study of its geometry leads to the important conclusion that, once the law for magnetizing force, H, against x is known, all other quantities can be deduced therefrom, whether the region is linear or saturated. It is this conclusion that has led to a law governing the distribution of H. Based on this we are led to simple expressions for the calculation of the various quantities. Lastly, it is to be expected that in the study of the solid-rotor machine where performance has to be calculated over a wide range of frequencies, the results of Table 1 will be of value.

(8) ACKNOWLEDGMENTS

The authors are grateful to the Director, Indian Institute of Technology, Kharagpur (India), for granting facilities for the work described in the paper, and also to Mr. E. M. Gopal for the assistance he rendered.

(9) REFERENCES

(1) ROSSENBERG, E.: 'Solid Iron Conductors and Current Breakers', *Electrotechnik und Maschinenbau*, 1923, **41**, p. 701.

(2) MCCONNELL, H. M.: 'Eddy Current Phenomena in Ferro-Magnetic Materials', *Transactions of the American I.E.E.*, 1954, **73**, Part I, p. 226.

(3) MCCONNELL, H. M., and SVERDRUP, E. F.: 'The Induction Machine with Solid Iron Rotor', *ibid.*, 1955, **74**, Part II, p. 343.

(4) POHL, R.: 'Electromagnetic and Mechanical Effects in Solid Iron due to an Alternating or Rotating Magnetic Field', *Journal I.E.E.*, 1944, **91**, Part II, p. 239.

(5) HAY, A.: 'A Graphical Treatment of the Skin Effect', *ibid.*, 1911, **46**, p. 487.

DISCUSSION ON

'THE PRODUCTION OF A SINUSOIDAL FLUX WAVE, WITH PARTICULAR REFERENCE TO THE INDUCTOR ALTERNATOR'*

Mr. G. Barello (*France: communicated*): I was greatly interested by Mr. Hancock's monograph, as his main theoretical results are the same as those I published† following a patent application filed in 1943. The agreement between the results can be considered as a proof of their soundness.

However, the designers of inductor alternators do not appear to be aware of the importance of adopting a rotor profile approaching the ideal shape. It is true that in practice a sinusoidal waveform of the generated voltage cannot be obtained solely by this means.

Armature reaction and hysteresis are important causes of distortion of the voltage wave in this type of alternator, generally built with only one slot per pole per phase. Hysteresis produces a trough in the rising branch and a peak in the falling branch of each half-wave. However, the suggested rotor shape offers other advantages. For instance, it is known that the voltage/excitation characteristic of a common inductor alternator, after reaching a maximum, falls at high values of exciting current, owing to the saturation of the rotor teeth.

With the improved form of the rotor saliencies this effect is very attenuated, because the rotor induction corresponding to a given flux is lower. Moreover, taking also into account the smaller height of the rotor saliences, the excitation m.m.f. is considerably reduced.

Even if it is not especially intended to obtain a sinusoidal flux distribution, the foregoing gives a clue for improving an ordinary rotor. This can be seen if one considers the known magnetic field plot of a rotor with rectangular slots placed in front of an unslotted stator; if the rotor and stator surfaces are both supposed to be equipotentials, any other equipotential line of the corresponding field plot should be adopted as the rotor profile and would give the same flux distribution on the stator bore, when the proper m.m.f. was applied between the two surfaces. The field plot shows that, for a slightly smaller air-gap at the centre-line of the saliences, the equipotential surfaces corresponding to a given rectangular slot will give rotor slots which are rounded and shallower than the original slots. A more careful analysis of the consequences of this modification shows that it is always favourable.

Mr. N. N. Hancock (*in reply*): The objection put forward by designers to the use of these profiles is, with some justification, based mainly on the distortion caused by armature reaction. There are, however, designers who are not aware that there are practicable pole profiles which result in sinusoidal no-load e.m.f.'s. In this connection I must myself apologize to Mr. Barello for my ignorance of his prior work. I find his remarks on hysteresis particularly interesting as I had not given any consideration to this effect.

* Hancock, N. N.: Monograph No. 204 S, October, 1956 (see **104** C, p. 167).
† *Elettrotecnica*, 1946, 33, p. 313.

DISCUSSION ON

'AN ANALYSIS OF COMMUTATION FOR THE UNIFIED-MACHINE THEORY'*

Mr. M. J. Jevons (*communicated*): Mr. Jones's method of including a second coil in the unified theory is both novel and informative. The issues of the short-circuited coil, with an axis coincident with the main stator axis have long been debated, in classical terms, for the a.c. commutator machine, in which the problems of commutation are particularly serious.

The dynamic performance of any electro-mechanical device is described in a minimum number of equations derived from the holonomic Lagrange equation, and, by definition, forms a symmetric set. The equations are made linear by a transformation into quasi-holonomic axes, but, it is argued, this latter set is not basic to the commutator machine. The equations of this machine are obtained from a 'layered' slip-ring primitive machine by constraining non-holonomic reference axes to be holonomic over the commutating region only, and equating this to zero in the limit. This idealizes the process of commutation and at the same time linearizes the set of equations. The equations thus obtained are symmetric and are reduced to the conventional form by eliminating the axes of the additional coils.

This method of including commutation is suitable for the 2-brush machine, but would be unsuitable for unbalanced conditions such as obtain in the Metadyne or commutator version of the single-phase induction motor. An approximation might be made by the use of a 3-layer primitive, but the increased complexity would limit the usefuless of the equations.

Mr. C. V. Jones (*in reply*): The analysis given in the paper was confined to the simple case of a 2-brush commutator machine merely for the sake of clarity. No new principle is involved however, in the extension of the analysis to the 4-winding commutator machine. This is straightforward, and the appropriate results have been considered in a previous discussion of the paper.†

* Jones, C. V.: Monograph No. 302 U, April, 1958 (see **105** C, p. 476).
† *Proceedings I.E.E.*, 1959, **106** C, p. 1.

INDEX TO VOLUME 106, PART C

1959

ABBREVIATIONS

(P)—Paper. (D)—Discussion.

PROCEEDINGS OF THE INSTITUTION OF ELECTRICAL ENGINEERS

PART C—MONOGRAPHS, SEPTEMBER 1959

CONTENTS

Bibliographical References.—It is requested that bibliographical reference to an Institution paper should always include the serial number of the paper and the month and year of publication, which will be found at the top right-hand corner of the first page of the paper. This information should precede the reference to the Volume and Part.

Example.—SMITH, J.: "Reflections from the Ionosphere," *Proceedings I.E.E.*, Paper No. 4001 R, December, 1954 (102 B, p. 1234).

Published by The Institution, Savoy Place, London, W.C.2. *Telephone:* COVent Garden 1871. *Telegrams:* 'Voltampere, Phone, London.'
Printed by Unwin Brothers Limited, Woking and London.